



GEORG-AUGUST-UNIVERSITÄT  
GÖTTINGEN



***Analysis of the Cell Entry of Enveloped Viruses  
and Identification of Potential Intervention Strategies***

Dissertation  
for the award of the degree

“Doctor rerum naturalium”

of the Georg-August-Universität Göttingen

within the doctoral program

*Emerging Infectious Diseases (EIDIS)*

of the Georg-August University School of Science (GAUSS)

submitted by

**Bojan Fabio Hörnich**

from Berlin, Germany

Göttingen 2021

---

## **Thesis Committee**

Dr. Alexander Hahn

Junior Research Group Herpesviruses, German Primate Center, Göttingen

Prof. Dr. Lutz Walter

Primate Genetics Laboratory, German Primate Center, Göttingen

Dr. Christiane Stahl-Hennig

Unit of Infection Models, German Primate Center, Göttingen

## **Members of the Examination Board**

Referee: Dr. Alexander Hahn

Junior Research Group Herpesviruses, German Primate Center, Göttingen

2<sup>nd</sup> Referee: Prof. Dr. Stefan Pöhlmann

Infection Biology Unit, German Primate Center, Göttingen

## **Further members of the Examination Board**

Prof. Dr. Lutz Walter

Primate Genetics Laboratory, German Primate Center, Göttingen

PD Dr. Michael Winkler

Infection Biology Unit, German Primate Center, Göttingen

Prof. Dr. Rüdiger Behr

Platform Degenerative Diseases, German Primate Center, Göttingen

Prof. Dr. Christian Roos

Primate Genetics Laboratory, German Primate Center, Göttingen

Date of oral examination: 17.01.2022



---

## Table of Contents

<b>1</b>	<b>ABSTRACT .....</b>	<b>1</b>
<b>2</b>	<b>INTRODUCTION .....</b>	<b>3</b>
2.1	VIRAL BIOLOGY AND PATHOGENESIS .....	3
2.1.1	<i>The pandemic zoonotic virus SARS-CoV-2.....</i>	3
2.1.2	<i>The human oncogenic virus KSHV.....</i>	4
2.2	VIRAL REPLICATION CYCLE AND CELL-CELL FUSION.....	5
2.3	VIRAL ENTRY AND CELLULAR RECEPTORS .....	7
2.3.1	<i>SARS-CoV-2 entry.....</i>	7
2.3.2	<i>KSHV entry.....</i>	9
2.4	VIRAL MEMBRANE FUSION .....	11
2.4.1	<i>SARS-CoV-2 Spike-mediated fusion.....</i>	12
2.4.2	<i>gB the herpesvirus fusion protein .....</i>	14
2.5	STRATEGIES TO PREVENT VIRAL ENTRY AND MEMBRANE FUSION .....	17
2.5.1	<i>Inhibitors of viral membrane fusion.....</i>	17
2.5.2	<i>Host fusion preventors IFITMs.....</i>	18
2.6	THESIS AIM.....	21
<b>3</b>	<b>PUBLICATIONS/RESULTS .....</b>	<b>22</b>
3.1	PUBLICATION 1: SARS-CoV-2 AND SARS-CoV SPIKE-MEDIATED CELL-CELL FUSION DIFFER IN THEIR REQUIREMENTS FOR RECEPTOR EXPRESSION AND PROTEOLYTIC ACTIVATION .....	22
3.2	PUBLICATION 2: INTERFERON-INDUCED TRANSMEMBRANE PROTEINS INHIBIT INFECTION BY THE KAPOSI'S SARCOMA-ASSOCIATED HERPESVIRUS AND THE RELATED RHESUS MONKEY RHADINOVIRUS IN A CELL-SPECIFIC MANNER.....	49
<b>4</b>	<b>DISCUSSION.....</b>	<b>75</b>
4.1	PROTEOLYTIC ACTIVATION OF THE SARS-CoV-2 SPIKE– IMPLICATIONS FOR PATHOGENESIS AND CLINICAL INTERVENTION STRATEGIES.....	75
4.1.1	<i>The SARS-CoV-2 Spike– Contribution of syncytia formation and matrix-metalloprotease activation to SARS-CoV-2 pathogenesis.....</i>	75
4.1.2	<i>Proteolytic fusion activation of the SARS-CoV-2 Spike has critical implications for clinical intervention .....</i>	78
4.1.3	<i>A potential role of Ambroxol in COVID-19 treatment.....</i>	80
4.2	DIFFERENTIAL ANTIVIRAL ACTIVITY OF IFITMS TOWARDS GAMMA-2-HERPESVIRUSES– HINTS TO THE IFITM FUNCTION AND VIRAL EVASION STRATEGIES.....	82
4.2.1	<i>Differential effects of IFITMs on gamma-2-herpesviruses- Implications for the IFITM function.....</i>	83
4.2.2	<i>IFITM evasion of KSHV and RRV.....</i>	85
4.2.3	<i>Viral adaptation to IFITMs and influence on in vivo importance .....</i>	87
<b>5</b>	<b>OUTLOOK.....</b>	<b>90</b>
<b>6</b>	<b>REFERENCES .....</b>	<b>92</b>
<b>7</b>	<b>APPENDIX.....</b>	<b>A</b>
7.1	LIST OF FIGURES .....	A
7.2	LIST OF ABBREVIATIONS .....	A
7.3	LIST OF PUBLICATIONS .....	D
7.4	CONFERENCE PARTICIPATIONS.....	D
7.5	ACKNOWLEDGEMENT .....	E
7.6	CURRICULUM VITAE .....	F



## 1 Abstract

Viruses are a continuous threat for the human population. They are causing tremendous damage to human health and economy. Not only zoonotic viruses, which jump from animals to humans, but also the spread of highly adapted human pathogens, results in an increase of epidemics. To be prepared for future challenges it is necessary to gain fundamental knowledge of viruses and utilize this knowledge to invent applicable counteractions. Antiviral intervention is possible at several key points of the viral replication cycle. Preventing already the entry of the virus into the host cell holds great potential for effective treatment strategies, as it completely prevents virus induced damage to the cell. We therefore investigated fundamental basics of the entry and fusion mechanism as well as potential intervention strategies of two distinct viruses, one zoonotic and recently emerged, the other one evolutionary ancient and highly adapted.

First, we analyzed the viral surface glycoprotein Spike (S) of the recently emerged severe acute respiratory syndrome coronavirus 2 (SARS-CoV-2) and compared it with the Spike of the severe acute respiratory syndrome coronavirus (SARS-CoV). Both viruses require the viral surface protein Spike, the cell surface receptor ACE2 and an activating protease to enter the cell. We were able to show that SARS-CoV-2 Spike-mediated cell-cell fusion was less dependent on the protease TMPRSS2 and more on the receptor ACE2; Vice versa the SARS-CoV Spike-mediated cell-cell fusion was more dependent on TMPRSS2 and less on ACE2 expression. We could show that this observation was based on the fact that the SARS-CoV-2 Spike can be activated, in addition to members of the transmembrane protease serine subtype (TMPRSS)-family and cathepsins, by metalloproteases. The TMPRSS2-independent activation of the Spike for cell-cell fusion and the ability of forming syncytia was related to the multibasic cleavage motif present in the SARS-CoV-2 Spike. Furthermore, we identified a KR-motif in the SARS-CoV-2 Spike subunit 2 (S2) as the key site for TMPRSS2 proteolytic activation. While mutation of this site abolished any TMPRSS2-related activation, the SARS-CoV-2 Spike was still proteolytically activated by metalloproteases for cell-cell fusion and cathepsins for particle entry. In addition, we were able to identify the over-the-counter medication Ambroxol as inhibitor of SARS-CoV-2 replication in Calu-3 cells.

In contrast to the entry of SARS-CoV-2, the high degree of complexity of the entry of Kaposi's sarcoma herpesvirus (KSHV) does not allow for a simple intervention. We therefore analyzed the antiviral activity of the host cell broad-spectrum restriction factors Interferon (IFN)-inducible transmembrane proteins (IFITMs) on the gamma-2-herpesviruses KSHV and the closely related primate virus rhesus monkey rhadinovirus (RRV). We were able to show that the entry of KSHV and RRV is inhibited by IFITM1 in a cell-dependent manner. While knockout of IFITMs in cells of epithelial and fibroblast origin enhanced KSHV and RRV infection, IFITM-knockout in endothelial cells remained without effect. We could furthermore show that in epithelial and fibroblast cells, IFITM1 overexpression inhibited the KSHV and RRV infection more effectively than IFITM2 and IFITM3. By showing that all IFITMs inhibit gamma-2-herpesvirus glycoprotein-mediated cell-cell fusion and that KSHV partially evades this restriction, likely by avoiding IFITM-positive compartments, we could contribute to the understanding of the IFITM mechanism against the entry of enveloped viruses.

Taken together this thesis investigated fundamental basics of SARS-CoV-2 entry and fusion as well as the impact of IFITMs on gamma-2-herpesviruses, leading to future perspectives for intervention strategies against the entry process of enveloped viruses.

## 2 Introduction

### 2.1 Viral biology and pathogenesis

#### 2.1.1 The pandemic zoonotic virus SARS-CoV-2

Development of fatal disease is a rare event when pathogens are adapted to their respective host. However, when viral infections occur in a non-natural host, severe diseases can arise. Viruses with a zoonotic origin like influenza A virus (IAV), human immunodeficiency virus (HIV) and Ebola virus (EBOV) caused epidemics with severe outcomes and in case of IAV, the 1918 pandemic (1–3). Although coronaviruses (CoVs) are also found natively in the human population, where they can cause common cold, zoonotic spillover of severe acute respiratory syndrome coronavirus (SARS-CoV), middle east respiratory syndrome coronavirus (MERS-CoV) caused epidemics and SARS-CoV-2 an ongoing pandemic (4). SARS-CoV-2 has a non-segmented positive single stranded RNA genome with a size of 29.8-29.9 kb, coding for at least 23 ORFs (5). The origin of SARS-CoV-2 is still unclear; It shares similarities with bat and pangolin CoVs (6–10). Initially, the bat CoV RaTG13 was identified as the CoV with the highest similarity to SARS-CoV-2 (6). Recent studies identified several bat CoVs that are even closer related to SARS-CoV-2 than RaTG13 (8, 11, 12). However, these viruses are believed to be too distantly related to serve as origin of SARS-CoV-2 (8, 11–14). It is therefore assumed that transmission from bat to human involved an intermediate host as shown for SARS-CoV (13). While, the residues found in the receptor binding domain (RBD) share similarity with pangolin CoVs (7, 15, 16), key residues in the RBD and the S1/S2-site (see chapter 2.3.1) significantly differ (17), leaving the search for an intermediate host still open. However, regarding receptor usage, proteolytic priming and pathogenesis, SARS-CoV-2 displays similarities to the more distantly related SARS-CoV (7, 18). In principle, SARS-CoV-2 is an airborne virus which is mainly transmitted via respiratory droplets, but infection through aerosols, contaminated surfaces, and fecal–oral transmission, similar to SARS-CoV, might be possible as well (15, 16, 19). The most astonishing characteristic of SARS-CoV-2 is the spectrum of disease symptoms which reaches from asymptomatic cases to fatal pneumonia. SARS-CoV-2 causes the coronavirus disease 2019 (COVID-19). While most symptomatic cases involve symptoms of common cold or flu, the disease can rapidly progress to the acute respiratory distress syndrome with fatal outcome (20, 21).

The severeness of COVID-19 is related to different risk factors like age and pre-existing diseases (22, 23). Besides the clear initial disease characteristics, long lasting symptoms including fatigue, periodic headache as well as cognitive impairment are also reported and are now called long COVID (24–26). While initially thought to be unaffected by SARS-CoV-2 infection, also children can acquire a severe post-infectious complication named pediatric inflammatory multisystem syndrome (27, 28). Meanwhile several vaccines are available, however due to the emerge of new SARS-CoV-2 variants with increasing chance of immune escape, there is still a demand for effective COVID-19 treatment options (29, 30).

### 2.1.2 The human oncogenic virus KSHV

Some members of the herpesvirus family belong to the most widespread viruses in the world. Herpes simplex virus 1 (HSV-1) and Epstein-Barr virus (EBV) were shown to have a seroprevalence of at least 60% in the human population and up to 80% in some countries (31, 32). Herpesviruses are highly adapted pathogens and are constantly coevolving with their respective hosts (33, 34). Upon primary infection they establish a lifelong persistence (35, 36). The herpesvirus family is divided into the alpha-, beta- and gammaherpesviruses (37). Key feature of all herpesviruses is a biphasic replication cycle. The latent phase allows efficient immune evasion with just a small subset of viral proteins expressed (36, 38, 39). During this phase, the viral genome is maintained alongside with the host genome as episome (40). Sensing of environmental changes results in expression of lytic genes and reactivation (36, 41–44). While most herpesvirus infections do not cause severe diseases in healthy individuals, the gammaherpesvirus family harbors two of the seven known tumorigenic viruses, EBV and the gamma-2-herpesvirus Kaposi's sarcoma herpesvirus (KSHV) (45). In addition to KSHV, the gamma-2-herpesvirus sub-family also contains the rhesus monkey rhadinovirus (RRV), which is used to study gamma-2-herpesvirus biology in animal models and shares similarities with KSHV. Like all herpesviruses, KSHV and RRV have a double-stranded DNA genome that is enclosed by the icosahedral capsid. The viral tegument is a layer of proteins that are involved in viral assembly, particle transport as well as immune evasion and separates the capsid from the lipid envelope (46, 47). KSHV causes Kaposi's sarcoma (KS), a highly vascularized tumor, which was first described in 1872 by Moritz Kaposi (48). Since then, four main types of KS have been described: The classical KS mainly occurs in elderly men of Mediterranean or

Jewish ancestry (48), while the endemic KS, that is predominately found in Africa, also affects children (49), the epidemic or acquired immune deficiency syndrome related KS is linked to HIV infection (50) and the iatrogenic KS is found in organ transplant recipients (51). Today, KSHV is also associated to primary effusion lymphoma (PEL) (52), multicentric Castleman disease (MCD) (53), KSHV inflammatory cytokine syndrome (54) and cases of osteosarcoma (55). Although the exact mechanism of KSHV oncogenesis is not completely understood in detail, several of the KSHV genes that are expressed during latency and reactivation promote enhanced cell survival, proliferation as well as secretion of growth and angiogenic factors and thus likely contribute to oncogenesis (46). The main transmission route of KSHV is via saliva, but it is also transmitted via sexual contact, blood or solid organ transplantation (51, 56). Seroprevalence of KSHV is distributed with high regional differences; The highest seroprevalence is found in sub-Saharan Africa with up to 90%, followed by 20-30% in the Mediterranean area and under 10% in northern Europe, Asia and the USA (57). This is also reflected by the KSHV-associated disease incidence. While occurrence of KSHV-associated disease is rather low in industrial countries, KSHV-associated malignancies belong to the most common cancers in endemic areas like sub-Saharan Africa (57–59). Treatments against KSHV-associated diseases mainly involves anti-HIV therapy or chemotherapy, but to date no vaccine is available and especially in PEL and MCD patients, treatment options are limited, often leading to poor prognosis (46, 57).

## **2.2 Viral replication cycle and cell-cell fusion**

Viruses are per se no living organisms, they are obligate parasites that depend on host organisms to promote their propagation. To successfully infect and spread in an organism, a concerted sequence of events must occur in which viruses hijack the host cell machinery to produce infectious offspring. The first step in the viral replication cycle is the attachment to a host cell (Figure 1; (60)). There are two major possibilities for attachment: While some viruses attach directly through interaction of their surface protein with the respective cellular receptor that also triggers entry into the cell, other viruses first attach via interaction with cell surface carbohydrates like heparan sulfate proteoglycan (HSPG) or sialic acid, which not directly facilitate entry in most cases (60,

61). These abundant cell surface molecules increase the local particle concentration, which decreases the required affinity to bind the entry receptor (62). In contrast, binding to the viral entry receptor actively promotes the entry into the target cell e.g. by initiation of conformational changes of the viral surface protein that results in direct fusion at the plasma membrane (63, 64), passive endocytic internalization (65, 66) or direct activation of endocytosis (67, 68). Although plasma membrane fusion is seen for viruses like HIV-1 (69) and HSV-1 (70), endocytic entry is often favored as it may allow avoidance of the crowded intracellular meshwork and immune surveillance. The major route of endocytic entry used by a variety of viruses is the clathrin-mediated endocytosis. Besides this, viruses can also enter the cell via caveolin-mediated endocytosis, macropinocytosis as well as several uncharacterized clathrin/caveolin-independent routes (71, 72). Most of these pathways ultimately end in the endolysosomal pathway where the fusion of the viral and host membrane results in the release of the viral content into the host cell. In case of most negative and positive single-stranded RNA viruses, the replication of the viral genome and translation of viral proteins starts already in the cytosol. In case of retroviruses and DNA-viruses, like herpesviruses, the genome is transported to the nucleus where it is replicated and transcribed (35, 73). The produced viral proteins, together with the viral genome are then assembled to progeny virus. The budding of the progeny virus then takes place and new virions are released.

Another possibility for the virus to spread is the formation of syncytia. Syncytia are formed when infected cells fuse with uninfected neighboring cells and are characterized by multinucleation (74). The formation of syncytia allows viral spread to nearby cells without the production of assembled viral particles. The syncytia formation is mediated by the viral surface fusion protein (chapter 2.4) and likely contributes to enhanced viral replication, escape of immune surveillance as well as tissue damage by cytopathic effects (75–77). Cell-cell fusion is mainly observed when viral fusion proteins are capable to mediate direct fusion at the plasma membrane (see chapter 2.4) (78–80). When the viral fusion proteins are found at the host cell surface, fusion can be activated by interaction with the host receptors present on neighboring cells (80). Replication and transcription/translation of the viral genome can then occur as described for above.

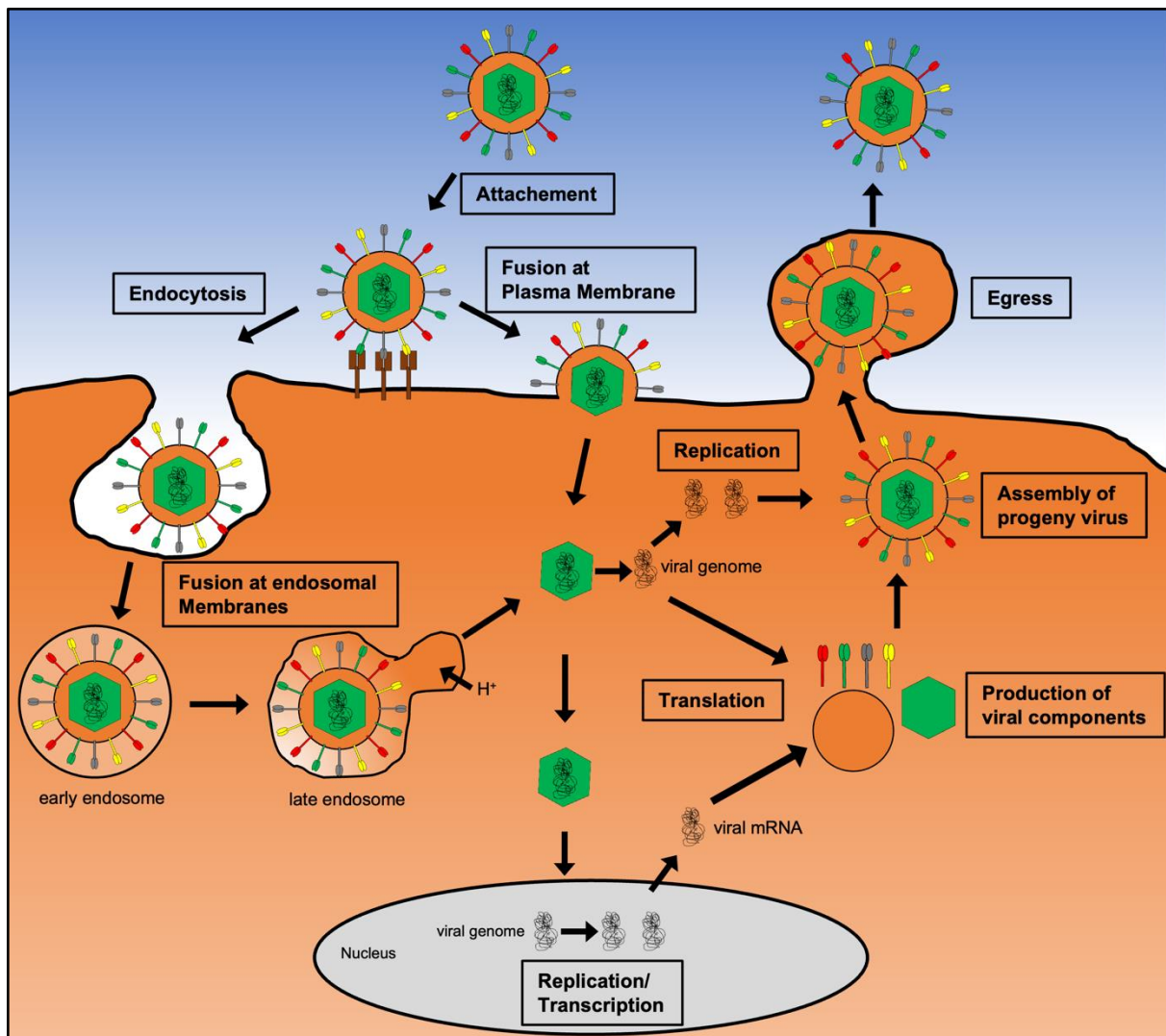


**Figure 1:** Simplified viral replication cycle. The viral particle binds to the host cell via attachment factors or the viral entry receptor. Binding to the entry receptor triggers direct fusion at the plasma membrane or internalization of the viral particle via endocytosis. Fusion of the viral and host membrane either at the plasma membrane or the endolysosomal pathway results in the release of the viral genome into the host cell. The viral genome is either directly replicated, transcribed, and translated in the cytosol or transported to the nucleus where replication of the viral genome and/or transcription takes place. Transcription of viral transcribed mRNA results in production of viral proteins, together with the replicated viral genome, these are assembled to progeny virus. The progeny viral particles then egress via exocytosis or cell lysis (60).

## 2.3 Viral entry and cellular receptors

### 2.3.1 SARS-CoV-2 entry

SARS-CoV-2 only expresses a single viral surface glycoprotein which mediates receptor binding and fusion. This Spike (S) protein is highly conserved among coronaviruses regarding function and domain organization. During maturation of the Spike, it is cleaved into the subunit 1 (S1) and subunit 2 (S2) (Figure 2A; (18, 79, 81)).

The SARS-CoV-2 S1 contains the receptor binding domain (RBD), which promotes binding to the SARS-CoV-2 entry receptor ACE2 (18, 79). Binding to ACE2 was already shown for SARS-CoV and the bat CoV RaTG13 (14, 82). The affinity of SARS-CoV-2 Spike to hACE2 is, however, 1000-fold higher than RaTG13 Spike (14), while the binding affinity of SARS-CoV-2 Spike and the more distantly related SARS-CoV Spike to hACE2 is in a similar range, although with slight differences (83–85). In addition to ACE2, also Neuropilin-1 was shown to enhance the entry of SARS-CoV-2 (86, 87). The SARS-CoV-2 Spike binds HSPG and sialic acid, which might serve as attachment factors and this binding is predicted to occur via the N-terminal domain (NTD) (83, 88–91). Processing of the SARS-CoV-2 Spike into the S1- and S2-subunit occurs at the S1/S2-site, which contains a multibasic cleavage site and is mediated by the host cellular protease furin as well as related enzymes (79, 81, 92). Interestingly, a multibasic cleavage motif at the S1/S2-site is also found in the Spike proteins of MERS-CoV (93) and human OC43 (79), but not SARS-CoV (94) or RaTG13 (14). The SARS-CoV-2 S1/S2-site was shown to be important for entry into Calu-3 lung cells (79), but not for entry into Vero or 293T-ACE2 cells (95). Although deletion variants of the multibasic cleavage motif at the S1/S2-site were isolated *in vitro* and *in vivo* (96, 97), it was demonstrated that the cleavage at the S1/S2-site is essential for transmission (95, 98). While the RBD containing S1-subunit mediates the initial binding and attachment to the host cell, the S2-subunit contains the proposed proteolytic priming site (S2'-site), which was identified in SARS-CoV and MERS-CoV (93, 94, 99), the fusion peptide (FP) as well as the heptad repeat regions 1 and 2 (HR1, HR2), responsible for membrane fusion (see chapter 2.4.1; Figure 2A; (18, 100)). SARS-CoV-2 can directly fuse near or at the plasma membrane and this fusion depends on members of the TMPRSS-family, in particular TMPRSS2 (18, 101–103). When TMPRSS2 is not present or low abundant, the SARS-CoV-2 particles are internalized, in case of 293T-ACE2 cells (104) via clathrin-mediated endocytosis and activation occurs via endosomal cathepsins (see Figure 2B; (18)). Following fusion at the cell-membrane or endosomal membranes the viral genome is released into the cell and the viral replication cycle progresses as described in chapter 2.2.



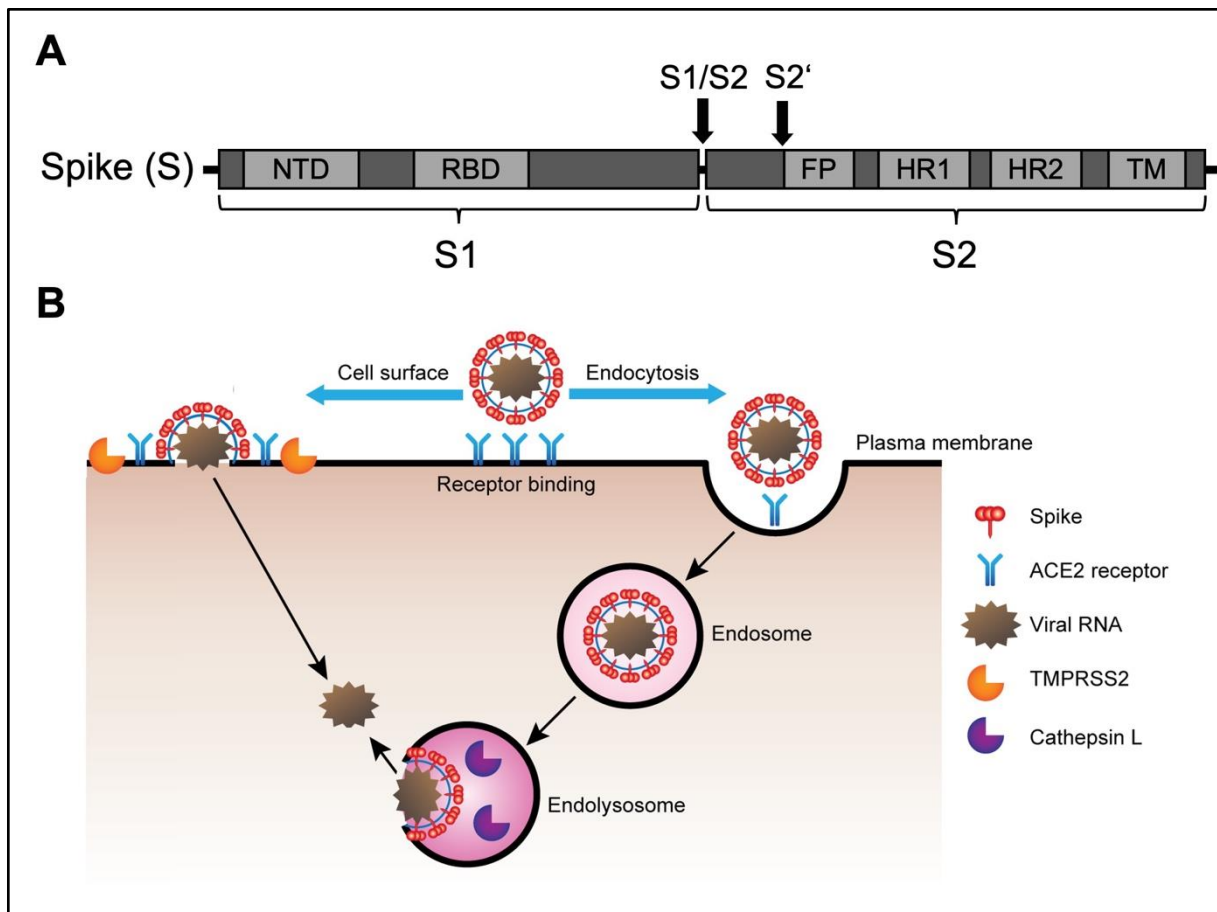


**Figure 2:** SARS-CoV-2 Spike protein structure and particle entry. **A** Schematic representation of the SARS-CoV-2 Spike (not exactly drawn to scale). After cleavage at the multibasic cleavage motif (RRAR) at the S1/S2-site, the Spike is separated into the S1- and S2-subunit. The S1-subunit contains the N-terminal domain (NTD) and the receptor binding domain (RBD). The S2-subunit contains the fusion peptide (FP), the heptad repeats 1 and 2 (HR1, HR2), the transmembrane domain (TM) and the proposed proteolytic priming site (S2') (18, 100). **B** Schematic representation of the SARS-CoV-2 particle entry adapted from Murgolo et al. (105). After receptor binding, the SARS-CoV-2 particle can either directly fuse at the plasma membrane, if TMPRSS2 or related proteases are present, or it is internalized via endocytosis. Fusion of endocytosed particles takes place in cathepsin containing endolysosomal compartments (105).

### 2.3.2 KSHV entry

KSHV expresses several glycoproteins (g) that have a variety of functions, but mainly interact with attachment factors or entry receptors. While the glycoproteins gH, gL, gB, gM and gN are conserved among herpesviruses, ORF4, K8.1, K1, K14, and K15 are KSHV-specific glycoproteins (106, 107). However, only ORF4, gB, gH/gL, gM/gN, and K8.1 were demonstrated to be incorporated into the lipid bilayer of virions (107, 108). Attachment to ubiquitous cell surface HSPGs is mainly mediated by gH, gB, and K8.1 (109–111). This together with the fact that KSHV binds multiple entry receptors results in a broad cell tropism and redundancy of receptors. Inhibition or knockout/knockdown of a single entry receptor drastically reduces, but often not completely prevents

infection (112–115). The KSHV tropism includes human endothelial cells, epithelial cells, keratinocytes, B cells, macrophages, dendritic cells, T-cells, fibroblast cells and a variety of animal cells (113, 116, 117). Entry into cells of epithelial and endothelial origin was shown to be mediated by members of the ephrin receptor family, mainly EphA2, although other Eph-members were reported but with lower efficiency (113, 118, 119). The Eph interaction is mainly mediated by the glycoprotein complex gH/gL (112, 114, 118). Additional receptors like integrins were also demonstrated to be involved in KSHV-mediated downstream signaling as well as entry into epithelial, endothelial and fibroblast cells (111, 114, 119, 120). However, the exact nature of the integrin binding is still debated; While  $\alpha V\beta 3$ ,  $\alpha V\beta 5$  and  $\alpha 3\beta 1$  (121, 122) were initially shown to be important for the cell entry, recent results imply that successful KSHV infection of some cells might be independent of members of the  $\alpha V$ - and  $\beta 1$ -family of integrins and mainly depends on EphA2 and HSPG expression (119). Furthermore, it was demonstrated that KSHV utilizes DC-SIGN to enter human myeloid dendritic cells, macrophages, and activated B cells (123–125). The most interesting point is that the proposed site of KSHV latency, the B cells, are only partially susceptible to free virus infection (116, 126). Entry into the B cell line MC116 and into tonsillar B cells depend on K8.1 and a yet unknown receptor (117). Another B cell line, BJAB, was shown to be entered in a EphA7-dependent manner via cell-to-cell spread (115). Like other enveloped viruses, KSHV virions have to fuse with the lipid bilayer of the host membrane. Although some herpesviruses can fuse directly at the plasma membrane, KSHV enters most studied cell types via different modes of endocytosis (113, 127, 128). Using inhibitors of macropinocytosis and colocalization studies with the macropinocytosis marker dextran it was demonstrated that macropinocytosis is the main entry route of KSHV into the endothelial cell lines HMVEC-d and HUVEC (127). HFF are predominantly entered via clathrin-mediated endocytosis and 293T via an yet unidentified pH-dependent endocytosis pathway (128, 129). Following internalization, KSHV utilizes the gH/gL and gB complex, which represents the herpesvirus core fusion machinery, to promote fusion of the viral and host membrane (130–132). Subsequently, the viral capsid is released into the cytosol and is transported to the nucleus along the microtubular cytoskeleton. Following capsid disassembly, the viral genome is released into the nucleus.

## 2.4 Viral membrane fusion

A key process in the entry of enveloped viruses is the virus-host membrane fusion, which ultimately leads to the release of the viral content into the host cell. Although the process of membrane fusion is, in principle, thermodynamically favored, it is prevented by short distance repulsive forces and sterical hindrance caused by membrane proteins. This limits the distance in which two membranes can come in contact without external energy to approx. 20 nm (133). The additional energy is provided by the viral fusion protein, which is a viral surface protein that catalyzes the viral-host membrane fusion process. While viral fusion proteins are often not well conserved on the genomic or amino-acid level, they share a surprisingly homologous tertiary structure, which hints towards a common ancestor or convergent evolution (134).

Most viral fusion proteins studied this far can be grouped into three distinct classes of fusion proteins based on structural differences of the pre- and post-fusion complexes: Class I fusion proteins are present as homotrimers and are characterized by a central bundle of six alpha-helices (6HB), which is formed by a trimer of  $\alpha$ -helical N-terminal coiled coils and three C-terminal helices (135). An interesting feature of class I fusion proteins is that their fusion activity can be triggered by various mechanisms. While binding of the HIV envelope (Env) protein to the receptor is sufficient to trigger fusion (136), the IAV hemagglutinin (HA) has to be activated by protonation at low pH (137) and the CoV Spike by proteolytic cleavage following receptor binding (18, 93, 94). Class II fusion proteins share a common dimeric  $\beta$ -sheet structure where the fusion loops are found at the tips of those  $\beta$ -strands. In contrast to class I fusion proteins, all class II fusion proteins identified, are solely activated in a pH-dependent manner (135, 138). The class III fusion proteins, share architecture and activation principles of the two other classes. They are trimers and contain a central  $\alpha$ -helical coiled-coils, similar to class I fusion proteins, however, the  $\beta$ -strand structure of the fusion loops resembles more that of class II fusion proteins (139).

Although there are differences in structure and activation of the distinct classes of fusion proteins, the overall catalytic principle of the membrane fusion is highly comparable between different viruses and progresses through several steps, which are mediated via the various domains of the viral fusion protein (Figure 3):

After the attachment and/or receptor binding, which brings the viral and host membrane into proximity, the activated fusion protein changes into an extended position and bridges the two membranes. This first step is mediated by the two membrane-

interacting elements, the viral membrane-anchored C-terminal transmembrane anchor and a hydrophobic domain that is inserted into the target membrane. This structure is often referred to as the pre-hairpin or extended intermediate and represents a homotrimer in all viral fusion proteins studied this far. In second step, the pre-hairpin intermediate undergoes intramolecular structural rearrangements which draws the fusion peptide-anchored target membrane, and the transmembrane-anchored viral membrane together and thus overcomes the repulsive energy. This results in the third step, the formation of a hemifusion intermediate, where the opposed proximal leaflets of the two membranes merge. Progression through hemifusion then results in the opening of the fusion pore (step 4) and release of the viral content into the host cell (133, 134, 138).

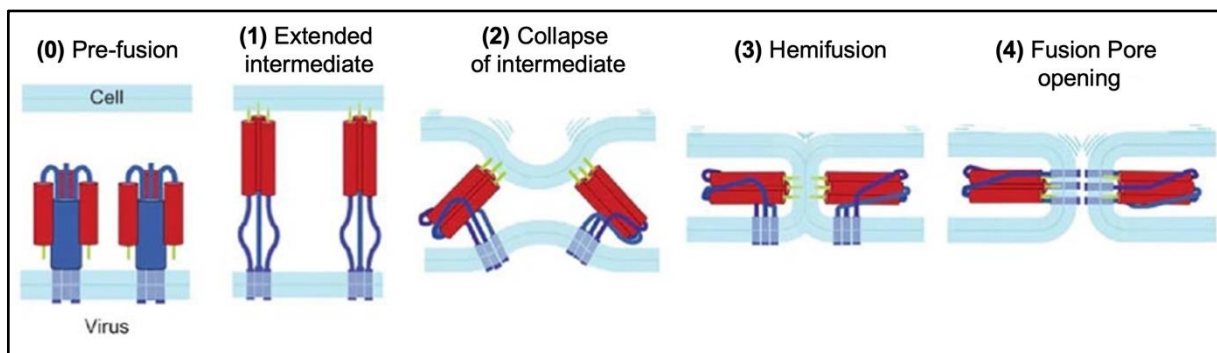


**Figure 3:** Viral membrane fusion adapted from Harrison et al. (134). 0 In the pre-fusion complex, the fusion protein is buried in the viral membrane. 1 Upon external trigger, the fusion protein trimer elongates, and the hydrophobic domain insert into the host membrane. 2 The following structural rearrangement of the viral fusion protein provides the energy to reduce the distance between the host and the viral membrane. 3 Catalyzed by the viral fusion proteins the opposing leaflets fuse and form the hemifusion intermediate. 4 In the final step the hemifusion intermediate progresses to the fusion pore opening (133, 134, 138).

#### 2.4.1 SARS-CoV-2 Spike-mediated fusion

The Spike protein is highly conserved among coronaviruses and shares a common structure and function. At amino acid level the Spike proteins of SARS-CoV-2 and SARS-CoV share about 76% identity (140). The SARS-CoV-2 Spike is a class I fusion protein and comprises two subunits, S1 and S2. The S1-subunit harbors the ACE2 binding RBD (18, 83), while the S2-subunit is the actual fusion protein and contains the upstream helices (UH), FP, central helix (CH), subdomain 3 (SD3), a linker domain (L), the HR1 and HR2, which form the fusion core region (6HB) as well as the viral-membrane anchored transmembrane domain (TM) (Figure 4A; (141)). On the virion surface, the Spike trimers exist in a closed conformation in which the membrane fusion

components of the S2-subunits are shielded by the RBDs of the anticlockwise neighboring S1-subunits (142). The RBD undergoes conformational changes that results in either accessibility or inaccessibility of ACE2 and represents open and closed conformation of the Spike (Figure 4B; (85, 142–144)). Priming or pre-processing at the S1/S2-site recognition motif is thought to enhance the accessibility (open conformation) of the RBD and thus facilitate ACE2-binding (14, 142). In crystal structure studies, asymmetrical trimers in which only one RBD was in an open position were frequently observed (85, 142–144). The following model of SARS-CoV-2 Spike membrane fusion was first described by Fan et al. and was modified after Benton et al. (Figure 4; (141, 142)):

Successive binding of ACE2 by the Spike RBD can finally result in an unstable three-RBD open conformation, in which the Spike is able to bind up to three ACE2 molecules (Figure 4B; (142)). ACE2 binding results in a movement that reduces the contact area of the ACE2-bound S1 to each other and the central S2-core, the three S1 of the trimer are then arranged as a trimeric ring that is attached only via intermediate subdomains (142). In this unshielded conformation, the proteolytic priming sites in the S2-subunit are exposed and accessible for activation (142). Proteolytic cleavage downstream of the FP in S2-subunit, either by members of the TMPRSS-family or cathepsins (18, 103), results in structural rearrangements and exposure of the FP, which then inserts into the host membrane (142). Refolding involves formation of the characteristic 6HB by HR1 and HR2 and brings the TM-bound viral membrane as well as the FP-bound host membrane in a proximity that allows for successful membrane fusion by progression through the steps described in chapter 2.4 (141).

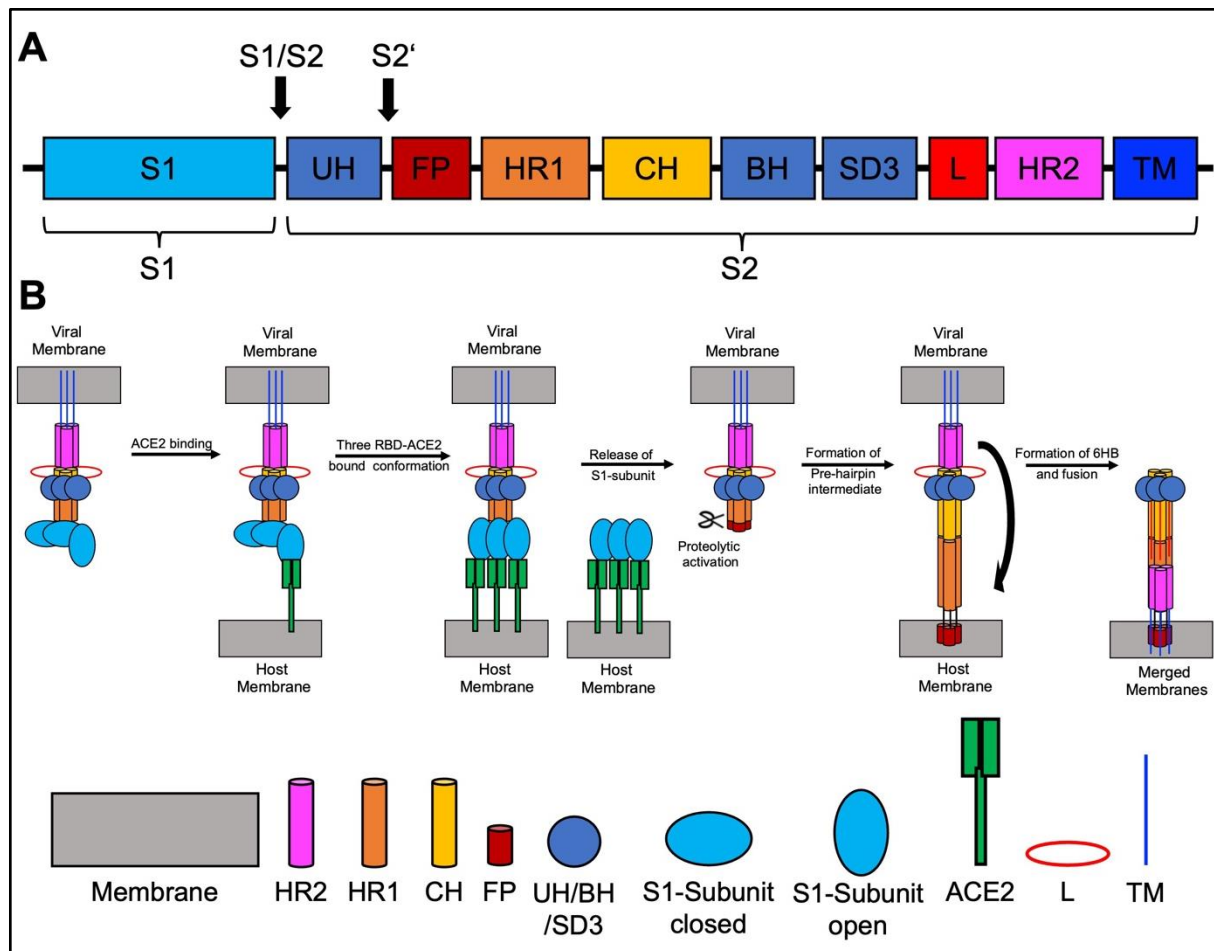


**Figure 4:** Schematic representation of the proposed model of SARS-CoV-2 Spike-mediated membrane fusion. **A** Schematic representation of the domains of the SARS-CoV-2 Spike domains relevant for membrane fusion, adapted from Fan et al. (141) (not exactly drawn to scale). Shown are the S1- and S2-subunit, which contains the upstream helices (UH), hydrophobic fusion peptide (FP), heptad repeats 1 (HR1), central helix (CH), subdomain 3 (SD3), linker domain (L), heptad repeats 2 (HR2), and transmembrane domain (TM). The recognition site for proteolytic cleavage into S1- and S2-subunits (S1/S2-site) and the proteolytic priming site (S2') are indicated by arrows. **B** Model of the SARS-CoV-2 Spike-mediated membrane fusion adapted from Fan et al. (141) and modified after Benton et al. (142). The first picture (starting left) shows a schematic of the pre-fusion structure of the SARS-CoV-2 Spike with one of the receptor binding domains (RBDs) in the S1-subunit in an open position. The RBD of the opened S1-subunit binds to the receptor ACE2, which results in subsequent formation of a three S1-subunit open formation and up to three bound ACE2 proteins. Binding of ACE2 results in release of the S1-subunit and unshielding of the S2' proteolytic priming site in the S2-subunit. Following proteolytic activation of the S2-subunit, the FP inserts into the host membrane and forms the theoretical pre-hairpin structure that bridges the viral and host membrane. Movement of the HR2 towards the HR1 results in the formation of the post-fusion structure of SARS-CoV-2 Spike with the 6 helix bundle (6HB) and fusion of the viral and host membrane (141, 142).

#### 2.4.2 gB the herpesvirus fusion protein

While the membrane fusion process of SARS-CoV-2 involves one viral surface glycoprotein, which serves both as attachment factor and fusion executor, the fusion process of herpesviruses is far more complex. The essential fusion machinery of all studied herpesviruses is formed by a heterotrimeric complex of the viral surface glycoproteins gH and gL together with gB (130–132), but in case of several

herpesviruses at least one additional glycoprotein is required for attachment and receptor binding (145). gB is structurally conserved among all herpesviruses and is the actual fusion protein. Its structure is highly similar to the VSV glycoprotein (G) and is thus designated as a type III fusion protein (139). Post-fusion crystal structures of HSV-1 (146), pseudorabies virus (147), human cytomegalovirus (HCMV) (148) and EBV (149) gB, as well as the recently published prefusion structures of HSV-1 (150) and HCMV (151) gB, together with the well characterized fusion process mediated by VSV-G, give insights into the domain structure and distinct steps of the herpesvirus membrane fusion. gB harbours a trimeric pedestal, which is formed by the membrane proximal region (MPR), the transmembrane domain (TM) and the cytoplasmic tail domain (CTD). The gB ectodomain is further divided into domains I-V (DI-DV) (Figure 5A; (150–152)). Activation of gB is thought to occur following the wedge and clamp model. In this model, the CTD serves as a clamp that stabilizes the pre-fusion conformation of the gB ectodomain (153). Although the exact function of the gH/gL-complex in this process is not completely understood and might vary in different herpesviruses, it is proposed that gH/gL either stabilize the pre-fusion complex or that the CTD of gH transmits a signal that releases the clamp on gB and allows activation (153). In HSV-1 fusion, this signal is hypothesized to involve and depend on the interaction of gD with the cell surface receptor and ultimately with gH/gL as well as gB (152). However, in case of KSHV and RRV, where the gH/gL-complex already mediates the interaction with the cell surface receptor, the complex of gH/gL with gB is enough to execute fusion (130–132). The actual steps of the proposed gB membrane fusion model are very similar to VSV-G and all other viral fusion proteins as described in chapter 2.4. To progress from the pre-fusion to the post-fusion complex, gB undergoes large structural rearrangements. The following model of gB fusion was described by Liu et al. for HCMV gB (Figure 5B; (151)): Following receptor binding induced release of the CTD-clamp, the fusion process is initiated when the interaction of the fusion loop with the MPR breaks (151). This leads to a rearrangement where DI and DII rotate to nearly 180° and allow that the fusion loops are inserted into the host membrane (pre-hairpin intermediate) (151). Refolding induced extension of DV towards the fusion loops, which results in formation of the 6HB, brings the TM-bound viral membrane and the fusion loop-bound host membrane into close proximity, resulting in hemifusion, fusion pore opening (150–152, 154).



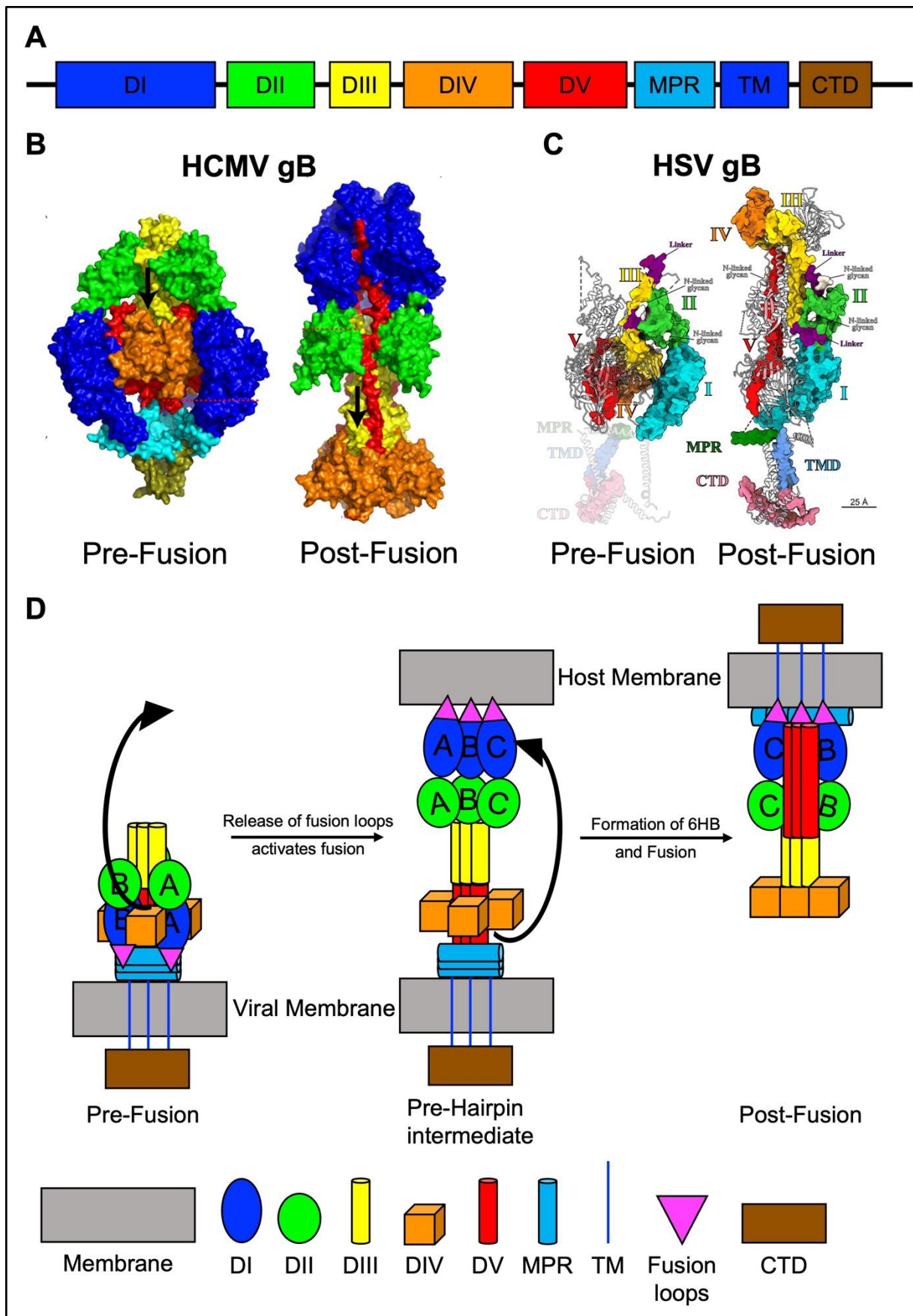


**Figure 5:** Schematic representation of the proposed model of herpesviral gB-mediated fusion. **A** Schematic representation of the domains of the HCMV gB domains relevant for membrane fusion adapted from Liu et al. (151) (not exactly drawn to scale). The HCMV gB contains the Domain I (DI), Domain II (DII), Domain III (DIII), Domain IV (DIV), Domain V (DV), the membrane proximal region



(MPR), the transmembrane domain (TM) the fusion loops and the C-terminal domain (CTD). **B** Space filling models of the HCMV gB crystal structures of the pre-fusion (left) and the post-fusion (right) trimers, adapted from Liu et al. (151). **C** Rigid body fit of the monomers of the HSV-1 gB pre-fusion (left) and the post-fusion (right) crystal structures adapted from Vollmer et al. (150), coloring diverges from A and B. **D** Schematic representation of the model of HCMV gB mediated fusion adapted from Liu et al. (151). The first picture (starting left) shows a schematic of the HCMV gB pre-fusion complex, where the fusion loops are buried in the MPR. Upon signal from the CTD, the interaction of the fusion loops with the MPR breaks. The following rearrangement results in rotation of the DI and DII to nearly 180° and allows insertion of the fusion loops into the host membrane and formation of the hypothetical pre-hairpin intermediat. Refolding of the DV towards the host membrane inserted fusion loops results in the post-fusion gB structure, formation of a 6 helix bundel (6HB) and subsequent fusion of the viral and host membrane (150, 151).

## 2.5 Strategies to prevent viral entry and membrane fusion

### 2.5.1 Inhibitors of viral membrane fusion

Advances in crystal structure analysis and better understanding of the viral fusion process resulted in the development of several viral fusion inhibitors. Most of the fusion inhibitors developed in recent years aimed to target the fusion core of the viral fusion trimer. In case of several class I fusion proteins, peptides derived from either the HR1 or the HR2 were developed (155, 156). These analogs interact with the counterpart HR and thus prevent the formation of the central 6HB. Cp32M (157), Sifuvirtide (158), and T2635 (159) are based on the HR1 of HIV gp41 and inhibit the membrane fusion of wild type (wt) and HIV variants. Similarly, peptide mimics of the HR2 regions of several paramyxoviruses like Newcastle disease virus, respiratory syncytial virus (RSV) were developed (160, 161). Due to the conserved nature of the S2-subunit of coronaviruses, the peptide EK1 derived from the HR1 of human CoVs spike was shown to effectively inhibit Spike-mediated membrane fusion of SARS-CoV, MERS-CoV and SARS-CoV-2 (162, 163). Aside from HR-peptide mimics, there are several small molecule inhibitors. An example are indole-based chemicals, which bind into the hydrophobic pocket inside the trimer core and also prevent formation of the 6HB (164). A very interesting class of broadly antiviral fusion inhibitors was identified to modify the biophysical properties of membranes making them less fusiogenic. Both, amphiphilic thiazolidine derivatives (165, 166) and rigid amphipathic fusion inhibitors (167, 168) are light activated molecules, which modify the membrane phospholipids (169). The resulting increase in positive curvature and reduced fluidity of membranes elevate the energy levels required for membrane fusion (170, 171). While all of these inhibition modes target the physical process of membrane fusion, especially class I fusion

proteins harbors the potential of an additional target step, the activation (see chapters 2.3.1 and 2.4.1). As several class I fusion proteins require at least one proteolytic activation step for transition into their fusion-active form, protease inhibitors harbor great potential as antiviral drugs. In case of SARS-CoV-2, several inhibitors against the main activating protease TMPRSS2, but also other proteases are currently tested in ongoing clinical trials.

### 2.5.2 IFITMs– Host viral entry inhibitors

While great effort was put into identification of inhibitors of viral entry, nature has already developed efficient broadly acting entry inhibitors, the Interferon (IFN)-inducible transmembrane proteins (IFITMs). IFITMs are small helical membrane proteins, which are highly conserved among all vertebrate species (172, 173). The antiviral activity of IFITM3 was identified in an siRNA screen for IAV restriction factors (174). In this study IFITM1, IFITM2 and IFITM3 were identified to potently inhibit the entry of viral particles that were decorated with the viral surface proteins of IAV, West Nile virus (WNV) and Dengue virus (DENV), so called pseudoparticles (174). In the following years a growing list of viruses, now including several flaviviruses, filoviruses, bunyaviruses, and coronaviruses, were shown to be restricted by members of the IFITM-family (174–179). In addition to the IFN-inducible IFITM1, IFITM2 and IFITM3, the IFITM-cluster on chromosome 11 in the human genome also contains the non- IFN inducible, non-immune related IFITM5 and IFITM10 (178, 180). IFITMs localize to different cellular compartments. Although the localization of IFITMs likely also depends on the cell type and on expression levels, IFITM1 displays mainly plasma membrane localization, while IFITM2 and IFITM3 are predominantly found in the endolysosomal pathway (181–183). A YxxΦ -motif found in the N-terminal domain of IFITM2 and IFITM3 was demonstrated to be responsible for the correct subcellular location (Figure 6A). Disruption of this motif localized IFITM3 to the plasma membrane and rendered it less functional (184). Similarly, exchange of residues 43-48 to alanine delocalized IFITM3 from late endosomes to the cell periphery. This reduced the antiviral effect to IAV but not to DENV (185). Analogous, delocalization of IFITM1 from the plasma to the cell interior by mutation of the conserved intracellular loop (CIL)-domain (Figure 6A), reduced the IFITM1-mediated antiviral activity against IAV, mumps and measles virus (183). While it is clear that IFITMs interfere with viral entry, the exact mechanism

of the IFITM-mediated restriction is unclear. After the initial discovery of IFITMs a variety of potential mechanisms were proposed (Figure 6B; (178, 186)):

One mechanism suggests that IFITMs modify the biophysical properties of membranes and make them less fusogenic. This model of IFITM function is based on the observation, that IFITMs are capable to restrict viral fusion protein-mediated cell-cell fusion (187–189) and on experiments showing that IFITMs reduce the membrane curvature and increase the lipid order of membranes, which likely prevents fusion pore opening (187, 190, 191). Other mechanisms involve interaction with additional proteins like the metalloprotease ZMPSTE24. Although the exact mechanism of the interplay between ZMPSTE24 and IFITM3 is unclear, the authors claim, that ZMPSTE24 is a IFITM3 downstream effector and necessary for the antiviral activity of IFITM3. Indeed, knockout of ZMPSTE24 in A549 cells abrogates antiviral activity of IFITM3 and the IFITM3 antiviral activity was restored upon ectopic expression of ZMPSTE24 (192). However, this model was not studied in detail and awaits further investigation. The third mechanism claims that IFITM3 affects endosomal acidification and is based on the observation that a majority of IFITM-restricted viruses enter the cell in an endosomal pH-dependent manner (174, 176, 193–195). This mechanism is also supported by the finding that IFITM3 influences the trafficking of the vacuolar ATPase (196). Lastly, IFITM3 was also demonstrated to interact with Vesicle-membrane-protein-associated protein (VAPA) and influence the cholesterol content of the endosomes, which was shown to affect the membrane fusion process (197, 198). However, an involvement of VAPA and cholesterol in the antiviral activity of IFITMs was challenged in other studies (190, 199). Whether one mechanism alone explains the broad IFITM-mediated restriction of viral entry, or all mechanisms are utilized at a time remains enigmatic. However, advances in live cell imaging and single viral particle tracking underlined the importance of the IFITM localization. Viral particles of the highly restricted IAV were demonstrated to colocalize with IFITM3-positive compartments, while the pseudoparticles of the unrestricted Lassa virus (LASV) did not (200–202). In recent years a large number of viruses was identified to be restricted by one or several IFITMs. However, the majority of restricted viruses identified so far are mainly RNA viruses. Although most viruses tested so far are restricted, there are some viruses that seem to be resistant against the IFITM-mediated restriction. Especially in the group of DNA viruses, several viruses were identified to be resistant against IFITMs.



## 2.6 Thesis aim

The development of therapeutics against viruses comes with the caveat that viruses often utilize host cellular components and processes for their own propagation. This hampers the effort to identify drugs without undesired side effects. Several drugs that were developed in recent years often target viral polymerases. However, targeting steps late in the viral replication cycle often does not reduce virus induced cell damages. Inhibition of the earliest step in the viral replication cycle, the entry or even more precise, the membrane fusion, would prevent any viral induced damage and therefore holds great potential for potent drugs. In recent years, several specific but also broadly acting viral fusion inhibitors were identified. A key to the development of effective fusion inhibitors lies in the understanding of viral fusion processes.

Therefore, the first aim of this study was to gain a better understanding of the entry and fusion process of the zoonotic virus SARS-CoV-2 and identify, using this knowledge, new therapeutic treatment options. While the entry process of SARS-CoV-2 holds potential for therapeutical intervention, the high degree of redundancy as well as the complexity of the KSHV entry and herpesvirus membrane fusion, impedes development of new therapeutics. Where science struggles, nature has already developed broadly acting entry inhibitors, the IFITMs. Therefore, a second aim was to investigate whether IFITMs can inhibit the gamma-2-herpesviruses KSHV and the closely related RRV.

### 3 Publications/Results

#### 3.1 Publication 1: SARS-CoV-2 and SARS-CoV Spike-Mediated Cell-Cell Fusion Differ in Their Requirements for Receptor Expression and Proteolytic Activation

Bojan F. Hörnich,<sup>a</sup> Anna K. Großkopf,<sup>a</sup> Sarah Schlagowski,<sup>a</sup> Matthias Tenbusch,<sup>b</sup> Hannah Kleine-Weber,<sup>c</sup> Frank Neipel,<sup>b</sup> Christiane Stahl-Hennig,<sup>d</sup> Alexander S. Hahn<sup>a</sup>

a Nachwuchsgruppe Herpesviren, Abteilung Infektionsbiologie, Deutsches Primatenzentrum–Leibniz-Institut für Primatenforschung, Göttingen, Germany

b Virologisches Institut, Universitätsklinikum Erlangen, Erlangen, Germany

c Abteilung Infektionsbiologie, Deutsches Primatenzentrum–Leibniz-Institut für Primatenforschung, Göttingen, Germany

d Abteilung Infektionsmodelle, Deutsches Primatenzentrum–Leibniz-Institut für Primatenforschung, Göttingen, Germany

Status of Publication: Published in the Journal of Virology.

Contribution: I was responsible for the methodology, formal analysis, data analysis, visualization, reviewing/editing and investigation. Investigation was performed for experiments that lead to Figure 1 A-B, Figure 1 D-F, Figure 2, Figure 3 A-B, Figure 4, Figure 5, Figure 6 A-B, Figure 6 D-E, Figure 7, Figure 8B. For Figure 8 C-D the cells were seeded and inhibitor treatment prior to infection was performed.





## SARS-CoV-2 and SARS-CoV Spike-Mediated Cell-Cell Fusion Differ in Their Requirements for Receptor Expression and Proteolytic Activation

Bojan F. Hörnich,<sup>a</sup> Anna K. Großkopf,<sup>a</sup> Sarah Schlagowski,<sup>a</sup> Matthias Tenbusch,<sup>b</sup> Hannah Kleine-Weber,<sup>c</sup> Frank Neipel,<sup>b</sup> Christiane Stahl-Hennig,<sup>d</sup> Alexander S. Hahn<sup>a</sup>

<sup>a</sup>Nachwuchsgruppe Herpesviren, Abteilung Infektionsbiologie, Deutsches Primatenzentrum–Leibniz-Institut für Primatenforschung, Göttingen, Germany

<sup>b</sup>Virologisches Institut, Universitätsklinikum Erlangen, Erlangen, Germany

<sup>c</sup>Abteilung Infektionsbiologie, Deutsches Primatenzentrum–Leibniz-Institut für Primatenforschung, Göttingen, Germany

<sup>d</sup>Abteilung Infektionsmodelle, Deutsches Primatenzentrum–Leibniz-Institut für Primatenforschung, Göttingen, Germany

**ABSTRACT** Severe acute respiratory syndrome-related coronavirus 2 (SARS-CoV-2) infects cells through interaction of its spike protein (SARS2-S) with angiotensin-converting enzyme 2 (ACE2) and activation by proteases, in particular transmembrane protease serine 2 (TMPRSS2). Viruses can also spread through fusion of infected with uninfected cells. We compared the requirements of ACE2 expression, proteolytic activation, and sensitivity to inhibitors for SARS2-S-mediated and SARS-CoV-S (SARS1-S)-mediated cell-cell fusion. SARS2-S-driven fusion was moderately increased by TMPRSS2 and strongly by ACE2, while SARS1-S-driven fusion was strongly increased by TMPRSS2 and less so by ACE2 expression. In contrast to that of SARS1-S, SARS2-S-mediated cell-cell fusion was efficiently activated by batimastat-sensitive metalloproteases. Mutation of the S1/S2 proteolytic cleavage site reduced effector cell-target cell fusion when ACE2 or TMPRSS2 was limiting and rendered SARS2-S-driven cell-cell fusion more dependent on TMPRSS2. When both ACE2 and TMPRSS2 were abundant, initial target cell-effector cell fusion was unaltered compared to that of wild-type (wt) SARS2-S, but syncytia remained smaller. Mutation of the S2 cleavage (S2') site specifically abrogated activation by TMPRSS2 for both cell-cell fusion and SARS2-S-driven pseudoparticle entry but still allowed for activation by metalloproteases for cell-cell fusion and by cathepsins for particle entry. Finally, we found that the TMPRSS2 inhibitor bromhexine, unlike the inhibitor camostat, was unable to reduce TMPRSS2-activated cell-cell fusion by SARS1-S and SARS2-S. Paradoxically, bromhexine enhanced cell-cell fusion in the presence of TMPRSS2, while its metabolite ambroxol exhibited inhibitory activity under some conditions. On Calu-3 lung cells, ambroxol weakly inhibited SARS2-S-driven lentiviral pseudoparticle entry, and both substances exhibited a dose-dependent trend toward weak inhibition of authentic SARS-CoV-2.

**IMPORTANCE** Cell-cell fusion allows viruses to infect neighboring cells without the need to produce free virus and contributes to tissue damage by creating virus-infected syncytia. Our results demonstrate that the S2' cleavage site is essential for activation by TMPRSS2 and unravel important differences between SARS-CoV and SARS-CoV-2, among those, greater dependence of SARS-CoV-2 on ACE2 expression and activation by metalloproteases for cell-cell fusion. Bromhexine, reportedly an inhibitor of TMPRSS2, is currently being tested in clinical trials against coronavirus disease 2019. Our results indicate that bromhexine enhances fusion under some conditions. We therefore caution against the use of bromhexine in high dosages until its effects on SARS-CoV-2 spike activation are better understood. The related compound ambroxol, which similarly to bromhexine is clinically used as an expectorant, did not exhibit activating effects on cell-cell fusion.

**Citation** Hörnich BF, Großkopf AK, Schlagowski S, Tenbusch M, Kleine-Weber H, Neipel F, Stahl-Hennig C, Hahn AS. 2021. SARS-CoV-2 and SARS-CoV spike-mediated cell-cell fusion differ in their requirements for receptor expression and proteolytic activation. *J Virol* 95:e00002-21. <https://doi.org/10.1128/JVI.00002-21>.

**Editor** Tom Gallagher, Loyola University Chicago

**Copyright** © 2021 American Society for Microbiology. All Rights Reserved.

Address correspondence to Alexander S. Hahn, [ahahn@dpz.eu](mailto:ahahn@dpz.eu).

**Received** 5 January 2021

**Accepted** 14 February 2021

**Accepted manuscript posted online** 19 February 2021

**Published** 12 April 2021

Both compounds exhibited weak inhibitory activity against SARS-CoV-2 infection at high concentrations, which might be clinically attainable for ambroxol.

**KEYWORDS** COVID-19, SARS-CoV-2, TMPRSS2, cell-cell fusion, spike, virus entry

The coronavirus disease 2019 (COVID-19) disease spectrum is caused by severe acute respiratory syndrome-related coronavirus 2 (SARS-CoV-2), which was first identified in patients with pneumonia of unknown origin in the city of Wuhan, China (1). While first characterized as a pneumonia, COVID-19 probably affects a number of organ systems (2–4). SARS-CoV-2 was shown to use the angiotensin-converting enzyme 2 (ACE2) receptor, which was previously described as the receptor for the closely related severe acute respiratory syndrome-related coronavirus (SARS-CoV) (5), for the infection of human cells (1, 6, 7). For the proteolytic activation of the viral spike protein, a prerequisite for the fusion activity of coronaviruses (reviewed in reference 8), transmembrane protease serine 2 (TMPRSS2) (7, 9), as well as the related TMPRSS4 (2), was reported to be of critical importance. In addition, TMPRSS2 was demonstrated to colocalize with the ACE2 receptor (10) and therefore may be biologically particularly relevant. Depending on the cell type, SARS-CoV-2 spike (SARS2-S)-driven entry can also occur through endocytotic pathways where virus-cell fusion is most likely activated by cathepsins (7). Another study reported that several members of the TMPRSS family can activate SARS2-S-mediated membrane fusion (11). The proposed mechanisms for spike priming and initiation of fusion therefore require further clarification, e.g., whether serine protease activity is required under all circumstances or whether fusion can also occur without the action of serine proteases, when these proteases act on the spike protein, and whether there are differences between cell-cell and cell-particle fusions.

It was recently discovered that the polybasic S1/S2 cleavage site of SARS2-S is required for efficient infection of lung-derived cells and promotes the formation of syncytia (12). Understanding syncytium formation may be important, as large syncytial elements are reported to constitute a hallmark of COVID-19-associated pathology (13). Nevertheless, the exact contribution of the two known proteolytic priming sites to cell-cell fusion and their protease usage are not entirely clear. To address these questions, we mutated the S1/S2 site as well as the S2 cleavage (S2') site, we assessed the effects of proteolytic activation by using inhibitors of TMPRSS2 and other proteases, and we analyzed the effects of different levels of protease and receptor expression on SARS-CoV spike (SARS1-S) and SARS2-S fusion activity.

TMPRSS2, which is expressed in airway cells (14), may be amenable to specific inhibition by bromhexine (15), a molecule normally used as an expectorant that thins phlegm, eases coughing, and is widely known as a popular over-the-counter medication, which would make its repurposing for COVID-19 particularly attractive. For these or additional reasons, bromhexine is now being tested in at least three clinical trials (NCT04355026, NCT04273763, NCT04340349) for efficacy against COVID-19. We therefore tested the effect of the TMPRSS2 inhibitor bromhexine on spike-mediated cell-cell fusion and SARS2-S-driven cell entry and compared its potency to that of the serine protease inhibitor camostat. We also included ambroxol, an active metabolite of bromhexine, in our studies (16). Ambroxol has often replaced bromhexine as an over-the-counter medication, and its structural similarity to bromhexine may hint at potential inhibitory effects toward TMPRSS2. Ambroxol may also exhibit weak but broad antiviral activity, as it was shown to reduce the occurrence of respiratory infections (17) and to inhibit proteolytic activation of influenza virus by triggering the release of antiviral factors (18), and it is used to treat acute respiratory distress syndrome in adults and antenatally in infants (19, 20). Further, two recent preprints, one describing modulation of the ACE2-SARS2-S interaction by both bromhexine and ambroxol (21) and the other reporting weak inhibitory activity of ambroxol against SARS-CoV-2 replication (22) in Vero E6 cells, point at a potential utility of these molecules in the therapy of COVID-19.

## RESULTS

**SARS2-S mediates robust fusion of 293T cells transfected with ACE2 with and without coexpression of TMPRSS2.** In order to investigate the fusion mechanism of SARS-CoV-2, we generated several SARS2-S mutants (Fig. 1A, schematic after reference



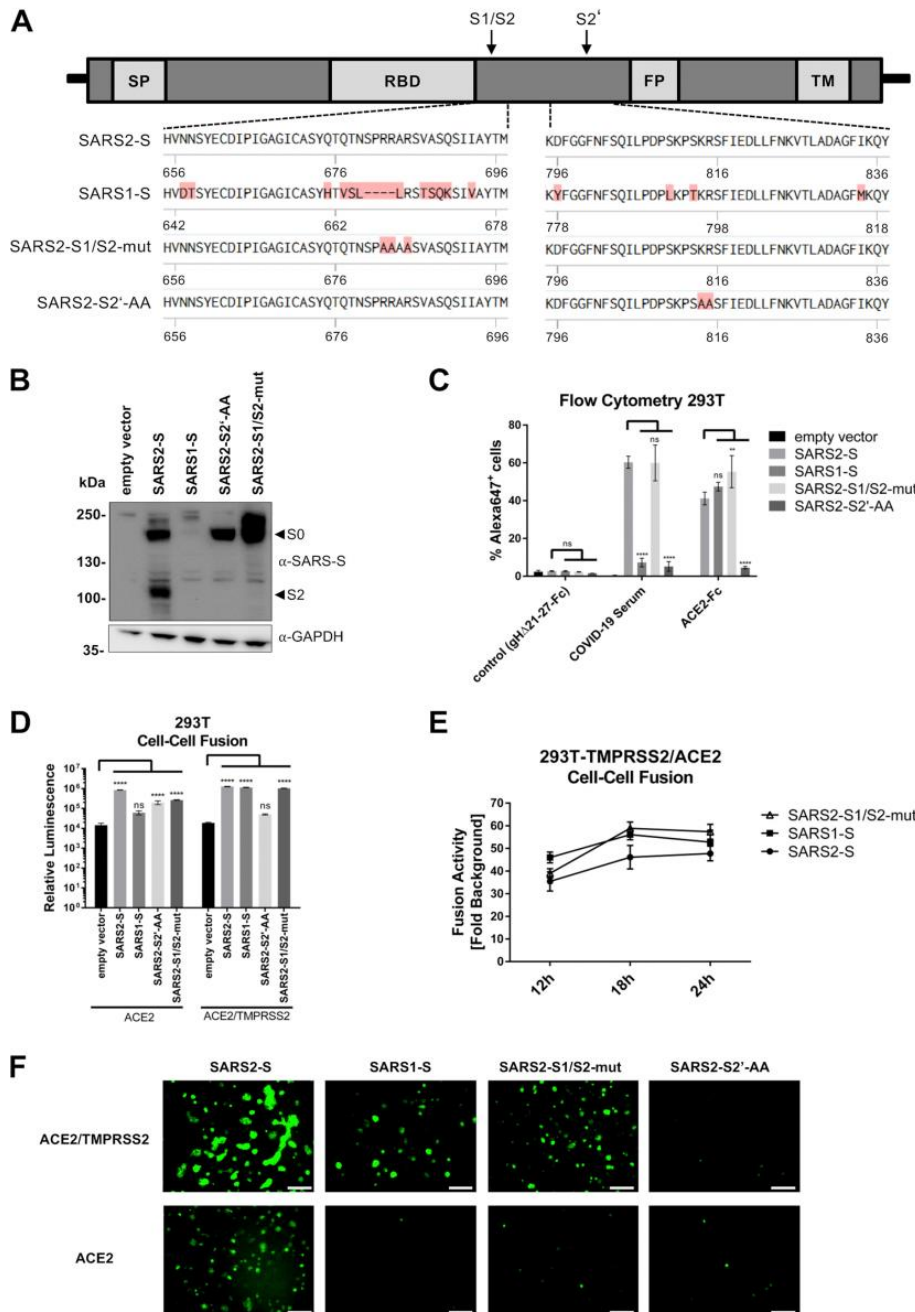


**FIG 1** SARS-2-S mediates robust fusion activity in the presence of ACE2 or ACE2 and TMPRSS2 on target cells, and ablation of the S1/S2 or S2' proteolytic cleavage site affects fusion activity differently. (A) Schematic illustration of the coronavirus spike protein showing the

(Continued on next page)

23). It was reported that the furin recognition motif at the S1/S2 cleavage site of SARS2-S, which is not found in SARS1-S, plays a role in the infection of airway cells, like Calu-3 cells, but is dispensable in other cell types (12). Thus, we generated a mutant, SARS2-S1/S2-mut, where the furin recognition motif and the cleavage site were replaced by alanines (Fig. 1A). Unlike with already published S1/S2 mutants (12, 24), we did not delete the site, as we suspected that this may influence protein conformation and flexibility, but we mutated the proposed furin cleavage site (25) to fully abrogate processing at this site. We furthermore generated an S2' site mutant, SARS2-S2'-AA, by changing K814 and R815 to alanine. The S2' site was shown to be important for proteolytic priming in SARS1-S and is highly conserved among coronavirus spikes (26). We therefore suspected that this site is also important for proteolytic processing of SARS2-S. Clearly detectable bands of lower molecular weights, indicative of proteolytic processing, were observed only with wild-type (wt) SARS2-S (Fig. 1B). As expected, the S1/S2 mutant exhibited no processing at the S1/S2 site, indicated by a missing S2 fragment in a Western blot of transfected 293T cell lysate (Fig. 1B). This is similar to what occurs with SARS1-S, which has no furin cleavage site at this position. As not all mutants might be efficiently expressed at the cell surface, we performed cell surface staining with a COVID-19 convalescent-phase serum, followed by flow cytometry (Fig. 1C, middle column group), which revealed detectable but strongly reduced cell surface expression of the SARS2-S2'-AA mutant, as well as reduced ACE2 binding when the same assay was performed with an ACE2-Fc fusion protein (Fig. 1C, right column group). SARS1-S was only weakly recognized by the COVID-19 convalescent-phase serum. RRV gHΔ21-27-Fc, an Fc fusion protein of RRV gH that lacks any detectable receptor interactions (27), served as a control.

In order to study spike-mediated cell-cell fusion, we established a quantitative reporter gene assay. We chose 293T cells as effector cells, i.e., the cell expressing the viral glycoproteins, because (i) 293T cells exhibit high transfection efficiency and protein expression and (ii) 293T cells can be lifted without trypsinization. We resorted to a system that is also used for two-hybrid screenings, using a VP16-Gal4 transcription factor in one cell and a Gal4 response element-driven reporter construct in the other cell, which results in strong transactivation and reporter gene expression after cell-cell fusion. We transfected 293T target cells with ACE2 and TMPRSS2 expression plasmids and a Gal4 response element-driven TurboGFP-luciferase reporter plasmid (Gal4-TurboGFP-Luc) and effector cells with spike expression constructs, as well as with a plasmid encoding the Gal4 DNA binding domain fused to the VP16 transactivator. Apparent expression levels of SARS1-S as assayed by Western blotting were lower than those of SARS2-S (Fig. 1B), but this may be owing to different levels of glycosylation, proteolytic cleavage, and transfer or detection and was not reflected in its surface expression as measured by ACE2 binding (Fig. 1C) and its fusion activity (Fig. 1D). We

#### FIG 1 Legend (Continued)

signal peptide (SP), the receptor binding domain (RBD), the fusion peptide (FP), the transmembrane domain (TM), the S1/S2 cleavage site (S1/S2), and the S2 cleavage site (S2'), together with amino acid sequence alignments of the spike proteins of SARS-CoV-2 and SARS-CoV and the SARS2-S cleavage site mutants analyzed in this study (not exactly drawn to scale). (B) Expression of spike variants in 293T cells. The unprocessed spike (S0) and the S1/S2 site-processed spike (S2) are indicated by arrows. The expression of GAPDH served as a loading control. (C) Cell surface expression and ACE2 binding. Cell surface expression as measured by antibody binding from a COVID-19 patient convalescent-phase serum and binding of soluble ACE2-Fc to 293T cells expressing the indicated spike proteins were determined via flow cytometry analysis and detection with an Alexa 647-coupled secondary antibody to human IgG. The percentages of Alexa 647-positive cells are shown. Error bars represent the standard deviations from three independent experiments. (D) Cell-cell fusion assay. Effector cells (293T cells transfected with either an empty vector or expression plasmids for the indicated spike variants and Vp16-Gal4 transactivator) were cocultured with target cells (293T cells transfected with ACE2 or ACE2/TMPRSS2 expression plasmids and the Gal4-TurboGFP-Luc reporter plasmid). After 24 h, luciferase activity was measured. The data show averaged relative luminescence units, and error bars represent the standard deviations from one representative experiment performed in triplicate. (E) Experiment as shown in panel D, except that only ACE2/TMPRSS2 target cells were analyzed. After 12 h, 18 h, and 24 h, luciferase activity was measured. The data show averaged fusion activities normalized to that with empty vector-transfected effector cells, and error bars represent the standard deviations from one representative experiment performed in triplicate. (F) Representative GFP fluorescence microscopy images of a cell-cell fusion assay with ACE2- and ACE2/TMPRSS2-expressing target cells and effector cells expressing the indicated spike variants (200- $\mu$ m scale bar). Statistical significance in panels C and D was determined by two-way ANOVA, and *P* values were corrected for multiple comparisons by Sidak's method (*P* > 0.05, not significant [ns]; *P* ≤ 0.05, \*; *P* ≤ 0.01, \*\*; *P* ≤ 0.001, \*\*\*; *P* ≤ 0.0001, \*\*\*\*).



found that when only ACE2 was overexpressed (Fig. 1D, left), all SARS2-S constructs exhibited fusion activity that was statistically different from background. SARS1-S had visible activity, but that did not remain significant after correction for multiple comparisons. On 293T cells that were cotransfected with ACE2/TMPRSS2 expression constructs, all spike variants exhibited fusion activity significantly over background (Fig. 1D, right), except for the SARS2-S2'-AA mutant, which exhibited visible but not statistically significant activity. We chose a logarithmic scale in Fig. 1D for an initial overview of the considerably different fusion activities and how they relate to background activity. Testing activity in a time-lapse experiment on 293T cells that were cotransfected with ACE2/TMPRSS2 expression constructs, we observed that luciferase activity increased up to 18 h for SARS1-S and SARS2-S1/S2-mut and possibly up to 24 h for SARS2-S (Fig. 1E). Also, activities between SARS1-S, SARS2-S, and SARS2-S1/S2-mut were not meaningfully different at any time point. Activity is shown on a linear scale here, which allows for discrimination of smaller differences and which we use from here on.

**The S1/S2 site is critical for syncytium size.** Our results demonstrated mostly normal fusion activity of the S1/S2 mutant in our system when TMPRSS2 was present. Therefore, we wanted to address how mutation of the S1/S2 site translates into syncytium formation in our system, as several reports clearly demonstrated that the S1/S2 site is important for this process (12, 25). It should be noted that initial cell-cell fusion and syncytium formation may not necessarily be the exact same thing. After the initial fusion event, all factors that were originally present in separate cells, i.e., viral glycoprotein, receptor, and activating proteases, are then together in a single syncytial cell and can interact directly upon coexpression. As our reporter also encodes a TurboGFP that is fused to firefly luciferase, syncytium formation can be conveniently visualized. Under the microscope, we indeed observed that in the presence of ACE2 and TMPRSS2, the S1/S2 mutant formed small but numerous syncytia, while wt SARS2-S formed larger syncytia (Fig. 1F). Luciferase reporter activities were comparable. The formation of extended syncytia is obviously a quality that our luciferase reporter does not capture, and interestingly, this is not a matter of the timing of the measurement (Fig. 1E), as even at earlier time points, the luciferase activities between wt SARS2-S and the S1/S2 mutant as well as SARS1-S were similar. We conclude that our luciferase assay measures primarily the initial fusion between effector and target cells and not the formation of extended syncytia.

**SARS2-S-mediated cell-cell fusion is dependent on ACE2 receptor expression and is less restricted by TMPRSS2-mediated activation in *trans* than SARS1-S-mediated fusion.** As we found SARS2-S capable of fusing 293T cells efficiently when ACE2 was expressed without TMPRSS2, while SARS1-S was fully fusogenic only in the presence of TMPRSS2, we decided to analyze SARS2-S, SARS1-S, and SARS2-S1/S2-mut as well as the SARS2-S2'-AA mutant in the context of different ACE2 and TMPRSS2 expression levels (Fig. 2). In this setting, we again observed the robust fusion activity of SARS2-S, which was essentially unaltered by different levels of TMPRSS2 but required the presence of ACE2 (Fig. 2A). SARS1-S, on the other hand, exhibited high activity under all conditions with TMPRSS2 present, whether ACE2 was recombinantly expressed or not. The activity of the SARS2-S2'-AA mutant was low under all conditions but was highest under the condition with maximal ACE2 expression and not responsive to changes in TMPRSS2 levels. SARS2-S1/S2-mut exhibited an interesting behavior in that it exhibited reduced fusion activity when either ACE2 or TMPRSS2 was absent but was fully fusion competent under all conditions in between, with probably a slight trend toward highest activity with comparatively low TMPRSS2 levels, and so it was similar in that respect to SARS1-S. The respective protein levels present at the end of the coculture are shown in Fig. 2B. We labeled the fully processed S2 fragment with an asterisk, as the exact nature of this fragment cannot be deduced with full confidence from its apparent molecular size, even if it may be the so-called S2' fragment after cleavage at this site. Interestingly, the S0 and S2 fragments of SARS2-S are visibly processed to a large degree into smaller

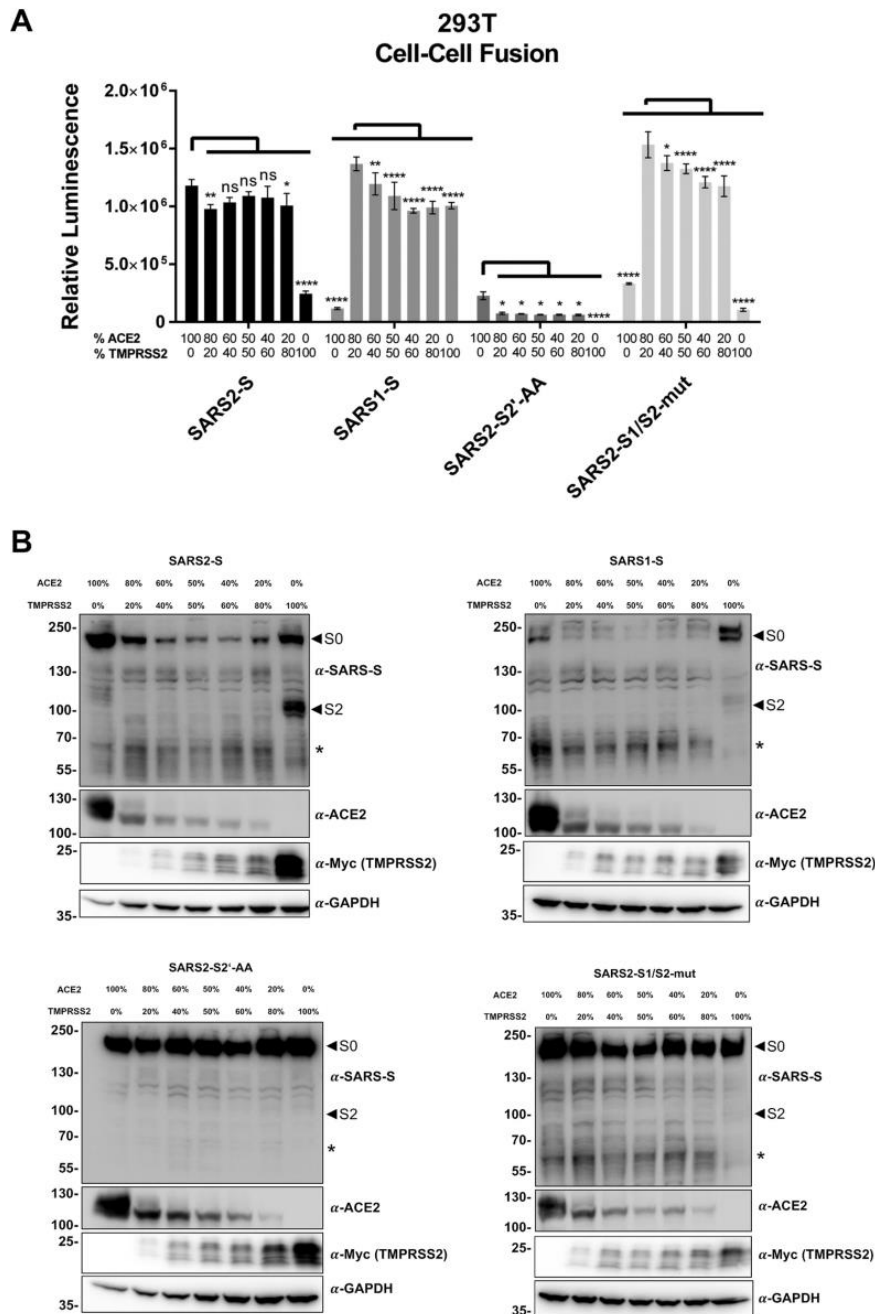


**FIG 2** SARS2-S-mediated cell-cell fusion depends on ACE2 receptor expression, whereas SARS1-S-mediated fusion depends on TMPRSS2 activity in 293T cells. (A) Cell-cell fusion assay. Effector cells (293T cells transfected with either an empty vector or (Continued on next page)



fragments under conditions that allow for high fusion activity. We decided to continue with transfecting equal amounts of ACE2 and TMPRSS2 expression plasmids.

**Differential effects of the TMPRSS2 inhibitors camostat and bromhexine and the bromhexine metabolite ambroxol on SARS1-S- and SARS2-S-mediated fusion.**

For a comprehensive analysis, we measured fusion with target cells that were cotransfected with ACE2 and TMPRSS2 expression plasmids, in addition to cells transfected with either the ACE2 or TMPRSS2 expression plasmid alone. As fusion effectors, SARS1-S and SARS2-S as well as SARS2-S1/S2-mut and SARS2-S2'-AA were included. To test the effects of TMPRSS2 inhibition by small molecules on the activation of wt SARS2-S and the two mutants as well as SARS1-S, we incubated the different target cells with bromhexine (reportedly a specific inhibitor of TMPRSS2 [15]), the chemically related compound ambroxol, or camostat (an irreversible inhibitor of TMPRSS2 and many serine proteases in general [28, 29]) at 50  $\mu$ M (Fig. 3A). We chose this high concentration, which is most likely outside any therapeutic range except for that of ambroxol, as overexpression of TMPRSS2 may shift the 50% effective concentration ( $EC_{50}$ ) considerably upwards.

As observed before (Fig. 1D), in the presence of ACE2 and TMPRSS2, both SARS1-S and SARS2-S exhibited strong fusion activity, as did SARS2-S1/S2-mut. SARS2-S2'-AA, on the other hand, was strongly impaired under these conditions.

ACE2 expression alone was sufficient for inducing the high fusion activity of SARS2-S but induced only moderate activity of SARS1-S. Levels of ACE2 expression were higher in single-transfected cells (Fig. 3B). This observation is compatible with data from the literature stating that ACE2 is cleaved by TMPRSS2 (10), which conceivably reduces detection by Western blotting, in addition to potential competition effects between expression plasmids.

Nevertheless, SARS2-S-driven fusion was clearly not limited by TMPRSS2 expression and reached its highest activity when only ACE2 was expressed. The S1/S2 cleavage site mutant of SARS2-S, on the other hand, exhibited reduced activation in the presence of ACE2 without additional TMPRSS2 activity, whereas the SARS2-S2'-AA mutant again exhibited low but detectable fusion activity when ACE2 was overexpressed. Overexpression of TMPRSS2 did not increase the fusion activity of SARS2-S2'-AA. Conversely, SARS1-S-driven fusion was clearly more enhanced by the overexpression of TMPRSS2 than by the overexpression of ACE2, reaching high activity under conditions where only TMPRSS2 was recombinantly expressed, and was only weakly activated by ACE2 expression in the absence of recombinant TMPRSS2 expression (Fig. 2A and 3A).

We observed that cell-cell fusion by SARS1-S and SARS2-S was not inhibited by bromhexine and that only SARS1-S activity was slightly inhibited by ambroxol in the presence of TMPRSS2. Surprisingly, we observed an induction of SARS2-S fusion activity in the presence of bromhexine, significantly so when ACE2 and TMPRSS2 were coexpressed. Camostat did not reduce SARS2-S-mediated fusion in this setting unless TMPRSS2 was overexpressed without ACE2. However, both SARS2-S1/S2-mut and even more pronouncedly SARS1-S exhibited a significantly reduced fusion activity in the presence of camostat. The strong induction of SARS1-S-mediated fusion by TMPRSS2 was clearly reversed by camostat but not by bromhexine. Notably, camostat did not exert any inhibitory effect on the remaining fusion activity of the SARS2-S2'-AA mu-

**FIG 2** Legend (Continued)

expression plasmids for the indicated spike variants and Vp16-Gal4 transactivator) were cultured together with target cells (293T cells transfected with ACE2 or TMPRSS2 expression plasmids at the indicated ratios and the Gal4-TurboGFP-Luc reporter plasmid). After 24 h, luciferase activity was measured. The data show averaged relative luminescence units, and error bars represent the standard deviations from one representative experiment performed in triplicate. Comparisons were made against the condition with maximum activation using two-way ANOVA, and *P* values were corrected for multiple comparisons by Sidak's method (*P* > 0.05, ns; *P*  $\leq$  0.05, \*; *P*  $\leq$  0.01, \*\*; *P*  $\leq$  0.001, \*\*\*; *P*  $\leq$  0.0001, \*\*\*\*). (B) The expression of proteins in target cells and effector cells after cocultivation was analyzed by Western blotting from lysates harvested for determination of the luciferase activity in panel A. The unprocessed spike (S0) and the S1/S2-site processed spike (S2) are indicated by arrows. An additional cleavage product marked with an asterisk was observed. The predominant, processed, low-molecular-weight TMPRSS2 fragment is shown. The expression of GAPDH served as a loading control. One representative Western blot is shown.

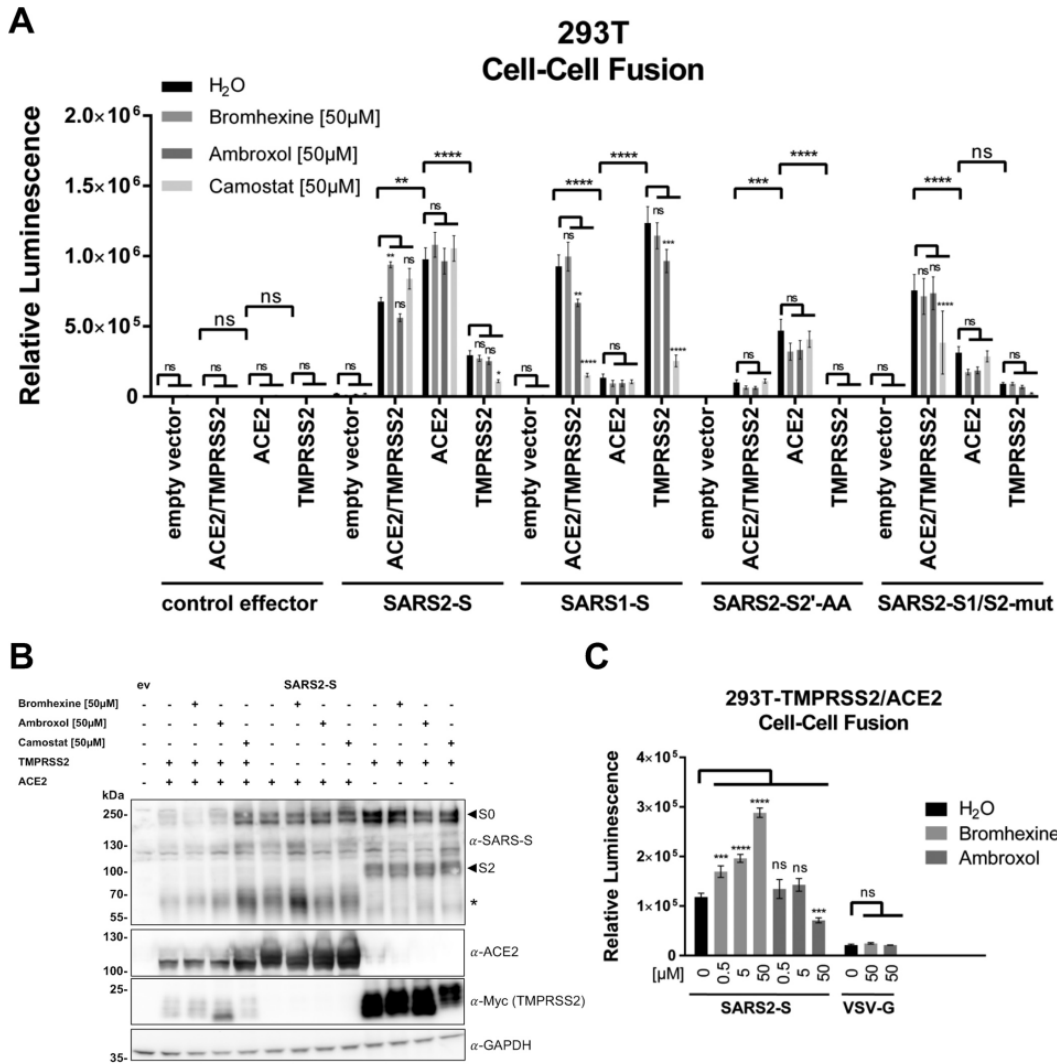


**FIG 3** SARS2-S-mediated cell-cell fusion of 293T cells is enhanced by bromhexine in the presence of TMPRSS2. (A) Cell-cell fusion assay. Effector cells (293T cells transfected with either empty vector or expression plasmids for the indicated spike variants together with the Vp16-Gal4 expression plasmid) were added to target cells (293T cells transfected with empty vector, expression plasmids for ACE2 and TMPRSS2, alone or in combination, and the Gal4-TurboGFP-Luc reporter plasmid) that had been preincubated for 30 min with bromhexine, ambroxol, or camostat. After addition of effector cells, effector and target cells were cocultured in the presence of the respective inhibitors at 50  $\mu$ M. After 24 h, luciferase activity was measured. The data show averaged relative luminescence units, and the error bars represent the standard errors of the means from four independent experiments, each performed in triplicate. Statistical significance was determined by two-way ANOVA, and *P* values were corrected for multiple comparisons by Sidak's method ( $P > 0.05$ , ns;  $P \leq 0.05$ , \*;  $P \leq 0.01$ , \*\*;  $P \leq 0.001$ , \*\*\*;  $P \leq 0.0001$ , \*\*\*\*). For the comparison between inhibitor treatments, the three comparisons within each family were corrected for. The *P* values for comparisons between different H<sub>2</sub>O (control)-treated target cell populations were corrected for multiple comparisons of each target cell and effector cell combination in the inhibitor group (in total, 190 possible comparisons). (B) The expression of proteins in treated target cells and effector cells after cocultivation was analyzed by Western blotting from lysates harvested for determination of the luciferase activity shown in panel A. The unprocessed spike (S0) and the S1/S2 site-processed spike (S2) are indicated by arrows. An additional cleavage product marked with an asterisk was observed. The predominant, processed, low-molecular-weight TMPRSS2 fragment is shown. The expression of GAPDH served as a loading control. One representative Western blot is shown. ev, empty vector. (C) Cell-cell fusion assay. Effector cells (293T cells transfected with the indicated glycoprotein expression plasmids and the Gal4-Luc reporter plasmid) were cocultured with target cells (293T cells transfected with ACE2 and TMPRSS2 (Continued on next page)

tant, nor did TMPRSS2 expression induce the activity of this mutant, compatible with the S2' site being the primary target of TMPRSS2-mediated activation in *trans*.

The results were also mirrored by Western blotting (Fig. 3B) of SARS2-S under the same conditions, if generation of the fully processed S2 fragment, which we labeled with an asterisk, is analyzed. Generation of this fragment was clearly visible under all conditions that allowed for high fusion activity, e.g., when ACE2 was present but less so with TMPRSS2 alone. Interestingly, the addition of camostat increased the detectable amount of ACE2, probably explaining the slight trend toward higher activity in its presence. Further, ambroxol reproducibly induced the generation of an atypical TMPRSS2 autoproteolytic fragment, which may hint at some sort of modulating activity of ambroxol toward TMPRSS2 (Fig. 3B, fourth lane).

Taken together, we observed robust SARS2-S-mediated cell-cell fusion with ACE2-overexpressing cells that was not dependent on exogenous TMPRSS2 expression and that was not inhibited by bromhexine. Instead, fusion was enhanced by bromhexine. Cell-cell fusion mediated by SARS2-S was clearly not at all or to a much lesser degree restricted by serine protease activity on target cells than fusion by SARS1-S. Interestingly, ambroxol exhibited some activity against TMPRSS2-mediated activation of SARS1-S.

#### **Bromhexine enhances SARS2-S-mediated fusion in the presence of TMPRSS2.**

To further explore the paradoxical effect of the putative TMPRSS2 inhibitor bromhexine on fusion activity, we performed fusion reactions in the presence of bromhexine and ambroxol at different concentrations (Fig. 3C). In order to eliminate potential systematic errors, we deviated from our previous protocol in that we cocultured for 48 h instead of 24 h and cotransfected the reporter plasmid into the effector instead of the target cells, this time using a different luciferase reporter without TurboGFP. We again did not observe inhibition by bromhexine but a dose-dependent enhancement. Ambroxol treatment, on the other hand, did not lead to a similar enhancement but to a slight decrease in activity at 50  $\mu$ M. As a control fusion protein that works with practically any cell type, we included vesicular stomatitis virus glycoprotein (VSV-G). While VSV-G is physiologically pH activated for full fusion activity (30), it reportedly exhibits considerable activity without pH priming (31, 32). VSV-G-mediated fusion activity was not increased by bromhexine.

**SARS2-S-mediated cell-cell fusion is sensitive to the inhibition of matrix metalloproteases.** The robust cell-cell fusion that we observed with SARS2-S in the absence of TMPRSS2 activity should most likely be triggered by proteolytic processing, if the mechanism is analogous to what was observed for SARS-CoV (8, 33). Therefore, we tested the effects of different protease inhibitors on SARS2-S-mediated fusion of ACE2-expressing 293T cells without exogenous TMPRSS2 activity. As we wanted to exclude the possibility that preactivation on the producer cells plays a role, we tested the inhibitors both in the coculture (Fig. 4A) and with preincubation of both effector and target cells (Fig. 4B). Values were normalized to those for the respective solvent control for better comparison. We observed some inhibitory effect on SARS2-S and SARS1-S fusion activity by the broadband serine protease inhibitor 4-(2-aminoethyl) benzenesulfonyl fluoride hydrochloride (AEBSF) and by a protease inhibitor cocktail whose main ingredients are the serine protease inhibitors AEBSF and aprotinin and the cysteine protease inhibitors E64 and leupeptin. The S1/S2 cleavage site mutant was not sensitive to this inhibitor cocktail, suggestive of action at this site in the wild-type SARS-CoV-2 spike. These effects were more pronounced and significant with preincubation of the effector cells (Fig. 4B), in particular for the SARS2-S2'-AA mutant. Interestingly, the inhibitor cocktail almost completely abrogated the remaining fusion activity of SARS1-S. The furin inhibitor decanoyl-RVKR-chloromethylketone (CMK) did

#### **FIG 3 Legend (Continued)**

expression plasmids and the Vp16-Gal4 expression plasmid) that had been preincubated for 30 min with bromhexine or ambroxol. After addition of effector cells, effector and target cells were cocultured with inhibitors at the indicated concentrations, and the luciferase activity of cell lysates was measured after 48 h. Data show averaged relative luminescence units of one experiment performed in triplicate, and error bars represent standard deviations.



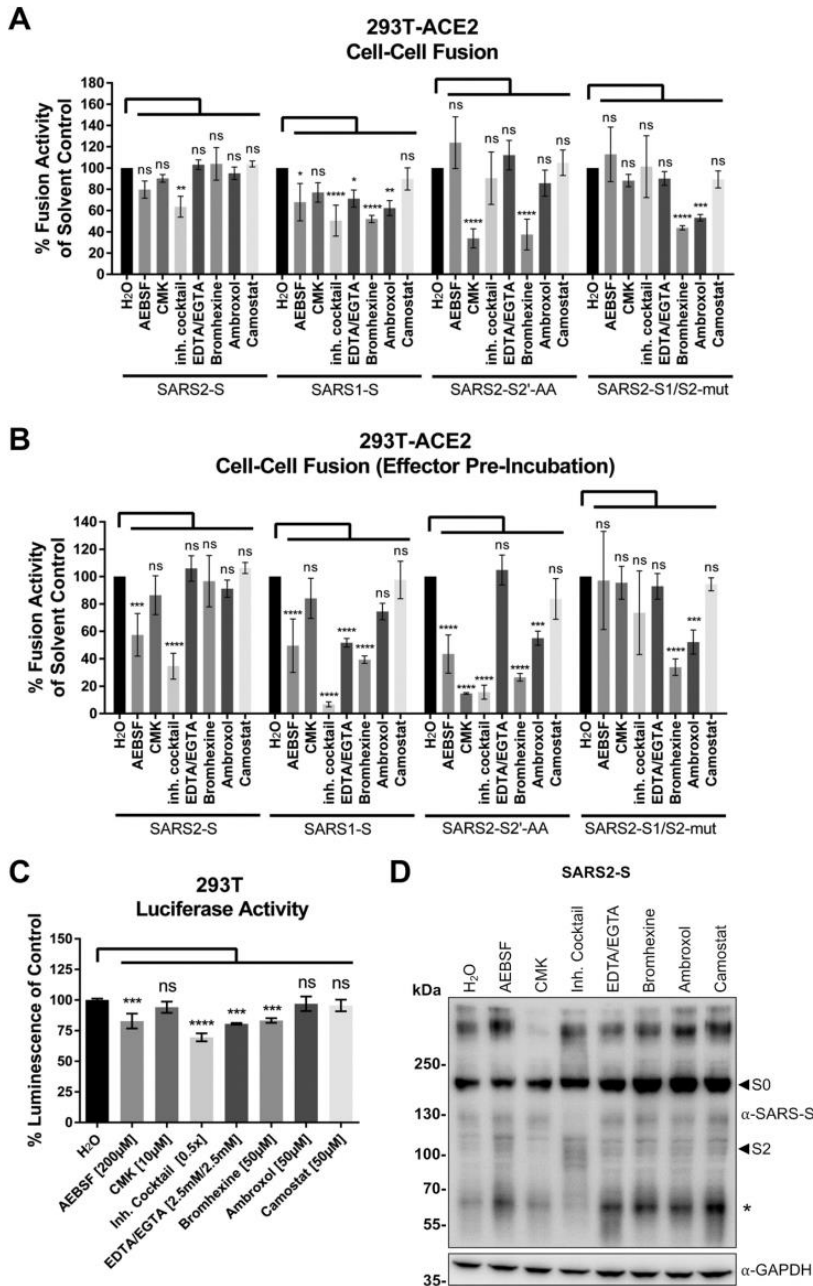


**FIG 4** Sensitivity of SARS2-S-mediated 293T cell-cell fusion to different inhibitors. (A) Cell-cell fusion assay. Effector cells (293T cells transfected with expression plasmids for the indicated spike variants together with the Vp16-Gal4 expression plasmid) were added to target cells (293T cells transfected with expression plasmids for ACE2 and the Gal4-TurboGFP-Luc (Continued on next page)



not significantly inhibit any of the spikes except for the S2' mutant (Fig. 4A and B). This was somewhat surprising for us, but it may reflect the fact that proteases other than furin can cleave at the S1/S2 site (34), which may in turn partially obviate furin cleavage in our system. We also tested EDTA/EGTA, bromhexine, ambroxol, and camostat, which as expected had no effect in this TMPRSS2-free system. EDTA/EGTA had a mild impact on SARS1-S fusion activity with and without preincubation (Fig. 4A and B). Bromhexine and ambroxol exhibited an interesting behavior in this assay. We observed inhibitory activity of bromhexine and ambroxol toward SARS1-S and the SARS2-S1/S2-mut and SARS2-S2'-AA mutants in this TMPRSS2-free cell system, suggesting that these substances somehow interact with the spike proteins or ACE2. The luciferase activity of control cells, which were transfected with both the Gal4 response element-driven reporter and the Gal4 transactivator constructs, was only mildly affected by AEBSF, the inhibitor cocktail, EDTA/EGTA, and bromhexine, not by the other substances (Fig. 4C). In particular, any reductions observed with ambroxol cannot be explained by nonspecific effects on the luciferase reporter system and most likely represent real inhibitory activity against SARS1-S-mediated fusion activity and fusion mediated by the two SARS2-S cleavage site mutants.

Western blot analysis suggested that the protease inhibitor cocktail may have had a somewhat stabilizing effect on the S2 intermediate form of SARS2-S (Fig. 4D), which resulted in less processing into the putative S2' form (marked by an asterisk). CMK both reduced "smear" at higher molecular weight, which likely represents glycosylation variants, and reduced the abundance of the S2 proteolytic product, which should be generated through cleavage at the polybasic cleavage site, compatible with furin inhibition. As none of the tested inhibitors resulted in a meaningful reduction of the fusion activity of wt SARS2-S that could not also be explained by toxicity, we decided to test a more potent inhibitor of metalloproteases than EDTA/EGTA, whose maximum concentration is limited by its effects on cell adhesion and viability. The EDTA/EGTA concentration that was used by us was most likely too low to meaningfully impact protease activity, in particular as the cell culture medium contains calcium and magnesium. We therefore tested batimastat, which inhibits matrix metalloproteases (35, 36).

Batimastat indeed inhibited SARS2-S-dependent fusion in the absence of TMPRSS2 in a dose-dependent manner (Fig. 5A). Interestingly, no inhibition was observed in the presence of both ACE2 and TMPRSS2 or in the presence of TMPRSS2 alone unless TMPRSS2 was inhibited by camostat (Fig. 5A). Therefore, batimastat-sensitive metalloproteases cleave SARS2-S to activate cell-cell fusion. This notion is supported by the finding that TMPRSS2 expression can overcome the batimastat-induced block. Western blot analysis of the fusion reactions indicated that batimastat probably induced a subtle change in the migration pattern of the SARS2-S S2 fragment in the presence of ACE2 but without TMPRSS2 (Fig. 5B). We next decided to test the effect of batimastat

#### FIG 4 Legend (Continued)

reporter plasmid) that had been preincubated for 30 min with twice the final concentration of AEBSF (200  $\mu$ M), the furin inhibitor CMK (10  $\mu$ M), proteinase inhibitor cocktail, EDTA/EGTA (2.5 mM each), bromhexine (50  $\mu$ M), ambroxol (50  $\mu$ M), and camostat (50  $\mu$ M). After addition of effector cells, effector and target cells were cocultured in the presence of the respective inhibitors. After 24 h, luciferase activity was measured. The data show values normalized to those after solvent treatment, which was set to 100%, and the error bars represent the standard deviations from three independent experiments, each performed in triplicate. (B) Cell-cell fusion assay as shown in panel A, except that effector cells were preincubated with the indicated inhibitors for 18 h before being cocultured with target cells. The target cells were preincubated with the indicated inhibitors for 30 min before the addition of effector cells. After 24 h, luciferase activity was measured. The data show values normalized to those after solvent treatment, which were set to 100%, and the error bars represent the standard deviations from three independent experiments, each performed in triplicate. (C) 293T cells were transfected with Vp16-Gal4 and Gal4-TurboGFP-Luc reporter expression plasmids and were incubated with inhibitors as described for panel A. After 24 h, luciferase activity was measured. The data show values normalized to those after solvent treatment, which were set to 100%, and error bars represent the standard deviations from one representative experiment performed in triplicate. (D) The expression of proteins in treated target cells and effector cells after cocultivation was analyzed by Western blotting from lysates harvested for determination of the luciferase activity shown in panel A. The unprocessed spike (S0) and the S1/S2 site-processed spike (S2) are indicated by arrows. An additional cleavage product marked with an asterisk was observed. The predominant, processed, low-molecular-weight TMPRSS2 fragment is shown. The expression of GAPDH served as a loading control. One representative Western blot is shown.

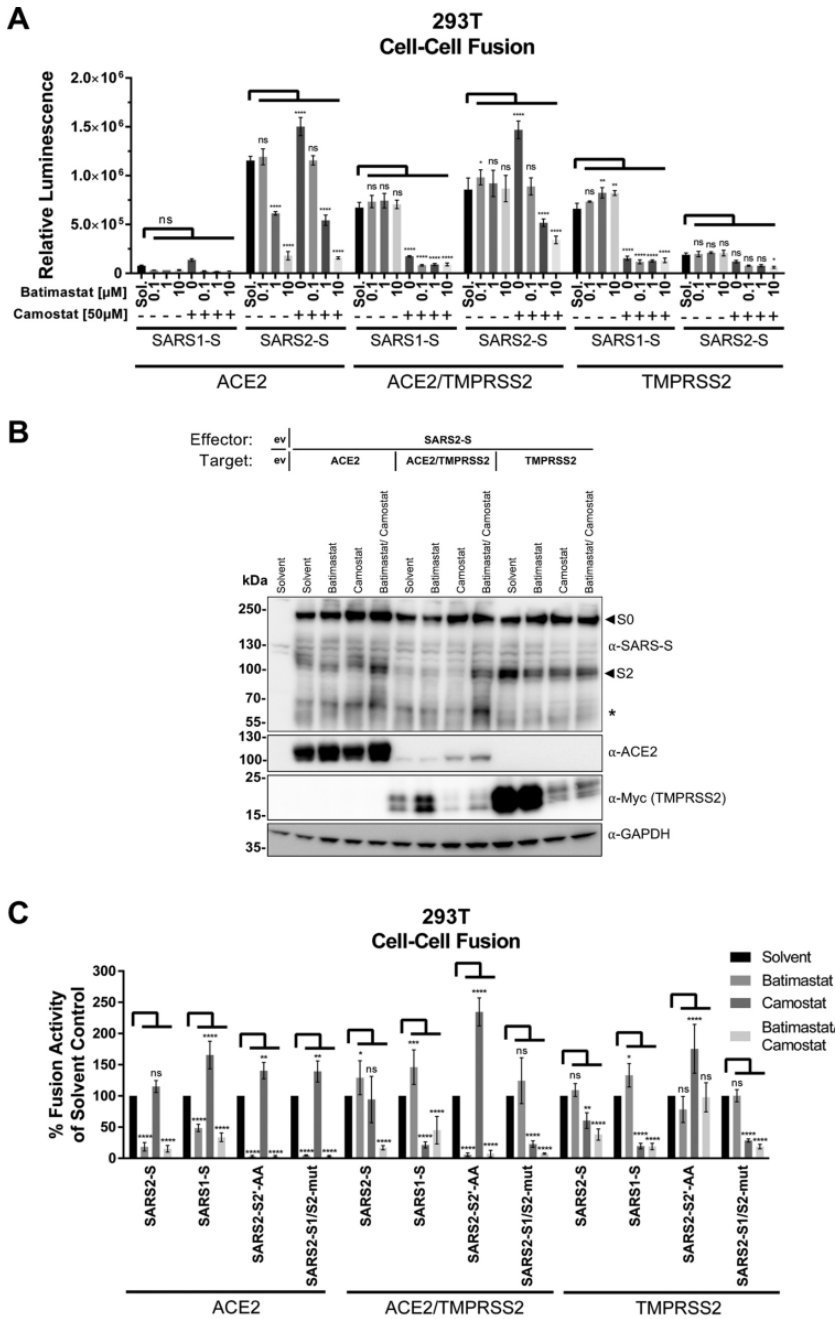


**FIG 5** The matrix metalloproteinase inhibitor batimastat inhibits SARS2-S-mediated cell-cell fusion. (A) Cell-cell fusion assay. Effector cells (293T cells transfected with expression plasmids for the indicated spike variants together with the (Continued on next page)

on the fusion activity of the S1/S2 mutant and the S2'-AA mutant under conditions of ACE2 overexpression without TMPRSS2 (Fig. 5C, left). Both mutants were inhibited by batimastat, indicating that matrix metalloproteases can cleave irrespective of an intact S1/S2 or S2' cleavage site, although this does not necessarily rule out a modulating effect in particular by S1/S2 cleavage, as mutation of S1/S2 leads to impaired activity without TMPRSS2. SARS1-S was also slightly affected by batimastat under these conditions but at an overall very low activity level (compare Fig. 5A). Under conditions of ACE2 and TMPRSS2 coexpression, which leads to lower ACE2 levels (compare Fig. 2B, 3B, and 5B), SARS2-S1/S2-mut was not impacted by batimastat unless TMPRSS2 was again inhibited by the addition of camostat (Fig. 5C, middle), whereas the activity of the S2' mutant was inhibited in the presence of batimastat alone, strongly suggesting that TMPRSS2 activates via the S2' site. Under conditions of TMPRSS2 overexpression without ACE2 overexpression (Fig. 5C, right), batimastat was again without effect. Results with the SARS2-S2'-AA mutant come with the caveat that this mutant was barely active at all under these conditions (Fig. 2A and 3A). In summary, these experiments demonstrate that in the presence of the ACE2 receptor, matrix metalloproteases can efficiently activate SARS2-S for cell-cell fusion.

**The SARS2-S S2' site is the target site for TMPRSS2-mediated proteolytic activation.** While our results with the SARS2-S2'-AA mutant were already strongly suggestive of S2' being the target site for TMPRSS2, this conclusion remained slightly ambiguous in light of the relatively low surface expression and inefficient proteolytic processing of this mutant (Fig. 1B and C). We therefore set out to generate an S2' mutant that is still efficiently processed and expressed at the cell surface. We permuted several amino acids to replace the original KR (Fig. 1A) sequence motif and tested fusion activity in the presence of ACE2, TMPRSS2, and ACE2/TMPRSS2. We found that SARS2-S2'-GH and -HH mutants were active in our fusion assay, whereas EE and ES resulted in abrogation of fusion activity to below the levels achieved with the AA mutant (Fig. 6A). The GH mutant was also processed (Fig. 6B) and efficiently expressed at the cell surface and exhibited high ACE2 binding capacity (Fig. 6C). For further experiments, we continued with the SARS2-S2'-GH mutant. Interestingly, when we tested the furin inhibitor CMK for its effects in the absence of TMPRSS2, all spike variants were slightly less active, but only the S2'-GH variant was significantly inhibited, suggesting increased dependence on prepriming by furin in the absence of the S2' site (Fig. 6D).

Confirming the results of our prior fusion assays with the AA mutant, SARS2-S2'-GH and SARS2-S2'-HH fusion activities on 293T cells in the presence of only ACE2 were sensitive to batimastat (Fig. 6E, left), and on 293T cells expressing ACE2/TMPRSS2, both SARS2-S2'-GH and SARS2-S2'-HH were insensitive to camostat but again highly sensitive to batimastat (Fig. 6E, right). The fusion activities of the S2 mutants were even increased in the presence of camostat, likely because inhibition of TMPRSS2 increases ACE2 levels, as demonstrated in Fig. 3B. This unequivocally identifies the S2' site as the

#### FIG 5 Legend (Continued)

Vp16-Gal4 expression plasmid) were added to target cells (293T cells transfected with expression plasmids for ACE2, ACE2/TMPRSS2, or TMPRSS2 and the Gal4-TurboGFP-Luc reporter plasmid) that had been preincubated with batimastat or camostat for 30 min at twice the indicated final concentration. After 24 h, luciferase activity was measured. The data show averaged relative luminescence units, and error bars represent the standard deviations from one representative experiment performed in triplicate. (B) The expression of proteins in treated target cells and effector cells after cocultivation was analyzed by Western blotting from lysates harvested for determination of luciferase activity shown in panel A. The unprocessed spike (S0) and the S1/S2 site-processed spike (S2) are indicated by arrows. An additional cleavage product marked with an asterisk was observed. The predominant, processed, low-molecular-weight TMPRSS2 fragment is shown. The expression of GAPDH served as a loading control. One representative Western blot is shown. ev, empty vector. (C) Cell-cell fusion assay. Effector cells (293T cells transfected with expression plasmids for the indicated spike variants together with the Vp16-Gal4 expression plasmid) were added to target cells (293T cells transfected with expression plasmids for ACE2, ACE2/TMPRSS2, or TMPRSS2 and the Gal4-TurboGFP-Luc reporter plasmid) that had been preincubated for 30 min with batimastat (10  $\mu$ M) and/or camostat (50  $\mu$ M) at twice the final concentration. After 24 h, luciferase activity was measured. The data show values normalized to those after solvent treatment, which were set to 100%, and the error bars represent the standard deviations from three independent experiments, each performed in triplicate. Statistical significance in panels A and C was determined by two-way ANOVA, and *P* values were corrected for multiple comparisons by Sidak's method (*P* > 0.05, ns; *P*  $\leq$  0.05, \*; *P*  $\leq$  0.01, \*\*; *P*  $\leq$  0.001, \*\*\*; *P*  $\leq$  0.0001, \*\*\*\*).



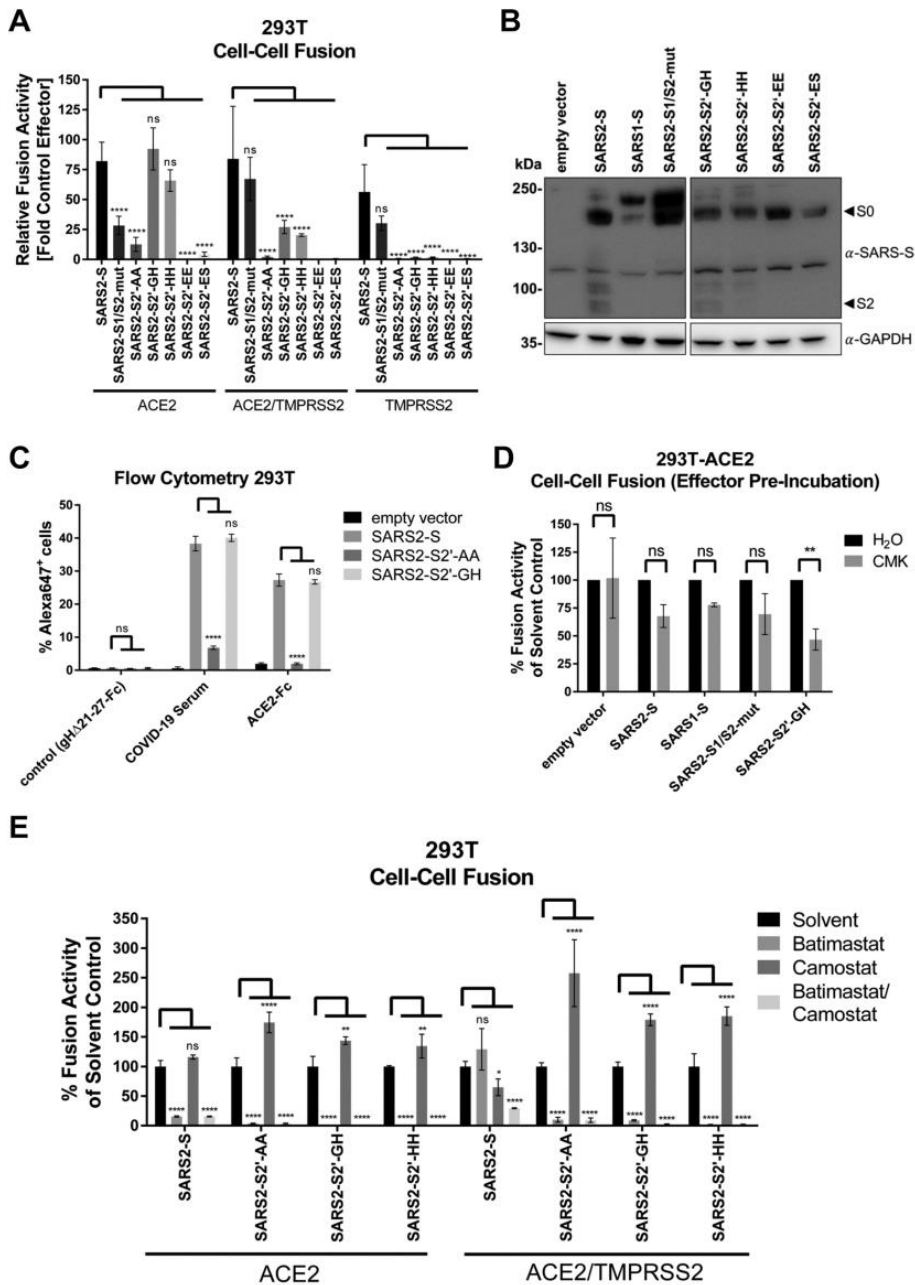


**FIG 6** The conserved S2' site is the site of TMPRSS2-mediated activation of SARS2-S for cell-cell fusion. (A) Cell-cell fusion assay. Effector cells (293T cells transfected with expression plasmids for the indicated spike variants together with the Vp16-Gal4 expression plasmid) were added to target cells (293T cells transfected with expression plasmids for ACE2, ACE2/TMPRSS2, or TMPRSS2 and the

(Continued on next page)

TMPRSS2 target site and, interestingly, as the only TMPRSS2 target site, at least for the activation of fusion.

**The entry of SARS2-S-pseudotyped lentiviruses is enhanced by TMPRSS2 and is not inhibited by bromhexine.** To compare our findings on cell-cell fusion to spike protein-driven entry, we used lentiviral particles expressing green fluorescent protein (GFP) as a reporter gene, pseudotyped with SARS2-S. We found that TMPRSS2 expression was clearly required for efficient infection of 293T cells by SARS2-S-pseudotyped particles (Fig. 7A). ACE2 overexpression alone also enhanced infection but considerably less efficiently and barely above the detection limit, which may be owing to our lentiviral GFP system. TMPRSS2-mediated enhancement was reduced by the addition of camostat but not by the addition of bromhexine or ambroxol, both of which may even slightly enhance infection in this setting. These observations were corroborated by fluorescence microscopy (Fig. 7B). As luciferase is more sensitive than GFP as a reporter gene, we switched to luciferase detection (Fig. 7C). We also included the SARS2-S D614G variant. As previously reported, D614G-driven infection was more efficient (37). It was also strongly enhanced by TMPRSS2, as evidenced by potent camostat-mediated inhibition. Ambroxol and bromhexine had no activity in this system, as opposed to camostat. Batimastat did not alter SARS2-S-driven entry. A VSV-G-pseudotyped lentivirus was not significantly affected by either substance.

**Mutation of the S2' site uncouples infection from TMPRSS2.** Next, we aimed to corroborate our findings regarding the S2' site as TMPRSS2's target site for cell-cell fusion in pseudoparticle infection. Our SARS2-S2'-GH mutant was efficiently incorporated into lentiviral particles, as was SARS2-S1/S2-mut (Fig. 7D). Both spike mutants could drive entry into 293T cells expressing ACE2/TMPRSS2, but SARS2-S2'-GH did so with reduced efficiency and SARS2-S1/S2-mut probably with increased efficiency, although we did not test for the latter (Fig. 7E). None of the spike variants was inhibited by batimastat. SARS2-S wt and SARS2-S1/S2-mut were inhibited by camostat, but not by batimastat or E64-d, indicating proteolytic activation by TMPRSS2. The S2' mutant, on the other hand, was exclusively inhibited by E64-d, indicating that it was refractory to activation by TMPRSS2 and dependent on activation by cathepsins.

**SARS-CoV-2 is weakly inhibited by ambroxol on Calu-3 lung cells.** As transfected 293T cells express TMPRSS2 at high and possibly variable levels between cells and allow for at least some entry via endocytosis, weak modulatory effects on ACE2 or TMPRSS2 might be missed in that system. Calu-3 cells express TMPRSS2 to much higher levels than 293T cells (Fig. 8A), which are practically negative, but still at endogenous levels. We therefore infected the Calu-3 lung cell line with our lentiviral pseudoparticles (Fig. 8B). These cells allow for infection by our lentiviral pseudoparticles only at very low levels (not shown). In order to achieve infection at faithfully detectable levels, we used the D614G variant, which exhibited the same sensitivity profile to

#### FIG 6 Legend (Continued)

Gal4-TurboGFP-Luc reporter plasmid). After 24 h, luciferase activity was measured. The data show fold values for the empty vector control, and the error bars represent the standard deviations of results from three independent experiments, each performed in triplicate. (B) Expression of analyzed spike variants in 293T cells. The unprocessed spike (S0) and the S1/S2 site-processed spike (S2) are indicated by arrows. The expression of GAPDH served as a loading control. (C) Cell surface expression and ACE2 binding. Cell surface expression and binding of soluble ACE2-Fc by the indicated spike variants was determined by flow cytometry. Analysis was performed as in Fig. 1C. (D) Cell-cell fusion assay. Effector cells (293T cells transfected with expression plasmids for the indicated spike variants together with the Vp16-Gal4 expression plasmid) were preincubated with the furin inhibitor CMK (10  $\mu$ M) and after 16 h were added to target cells (293T cells transfected with expression plasmids for ACE2 and the Gal4-TurboGFP-Luc reporter plasmid) that had been preincubated for 30 min with the same inhibitor concentration. After the addition of effector cells, effector and target cells were cocultured in the presence of CMK. After 24 h, luciferase activity was measured. The data show values normalized to those for solvent treatment, which were set to 100%, and the error bars represent the standard deviations from two independent experiments, each performed in triplicate. (E) Cell-cell fusion assay. Effector cells (293T cells transfected with expression plasmids for the indicated spike variants together with the Vp16-Gal4 expression plasmid) were added to target cells (293T cells transfected with expression plasmids for ACE2, ACE2/TMPRSS2, or TMPRSS2 and the Gal4-TurboGFP-Luc reporter plasmid) that had been preincubated with batimastat and/or camostat for 30 min at twice the final concentration; final concentrations were 10  $\mu$ M batimastat and/or 50  $\mu$ M camostat. After 24 h, luciferase activity was measured. The data show values normalized to those for solvent treatment, which were set to 100%, and the error bars represent the standard deviations from two independent experiments, each performed in triplicate. Statistical significance in panels A, C, D, and E was determined by two-way ANOVA, and *P* values were corrected for multiple comparisons by Sidak's method (*P* > 0.05, ns; *P*  $\leq$  0.05, \*; *P*  $\leq$  0.01, \*\*; *P*  $\leq$  0.001, \*\*\*; *P*  $\leq$  0.0001, \*\*\*\*).

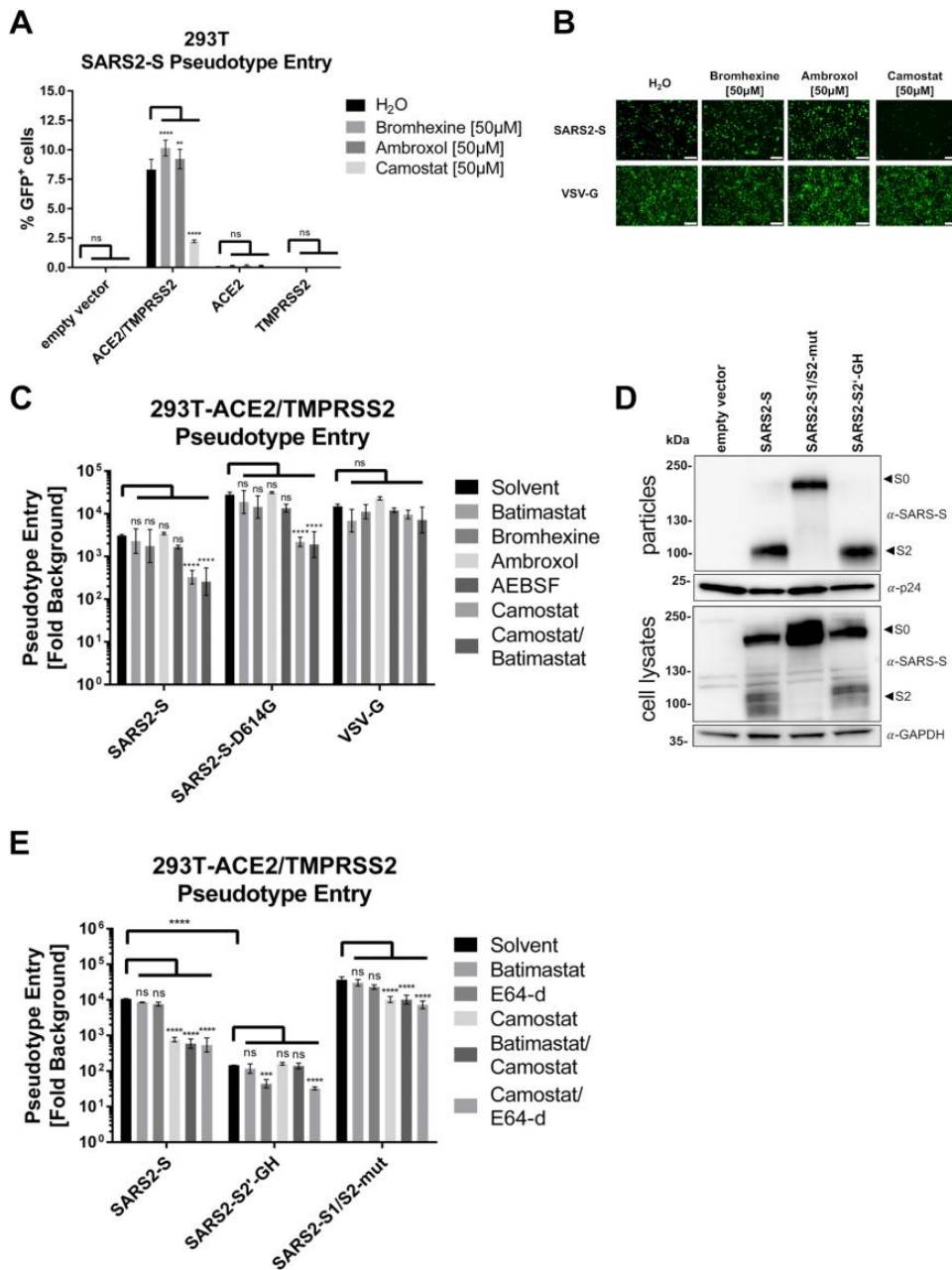


**FIG 7** Requirements for the entry of SARS2-S-pseudotyped lentiviral particles differ from requirements for SARS2-S-mediated cell-cell fusion. (A) 293T cells transfected with an empty vector or ACE2/TMPRSS2, ACE2, or TMPRSS2 plasmid were preincubated with bromhexine, ambroxol, or camostat at the indicated concentration before the addition of lentiviral particles pseudotyped with SARS2-S. Forty-eight hours after transduction, the cells were analyzed via flow cytometry. Data show averaged percentages of GFP-positive cells, and error bars (Continued on next page)



inhibitors but was about 1 log more efficient at driving entry (Fig. 7C). By now, D614G has become the dominant variant globally and is therefore probably also more relevant. As expected, SARS2-S-driven entry was practically abrogated by 50  $\mu$ M camostat. Bromhexine again had no detectable impact on SARS2-S-driven entry. Ambroxol, on the other hand, exhibited a weakly inhibitory effect on SARS2-S-driven infection in this system, even if that needs a linear scale for proper visualization. Interestingly, both substances, but bromhexine more so, affected entry of VSV-G-pseudotyped particles negatively. This is likely owing to the targeting of lysosomal processes by these two substances (38, 39). Finally, we wanted to test whether this small but detectable effect would translate into inhibition of authentic virus. We therefore infected Calu-3 cells with a clinical isolate of SARS-CoV-2 at a low multiplicity of infection (MOI) and quantified the viral RNA after 20 to 24 h by reverse transcription-quantitative PCR (RT-qPCR) (Fig. 8C). We chose 5  $\mu$ M and 50  $\mu$ M as concentrations for ambroxol and bromhexine and 10  $\mu$ M for batimastat. For ambroxol, which is heavily enriched in lung tissue, 50  $\mu$ M might be a clinically attainable concentration. Interestingly, for ambroxol and bromhexine, viral RNA copy number trended lower upon treatment and in a dose-dependent manner, as can be observed in the raw cycle threshold ( $C_T$ ) values (Fig. 8C) and after relative quantification (Fig. 8D). Reduction by both ambroxol and bromhexine at 50  $\mu$ M was significant, even if inhibition by ambroxol remained significant only without correction for multiple comparisons, which is appropriate in light of a dose response (analysis of variance [ANOVA] with a posttest for the linear trend in  $C_T$  values at 0  $\mu$ M, 5  $\mu$ M, and 50  $\mu$ M; results were significant for ambroxol and bromhexine). Ten micromolar batimastat (compared to the dimethyl sulfoxide [DMSO] solvent) had no significant effect on SARS-CoV-2 mRNA level, even if DMSO alone had quite some impact compared to water, most likely due to the high concentration needed, which was 1%. In a cell viability assay with Calu-3 cells using dilutions of commercial over-the-counter cough thinners, neither bromhexine nor ambroxol exhibited significant effects up to 10  $\mu$ M (Fig. 8E). We used the cough thinners as an alternative source of ambroxol and bromhexine for some control experiments, which were not included in this paper, to control for the specificity of the observed effects and their independence from the source of the two substances. Bromhexine but not ambroxol clearly impacted cell viability at 100  $\mu$ M, which is compatible with our observations of 293T cells (Fig. 4C), although it should be noted that the toxicity of bromhexine may have been overestimated in Fig. 8E due to nonactive ingredients of the cough thinner.

## DISCUSSION

We have established a two-hybrid-based protocol for measuring spike-mediated cell-cell fusion that allows for the quantitation of cell-cell fusion by luciferase activity and visualization of syncytia by GFP fluorescence. Our finding that SARS1-S-mediated and SARS2-S-mediated fusion activity is activated by the ACE2 receptor is in accord-

### FIG 7 Legend (Continued)

represent the standard deviations from one representative experiment performed in triplicate. (B) Micrographs of ACE2- and TMPRSS2-transfected cells that were infected with the respective lentiviral GFP-encoding pseudotype particles. (C) 293T cells transfected with ACE2/TMPRSS2 were preincubated with batimastat (10  $\mu$ M), bromhexine (50  $\mu$ M), ambroxol (50  $\mu$ M), AEBSF (200  $\mu$ M), camostat (50  $\mu$ M), or batimastat (10  $\mu$ M) in combination with camostat (50  $\mu$ M) before the addition of lentiviral particles pseudotyped with the respective glycoprotein. Forty-eight hours after transduction, the cells were lysed and luciferase activity was determined. Data show fold changes over background (bald particles with solvent control), and error bars represent the standard deviations from three independent experiments, each performed in triplicate; raw values were  $\log_{10}$  transformed before analysis. (D) Western blot analysis of incorporation of the respective spike variants into lentiviral particles used in panel E and lysate control of transfected 293T cells used for the production of lentiviral particles. p24 and GAPDH served as loading controls. (E) 293T cells transfected with ACE2/TMPRSS2 were preincubated with batimastat (10  $\mu$ M), E64-d (25  $\mu$ M), camostat (50  $\mu$ M), or batimastat (10  $\mu$ M)/E64-d (25  $\mu$ M) in combination with camostat (50  $\mu$ M) before the addition of lentiviral particles pseudotyped with the respective glycoproteins. Forty-eight hours after transduction, the cells were lysed and luciferase activity was determined. Data show fold changes over background (bald particles with the solvent control), and error bars represent the standard deviations from two independent experiments, each performed in triplicate; raw values were  $\log_{10}$  transformed before analysis. Statistical significance in panels A, C, and E was determined by two-way ANOVA, and *P* values were corrected for multiple comparisons by Sidak's method ( $P > 0.05$ , ns;  $P \leq 0.05$ , \*;  $P \leq 0.01$ , \*\*;  $P \leq 0.001$ , \*\*\*;  $P \leq 0.0001$ , \*\*\*\*).

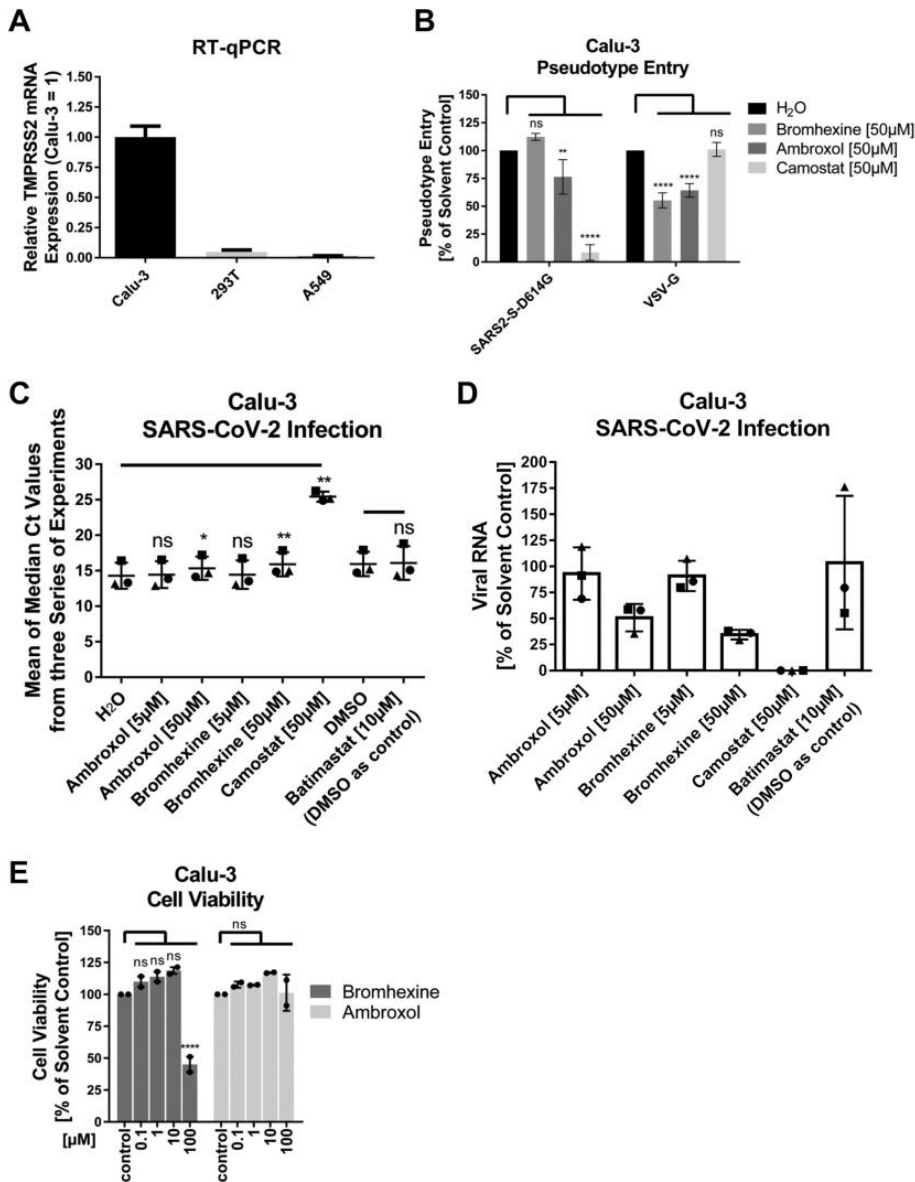


**FIG 8** SARS-CoV-2 is weakly inhibited by bromhexine and ambroxol on Calu-3 cells. (A) RT-qPCR analysis of TMPRSS2 expression. Fold TMPRSS2 mRNA expression in Calu-3 cells, 293T cells, and A549 cells was measured by RT-qPCR using the  $\Delta\Delta C_t$  method. The -RT control (without reverse transcription) for the GAPDH mRNA was not negative as expected, but the contamination was considered irrelevant as its  $C_t$  was more than 19 cycles over the value of the sample, representing a contamination of less than 0.01%. Error bars represent the upper error bounds calculated from the sum of the standard deviations (SDs) of the  $\Delta C_t$  values for each cell line. (B) Calu-3 cells were infected with lentiviral particles encoding a TurboGFP-Luciferase reporter gene pseudotyped with SARS2-S in the presence of 50  $\mu$ M bromhexine, ambroxol, or camostat. Forty-eight hours after transduction, the cells were lysed and luciferase activity was determined. The data show values normalized to those for solvent treatment, which were set to 100%, and the error bars represent the standard deviations from three independent experiments, each performed in triplicate. (C) Viral RNA load. Calu-3 cells were

(Continued on next page)



ance with published data (11), whereas our finding that SARS2-S-mediated cell-cell fusion is relatively more restricted by ACE2 expression and less by proteolytic activation than SARS1-S-mediated fusion is novel. This is because SARS-CoV-2 can efficiently utilize metalloproteases for activation of cell-cell fusion. Further, we have faithfully established the S2' site of SARS2-S as the target for TMPRSS2-mediated activation through generation of a mutant that is defective for TMPRSS2 activation but otherwise fully functional.

In our system, TMPRSS2 coexpression on ACE2-expressing target cells was not required for SARS2-S-mediated fusion of ACE2-overexpressing 293T cells, comparable with the results of Ou et al., in whose study ACE2 expression alone was also sufficient to induce cell-cell fusion without the addition of exogenous protease (11), which was corroborated by a very recent report (40). Furthermore, we did not observe any effect on SARS2-S-mediated fusion activity upon inhibition of TMPRSS2 on target cells by the serine protease inhibitor camostat when ACE2 was present. Together, these results imply that proteolytic activation by TMPRSS2 may not be a limiting factor for cell-cell fusion in 293T cells. A recent report demonstrated that upon cotransfection of spike, ACE2, and TMPRSS2, TMPRSS2 accelerates fusion. The size of the resulting syncytia showed a TMPRSS2 dependency only within the first 12 h but was independent after 24 h in that report (41), which is compatible with our observations of efficient cell-cell fusion without TMPRSS2 in 293T cells.

While SARS1-S-mediated cell-cell fusion was also weakly activated when ACE2 was expressed alone, activation was much higher in the presence of TMPRSS2, indicating stronger dependence of SARS1-S on TMPRSS2, compatible with the monobasic S1/S2 cleavage site in the SARS-CoV spike protein. Surprisingly, we even observed maximal activation with overexpression of only TMPRSS2, indicating that SARS1-S-mediated cell-cell fusion is mostly protease and not ACE2 driven. In line with this observation, SARS1-S-mediated cell-cell fusion was clearly sensitive to camostat, which reversed the TMPRSS2-mediated activation (Fig. 3A).

Interestingly, mutational ablation of the S1/S2 cleavage site of SARS2-S rendered the mutated spike protein sensitive to inhibition by camostat in the presence of ACE2 and TMPRSS2 (Fig. 3A), suggesting that TMPRSS2 or a related protease is required for processing at the S2' site to reach full activation when the S1/S2 site is not cleaved. In addition, in the absence of recombinantly expressed TMPRSS2, SARS2-S1/S2-mut was clearly impaired with regard to fusion activity (Fig. 2A). Conversely, mutation of the S2' priming site abrogated any effects of TMPRSS2 on SARS2-S-mediated fusion, e.g., when TMPRSS2 alone was provided by means of recombinant expression (Fig. 3A and 6A) or when TMPRSS2 was inhibited by camostat (Fig. 6E). It should be noted that the SARS2-S S2' mutants were still fusogenic in the presence of high levels of the ACE2 receptor (Fig. 2A, 3A, and 6A and E), in the case of the GH and HH S2' mutants even at moderate ACE2 levels, and in the absence of TMPRSS2 with activity similar to that of the wild type (Fig. 6A). The S2' GH mutant was also efficiently incorporated (Fig. 7D) and able to drive the infection of pseudotyped lentiviral particles (Fig. 7E). With wt SARS2-S or SARS2-S1/S2-mut, but not with the SARS2-S S2' mutants, recombinant expression of TMPRSS2 led to low but detectable fusion activity (Fig. 2A and 6A).

#### FIG 8 Legend (Continued)

infected with SARS-CoV-2 in the presence of bromhexine, ambroxol, camostat, or batimastat at the indicated concentrations. Viral RNA was quantified by RT-qPCR 24 h (experiment 1 and 2) or 20 h (experiment 3) postinfection. The median  $C_T$  values of three experiments (each experiment was performed in biological triplicates) are plotted (experiment 1, dots; experiment 2, triangles; experiment 3, squares), and the mean was determined. Significant differences from solvent controls are indicated by asterisks. Significance was determined using repeated-measures one-way ANOVA and Fisher's least significant difference test without correcting for multiple comparisons. Differences were also significant using two-way ANOVA without correction for multiple comparisons and all available data, but the use of the median from each experiment reduced variance. All samples were compared to water except for batimastat, which was compared to DMSO. (D) Relative viral RNA expression. Using the median  $C_T$  values from each experiment series, as described above, and the experimentally determined PCR efficiency, the amount of viral RNA was calculated as the percentage of the solvent control for each inhibitor. (E) Cell viability. The cell viability of Calu-3 cells was determined after culture in the presence of the indicated compounds in two independent assays, each performed in biological triplicate. Statistical significance was determined using two-way ANOVA ( $P \geq 0.05$ , ns;  $P \leq 0.05$ , \*;  $P \leq 0.01$ , \*\*;  $P \leq 0.0001$ , \*\*\*\*).

Collectively, these findings identify the S2' site as the primary target of TMPRSS2 for fusion activation.

Another observation was that the S2'-AA mutant, as observed in Fig. 1C and 6C, exhibited drastically reduced surface expression. In fact, a similar incorporation defect has been described in the literature for SARS-CoV (26). Whatever the reason for this defect, we were able to overcome it completely by replacing the S2' motif KR with the amino acids GH, which restored surface expression (Fig. 6C), processing into S1 and S2 subunits (Fig. 6B), and particle incorporation (Fig. 7D). The reasons for this phenomenon are unclear. Charge reversal of S2' from KR to EE was definitely detrimental to activity, indicating that solubility may not be the critical point. As histidine may carry a positive charge depending on the local environment, our findings might hint at a requirement for at least one positive charge at this position.

Our results clearly demonstrate that cleavage at the S1/S2 site alone is not sufficient for fusion activity in the presence of ACE2 and requires additional processing at S2' or another site. This has been established for particle entry (12), but it was not entirely clear for cell-cell fusion, as the precleaved spike was clearly fusogenic also in conditions without exogenous protease activity in several reports (11, 12, 25, 41), which may have been interpreted as a cell-cell fusion-ready state after S1/S2 cleavage. While our initial attempts to block the fusion activity of wt SARS2-S and the S1/S2 mutant in the presence of ACE2 receptor but without TMPRSS2 were relatively unsuccessful, treatment with the metalloprotease inhibitor batimastat reduced fusion by both the wt (Fig. 5A) and the S1/S2 mutant (Fig. 5C), as well as fusion by the S2' mutants (Fig. 6E). These findings indicate that metalloproteases can activate SARS2-S and that this activation occurs at least in part independently of the S1/S2 site and of the S2' site, as both mutants were still batimastat sensitive. On the other hand, the S1/S2 mutant was clearly less active in the absence of TMPRSS2, indicating that matrix metalloproteases activate more efficiently when the S1/S2 site is present. These findings are in line with a very recent report describing similar observations using different inhibitors (40).

As SARS2-S did not require TMPRSS2 on target cells for robust cell-cell fusion, our attempts to test the impact of bromhexine as a specific inhibitor of TMPRSS2 on SARS2-S-mediated fusion activity were somewhat artificial. Nevertheless, SARS1-S-mediated fusion was clearly enhanced by TMPRSS2, as was fusion by SARS2-S1/S2-mut, and both were inhibited by camostat but not by bromhexine. Therefore, our finding that bromhexine specifically enhanced the fusion of 293T cells in the presence of SARS2-S, ACE2, and TMPRSS2 is something that we cannot explain easily. According to our results, the bromhexine-mediated enhancement was specific for SARS2-S and was not seen with VSV-G as a fusion effector (Fig. 3C), nor did we observe significant effects with the SARS2-S mutants or SARS1-S (Fig. 3A). We observed some inhibition of SARS1-S-mediated fusion in the presence of 50  $\mu$ M ambroxol (Fig. 3A) and also with SARS2-S with longer incubation times (Fig. 3C), which may hint at some activity of this substance against TMPRSS2, which would fit with the observation of an atypical autoproteolytic fragment of TMPRSS2 in the presence of ambroxol. The observation of the paradoxical effect of bromhexine in the presence of TMPRSS2 suggests that bromhexine somehow modulates proteolytic processing. It is at the moment not clear by what mechanism of action bromhexine modulates TMPRSS2 activity, if it does so, and we therefore cannot exclude the possibility that processing of some substrates is actually enhanced or altered instead of inhibited, as reported for several substrates (15, 42). Recently, another study also reported the lack of an inhibitory activity of bromhexine against TMPRSS2 (29). The activity of bromhexine against TMPRSS2-mediated receptor shedding, which may also explain our observations, was not observed, unlike with camostat, which increased ACE2 expression levels in the presence of TMPRSS2 (Fig. 3B and 5B). This may explain the slight increase, even if not always statistically significant, in fusion activity that we observed in some experiments with SARS2-S in the presence of camostat when ACE2 and TMPRSS2 were coexpressed (Fig. 3A and 5A).



Compared to another study (43), our fusion assay yielded slightly different results, with SARS2-S-mediated fusion appearing less dependent on activation by TMPRSS2. This may be due to differences in the protocol. The study by Yamamoto et al. (43) allowed only for very short contact times of 4 h and used nonadherent 293T FT cells, whereas we cocultured the cells for a longer time, which allows for extended contact between cells and may enable the action of matrix metalloproteases. Our finding that TMPRSS2 is not required for fusion is in line with several reports making the same observation (11, 12, 25, 40, 41, 44). In general, we observed a higher fusion activity with our SARS2-S1/S2-mut spike mutant than was observed with furin cleavage site mutants in previous studies (12, 25), but we observed this only when TMPRSS2 was recombinantly overexpressed together with ACE2. When only ACE2 or only TMPRSS2 was recombinantly expressed, SARS2-S1/S2-mut fusion activity was strongly impaired (Fig. 2A). It should be noted, that we left the loop intact and replaced only the basic residues with alanine in our mutant, whereas other groups deleted the loop structure, which may result in a less flexible conformation. Nevertheless, our mutational approach for ablating the furin cleavage site clearly rendered the spike protein more dependent on additional serine protease activity by recombinantly expressed TMPRSS2. This proteolytic activity was directed toward the S2' site, as SARS2-S1/S2-mut fusion activity was dependent on TMPRSS2 and was significantly inhibited by camostat (Fig. 3A) in the presence of TMPRSS2.

Taken together, our results actually reconcile several seemingly conflicting observations by other groups. The strong reduction in fusion activity by mutation of the S1/S2 site observed in one study using Vero cells (12) is reflected in our experimental conditions with only TMPRSS2 and endogenous levels of ACE2 expression, whereas our findings of more or less normal fusion activity under conditions of high-level ACE2 and TMPRSS2 expression are similar to the findings of another group with ACE2-overexpressing cells and the addition of trypsin or human airway trypsin-like protease (HAT) (25).

Overall, we propose that the dependence on S1/S2 cleavage, the activity of TMPRSS2 or a related protease, and receptor expression are to a certain degree interdependent and that one factor can at least partially compensate for another; e.g., more extensive proteolytic activation at S2' can render the spike more fusogenic even with lower receptor levels, which was particularly observed for SARS1-S and to a lesser degree for SARS2-S (Fig. 2). Similarly, batimastat-sensitive metalloproteases can activate SARS2-S for cell-cell fusion (Fig. 5A). This is partially dependent on the S1/S2 site, as SARS2-S1/S2-mut was still impaired in the absence of TMPRSS2 but completely independent of the S2' site, as demonstrated by the full fusion activity of the SARS2-S2'-GH spike mutant on ACE2-expressing 293T cells (Fig. 6A).

According to our results, the requirements for cell-cell fusion and virus-cell fusion differ: additional TMPRSS2 activity drastically enhanced pseudotype entry into transfected 293T cells (Fig. 7A) but was not needed for cell-cell fusion with identically transfected 293T cells (Fig. 2A and 3A). In addition, the matrix metalloprotease inhibitor batimastat did not affect particle entry in the presence of the TMPRSS2 inhibitor camostat, indicating that matrix metalloproteases can activate cell-cell fusion but not particle-cell fusion (Fig. 7C and E), at least not in our experimental system. Similar observations were previously made for SARS-CoV (33). The interpretation of these results is complicated by the ability of virus particles to enter cells both through direct membrane fusion or an endocytotic pathway and by different prepriming states of viral spike proteins, depending on proteolytic activity in the producer cell (45). As activation of the spike protein is expected to differ between organ systems depending on the presence of different proteolytic activities, these processes ultimately need to be studied in appropriate tissue systems or animal models. It is tempting to speculate that, relative to SARS-CoV, more relaxed requirements for cell-cell fusion with regard to proteolytic activation contribute to the broad organ tropism and neuroinvasion by SARS-CoV-2, as well as the clinically observed formation of extended syncytia (13). Irrespective of the role of cell-cell fusion in COVID-19, in light of the observed paradoxical activation

of cell-cell fusion by bromhexine and its lack of inhibitory activity against the entry of SARS2-5-pseudotyped lentiviruses on TMPRSS2-expressing cells, we at the moment caution against clinical use of bromhexine for the treatment or prophylaxis of COVID-19, at least at high concentrations that aim at the inhibition of TMPRSS2. A recent, small randomized trial showed promising results for bromhexine at 8 mg three times per day combined with hydroxychloroquine (46), which should result in bromhexine plasma concentrations in the range of 0.1  $\mu\text{M}$  (47). We are fairly confident to postulate that these favorable results are unlikely due to the inhibition of TMPRSS2, although we cannot fully exclude the possibility of extremely weak activity. This view is supported by a recent study that found no effect of bromhexine on TMPRSS2 activity (29). More likely, favorable patient outcomes are attributable to the beneficial effects of bromhexine or its main metabolite ambroxol on lung function, general defense mechanisms against airway infections, and inflammatory responses (16–19, 48). Another recent study by Olaleye et al. (21) specifically analyzed the effects of bromhexine and ambroxol on the interaction of ACE2 with the SARS-CoV-2 spike receptor binding domain (RBD) and reported a very peculiar behavior of these substances, which in part may explain the paradoxical results of our fusion assays and would support a beneficial effect of low-dose bromhexine, which is converted to ambroxol *in vivo*. While ambroxol weakly inhibited the ACE2-RBD interaction up to a 100  $\mu\text{M}$  concentration, bromhexine exhibited a biphasic behavior and was weakly inhibitory below 10  $\mu\text{M}$  but increased ACE2-RBD binding at higher concentrations in that study. Both substances were reported to weakly inhibit SARS-CoV-2-mediated cytopathic effect (CPE) in culture (22), and ambroxol was also shown to moderately impact the replication of SARS-CoV-2 in that report (22), albeit on Vero cells and not lung cells. Our results suggest that ambroxol can weakly inhibit spike-driven entry of lentiviral pseudotypes into Calu-3 cells at high but potentially attainable concentrations (Fig. 8B), and our experiments with authentic SARS-CoV-2 on Calu-3 cells (Fig. 8C and D) demonstrated a trend toward inhibition of replication by both ambroxol and bromhexine, with bromhexine possibly being slightly more potent but also more toxic (Fig. 4C and 8E). Thus, the specificity of bromhexine-mediated inhibition is questionable. In sum, it seems likely that ambroxol acts weakly on TMPRSS2, which would explain its modest but significant effect on the TMPRSS2-mediated activation of SARS1-5-mediated fusion (Fig. 3A). It should be noted that replication of the authentic virus can be influenced at numerous points, not necessarily only during entry, and that effects can be amplified over several replication cycles. Of course, compared to the potency of camostat, the effect of both substances is marginal. Nevertheless, ambroxol can be administered in high doses of 1 g and more intravenously (19) or orally (49) and reportedly accumulates strongly in lung tissue (50). Thus, ambroxol, which exhibited a trend toward the inhibition of SARS2-5-mediated entry and fusion in several assays without enhancing effects, as was observed with bromhexine at high concentrations, may represent an interesting option for supportive therapy at higher dosages, in particular as it is a proven therapeutic for antenatal respiratory distress syndrome (51) and has shown efficacy in the treatment of radiation-induced lung injury (48).

#### MATERIALS AND METHODS

**Cell culture.** All cell lines in this study were incubated at 37°C and 5% CO<sub>2</sub>. 293T cells (a kind gift from Vladan Rankovic and originally purchased from the ATCC, Göttingen, Germany) and Calu-3 cells (a kind gift from Stefan Ludwig) were cultured in Dulbecco's modified Eagle medium (DMEM), high glucose, GlutaMAX, 25 mM HEPES (Thermo Fisher Scientific) supplemented with 10% fetal calf serum (FCS) (Thermo Fisher Scientific) and 50  $\mu\text{g}/\text{ml}$  gentamicin (PAN Biotech). For Calu-3 cells, 1 mM sodium-pyruvate (Thermo Fisher Scientific) was added. For seeding and subculturing of cells, the medium was removed, and the cells were washed with phosphate-buffered saline (PBS; PAN-Biotech) and detached with trypsin (PAN-Biotech). All transfections were performed using polyethylenimine (PEI; Polysciences) in a 1:3 ratio ( $\mu\text{g}$  DNA/ $\mu\text{g}$  PEI) mixed in Opti-MEM. The cell viability assay with Calu-3 cells (Fig. 8E) was performed as described previously (7); unlike with the other assays in this series of experiments, bromhexine and ambroxol were used in the form of commercial cough suppressants (Krewel Meuselbach bromhexine at 12 mg/ml and Mucosolvan at 30 mg/5 ml; Sanofi-Aventis).



**Plasmids.** Expression plasmids for pQCKIPBL-HTMPRSS2 (52), pCG1-SARS-2-S<sub>2</sub>-humanized (7), pCG1-ACE2 (7), and pCG1-SARS S (53) are described elsewhere. For generation of pVAX1-SARS2-S, the codon-optimized sequence encoding the spike protein of SARS-CoV-2 was amplified by PCR and cloned into the pVAX1 backbone. psPAX2 and pMD2.G were a gift from Didier Trono (Addgene plasmid numbers 12260 and 12259), and pLenti CMV GFP Neo (657-2) was a gift from Eric Campeau and Paul Kaufman (Addgene plasmid number 17447). The expression plasmids SARS2-S<sub>2</sub>-AA, SARS2-S1/S2-mut, and SARS2-D614G were generated from humanized pCG1\_SL-Cov\_Wuhan-S\_SARS2-S by PCR-based mutation of the SARS2-S S1/S2 and the S<sub>2</sub>' cleavage site using around-the-horn PCR mutagenesis with S7 fusion PCR (Biozym) or Phusion PCR, T4 PNK, and Quick ligase (all from New England Biolabs) and using the following primers: S1-S2 AAAA mut for V2 (CTGCCTCTGTGGCCAGCCAGAGCATC), S1-S2 AAAA mut rev V2 (CAGCGCGGGGGCTTTGTCTGTCTGTCTG), S2 to AA mut\_Forward (GCCAGCTTCATCGAGGACCTGCTG), S2 to AA mut\_Reverse (AGCGCTGGGCTTGTAGGATCGG), SARS2S R815 H for (CACAGCTTCATCGAGGACCTGCTG), SARS2S K814H rev (GTGGCTGGGCTTGTAGGATCGG), SARS2S R815E for (GAGAGCTTCATCGAGGACCTGCTG), SARS2S K814E rev (CTGCCTGGGCTTGTAGGATCGG), SARS2S R815E for (GAGAGCTTCATCGAGGACCTGCTG), SARS2S R815S for (AGCAGCTTCATCGAGGACCTGCTG), SARS2S K814G rev (TCCGCTGGGCTTGTAGGATCGG), D614G for aroundthethom (GGGTGAACGTGACCGAAGTGCC), and D614G rev aroundthethom (CCGTGGTACAGCACTGCCACTG). Sequence integrity was verified by sequencing of the coding region. Plasmid pCG1-SARS2-S<sub>2</sub>'-mut contains a silent G-to-T mutation in the codon for leucine 441.

Expression plasmids pVAX1-SARS2-S<sub>2</sub>'-GH, pVAX1-SARS2-S1/S2-mut, and pVAX1-SARS2-S<sub>2</sub>-D614G were generated from pVAX1-SARS2-S by PCR-based mutation in a similar manner.

The Gal4-Luc reporter plasmid encoding firefly luciferase under the control of an activator sequence that binds the Gal4 transcription factor has been described elsewhere (33). The Gal4 DNA binding domain VP16 fusion plasmid corresponds to GenBank identifier X85976. The TurboGFP-luciferase fusion reporter gene was constructed using Gibson Assembly master mix (New England Biolabs) to insert the TurboGFP open reading frame with a Ser-Gly-Ser-Gly linker in front of the Met codon of the luciferase open reading frame. Before assembly, the two fragments were generated using Phusion PCR (New England Biolabs) by amplifying the TurboGFP open reading frame from the vector pGIPZ (Thermo Scientific Open Biosystems), using the primers TurboGFP for Gal4Luc before ATG ov (GGTACTGTGGTAAAATGGAGAGCGACGAGAGC) and TurboGFP rev (TTCTTACCAGGCTCTGCATC), and the Gal4-Luc backbone by amplification with primer Gal4Luc before ATG rev (TTTACCAACAGTACCGAATGC) and primer Luc for S<sub>6</sub>SG TurboGFP overhang (GATGCAGATGCCGGTGAAGAAAGCGGTATGGAGAGCGCAAAAACATAAAG).

The pLenti-CMV-TurboGFP-luciferase fusion reporter gene was constructed using Gibson Assembly master mix (New England Biolabs) to exchange the insert in pLenti-CMV-BLAST-EphA7-Strep (described elsewhere [54]) with the TurboGFP-luciferase open reading frame without the Strep tag; the two fragments were generated using CloneAmp HiFi PCR premix (TaKaRa Bio) by amplifying the TurboGFP-Luc open reading frame from the vector Gal4-TurboGFP-Luc using the primers GA\_TurboGFP-Luc\_pLentiBlast-StrepOneOv\_For (ACAAAAAGCAGGCTCCACCATGGAGAGCGACGAGAGC) and GA\_TurboGFP-Luc\_pLentiBlast-StrepOneOv\_Rev (TGTGGATGGCTCCAAGCGCTTACAAATTTGGACTTCCGCC), and the pLenti-CMV-BLAST-EphA7-Strep backbone by amplification with primer pLenti attB1 rev at ATG (CATGTGGAGCCTGC TTTTGTGAC) and OneStrep for (AGCGCTTGGACCATCCAC).

**Western blotting.** Protein expression was analyzed by polyacrylamide gel electrophoresis on 8% to 16% precast gradient gels (Thermo) and Western blotting using antibodies to ACE2 (AF933; R&D Systems), the c-Myc epitope (clone 9E10; Santa Cruz Biotechnology), SARS spike (NB10-56578; Novus Biologicals), HIV-1 Gag p24 (clone 749140; R&D), and GAPDH (glyceraldehyde-3-phosphate dehydrogenase; GenScript) in NETT-G (150 mM NaCl, 5 mM EDTA, 50 mM Tris, 0.05% Triton X-100, 0.25% gelatin, pH 7.5) and donkey anti-mouse horseradish peroxidase (HRP)-coupled (Dianova), goat anti-rabbit HRP-coupled (Life Technologies), or rabbit anti-goat HRP-coupled (Proteintech) secondary antibody in 5% dry milk powder in PBS with 0.05% Tween 20. Imaging was performed using the Immobilon Forte substrate (Merck) on an INTAS ECL ChemoCam system.

**Flow cytometry.** 293T cells were transfected with the respective spike expression constructs. On day 2 posttransfection, the cells were harvested by gentle pipetting in PBS and were fixed in 2% methanol-free formaldehyde in PBS for 15 min. The cells were then washed once in PBS and then incubated in 10% FCS in PBS for 30 min to block nonspecific binding. The cells were then incubated in either convalescent-phase serum at a 1:1,000 dilution or soluble ACE2-Fc fusion protein at 2 ng/ $\mu$ l, both described elsewhere (55), for 1 h in 10% FCS in PBS, followed by one wash in a large volume of PBS and then incubation with Alexa 647-coupled anti-human secondary antibody (Thermo Fisher Scientific) at 1:200 in 10% FCS in PBS. The RRV gH $\Delta$ 21-27-Fc fusion protein, which was used as a control protein, was generated from RRV 26-95 gH-Fc (56) by deletion of the codons for amino acids 21 to 27, which are important for receptor binding (27), and was produced analogously to the gH-Fc protein in the study of Hahn and Desrosiers (56). The cells were then washed once in a large volume of PBS and postfixed in 2% paraformaldehyde (PFA) in PBS before analysis on an LSRII flow cytometer (BD Biosciences). Data were analyzed using Flowing software (version 2.5) and GraphPad Prism, version 6, for Windows (GraphPad Software). COVID-19 convalescent-phase serum was collected previously (55) in accordance with ethical requirements (ethics committee UK Erlangen, license number AZ. 174\_20 B).

**Fusion assay.** 293T target cells were seeded in a 48-well plate at 50,000 cells/well and transfected with Vp16-Gal4 (Fig. 3C) or the Gal4-TurboGFP-luciferase expression plasmid (Gal4-TurboGFP-Luc in all other experiments) as well as expression plasmids for ACE2 and TMPRSS2, as indicated in the figure legends. In case only ACE2 or TMPRSS2 was transfected, the missing amount of DNA was replaced by an empty vector. 293T effector cells were seeded in a 10-cm dish at 70 to 80% confluence and transfected with either the Vp16-Gal4 (all experiments except Fig. 3C) or Gal4-luciferase (Fig. 3C) expression plasmid



as well as expression plasmids for SARS2-S, SARS2-S1/S2-mut, SARS2-S2'-AA, SARS2-S2'-GH, SARS2-S2'-HH, SARS2-S2'-EE, SARS2-S2'-ES, SARS1-S, VSV glycoproteins, or pcDNA6/V5-HisA (Thermo). For effector cell preincubation experiments, the medium of effector cells was changed to bromhexine hydrochloride (Merck), ambroxol hydrochloride (Merck), camostat mesylate (Tocris), batimastat (Merck), AEBSF (Merck), EDTA (Merck), EGTA (Merck), 100× animal-free cocktail set V (Calbiochem; Merck), or decanoyl-RVKKR-CMK (Merck) containing medium at a final concentration 6 h after transfection. Twenty-four hours after transfection, target cells were preincubated with bromhexine hydrochloride (Merck), ambroxol hydrochloride (Merck), camostat mesylate (Tocris), batimastat (Merck), AEBSF (Merck), EDTA (Merck), EGTA (Merck), or decanoyl-RVKKR-CMK (Merck) for 30 min at the concentrations indicated in the figure legends. Effector cells were then added to the target cells in a 1:1 ratio, reaching the final inhibitor concentration. After 24 to 48 h, GFP fluorescence was detected using a Vert.A1 fluorescence microscope and ZEN software (Zeiss), and luciferase activity was analyzed using the PromoKine firefly luciferase kit or Beetle-Juice luciferase assay (PKJ Biotech) according to the manufacturer's instructions and a BioTek Synergy 2 plate reader. Statistical analysis was performed using GraphPad Prism, version 6, for Windows (GraphPad Software).

**Production of lentiviral and pseudoparticles and pseudoparticle infection experiments.** Lentiviral pseudoparticles were produced by transfecting 293T cells with expression plasmids for psPAX2, pLenti-CMV-GFP, or pLenti-CMV-TurboGFP-luciferase and either SARS2-S variants (pVAX1-SARS2-S<sub>2</sub>'-GH, pVAX1-SARS2-S1/S2-mut, and pVAX1-SARS2-S<sub>2</sub>D614G) or VSV-G (pMD2.G; Addgene number 12259). The cell culture supernatants were harvested 24 to 72 h posttransfection, followed by the addition of fresh medium, and again after 48 to 72 h. The supernatants were passed through a 0.45- $\mu$ m cellulose acetate (CA) filter, and the SARS2-S pseudoparticles were concentrated via low-speed centrifugation at 4°C for 16 h at 4,200  $\times$  g. For detection of particle incorporation, the virus supernatant was further concentrated by centrifugation at 4°C for 2 h at 21,000  $\times$  g on 5% OptiPrep (Merck), the supernatant was removed, and the pellet was resuspended and subjected to Western blot analysis. The SARS-CoV-2 spike and VSV-G lentiviral pseudoparticles were used to transduce 293T cells transfected with TMPRSS2 and ACE2 expression plasmids or Calu-3 cells. Forty-eight hours after transfection with control or ACE2 and TMPRSS2 expression plasmids, the pseudoparticles were added to cells preincubated with the inhibitors bromhexine hydrochloride (Merck), ambroxol hydrochloride (Merck), camostat mesylate (Tocris), batimastat (Merck), AEBSF (Merck), and E64-d (Biomol) for 30 min at twice the concentration indicated in the figure legends, and the final concentration was reached after the addition of the inoculum. Cells transfected with pLenti-CMV-GFP pseudoparticles were harvested 48 h after transduction using trypsin. Bald particles from 293T cells that had been transfected with an empty vector instead of glycoprotein expression plasmids and the lentiviral packaging system were used as background control for normalization. Trypsin activity was inhibited by adding 5% FCS in PBS, and after being washed with PBS, the cells were fixed with 4% formaldehyde (Roth) in PBS. The percentages of GFP-positive cells were determined using a LSRII flow cytometer, and at least 10,000 cells were analyzed. Cells transfected with pLenti-CMV-TurboGFP-luciferase pseudoparticles were lysed after 48 h with luciferase lysis buffer (Promega) and detected using the Beetle-Juice luciferase assay according to manufacturer's instructions and a BioTek Synergy 2 plate reader. Statistical analysis was performed using GraphPad Prism 6.

**SARS-CoV-2 infections.** Primary SARS-CoV-2 isolate ER-PR2 was a kind gift from Klaus Überla, Erlangen, Germany, and was originally isolated on Vero cells. The virus stock was then grown on Calu-3 cells in DMEM plus 2% FCS plus penicillin/streptomycin. The virus-containing supernatant was harvested after CPE was clearly visible, and the supernatant was cleared by low-speed centrifugation at 1,200 rpm for 10 min before passage through a 0.2- $\mu$ m syringe filter (Mini-Sart; Sartorius). Virus stocks were aliquoted in 200- $\mu$ l aliquots and stored at  $-150^{\circ}\text{C}$ . Infectivity was determined by the method of Reed and Muench (57) at  $10^{6.1}$  50% tissue culture infectious doses (TCID<sub>50</sub>)/ml. Calu-3 cells were seeded 1 day (first experiment) or 2 days (other two experiments) before infection, and approximately 100,000 Calu-3 cells were infected at an MOI of approximately 0.002 in a 96-well plate in triplicates. The cells were preincubated with the respective inhibitors in 50  $\mu$ l at twice the concentration for  $\sim$ 1.5 h, and the virus was then added in 50  $\mu$ l medium. Total RNA from the cells and the culture supernatant was harvested 20 h (experiment 3) and 24 h (experiments 1 and 2) postinfection.

**RNA isolation, cDNA synthesis, and RT-qPCR.** RNA was isolated using the Direct-zol RNA Miniprep Plus kit (Zymo) according to the manufacturer's instructions. For quantification of viral RNA in infected cultures, the cells and cellular supernatant in a volume of 100  $\mu$ l were lysed and inactivated by addition of 300  $\mu$ l TRI reagent (Zymo). RT-qPCR of viral genomes was performed using the N1 CDC primer set from IDT (2019-nCoV\_N1-F, GACCCAAATCAGCGAAAT, and 2019-nCoV\_N1-R, TCTGGTACTGCCAGTGAATCTG, both at 500 nM, and 2019-nCoV\_N1-P, FAM-ACCCCGCATTACGTTTGGTGACC-BHQ1 [where FAM is 6-carboxyfluorescein and BHQ1 is black hole quencher 1] at 125 nM) and the SensiFAST Probe Hi-ROX one-step kit (Bioline) according to the manufacturer's instructions in a 20- $\mu$ l reaction mixture with a 5- $\mu$ l sample. All RT-qPCRs were performed in technical duplicates on a StepOne Plus (Thermo) real-time cyler. PCR conditions were 45°C for 10 min, 95°C for 2 min, and then 45 cycles of 95°C for 5 s followed by 55°C for 20 s. To determine the PCR efficiency across the whole dynamic range, a 7-step 10-fold dilution series with the H<sub>2</sub>O-treated SARS-CoV-2-infected Calu-3 cell sample was performed. These data points with the undiluted sample set to 1 was approximated by an exponential function using Microsoft Excel 2020. The measured PCR efficiency was additionally fitted by multiplication with a constant factor to match our RNA standard (Charité, Berlin, Germany), which was available only at 50, 500, and 5,000 copies, which confirmed our approach but was not used for relative quantification. Fit was performed by minimizing the sum of the squared relative deviations from the standard concentrations with an exactness of two digits.

For quantification of cellular TMPRSS2 and GAPDH expression, cDNA synthesis and qPCR were performed according to the manufacturer's instructions using the SensiFAST cDNA kit and SensiFAST SYBR



qPCR kit (both from Bioline). The qPCR was run on a StepOnePlus real-time PCR cycler (Thermo) and analyzed using the StepOne software, which was also used to calculate  $\Delta\Delta C_T$  values and error estimates for TMPRSS2 expression. TMPRSS2 mRNA was detected using primer set Hs.PT.58.39408998 (IDT) (forward primer GTCAAGGACGAGACCATGT, reverse primer TGCCAAAGCTTACAGACCAG). GAPDH mRNA was detected using primers GAPDH\_Hs-Mm\_s (CTTTGGTATCGTGAAGGACT) and GAPDH\_Hs-Mm\_as (GTAGAGGACGGATGATGTT). Amplifications with a  $C_T$  above 35 and nonmatching melting curve were scored as not detected.

#### ACKNOWLEDGMENTS

We thank Stefan Pöhlmann and Markus Hofmann for sharing reagents and for critical readings of the manuscript and helpful discussions. We thank Klaus Überla for sharing SARS-CoV-2 ER-PR2. We also thank Armin Ensser and Florian Full for helpful discussions.

This work was supported by grants HA 6013/4-1 and HA 6013/6-1 to A.S.H. from the Deutsche Forschungsgemeinschaft and by grant 2019.027.1 to A.S.H. from the Wilhelm-Sander-Stiftung.

#### REFERENCES

- Zhou P, Yang X-L, Wang X-G, Hu B, Zhang L, Zhang W, Si H-R, Zhu Y, Li B, Huang C-L, Chen H-D, Chen J, Luo Y, Guo H, Jiang R-D, Liu M-Q, Chen Y, Shen X-R, Wang X, Zheng X-S, Zhao K, Chen Q-J, Deng F, Liu L-L, Yan B, Zhan F-X, Wang Y-Y, Xiao G-F, Shi Z-L. 2020. A pneumonia outbreak associated with a new coronavirus of probable bat origin. *Nature* 579:270–273. <https://doi.org/10.1038/s41586-020-2012-7>.
- Zang R, Gomez Castro MF, McCune BT, Zeng Q, Rothlauf PW, Sonnek NM, Liu Z, Brulois KF, Wang X, Greenberg HB, Diamond MS, Ciorba MA, Whelan SPJ, Ding S. 2020. TMPRSS2 and TMPRSS4 promote SARS-CoV-2 infection of human small intestinal enterocytes. *Sci Immunol* 5:eabc3582. <https://doi.org/10.1126/sciimmunol.abc3582>.
- Bojkova D, McCreigh JE, McLaughlin K-M, Masterson SG, Wiedera M, Krähling V, Ciesek S, Wass MN, Michaelis M, Cinatl J. 2020. SARS-CoV-2 and SARS-CoV differ in their cell tropism and drug sensitivity profiles. *bioRxiv* 2020.04.03.024257.
- Hui KPY, Cheung M-C, Perera RAPM, Ng K-C, Bui CHT, Ho JCW, Ng MMT, Kuok DIT, Shih KC, Tsao S-W, Poon LLM, Peiris M, Nicholls JM, Chan MCW. 2020. Tropism, replication competence, and innate immune responses of the coronavirus SARS-CoV-2 in human respiratory tract and conjunctiva: an analysis in ex-vivo and in-vitro cultures. *Lancet Respir Med* 8:687–695. [https://doi.org/10.1016/S2213-2600\(20\)30193-4](https://doi.org/10.1016/S2213-2600(20)30193-4).
- Li W, Moore MJ, Vasilieva N, Sui J, Wong SK, Berne MA, Somasundaran M, Sullivan JL, Luzuriaga A, Greenough TC, Choe H, Farzan M. 2003. Angiotensin-converting enzyme 2 is a functional receptor for the SARS coronavirus. *Nature* 426:450–454. <https://doi.org/10.1038/nature02145>.
- Letko M, Marzi A, Munster V. 2020. Functional assessment of cell entry and receptor usage for SARS-CoV-2 and other lineage B betacoronaviruses. *Nat Microbiol* 5:562–569. <https://doi.org/10.1038/s41564-020-0688-y>.
- Hoffmann M, Kleine-Weber H, Schroeder S, Krüger N, Herrler T, Erichsen S, Schiergens TS, Herrler G, Wu N-H, Nitsche A, Müller MA, Drosten C, Pöhlmann S. 2020. SARS-CoV-2 cell entry depends on ACE2 and TMPRSS2 and is blocked by a clinically proven protease inhibitor. *Cell* 181:271–280. <https://doi.org/10.1016/j.cell.2020.02.052>.
- Heald-Sargent T, Gallagher T. 2012. Ready, set, fuse! The coronavirus spike protein and acquisition of fusion competence. *Viruses* 4:557–580. <https://doi.org/10.3390/v4040557>.
- Matsuyama S, Nao N, Shirato K, Kawase M, Saito S, Takayama I, Nagata N, Sekizuka T, Katoh H, Kato F, Sakata M, Tahara M, Kutsuna S, Ohmagari N, Kuroda M, Suzuki T, Kageyama T, Takeda M. 2020. Enhanced isolation of SARS-CoV-2 by TMPRSS2-expressing cells. *Proc Natl Acad Sci U S A* 117:7001–7003. <https://doi.org/10.1073/pnas.2002589117>.
- Shulla A, Heald-Sargent T, Subramanya G, Zhao J, Perlman S, Gallagher T. 2011. A transmembrane serine protease is linked to the severe acute respiratory syndrome coronavirus receptor and activates virus entry. *J Virol* 85:873–882. <https://doi.org/10.1128/JVI.02062-10>.
- Ou X, Liu Y, Lei X, Li P, Mi D, Ren L, Guo L, Guo R, Chen T, Hu J, Xiang Z, Mu Z, Chen X, Chen J, Hu K, Jin Q, Wang J, Qian Z. 2020. Characterization of spike glycoprotein of SARS-CoV-2 on virus entry and its immune cross-reactivity with SARS-CoV. *Nat Commun* 11:1620. <https://doi.org/10.1038/s41467-020-15562-9>.
- Hoffmann M, Kleine-Weber H, Pöhlmann S. 2020. A multibasic cleavage site in the spike protein of SARS-CoV-2 is essential for infection of human lung cells. *Mol Cell* 78:779–784.e5. <https://doi.org/10.1016/j.molcel.2020.04.022>.
- Giacca M, Bussani R, Schneider E, Zentilin L, Collesi C, Ali H, Braga L, Secco I, Volpe MC, Colliva A, Zanconati F, Berlot G, Silvestri F, Zacchigna S. 2020. Persistence of viral RNA, widespread thrombosis and abnormal cellular syncytia are hallmarks of COVID-19 lung pathology. *medRxiv* 2020.06.22.20136358.
- Ziegler CGK, Allon SJ, Nyquist SK, Mbano IM, Miao VN, Tzouanas CN, Cao Y, Yousif AS, Bals J, Hauser BM, Feldman J, Muus C, Wadsworth MH, Kazer SW, Hughes TK, Doran B, Gatter GJ, Vukovic M, Taliaferro F, Mead BE, Guo Z, Wang JP, Gras D, Plaisant M, Ansari M, Angelidis I, Adler H, Sucre JMS, Taylor CJ, Lin B, Waghay A, Mitsialis V, Dwyer DF, Buchheit KM, Boyce JA, Barrett NA, Laidlaw TM, Carroll SL, Colonna L, Tkachev V, Peterson CW, Yu A, Zheng HB, Gideon HP, Winchell CG, Lin PL, Bingle CD, Snapper SB, Kropski JA, Theis FJ. 2020. SARS-CoV-2 receptor ACE2 is an interferon-stimulated gene in human airway epithelial cells and is detected in specific cell subsets across tissues. *Cell* 181:1016–1035.e19. <https://doi.org/10.1016/j.cell.2020.04.035>.
- Lucas JM, Heinlein C, Kim T, Hernandez SA, Malik MS, True LD, Morrissey C, Corey E, Montgomery B, Mostaghel E, Clegg N, Coleman I, Brown CM, Schneider EL, Craik C, Simon J, Bedalov T, Nelson PS. 2014. The androgen-regulated protease TMPRSS2 activates a proteolytic cascade involving components of the tumor microenvironment and promotes prostate cancer metastasis. *Cancer Discov* 4:1310–1325. <https://doi.org/10.1158/2159-8290.CD-13-1010>.
- Renovanz VK. 1975. Results of some clinical-pharmacological studies on ambroxol (NA 872). *Arzneimittelforschung* 25:646–652. (In German.)
- Nobata K, Fujimura M, Ishiura Y, Myou S, Nakao S. 2006. Ambroxol for the prevention of acute upper respiratory disease. *Clin Exp Med* 6:79–83. <https://doi.org/10.1007/s10238-006-0099-2>.
- Yang B, Yao DF, Ohuchi M, Ide M, Yano M, Okumura Y, Kido H. 2002. Ambroxol suppresses influenza-virus proliferation in the mouse airway by increasing antiviral factor levels. *Eur Respir J* 19:952–958. <https://doi.org/10.1183/09031936.02.00253302>.
- Wu X, Li S, Zhang J, Zhang Y, Han L, Deng Q, Wan X. 2014. Meta-analysis of high doses of ambroxol treatment for acute lung injury/acute respiratory distress syndrome based on randomized controlled trials. *J Clin Pharmacol* 54:1199–1206. <https://doi.org/10.1002/jcph.389>.
- Wauer RR, Schmalisch G, Menzel K, Schröder M, Müller K, Tiller R, Methfessel G, Sitka U, Koepke E, Plath C, Schlegel C, Böttcher M, Köppe I, Fricke U, Severin K, Jacobi R, Schmidt W, Hinkel GK, Nitz I, Kunze D, Reichmann G, Lachmann B, Lampe K, Grauel EL. 1982. The antenatal use of ambroxol (bromhexine metabolite VIII) to prevent hyaline membrane disease: a controlled double-blind study. *Int J Biol Res Pregnancy* 3:84–91.
- Olaleye OA, Kaur M, Onyenaka CC. 2020. Ambroxol hydrochloride inhibits the interaction between severe acute respiratory syndrome coronavirus 2 spike protein's receptor binding domain and recombinant human ACE2. *bioRxiv* 2020.09.13.295691.



22. Bradfute SB, Ye C, Clarke EC, Kumar S, Timmins GS, Deretic V. 2020. Ambroxol and ciprofloxacin show activity against SARS-CoV2 in Vero E6 cells at clinically-relevant concentrations. *bioRxiv* 2020.08.11.245100.
23. Wrapp D, Wang N, Corbett KS, Goldsmith JA, Hsieh C-L, Abiona O, Graham BS, McLellan JS. 2020. Cryo-EM structure of the 2019-nCoV spike in the prefusion conformation. *Science* 367:1260–1263. <https://doi.org/10.1126/science.abb2507>.
24. Zhu Y, Feng F, Hu G, Wang Y, Yu Y, Zhu Y, Xu W, Cai X, Sun Z, Han W, Ye R, Chen H, Ding Q, Cai Q, Qu D, Xie Y, Yuan Z, Zhang R. 2021. The S1/S2 boundary of SARS-CoV-2 spike protein modulates cell entry pathways and transmission. *Microbiology* 12:961. <https://doi.org/10.1038/s41467-021-21213-4>.
25. Xia S, Lan Q, Su S, Wang X, Xu W, Liu Z, Zhu Y, Wang Q, Lu L, Jiang S. 2020. The role of furin cleavage site in SARS-CoV-2 spike protein-mediated membrane fusion in the presence or absence of trypsin. *Signal Transduct Target Ther* 5:92. <https://doi.org/10.1038/s41392-020-0184-0>.
26. Belouzard S, Chu VC, Whittaker GR. 2009. Activation of the SARS coronavirus spike protein via sequential proteolytic cleavage at two distinct sites. *Proc Natl Acad Sci U S A* 106:5871–5876. <https://doi.org/10.1073/pnas.0809524106>.
27. Großkopf AK, Schlagowski S, Ensser A, Desrosiers RC, Hahn AS. 2020. P1xdc family members are novel receptors for the rhesus monkey rhadinovirus (RRV). *bioRxiv* 2020.01.20.912246.
28. Nimishakavi S, Raymond WW, Gruenert DC, Caughey GH. 2015. Divergent inhibitor susceptibility among airway lumen-accessible tryptic proteases. *PLoS One* 10:e0141169. <https://doi.org/10.1371/journal.pone.0141169>.
29. Shrimp JH, Kales SC, Sanderson PE, Simeonov A, Shen M, Hall MD. 2020. An enzymatic TMPRSS2 assay for assessment of clinical candidates and discovery of inhibitors as potential treatment of COVID-19. *ACS Pharmacol Transl Sci* 3:997–1007. <https://doi.org/10.1021/acspstci.0c00106>.
30. Kim IS, Jenni S, Stanifer ML, Roth E, Whelan SPJ, van Oijen AM, Harrison SC. 2017. Mechanism of membrane fusion induced by vesicular stomatitis virus G protein. *Proc Natl Acad Sci U S A* 114:E28–E36. <https://doi.org/10.1073/pnas.1618883114>.
31. Hoffmann M, Wu Y-J, Gerber M, Berger-Rentsch M, Heimrich B, Schwemmle M, Zimmer G. 2010. Fusion-active glycoprotein G mediates the cytotoxicity of vesicular stomatitis virus M mutants lacking host shut-off activity. *J Gen Virol* 91:2782–2793. <https://doi.org/10.1099/vir.0.023978-0>.
32. Hoffmann D, Bayer W, Wildner O. 2007. Therapeutic immune response induced by intratumoral expression of the fusogenic membrane protein of vesicular stomatitis virus and cytokines encoded by adenoviral vectors. *Int J Mol Med* 20:673–681.
33. Simmons G, Bertram S, Glowacka I, Steffen I, Chaipan C, Agudelo J, Lu K, Rennekamp AJ, Hofmann H, Bates P, Pöhlmann S. 2011. Different host cell proteases activate the SARS-coronavirus spike-protein for cell-cell and virus-cell fusion. *Virology* 413:265–274. <https://doi.org/10.1016/j.virol.2011.02.020>.
34. Jaimes JA, Millet JK, Whittaker GR. 2020. Proteolytic cleavage of the SARS-CoV-2 spike protein and the role of the novel S1/S2 site. *iScience* 23:101212. <https://doi.org/10.1016/j.isci.2020.101212>.
35. Davies B, Brown PD, East N, Crimmin MJ, Balkwill FR. 1993. A synthetic matrix metalloproteinase inhibitor decreases tumor burden and prolongs survival of mice bearing human ovarian carcinoma xenografts. *Cancer Res* 53:2087–2091.
36. Wojtowicz-Praga SM, Dickson RB, Hawkins MJ. 1997. Matrix metalloproteinase inhibitors. *Invest New Drugs* 15:61–75. <https://doi.org/10.1023/a:1005722729132>.
37. Hou YJ, Chiba S, Halfmann P, Ehre C, Kuroda M, Dinnon KH, Leist SR, Schäfer A, Nakajima N, Takahashi K, Lee RE, Mascenik TM, Graham R, Edwards CE, Tse LV, Okuda K, Markmann AJ, Bartelt L, de Silva A, Margolis DM, Boucher RC, Randell SH, Suzuki T, Gralinski LE, Kawaoka Y, Baric RS. 2020. SARS-CoV-2 D614G variant exhibits efficient replication *ex vivo* and transmission *in vivo*. *Science* 370:1464–1468. <https://doi.org/10.1126/science.abe8499>.
38. Fois G, Hobi N, Felder E, Ziegler A, Miklavc P, Walther P, Radermacher P, Haller T, Dietl P. 2015. A new role for an old drug: ambroxol triggers lysosomal exocytosis via pH-dependent Ca<sup>2+</sup> release from acidic Ca<sup>2+</sup> stores. *Cell Calcium* 58:628–637. <https://doi.org/10.1016/j.ceca.2015.10.002>.
39. Takeda H, Misawa M, Yanaura S. 1983. A role of lysosomal enzymes in the mechanism of mucolytic action of bromhexine. *Jpn J Pharmacol* 33:455–461. <https://doi.org/10.1254/jip.33.455>.
40. Nguyen HT, Zhang S, Wang Q, Anang S, Wang J, Ding H, Kappes JC, Sodroski J. 2020. Spike glycoprotein and host cell determinants of SARS-CoV-2 entry and cytopathic effects. *J Virol* 95:e02304-20. <https://doi.org/10.1128/JVI.02304-20>.
41. Buchrieser J, Dufloo J, Hubert M, Monel B, Planas D, Rajah MM, Planchais C, Porrot F, Guivel-Benhassine F, Van der Werf S, Casarelli N, Mouquet H, Bruel T, Schwartz O. 2020. Syncytia formation by SARS-CoV-2-infected cells. *EMBO J* 39:e106267. <https://doi.org/10.15252/embj.2020106267>.
42. Azouz NP, Klingler AM, Rothenberg ME. 2020. Alpha 1 antitrypsin is an inhibitor of the SARS-CoV-2-priming protease TMPRSS2. *bioRxiv* 2020.05.04.077826.
43. Yamamoto M, Kiso M, Sakai-Tagawa Y, Iwatsuki-Horimoto K, Imai M, Takeda M, Kinoshita N, Ohmagari N, Gohda J, Semba K, Matsuda Z, Kawaguchi Y, Kawaoka Y, Inoue J. 2020. The anticoagulant nafamostat potentially inhibits SARS-CoV-2 infection *in vitro*: an existing drug with multiple possible therapeutic effects. *bioRxiv* 2020.04.22.054981.
44. Liu S, Selvaraj P, Lien CZ, Wu WW, Chou C-K, Wang TT. 2020. The PRRA insert at the S1/S2 site modulates cellular tropism of SARS-CoV-2 and ACE2 usage by the closely related Bat raTG13. *bioRxiv* 2020.07.20.213280.
45. Shang J, Wan Y, Luo C, Ye G, Geng Q, Auerbach A, Li F. 2020. Cell entry mechanisms of SARS-CoV-2. *Proc Natl Acad Sci U S A* 117:11727–11734. <https://doi.org/10.1073/pnas.2003138117>.
46. Ansarin K, Tolouian R, Ardalan M, Taghizadeh A, Varshochi M, Teimouri S, Vaezi T, Valizadeh H, Saleh P, Safiri S, Chapman KR. 2020. Effect of bromhexine on clinical outcomes and mortality in COVID-19 patients: a randomized clinical trial. *Bioimpacts* 10:209–215. <https://doi.org/10.34172/bi.2020.27>.
47. Bechgaard E, Nielsen A. 1982. Bioavailability of bromhexine tablets and preliminary pharmacokinetics in humans. *Biopharm Drug Dispos* 3:337–344. <https://doi.org/10.1002/bdd.2510030407>.
48. Xia D-H, Xi L, Xu C, Mao W-D, Shen W-S, Shu Z-Q, Yang H-Z, Dai M. 2010. The protective effects of ambroxol on radiation lung injury and influence on production of transforming growth factor beta1 and tumor necrosis factor alpha. *Med Oncol* 27:697–701. <https://doi.org/10.1007/s12032-009-9271-3>.
49. Mullin S, Smith L, Lee K, D'Souza G, Woodgate P, Elflein J, Hallqvist J, Toffoli M, Streeter A, Hosking J, Heywood WE, Khengar R, Campbell P, Hehir J, Cable S, Mills K, Zetterberg H, Limousin P, Libri V, Foletynie T, Schapira AHV. 2020. Ambroxol for the treatment of patients with Parkinson disease with and without glucocerebrosidase gene mutations: a non-randomized, noncontrolled trial. *JAMA Neurol* 77:427–434. <https://doi.org/10.1001/jamaneurol.2019.4611>.
50. Li Q, Yao G, Zhu X. 2012. High-dose ambroxol reduces pulmonary complications in patients with acute cervical spinal cord injury after surgery. *Neurocrit Care* 16:267–272. <https://doi.org/10.1007/s12028-011-9642-4>.
51. Zhang H, Liu J, Liu T, Wang Y, Dai W. 2018. Antenatal maternal medication administration in preventing respiratory distress syndrome of premature infants: a network meta-analysis. *Clin Respir J* 12:2480–2490. <https://doi.org/10.1111/crj.12923>.
52. Kleine-Weber H, Elzayat MT, Hoffmann M, Pöhlmann S. 2018. Functional analysis of potential cleavage sites in the MERS-coronavirus spike protein. *Sci Rep* 8:16597. <https://doi.org/10.1038/s41598-018-34859-w>.
53. Hoffmann M, Müller MA, Drexler JF, Glende J, Erdt M, Gützkow T, Losemann C, Binger T, Deng H, Schwegmann-Weßels C, Esser K-H, Drosten C, Herrler G. 2013. Differential sensitivity of bat cells to infection by enveloped RNA viruses: coronaviruses, paramyxoviruses, filoviruses, and influenza viruses. *PLoS One* 8:e72942. <https://doi.org/10.1371/journal.pone.0072942>.
54. Großkopf AK, Schlagowski S, Hörnich BF, Fricke T, Desrosiers RC, Hahn AS. 2019. EphA7 functions as receptor on BJAB cells for cell-to-cell transmission of the Kaposi's sarcoma-associated herpesvirus (KSHV) and for cell-free infection by the related rhesus monkey rhadinovirus (RRV). *J Virol* 93:e00064-19. <https://doi.org/10.1128/JVI.00064-19>.
55. Lapuente D, Maier C, Irgang P, Hübner J, Peter AS, Hoffmann M, Ensser A, Ziegler K, Winkler TH, Birkholz T, Kremer AE, Steininger P, Korn K, Neipel F, Überla K, Tenbusch M. 20 October 2020. Rapid response flow cytometric assay for the detection of antibody responses to SARS-CoV-2. *Eur J Clin Microbiol Infect Dis* <https://doi.org/10.1007/s10096-020-04072-7>.
56. Hahn AS, Desrosiers RC. 2013. Rhesus monkey rhadinovirus uses Eph family receptors for entry into B cells and endothelial cells but not fibroblasts. *PLoS Pathog* 9:e1003360. <https://doi.org/10.1371/journal.ppat.1003360>.
57. Reed LJ, Muench H. 1938. A simple method of estimating fifty per cent endpoints. *Am J Epidemiol* 27:493–497. <https://doi.org/10.1093/oxfordjournals.aje.a118408>.

### **3.2 Publication 2: Interferon-Induced Transmembrane Proteins Inhibit Infection by the Kaposi's Sarcoma-Associated Herpesvirus and the Related Rhesus Monkey Rhadinovirus in a Cell-Specific Manner.**

Bojan F. Hörnich<sup>a</sup>, Anna K. Großkopf<sup>a</sup>, Candice J. Dcosta<sup>a\*</sup>, Sarah Schlagowski<sup>a</sup>, Alexander S. Hahn<sup>a</sup>

a Junior Research Group Herpesviruses, German Primate Center – Leibniz-Institute for Primate Research, Göttingen, Germany

\*Current address: JMIR Publications, Toronto, Ontario

Status of Publication: Accepted for Publication in mBio.

#### Contribution:

I was responsible for the methodology, formal analysis, data analysis, visualization, writing of the original draft, reviewing/editing and investigation. Investigation was performed for experiments that lead to Figure 1, Figure 2, Figure 3A, Figure 4A, Figure 4C, Figure 6, Supplemental Figure 1, Supplemental Figure 3 A, B, D (Infection and Cytotoxicity of BafilomycinA1, MBCD), Supplemental Figure 5 and repeats for Figure 3B, Figure 4B, Figure 4D and Supplemental Figure 3 C and D (Infection and Cytotoxicity of EIPA). Purification and concentration of the virus stock and initial investigation was performed that resulted in experiments for Figure 5 B. Initial identification and screening of sgRNAs shown in Figure 2 was also performed.

25/11/21	22:12	ArtID:	DOI:10.1128/mBio.02113-21	CE: KGL-mar
Editor:		Section:	Designation:	
		Research Article		



RESEARCH ARTICLE



## Interferon-Induced Transmembrane Proteins Inhibit Infection by the Kaposi's Sarcoma-Associated Herpesvirus and the Related Rhesus Monkey Rhadinovirus in a Cell-Specific Manner

AQ: au **Bojan F. Hörnich,<sup>a</sup> Anna K. Großkopf,<sup>a</sup> Candice J. Dcosta,<sup>a\*</sup> Sarah Schlagowski,<sup>a</sup> Alexander S. Hahn<sup>a</sup>**

<sup>a</sup>Junior Research Group Herpesviruses, German Primate Center—Leibniz Institute for Primate Research, Göttingen, Germany

**ABSTRACT** The interferon-induced transmembrane proteins (IFITMs) are broad-spectrum antiviral proteins that inhibit the entry of enveloped viruses. We analyzed the effect of IFITMs on the gamma-2 herpesviruses Kaposi's sarcoma-associated herpesvirus (KSHV) and the closely related rhesus monkey rhadinovirus (RRV). We used CRISPR/Cas9-mediated gene knockout to generate A549 cells, human foreskin fibroblasts (HFF), and human umbilical vein endothelial cells (HUVEC) with combined IFITM1/2/3 knockout and identified IFITMs as cell-dependent inhibitors of KSHV and RRV infection in A549 cells and HFF but not HUVEC. IFITM overexpression revealed IFITM1 as the relevant IFITM that inhibits KSHV and RRV infection. Fluorescent KSHV particles did not pronouncedly colocalize with IFITM-positive compartments. However, we found that KSHV and RRV glycoprotein-mediated cell-cell fusion is enhanced upon IFITM1/2/3 knockout. Taken together, we identified IFITM1 as a cell-dependent restriction factor of KSHV and RRV that acts at the level of membrane fusion. Of note, our results indicate that recombinant IFITM overexpression may lead to results that are not representative for the situation at endogenous levels. Strikingly, we observed that the endotheliotropic KSHV circumvents IFITM-mediated restriction in HUVEC despite high IFITM expression, while influenza A virus (IAV) glycoprotein-driven entry into HUVEC is potently restricted by IFITMs even in the absence of interferon. Mechanistically, we found that KSHV colocalizes less with IFITM1 and IFITM2 in HUVEC than in A549 cells immediately after attachment, potentially contributing to the observed difference in restriction.

**IMPORTANCE** IFITM proteins are the first line of defense against infection by many pathogens and may also have therapeutic importance, as they, among other effectors, mediate the antiviral effect of interferons. Neither their function against herpesviruses nor their mechanism of action is well understood. We report here that in some cells but not in, for example, primary umbilical vein endothelial cells, IFITM1 restricts KSHV and RRV and that, mechanistically, this is likely effected by reducing the fusogenicity of the cell membrane. Further, we demonstrate potent inhibition of IAV glycoprotein-driven infection of cells of extrapulmonary origin by high constitutive IFITM expression.

**KEYWORDS** IFITMs, Kaposi's sarcoma-associated herpesvirus, influenza, interferons, virus entry

The family of interferon-induced transmembrane proteins (IFITMs) are small membrane proteins that exhibit antiviral activity toward a broad variety of viruses (1–6). There are five IFITMs present in the human genome, but only IFITM1, IFITM2, and IFITM3 are known to be immune related and interferon (IFN) inducible (reviewed in references 6 and 7). IFITM1 localizes to the plasma membrane, while IFITM2 and IFITM3 localize to endosomes/lysosomes (5, 8).

The exact mechanism of IFITM-mediated restriction of viral replication is not completely understood. It is, however, clear that restriction occurs mainly at the viral entry

**Editor** Peter Palese, Icahn School of Medicine at Mount Sinai

**Copyright** © 2021 Hörnich et al. This is an open-access article distributed under the terms of the [Creative Commons Attribution 4.0 International license](https://creativecommons.org/licenses/by/4.0/).

Address correspondence to Alexander S. Hahn, [ahahn@dpz.eu](mailto:ahahn@dpz.eu).

\*Present address: Candice J. Dcosta, JMIR Publications, Toronto, Ontario, Canada.

The authors declare no conflict of interest.

**Received** 15 July 2021

**Accepted** 15 November 2021

**Published**

AQ: A

November/December 2021 Volume 12 Issue 6 e02113-21

[mbio.asm.org](https://mbio.asm.org) 1

ID: [vinayak.bhelekar](https://doi.org/10.1128/mBio.02113-21)Time: 22:12 Path: //mumnasprod/home\$/VinayBhelekar\$/SM-MBIO210767



stage (3, 9, 10). According to some reports, IFITMs modify the overall membrane fusogenicity by modification of the membrane lipid composition and/or the membrane rigidity and thus prevent virus-host membrane fusion (11–14), probably causing arrest of the fusion pore opening following hemifusion (11, 12, 15). Other modes of action, such as, e.g., recruitment of additional antiviral factors, altered endocytic trafficking, and interference with vacuolar ATPase, have been postulated as well (reviewed in reference 16).

The majority of IFITM-restricted viruses are RNA viruses. The interplay of IFITMs with DNA viruses has been studied less extensively and with more ambiguous results. While vaccinia virus and herpes simplex virus 1 (HSV-1) are restricted by overexpression of individual IFITM proteins (17, 18), human papillomavirus 16 (HPV16) and the nonenveloped adenovirus type 5 are not (19). Interestingly, for the human cytomegalovirus (HCMV), small interfering RNA (siRNA)-mediated IFITM knockdown resulted in reduced infection and disturbed virus assembly (20). Varying results were obtained for Epstein-Barr virus (EBV), a gammaherpesvirus. While the initial entry of EBV was enhanced by overexpression of IFITM1 (21, 22), incorporation of IFITM2/3 into viral particles reduced the infectivity of progeny virus, whereas IFITM1 incorporation had no effect (23). Together, the literature on IFITM-mediated effects on the alphaherpesvirus HSV-1, the betaherpesvirus HCMV, and the gammaherpesvirus EBV indicate differences in the activity of IFITM proteins toward different herpesvirus subfamilies.

The Kaposi's sarcoma-associated herpesvirus (KSHV) and the related rhesus monkey rhadinovirus (RRV) belong to the gammaherpesvirus subfamily (24). KSHV is associated with Kaposi's sarcoma (KS), multicentric Castlemann's disease, primary effusion lymphoma (reviewed in reference 25), osteosarcoma (26), and KSHV inflammatory cytokine syndrome (KICS) (27). The incidence of KSHV-related disease and KSHV seroprevalence are low in industrial countries (28, 29), but KSHV represents a significant health burden in sub-Saharan Africa, where KSHV-related cancers are common (30, 31).

KSHV and RRV exhibit broad cell tropism *in vitro* (32, 33). Both viruses encode a set of glycoproteins (g) that mediate entry and are conserved among herpesviruses. Of these, gH, gL, and gB are the most extensively studied (reviewed in reference 34). KSHV and RRV enter many cell types through the interaction of the gH/gL complex with members of the ephrin receptor tyrosine kinase family (Ephs) (35–37) and, in the case of RRV, also with members of the plexin domain-containing protein family (38). KSHV also interacts with heparan sulfate and integrins (39–41). Entry of both viruses occurs mainly via endocytotic routes (33, 42–44). Following internalization, the viral membrane fuses with the host membrane. Several reports implicate the gH/gL complex together with gB as the minimal set of glycoproteins required for membrane fusion (38, 45, 46).

One study reported an enhancing role of IFITMs in the infection of the BJAB B cell line and human dermal microvascular endothelial cells (HMVEC-D) cells by KSHV, EBV, and herpes simplex virus 2 (HSV-2) (21). However, given the considerable differences between KSHV and RRV entry into B cells and different adherent cells (33, 36, 37), in particular since KSHV infection of B cell lines is, with a few exceptions, efficient only through cell-to-cell transfer (47–49), we hypothesized that IFITM-mediated restriction may be dependent on the nature of the target cell. Another question that we sought to address is whether IFITMs restrict RRV in human cells.

## RESULTS

**KSHV induces IFITM expression in A549 cells.** We first validated the specificity of the antibodies used in this study for Western blot analysis after directed expression (Fig. 1A). Next, we examined expression of IFITM proteins at baseline levels and after stimuli such as virus infection in the human lung epithelial cell line A549, which has been well characterized with regard to IFN signaling and IFITM expression (50–53). We infected the cells with KSHV BAC16 recombinant virus carrying a green fluorescent protein (GFP) reporter gene and RRV-YFP carrying a yellow fluorescent protein (YFP) reporter gene (Fig. 1B). Treatment with H<sub>2</sub>O and IFN- $\alpha$  served as negative and positive

F1

25/11/21 22:12 ArtID: DOI:10.1128/mBio.02113-21 CE: KGL-mar

IFITM-Mediated Restriction of KSHV and RRV

mBio

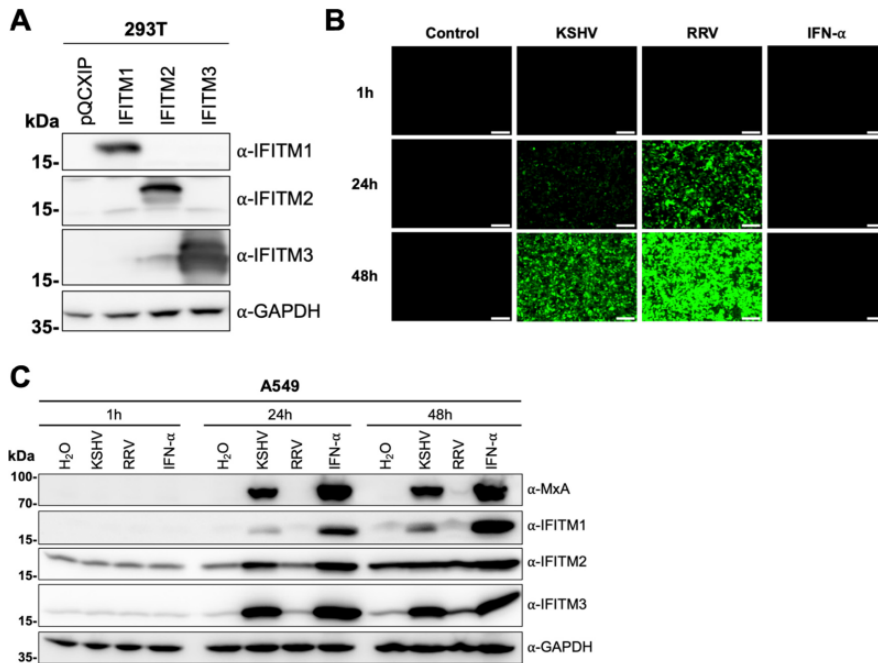


**FIG 1** KSHV induces IFITM1, IFITM2, and IFITM3 expression in A549 cells. (A) Western blot of 293T cells transfected with pQCXIP constructs to express IFITM1 to -3 or pQCXIP (empty vector). IFITMs were detected using the respective IFITM antibody, and GAPDH served as a loading control. (B and C) Fluorescence microscopy images (scale bar, 200  $\mu$ m) (B) and Western blot analysis (C) of A549 cells infected with KSHV-GFP or RRV-YFP or treated with H<sub>2</sub>O or IFN- $\alpha$  (5,000 U/ml) for the indicated time and harvested using SDS sample buffer. IFITM expression was detected with antibodies shown in panel A. MxA served as control for IFN-stimulated gene induction; GAPDH served as a loading control.

controls for IFITM induction, respectively. IFITM2 and IFITM3 were detected at low levels without IFN treatment, while IFITM1 and human myxovirus resistance protein 1 (MxA), another IFN-induced protein, were not detectable without stimulation (Fig. 1C). At the 1-h time point, neither treatment induced IFITM or MxA expression relative to the background. At the 24-h time point, induction over background levels of IFITM1, IFITM2, IFITM3, and MxA was observed in IFN- $\alpha$ -treated or KSHV-infected cells but not in RRV-infected cells. At 48 h, IFITM3 was also slightly induced by RRV, and IFITM2 induction relative to H<sub>2</sub>O treatment was barely discernible anymore. Basal IFITM expression also increased slightly over time after plating. In summary, KSHV-containing inoculum and IFN- $\alpha$  induced IFITM expression.

**Triple knockout of IFITM1/2/3 enhances KSHV and RRV infection of A549 cells and human foreskin fibroblasts (HFF).** Overexpression of IFITMs alters their subcellular localization (6; our observations), IFITMs are usually induced together, and recent studies report that IFITMs form homo- and hetero-oligomers (54–56) and might thus act synergistically. We therefore used CRISPR/Cas9 to generate triple IFITM1/2/3 knockout cells to study the effects of basal IFITM expression as well as IFN-induced IFITM expression on KSHV and RRV infection. We identified two single guide RNAs (sgRNAs) (sgIFITM1/2/3-a, sgIFITM1/2/3-b), which target the second exon of all three immune-related IFITMs (Fig. 2A and B). These sgRNAs were transduced together with Cas9 using the lentiCRISPRv2 system (57).

We chose the lung epithelial cell line A549 as an epithelial cell model. KSHV is occasionally detected in lung tissue (58), and A549 cells are well characterized with regard to IFITM-mediated restriction of different viruses (1, 9, 53). HFF were chosen as a

November/December 2021 Volume 12 Issue 6 e02113-21

mbio.asm.org 3

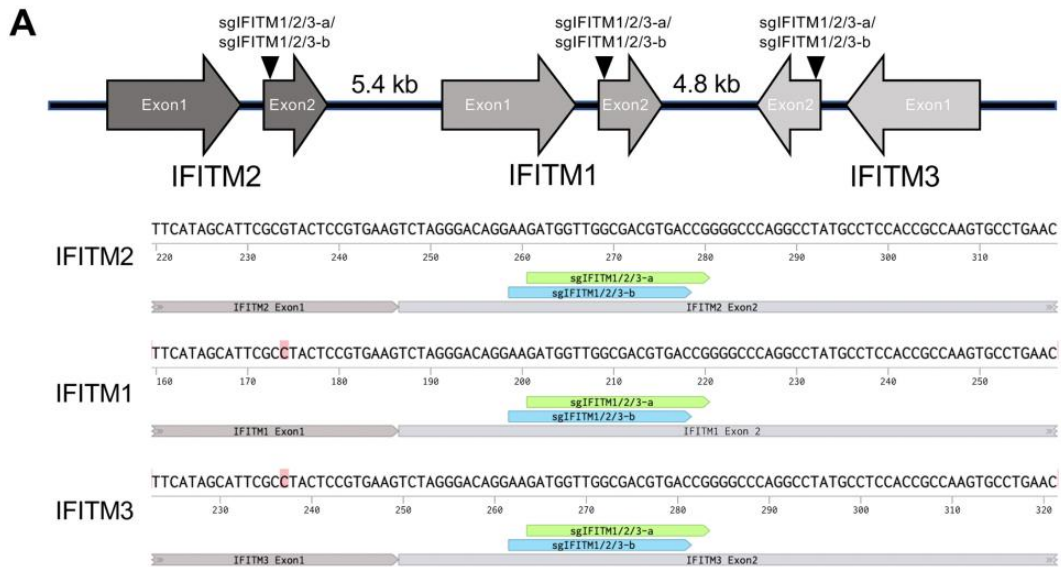
ID: vinayak.bhelekarTime: 22:12 Path: //mumnasprod/home\$/Vinay.Bhelekar\$/SM-MBIO210767



25/11/21 | 22:12 | ArtID: | DOI:10.1128/mBio.02113-21 | CE: KGL-mar

Hörnrich et al.

mBio



**B**

sgRNA	Target	Target-Sequence
sgNT-a	non-targeting	ATCGTTTCCGCTTAACGGCG
sgNT-b	non-targeting	TTCGCACGATTGCACCTTGG
sgIFITM1/2/3-a	IFITM1-IFITM3	GATGGTTGGCGACGTGACCG
sgIFITM1/2/3-b	IFITM1-IFITM3	AAGATGGTTGGCGACGTGAC

**FIG 2** Localization of the IFITM cluster on chromosome 11 in the human genome and sgRNAs used in this study. (A) Upper panel, schematic drawing (not to scale) of the localization of IFITM1, IFITM2, and IFITM3 on chromosome 11 in the human genome with target sites of sgRNAs targeting exon2 of IFITM1 to -3 (sgIFITM1/2/3-a, sgIFITM1/2/3-b). Lower panel, alignment of the target sites of sgIFITM1/2/3-a and sgIFITM1/2/3-b. (B) Sequences of sgRNAs used in this study.

fibroblast model, and human umbilical vein endothelial cells (HUVEC) as a model for endothelial cells. Knockout or substantial knockdown of IFITM1, IFITM2, and IFITM3 was achieved (Fig. 3A to C, right panels). Lentiviral particles (LP) encoding a GFP reporter gene pseudotyped with influenza A virus (IAV)-hemagglutinin (HA)/neuraminidase (NA) (IAV-LP) served as a positive control for IFITM-mediated restriction, while particles pseudotyped with IFITM-resistant amphotropic murine leukemia virus (MLV) envelope (MLV-LP) served as a negative control (1). Infections were performed with or without prior IFN- $\alpha$  stimulation. IFN- $\alpha$  treatment resulted in a significant reduction of KSHV, RRV, and IAV-LP infection in A549 cells (Fig. 3A, left panel). Both KSHV and RRV infection were enhanced in non-IFN- $\alpha$ -treated IFITM1/2/3 knockout A549 cells, indicating that basal IFITM levels or IFITM expression induced upon contact with the inoculum affect KSHV and RRV infection of A549 cells. In IFN- $\alpha$ -treated IFITM1/2/3 knockout cells, infection nearly reached levels

F3

November/December 2021 Volume 12 Issue 6 e02113-21

mbio.asm.org 4

ID: vinayak.bhelekarTime: 22:12I Path: //mumnasprod/home\$/Vinay.Bhelekar\$/SM-MBIO210767

25/11/21 | 22:12 | ArtID: | DOI:10.1128/mBio.02113-21 | CE: KGL-mar

IFITM-Mediated Restriction of KSHV and RRV

mBio

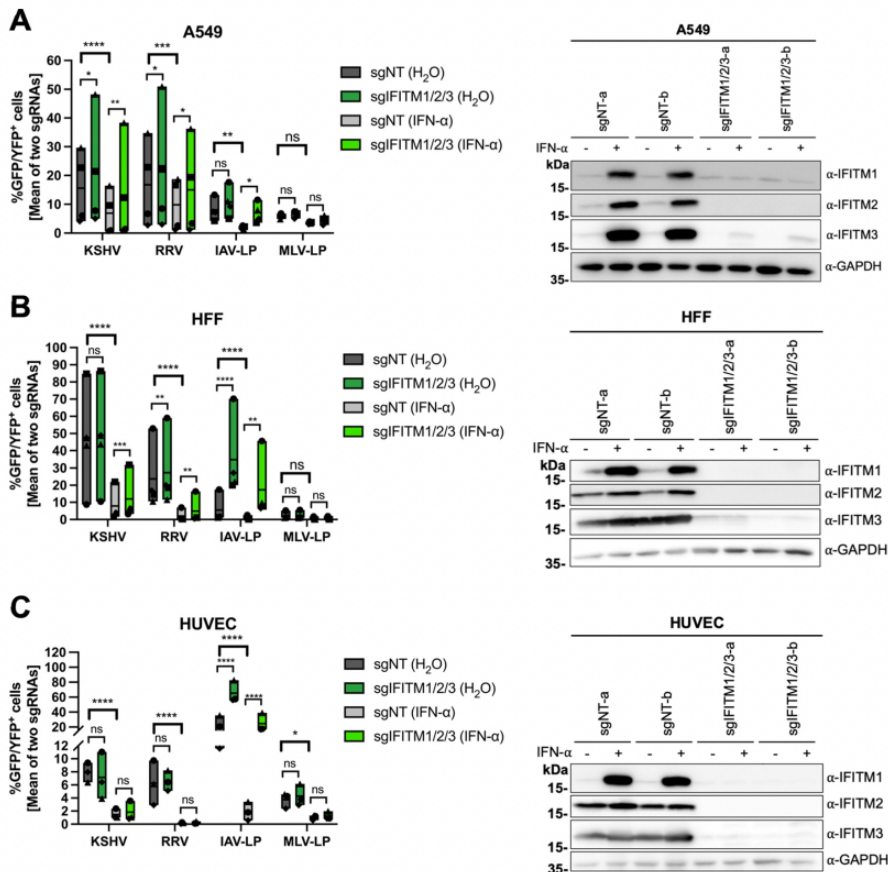


**FIG 3** IFITM1/2/3 triple knockout enhances KSHV and RRV infection in A549 cells and HFF. A549 cells (A), HFF (B), and HUVEC (C) were transduced with lentiviral vectors encoding Cas9 and the sgRNAs shown in Fig. 2. (A to C, left panels) IFITM knockout (sgIFITM1/2/3-a, sgIFITM1/2/3-b) or control (sgNT-a, sgNT-b) cells treated with IFN-α (5,000 U/ml) or H<sub>2</sub>O (control) and infected with KSHV-GFP, RRV-YFP, IAV lentiviral pseudotype (IAV-LP), or MLV lentiviral pseudotype (MLV-LP). Infection was measured using flow cytometry to detect expression of the fluorescent reporter gene. The graph shows individual data points representing averaged values for GFP<sup>+</sup>/YFP<sup>+</sup> cells of either two nontargeting (sgNT-a, sgNT-b) or IFITM1/2/3 knockout (sgIFITM1/2/3-a, sgIFITM1/2/3-b) transduced cells and floating bars representing the mean averaged from results of four independent experiments for A549 cells and HFF (A and B) and three independent experiments for HUVEC (C). Infections for each single experiment were performed in triplicate for each condition. Data points from the same experiment are labeled with identical symbols. The different sgRNAs were treated as biological replicates within each experiment. Statistical significance was determined by two-way analysis of variance (ANOVA), and *P* values were corrected for all possible multiple comparisons within one family by Tukey's method (nonsignificant [ns], *P* > 0.05; \*, *P* ≤ 0.05; \*\*, *P* ≤ 0.01; \*\*\*, *P* ≤ 0.001; \*\*\*\*, *P* ≤ 0.0001). (A to C, right panels) Representative Western blots of IFITM knockout (sgIFITM1/2/3-a or sgIFITM1/2/3-b) or control (sgNT-a or sgNT-b) cells treated with IFN-α (5,000 U/ml) or H<sub>2</sub>O. Indicated IFITM expression was detected with antibodies shown in Fig. 1A; GAPDH served as a loading control.

of control-treated sgNT-transduced cells. IAV-LP infection was dramatically increased upon IFITM1/2/3 knockout, while MLV-LP infection was not affected by IFITM1/2/3 knockout in A549 cells, in keeping with published results (1).

IFN-α pretreatment reduced KSHV and RRV infection of HFF more potently than infection of A549 cells (Fig. 3B, left panel). However, IFITM1/2/3 knockout in HFF enhanced KSHV infection only of IFN-α-treated cells, while RRV infection was slightly but significantly enhanced in both IFN-α and control-treated IFITM1/2/3 knockout cells. We observed relatively high basal IFITM2/3 expression in HFF, which was only



marginally increased by IFN- $\alpha$  (Fig. 3B, right panel). Infection of IFN- $\alpha$ -treated IFITM1/2/3 knockout HFF by KSHV or RRV did not reach levels of untreated sgNT-transduced cells, unlike what was observed with A549 cells, suggesting that IFITM-mediated restriction of KSHV and RRV infection plays a comparatively minor role in the overall IFN- $\alpha$ -mediated restriction of these two herpesviruses in HFF. The most potent effect of IFITM1/2/3 knockout was observed with IAV-LP infection, which was increased in both IFN- $\alpha$ - and control-treated cells. MLV-LP infection of HFF was not significantly affected by IFITM1/2/3 knockout.

Like HFF, HUVEC expressed IFITM2 and IFITM3 at high basal levels (Fig. 3C, right panel). IFN- $\alpha$  treatment of HUVEC resulted in a reduction of KSHV infection and an even more pronounced reduction of RRV infection (Fig. 3C, left panel). However, IFITM1/2/3 knockout had no significant effect on KSHV or RRV infection. Again, IAV-LP infection was strongly enhanced by IFITM1/2/3 knockout in both IFN- $\alpha$ - and control-treated HUVEC, while MLV-LP was not affected.

Overall, these results demonstrate IFITM-mediated restriction of KSHV and RRV infection of A549 cells and HFF but not HUVEC.

**IFITM1 overexpression reduces KSHV and RRV infection in a cell-dependent manner.** We next investigated the effect of individual IFITMs through directed expression by retroviral transduction (Fig. 4A to D) and included the following additional cell lines: (i) 293T cells as another cell line of either epithelial or neuroendocrine origin (59) and (ii) SLK cells, a clear renal carcinoma cell line (60) that is an established model for KSHV infection and propagation (61).

Overexpression of IFITM1 in A549 reduced KSHV and RRV infection by over 50%, whereas overexpression of IFITM2 and IFITM3 resulted in only a nonsignificant reduction (Fig. 4A, left panel), identifying IFITM1 as the IFITM that restricts KSHV and RRV in A549 cells. In agreement with the results in IFITM1/2/3 knockout experiments and published results (1), IAV-LP infection was reduced by all IFITMs, most prominently by IFITM3, and infection of MLV-LP was not affected. As directed expression of IFITM3 led to a slight if nonsignificant reduction in KSHV/RRV infection, we tested whether this effect would change through the introduction of well-characterized mutations into IFITM3 that change its subcellular localization from predominantly endosomal to a broader distribution (62, 63). While in this set of experiments in A549 cells (see Fig. S1A), effects were of similar magnitude as before, the ~30% reduction of KSHV infection by IFITM3 reached significance. Interestingly, this mild effect on KSHV infection was reduced by deletion of amino acids 1 to 21 ( $\Delta 1-21$ ) or by Y20A mutation in the N-terminal domain (62) or by the 43AS mutation (amino acids 43 to 48 changed to alanines) in the conserved intracellular loop (63). RRV infection, in contrast, was inhibited by IFITM3 bearing the mutations  $\Delta 1-21$  or Y20A but not by IFITM3 wild type (wt) or the 43AS mutant. Taken together, these results clearly implicate IFITM3's subcellular sorting motifs as major determinants of activity in particular against RRV.

IFITM1 overexpression also reduced RRV and KSHV infection of HFF (Fig. 4B, left panel), but the effect did not reach statistical significance, mostly because of a rather high pooled variance in this set of experiments, which may reflect the primary nature of HFF combined with comparatively high constitutive IFITM expression. In addition, we observed a nonsignificant but noticeable enhancement of RRV infection in IFITM2/3-overexpressing HFF. Again, these observations are in agreement with the effects observed in IFITM1/2/3 knockout HFF. While IAV-LP infection was reduced in HFF, MLV-LP infection was enhanced by overexpression of all IFITMs, significantly for IFITM2 and IFITM3.

A trend similar to that observed in A549 cells was also observed in 293T cells (Fig. 4C, left panel): IFITM1 overexpression reduced KSHV and RRV infection, although not significantly for RRV. MLV-LP infection was slightly increased by overexpression of IFITM3 in 293T cells.

In HUVEC, IFITM1 and IFITM3 overexpression also slightly decreased KSHV and RRV infection (Fig. S1B). Surprisingly, we also observed inhibition of MLV-LP by IFITM1 and -2 in this setting. Further, we noticed that HUVEC transduced to overexpress IFITMs exhibited a highly abnormal morphology (Fig. S1C).

25/11/21 22:12 ArtID: DOI:10.1128/mBio.02113-21 CE: KGL-mar

IFITM-Mediated Restriction of KSHV and RRV

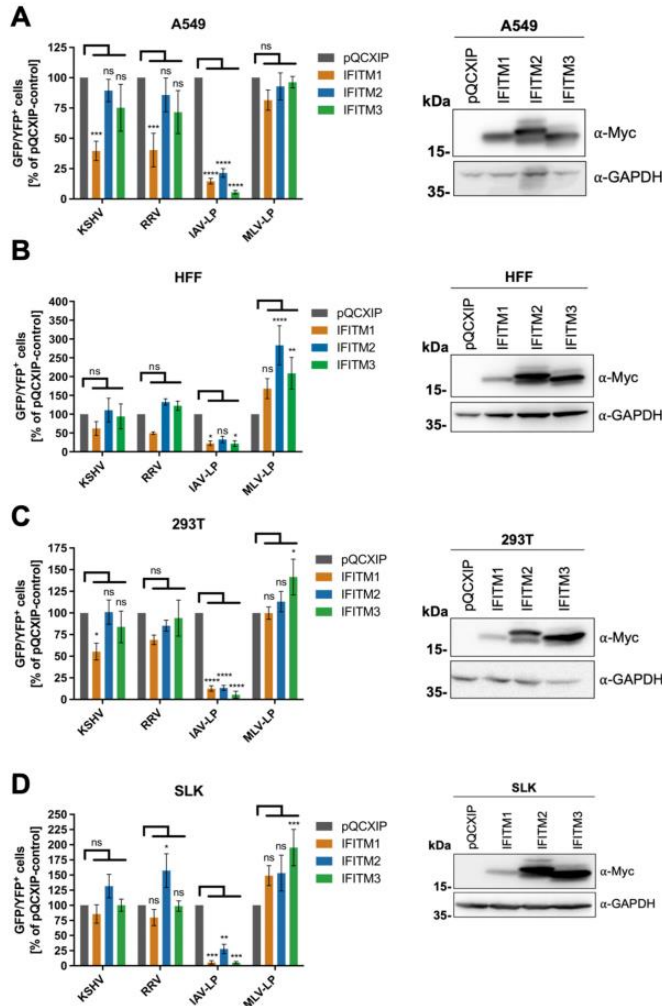


**FIG 4** Overexpression of IFITM1 inhibits KSHV and RRV infection in a cell-specific manner. A549 cells (A), HFF (B), 293T cells (C), and SLK cells (D) were transfected with pQCXIP constructs to express IFITM1-3 or pQCXIP (empty vector). (A to D, left panels) IFITM-overexpressing cells were infected with KSHV-GFP, RRV-YFP, IAV lentiviral pseudotype (IAV-LP), or MLV lentiviral pseudotype (MLV-LP). Infection was measured using flow cytometry to detect expression of the fluorescent reporter genes. The data show values normalized to pQCXIP empty vector, which was set to 100%, and the error bars represent the standard error of the mean of results of four independent experiments, each performed in triplicate. Statistical significance was determined by ordinary two-way ANOVA, and *P* values were corrected for multiple comparisons by Dunnett's method (ns, *P* > 0.05; \*, *P* ≤ 0.05; \*\*, *P* ≤ 0.01; \*\*\*, *P* ≤ 0.001; \*\*\*\*, *P* ≤ 0.0001). (A to C, right panels) Representative Western blots of IFITM-overexpressing cells. Expression of myc-tagged IFITMs was determined using anti-myc antibody; GAPDH served as a loading control.

A different observation was made in SLK cells (Fig. 4D, left panel), where neither IFITM1 nor IFITM3 overexpression resulted in reduced KSHV or RRV infection. Again, IFITM2 overexpression in SLK cells slightly enhanced KSHV infection and significantly enhanced RRV infection. An enhancement of infection by all IFITMs was observed with MLV, significantly for IFITM3.

November/December 2021 Volume 12 Issue 6 e02113-21

mbio.asm.org 7

ID: vinayak.bhelekarTime: 22:12 Path: //mumnasprod/home\$/Vinay.Bhelekar\$/SM-MBIO210767



25/11/21 | 22:12 | ArtID: | DOI:10.1128/mBio.02113-21 | CE: KGL-mar

Hörnich et al.

mBio®

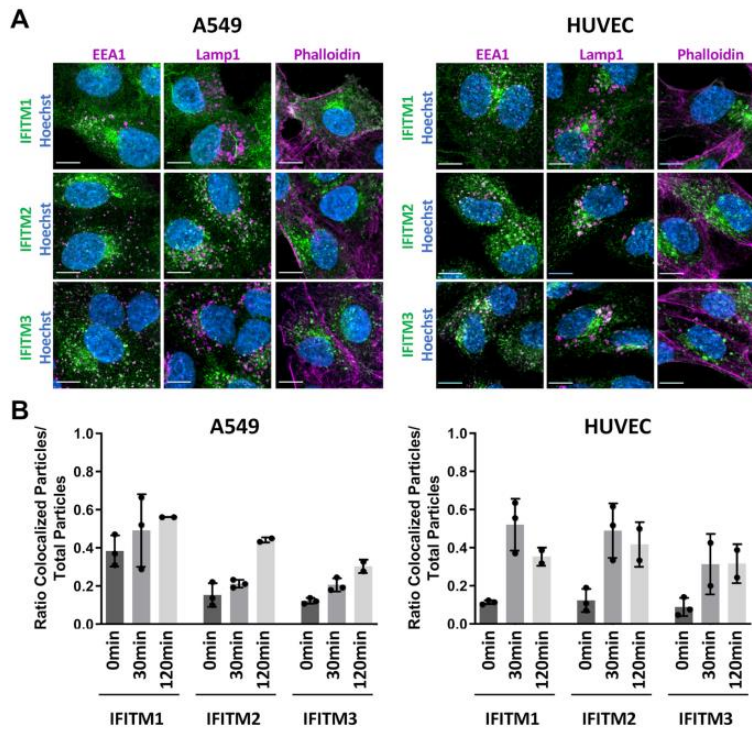


**FIG 5** Kinetics of colocalization of KSHV and IFITMs differ between HUVEC and A549 cells. (A) Confocal microscopy images of A549 cells (left panel) and HUVEC (right panel) treated with IFN- $\alpha$  (5,000 U/ml) for 16 h and stained with IFITM1, IFITM2, or IFITM3 antibody (all green). Costaining was performed with antibodies to EEA1, LAMP1, or phalloidin conjugate (all magenta) and Hoechst stain (blue). Scale bars, 10  $\mu$ m. (B) A549 cells (left panel) and HUVEC (right panel) were treated with IFN- $\alpha$  (5,000 U/ml) for 16 h and infected with KSHV\_mNeon-orf65. Colocalization of IFITM and mNeon signals was quantified. Data are shown as individual biological replicates together with the mean, and error bars represent the standard deviation. Per biological replicate and time point, at least three images were analyzed.

Taken together, our IFITM overexpression experiments corroborated the results observed in our IFITM1/2/3 knockout experiments and a cell-specific activity of individual IFITMs toward KSHV and RRV. Even if recombinant overexpression in HUVEC had some effect, this does not reflect the situation at endogenous expression levels. Restriction of the typically nonrestricted MLV-LP and drastically aberrant morphology with a “foamy” appearance (Fig. S1C) suggest that recombinantly overexpressed IFITMs in HUVEC, which naturally already express IFITM2 and IFITM3 at high levels, may lead to visibly distorted cellular membranes and vesicles and nonspecific effects on infection. Furthermore, IFITM1 was identified as the major contributor to IFITM-mediated restriction of KSHV and RRV.

**KSHV entry pathways and colocalization with IFITMs differ between A459 cells and HUVEC.** IFITM localization was reported to play a critical role in their antiviral effect (64, 65). For the highly restricted IAV, IFITM3-mediated restriction might be partially explained by the observation that IAV specifically colocalizes with IFITM3-positive vesicles (15, 53). As expected, we observed different subcellular localizations of IFITM1, IFITM2, and IFITM3 in both IFN- $\alpha$ -treated A549 cells and HUVEC (Fig. 5A; Fig. S2). IFITM2 and IFITM3 partially colocalized with the early endosome marker EEA1 and with the endolysosomal marker LAMP1, while IFITM1 localized to the plasma membrane and was distributed more toward the perimeter of the cell. IFITM1 was also found

F5

November/December 2021 Volume 12 Issue 6 e02113-21

mbio.asm.org 8

ID: vinayak.bhelekarTime: 22:12| Path: //mumnasprod/home\$/Vinay.Bhelekar\$/SM-MBIO210767

25/11/21 22:12 ArtID: DOI:10.1128/mBio.02113-21 CE: KGL-mar

IFITM-Mediated Restriction of KSHV and RRV



colocalized with EEA1 and LAMP1, particularly in HUVEC, but did generally show a less pronounced vesicular localization than IFITM2/IFITM3. As we observed IFITM1-mediated inhibition of KSHV and RRV infection in A549 cells, we examined how these viruses enter A549 by probing different entry pathways with inhibitors (Fig. S3). IFITM1 was reported to restrict viruses that directly fuse at the plasma membrane (18). KSHV and RRV infection of A549 cells was sensitive to bafilomycin A1 (Fig. S3A), indicating dependence on vesicular acidification, and were sensitive to methyl- $\beta$ -cyclodextrin (MBCD) (Fig. S3B), commonly believed to indicate a role for cholesterol-rich membrane domains (66, 67). 5-(*N*-Ethyl-*N*-isopropyl)amiloride (EIPA; an inhibitor of macropinocytosis [68]) had at best a marginal effect on KSHV and RRV on A549 cells, suggesting that neither KSHV nor RRV enter A549 cells predominantly via macropinocytosis. KSHV infection of HUVEC on the other hand was sensitive to EIPA (Fig. S3C), in agreement with published data (42) and suggesting macropinocytotic entry, whereas RRV infection of HUVEC was not EIPA sensitive. It should be noted that EIPA and MBCD at the first significantly effective concentrations caused minor yet significant changes in cellular ATP content (up to  $-20\%$ ) in our cell viability assay (Fig. S3D).

AQ: D

We next analyzed colocalization of KSHV particles with IFITMs in A549 cells and HUVEC. We utilized a KSHV\_mNeon-orf65, which is tagged with mNeonGreen at the capsid protein orf65, to visualize virions in IFN- $\alpha$ -treated cells at different time points (Fig. 5B; Fig. S4). KSHV\_mNeon-orf65 particles were detectable at the perimeter at the 0-min time point and were detected inside the cells from the 30-min time point on. Some particles reached the nucleus at the 120-min time point. As IFITMs are widely distributed throughout the cell, partial overlap with KSHV\_mNeon-orf65 particles was observed for all IFITMs, most prominently at later time points. While colocalization with all IFITMs followed roughly the same pattern over time in HUVEC, A549 cells exhibited differences between IFITM1 and IFITM2/3. In A549 cells, KSHV capsids were found to colocalize to the same degree with IFITM1 at all time points, while HUVEC showed a considerably lower extent of mNEON-IFITM1 overlap at the 0-min time point. While some particles localized to areas of high intensity in the IFITM staining, KSHV\_mNeon-orf65 particles were also frequently found in regions with overall lower IFITM signal. These areas were often adjacent to IFITM-positive areas, which might be compatible with the luminal spaces of large vesicles.

#### KSHV and RRV glycoprotein-mediated cell-cell fusion is reduced by IFITMs.

IFITMs were reported to modulate overall membrane fusogenicity and thereby entry of viral particles (11, 12, 69). We therefore utilized a cell-cell fusion assay to determine whether KSHV and RRV glycoprotein-mediated fusion activity is modulated by IFITMs. 293T effector cells were transfected with KSHV gH/gL or RRV gH/gL together with RRV gB and a plasmid encoding a VP16-Gal4 transactivator fusion protein. RRV gB was used because KSHV gB does not allow for efficient cell-cell fusion (46). Because of the low fusion activity of RRV gH/gL+gB, cell-cell fusion was analyzed after 48 h to reach robust levels of fusion activity (Fig. S5). Transfected effector cells were added to IFN- $\alpha$ -treated A549 IFITM1/2/3 knockout cells transduced with a lentiviral Gal4-driven TurboGFP-luciferase reporter construct or 293T cells transfected to express IFITM1, IFITM2, or IFITM3 and a Gal4-driven TurboGFP-luciferase reporter construct. Luciferase activity was measured as a readout for fusion.

F6

Treatment with IFITM-targeting sgRNAs resulted in an increase of KSHV and RRV gH/gL/gB-mediated cell-cell fusion compared to nontargeting controls (Fig. 6A). Viral glycoprotein expression and IFITM1/2/3 knockout in target cells was confirmed by Western blotting (Fig. 6B). Under conditions of recombinant overexpression, all three IFITMs were capable of reducing KSHV and RRV gH/gL/gB-mediated cell-cell fusion, with IFITM1 being the most effective (Fig. 6C). To exclude the possibility that the inhibition of KSHV and RRV glycoprotein-mediated cell-cell fusion occurs in response to changes in cell surface protein composition upon IFITM1/2/3 knockout, we measured cell surface expression of a set of selected cell surface receptors. Cell surface expression of the KSHV receptors EphA2 and integrin  $\alpha$ V as well as transferrin receptor (TrfR)

November/December 2021 Volume 12 Issue 6 e02113-21

mbio.asm.org 9

ID: vinayak.bhelekarTime: 22:12 Path: //mumnasprod/home\$/Vinay.Bhelekar\$/SM-MBIO210767



25/11/21 | 22:12 | ArtID: | DOI:10.1128/mBio.02113-21 | CE: KGL-mar

Hörnrich et al.

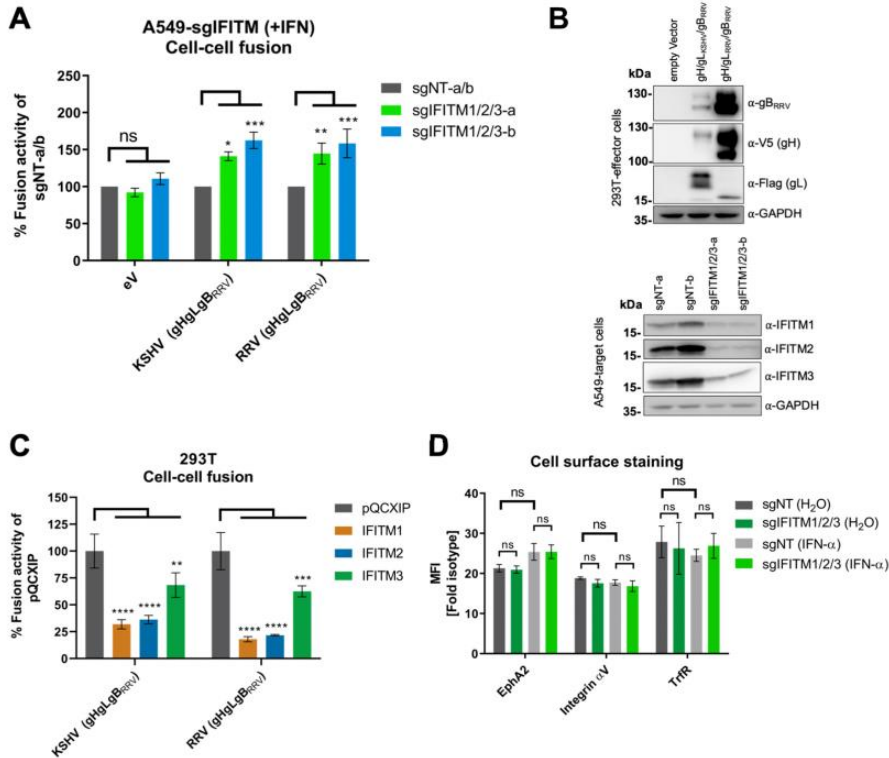


**FIG 6** IFITMs inhibit KSHV and RRV glycoprotein-mediated cell-cell fusion. (A) Cell-cell fusion assay. Effector cells (293T cells transfected with either empty vector [eV] or expression plasmids for the indicated viral glycoproteins together with Vp16-Gal4 expression plasmid) were added to target cells (A549 cells transfected with a Gal4-driven TurboGFP-luciferase construct and the respective CRISPR/Cas9 sgRNA construct), which had been preincubated for 16 h with IFN- $\alpha$  (5,000 U/ml). After 48 h, luciferase activity was measured. Values were normalized to the mean of the two nontargeting controls, sgNT-a and sgNT-b (sgNT-a/b), which was set to 100%, for each experiment. Error bars represent standard errors of the mean of the results of four independent experiments, each performed in triplicate. Statistical significance was determined by two-way ANOVA; *P* values were corrected for multiple comparisons by Dunnett's method (ns, *P* > 0.05; \*, *P* ≤ 0.05; \*\*, *P* ≤ 0.01; \*\*\*, *P* ≤ 0.001; \*\*\*\*, *P* ≤ 0.0001). (B) The expression of proteins in 293T effector and A549 target cells after cocultivation was analyzed by Western blotting from lysates harvested for determination of luciferase activity shown in panel A using the indicated antibodies. GAPDH served as a loading control. (C) Cell-cell fusion assay. Effector cells (293T cells transfected with expression plasmids for the indicated viral glycoproteins together with Vp16-Gal4 expression plasmid) were added to target cells (293T cells transfected with a Gal4-driven TurboGFP-luciferase construct and the respective pQCXIP-IFITM construct). After 48 h, luciferase activity was measured. Values were averaged from three independent experiments, each performed in triplicate. The data were normalized to empty vector control pQCXIP, which was set to 100%, and error bars represent the standard deviation. Statistical significance was determined by two-way ANOVA; *P* values were corrected for multiple comparisons by Dunnett's method (ns, *P* > 0.05; \*, *P* ≤ 0.05; \*\*, *P* ≤ 0.01; \*\*\*, *P* ≤ 0.001; \*\*\*\*, *P* ≤ 0.0001). (D) A549 cells were transfected with a lentiviral vector encoding Cas9 and sgRNAs shown in Fig. 2. IFITM knockout (sgIFITM1/2/3-a, sgIFITM1/2/3-b) or control (sgNT-a and sgNT-b) cells treated with IFN- $\alpha$  (5,000 U/ml) or H<sub>2</sub>O (control) were stained for cell surface expression of the indicated proteins. The graph shows fold values for the mean fluorescence intensity over that of the isotype control averaged from two nontargeting (sgNT-a, sgNT-b) or IFITM1/2/3 knockout (sgIFITM1/2/3-a, sgIFITM1/2/3-b) transfected cells from one representative experiment performed in triplicate. Error bars represent the standard deviation. Statistical significance was determined by two-way ANOVA; *P* values were corrected for multiple comparisons by Tukey's method (ns, *P* > 0.05; \*, *P* ≤ 0.05; \*\*, *P* ≤ 0.01; \*\*\*, *P* ≤ 0.001; \*\*\*\*, *P* ≤ 0.0001).

AQ: K

remained unchanged upon IFITM1/2/3 knockout (Fig. 6D). This suggests that IFITMs reduce cell-cell fusion through a mechanism distinct from receptor regulation.

**DISCUSSION**

Differences in the activity of IFITMs against several members of the herpesvirus family have already been reported (18–21, 23). Here, we report that human IFITM1 inhibits

25/11/21 22:12 ArtID: DOI:10.1128/mBio.02113-21 CE: KGL-mar

IFITM-Mediated Restriction of KSHV and RRV



the entry of KSHV and of the closely related rhesus macaque virus RRV in a cell-specific manner. We identified inhibition of membrane fusion as a potential mechanism through which IFITMs can modulate KSHV and RRV infection.

Combined knockout of all three IFITMs enabled us to study IFITM-mediated restriction through loss of function at expression levels that are induced through IFN signaling and free from potential artifacts through overexpression-induced mislocalization. Our approach revealed that KSHV and RRV infections are enhanced upon IFITM1/2/3 knockout in A549 cells and HFF but not in HUVEC. Similarly, overexpression of individual IFITMs did not result in measurable inhibition, e.g., in SLK cells, even though they were highly effective against IAV-LP. This finding may be explained by differences in entry routes that KSHV and RRV utilize to enter these different cells. KSHV was shown to enter HFF (70) and RRV rhesus fibroblasts (33, 44) via clathrin-mediated endocytosis, whereas KSHV enters HUVEC via macropinocytosis (see Fig. S3 in the supplemental material) (42). In contrast, KSHV infects A549 cells via a pH-dependent but largely macropinocytosis-independent pathway, as indicated by sensitivity to bafilomycin A but not to EIPA (Fig. S3). While most viruses that are restricted by IFITMs enter cells via clathrin- or caveolin-mediated endocytosis, only Ebola and Marburg viruses are restricted and enter their target cells predominantly via macropinocytosis (reviewed in reference 71). However, Ebola and Marburg virus glycoproteins are activated by endosomal cathepsins, which are found mainly in endolysosomal vesicles that also contain IFITMs (reviewed in references 72 and 73). In contrast, KSHV might already fuse in acidified IFITM-negative macropinocytotic compartments and thereby avoid IFITM restriction in HUVEC, in line with the observation that even overexpression of IFITMs in HUVEC has only a minor effect on KSHV infection (Fig. S1B) and knockout has no effect at all (Fig. 3C). A question that remains unanswered is why RRV is not affected by IFITMs in HUVEC at endogenous expression levels. RRV clearly does not enter these cells through the same EIPA-sensitive pathway that KSHV uses but also does not underlie the same restriction that IAV-LP does (Fig. 3 and 4; Fig. S3). Although IFITM1/2/3 knockout enhanced KSHV and RRV infection in A549 cells and HFF, the overall contribution to the IFN-mediated block to infection was different. In HFF, the enhancement was mainly observable in IFN- $\alpha$ -treated cells, while in A549 cells, the enhancement was also observable in non-IFN-treated cells. In A549, the IFITM1/2/3 knockout-mediated enhancement practically cancelled out the IFN- $\alpha$ -mediated inhibition of KSHV and RRV infection, similar to what was observed for the highly restricted IAV-LP. Despite minor differences, IFITM1/2/3 knockout similarly impacted KSHV and RRV infection, compatible with a broadly acting mechanism like decreasing membrane fusogenicity. Vice versa, it was also shown that primate IFITMs are effective against human viruses (74, 75), in line with the high degree of conservation of IFITMs in primate species (76, 77).

Overexpression of individual IFITMs in different cells revealed IFITM1 as the major contributor to IFITM-mediated restriction of KSHV and RRV. Similar to our observations, an antiviral effect of IFITM1 in A549 cells was also identified for the alphaherpesvirus HSV-1 in IFITM1 overexpression and siRNA-mediated knockdown experiments (18), which suggests broad activity of IFITM1 against herpesviruses. Of note, an effect of IFITM1 on KSHV infection has already been described by Hussein and Akula; however, in contrast to our study, their study reported that infection by KSHV, EBV, and HSV-2 was enhanced upon overexpression of IFITM1 in the BJAB B-cell line and in HMVEC-D cells (21). While we did not observe this phenomenon in the cells analyzed in this study, our observations of cell-specific antiviral activity do not rule out the possibility that in some cells infection might actually be enhanced by IFITM1 expression. In line with this notion, overexpression of IFITM2 resulted in a mild enhancement of RRV infection in SLK cells and HFF (Fig. 4). We observed a small reduction of KSHV infection of A549 cells as well by IFITM3 overexpression, which reached significance in one set of experiments (Fig. S1A). This effect was reduced when the Yxx $\Phi$  endocytic sorting motif ( $\Delta$ 1–21, Y20A) or the 43AS motif of IFITM3 was mutated (Fig. S1A). In contrast, RRV infection was significantly inhibited by overexpression of IFITM3 Y20A mutants

November/December 2021 Volume 12 Issue 6 e02113-21

mbio.asm.org 11

ID: vinayak.bhelekarTime: 22:12 Path: //mumnasprod/home\$/Vinay.Bhelekar/\$M-MBIO210767



and IFITM3 Y20A and  $\Delta 1-21$  mutants but not wt IFITM3, in this case clearly implicating these sorting signals and by extension localization of IFITMs in their mode of action. Given the higher susceptibility of KSHV than of RRV to bafilomycin A1 (Fig. S3), we speculate that a portion of RRV particles fuses at more peripheral sites, where infection is partially restricted by IFITM1 and IFITM3 Y20A and  $\Delta 1-21$  mutants. IFITM-mediated inhibition of KSHV or RRV infection was less pronounced than inhibition of IAV glycoprotein-driven entry. Several groups reported that IAV colocalized strongly with IFITM3 (15, 53, 78). We were unable to observe a pronounced colocalization of IFITMs with KSHV particles in the sense that many KSHV particles accumulate at regions of high IFITM intensity. However, we observed a clear difference in the colocalization of KSHV viral particles and IFITM1 in A549 cells and HUVEC at the 0-min time point, although the overall IFITM localization was similar in these cells (Fig. 5; Fig. S2). This observation fits well with the observation of different entry routes that KSHV utilizes to enter A549 cells and HUVEC and might explain the difference in susceptibility of KSHV toward IFITM1 between these two different cells. Interestingly, KSHV\_mNeon-orf65 particles that entered the cell were frequently observed in regions with low IFITM signal (Fig. S4). While these findings argue against concentration of IFITMs at viral particles, they would be compatible with indirect mechanisms of action such as rerouting of endocytotic pathways or reduction of membrane fusogenicity.

Mechanistically, we found that IFITMs modulate KSHV and RRV glycoprotein-induced membrane fusion at IFN- $\alpha$ -induced levels. Overexpression of IFITM1, IFITM2, and IFITM3 revealed that all three IFITMs can in principle reduce the KSHV and RRV glycoprotein-induced cell-cell fusion to a different degree. It should be noted that overexpression of IFITMs leads to abnormal localization, thereby potentially broadening activity. This supports the theory that all IFITMs are, in principle, capable of restricting fusion (6, 16, 79), which might be counteracted by avoidance of IFITM-positive compartments. In line with our experiments, IFITM overexpression was reported to reduce the fusion activity of other viral fusion proteins, including the IAV-HA (12, 13, 15) and severe acute respiratory syndrome coronavirus 2 spike (80) proteins as well as the glycoprotein of the otherwise non-restricted Lassa virus (15). Although cell-cell fusion does not universally mirror virus-cell fusion (81), our findings support a model of IFITM1 rendering the membrane less fusogenic. A general impact of IFITMs on membrane properties is also supported by a report that IFITMs inhibit trophoblast fusion (69). While our approach of a triple knockout was also intended to identify potential synergism between the three IFITMs, it did not do so. In HFF, IFITM1 might even counteract the mild enhancing effect that IFITM2 had on RRV infection (Fig. 4 B). Overexpression of IFITM1 was sufficient to effect inhibition with a similar magnitude as the enhancement that was observed after knockout. In light of our results and a recent report that IFITM3 blocks the IAV fusion process by increasing membrane stiffness (13), one might speculate that the three IFITMs exert their inhibitory activity through a similar mechanism at different locations.

Comparison of our experimental results in overexpression systems with those at interferon-induced expression levels and knockout of the three IFITMs allow a number of conclusions: (i) a significant discrepancy exists between results using gene knockout versus retroviral vector-driven overexpression in HUVEC; (ii) overexpression of IFITMs results in clearly aberrant morphology of HUVEC; and (iii) overexpression results in inhibition of MLV-LP, which is typically not restricted (2). These findings together with previous reports of mislocalization upon overexpression (6) and our finding that recombinant expression of the endosomal IFITM2 and IFITM3 results in inhibition of cell-cell fusion, which is strongly counterintuitive, suggest that results relying on overexpression of single IFITMs should be interpreted with caution. A recent study reported similar findings for SARS-CoV-2 (82). Gene knockout or knockdown may be essential to draw conclusions on function at naturally occurring expression levels.

Entry driven by the HA and NA glycoproteins of IAV, a respiratory pathogen, was far more potently restricted by IFITMs in fibroblasts and endothelial cells, particularly at constitutive expression levels, than in A549 lung epithelial cells. KSHV and likely RRV (83) are

25/11/21 22:12 ArtID: DOI:10.1128/mBio.02113-21 CE: KGL-mar

IFITM-Mediated Restriction of KSHV and RRV

AQ: L **TABLE 1** Cell lines

Cell line or type <sup>a</sup>	Origin
293T cells	Kind gift from Vladan Rankovic, Göttingen, Germany, and originally purchased from the ATCC
A549 cells	Laboratory of Stefan Pöhlmann, German Primate Center–Leibniz Institute for Primate Research, Göttingen, Germany
SLK cells	RRID:CVCL_9569; NIH AIDS Research and Reference Reagent program
HFF	Laboratory of Klaus Korn, Universitätsklinikum Erlangen, Institute for Clinical and Molecular Virology, Erlangen, Germany
RF	Laboratory of Rüdiger Behr, German Primate Center–Leibniz Institute for Primate Research, Göttingen, Germany
HUVEC	PromoCell
iSLK cells	Kind gift from Don Ganem (61)

<sup>a</sup>HFF, human foreskin fibroblasts; RF, rhesus monkey fibroblasts; HUVEC, human vascular endothelial cells.

endotheliotropic viruses and were restricted in lung epithelial cells but not endothelial cells. This suggests that IFITMs, which are constitutively expressed at high levels in HUVEC and fibroblasts, constitute a major line of defense against disseminated infection of extrapulmonary tissues by the respiratory pathogen IAV and that KSHV and RRV may have evolved to avoid IFITM-mediated restriction in their biological niche.

### MATERIALS AND METHODS

T1 **Cell culture.** All cell lines in this study (Table 1) were incubated at 37°C and 5% CO<sub>2</sub> and cultured in Dulbecco's modified Eagle medium, high glucose, GlutaMAX, 25 mM HEPES (Thermo Fisher Scientific) supplemented with 10% fetal calf serum (FCS; Thermo Fisher Scientific) and 50 µg/ml gentamicin (PAN-Biotech) (D10) except for HUVEC, which were maintained in standard endothelial cell growth medium 2 (PromoCell), and iSLK cells, which were maintained in D10 supplemented with 2.5 µg/ml puromycin (InvivoGen) and 250 µg/ml G418 (Carl Roth). IFN-α treatment was performed by supplementing the respective culture medium with IFN-α 2b (Sigma; 5,000 U/ml). For seeding and subculturing of cells, the medium was removed, and the cells were washed with phosphate-buffered saline (PBS; PAN-Biotech) and detached with trypsin (PAN-Biotech). All transfections were performed using polyethylenimine (PEI; Polysciences) at a 1:3 ratio (mg DNA/mg PEI) mixed in Opti-MEM (Thermo Fisher Scientific). Cytotoxicity was measured using the CellTiter-Glo luminescent cell viability assay (Promega) according to the manufacturer's instructions.

AQ: E  
AQ: F  
T2 **Retroviral vectors and pseudotyped lentiviral particles.** Retroviruses, lentiviruses, and lentiviral pseudotypes were produced by PEI-mediated transfection of 293T cells (plasmids are listed in Table 2). For retrovirus production, plasmids encoding gag/pol, pMD2.G encoding VSV-G, and the respective pQCXIP constructs were transfected (ratio, 1.6:1:1.6). For production of lentiviruses used for transduction, psPAX2 encoding gag/pol, pMD2.G encoding VSV-G, and the respective lentiviral construct, Gal4-driven TurboGFP-luciferase reporter lentivirus (AX526) or plentiCRISPRv2, were used (ratio, 2.57:1:3.57). For lentiviral pseudotypes psPAX2, pLenti CMV GFP Neo and expression plasmids for pCAGGS IAV\_WSN-HA and pCAGGS IAV\_WSN-NA for IAV-LP or paMLV\_env for MLV-LP were used (ratio, 1:1.4:2.4). Viruses were harvested twice, 24 to 48 h and 72 to 96 h after transfection, passed through a 0.45-µm CA filter, and frozen at –80°C. Transduction was performed by adding retroviruses and lentiviruses to cells for 48 h.

**TABLE 2** Plasmids

Plasmid	Source	Reference/identifier
psPAX2	Addgene (kind gift from Didier Trono)	Addgene no. 12260
VSV-G (pMD2.G)	Addgene (kind gift from Didier Trono)	Addgene no. 12259
plentiCRISPRv2	Addgene (kind gift from Feng Zhang)	Addgene no. 52961 (57)
gag/pol	Addgene (kind gift from Tannishtha Reya)	Addgene no. 14887
pLenti CMV GFP Neo	Addgene (kind gift from Eric Campeau and Paul Kaufman)	Addgene no. 17447
AX526 (Gal4-driven TurboGFP-luciferase reporter lentivirus)	Laboratory of Alexander Hahn	38
Gal4-TurboGFP-Luc (Gal4-driven TurboGFP-luciferase reporter plasmid)	Laboratory of Alexander Hahn	81
Vp16-Gal4	Laboratory of Alexander Hahn	81
pCAGGS IAV_WSN-HA	Laboratory of Michael Farzan	3
pCAGGS IAV_WSN-NA	Laboratory of Stefan Pöhlmann	3
paMLV_env	Laboratory of Michael Farzan	3
pQCXIP	Laboratory of Stefan Pöhlmann	3
pQCXIP-IFITM1	Laboratory of Stefan Pöhlmann	3
pQCXIP-IFITM2	Laboratory of Stefan Pöhlmann	3
pQCXIP-IFITM3	Laboratory of Stefan Pöhlmann	3
pQCXIP-IFITM3-Δ1-21	Laboratory of Stefan Pöhlmann	
pQCXIP-IFITM3-Y20A	Laboratory of Stefan Pöhlmann	
pQCXIP-IFITM3-43AS	Laboratory of Stefan Pöhlmann	
pEPkan-S	Addgene (kind gift from Nikolaus Osterrieder)	Addgene no. 41017

November/December 2021 Volume 12 Issue 6 e02113-21

mbio.asm.org 13

ID: vinayak.bhelekarTime: 22:12 Path: //mumnasprod/home\$/Vinay.Bhelekar\$/SM-MBIO210767



25/11/21 22:12 ArtID: DOI:10.1128/mBio.02113-21 CE: KGL-mar

Hörnrich et al.

mBio

**TABLE 3** Oligonucleotides

Oligonucleotide	Sequence
BAC16_downstream_of_GFP_STOP_overhang_plus_Zeo_3'	GGCGGAATTCCTCTAGTGCGGCCGAGTCGGGCCGCTTATCAGTCCTGCTCCTCGGCC
BAC16_upstream_of_GFP_ATG_antisense_strand_overhang_plus_EM7_P_start	GTAAGCTTGGTACCGAGCTCGGATCCACTAGTCCGCCACCTGTTGACAATTAATCATCGG
mNeonGreen_463-482_for	TACCCCAACGACAAAACCAT
mNeonGreen_504-523_rev	TGCCATTTCAGTGGGTAA
EPKans5_reverse_mNeon_463-482_ov	ATGGTTTTGTCGTTGGGGTACAACCAATTAACCAATCTGATTAG
EPKans_forward_mNeon_504-523_ov	TTACACCACTGGAAATGGCAGGATGACGACGATAAGTAGGGATAAC
mNeon-GS-KSHVorf65_for	TGTTGCGGGGAAGTGTTCCTCTGAGGCTATTTCCGCCCGCTGTGTGAAGATGGTGAG CAAGGGC
mNeon-GS-KSHVorf65_rev	TGATCCAGTCCTCTGGATCACGGGCTCTCACCTAAAGTTGGACATGCTCCCTT GTACAGCTCTGCC

Afterwards, selection was performed using 10  $\mu$ g/ml puromycin (InvivoGen; pQCXIP and plentiCRISPRv2 constructs) or 10  $\mu$ g/ml blasticidin (InvivoGen; AX526 lentivirus).

**Production of KSHV, KSHV\_mNeon-orf65, and RRV.** For the construction of KSHV\_mNeon-orf65, the GFP open reading frame of BAC16 was replaced with a Zeocin resistance gene by amplifying the resistance gene from pcDNA6 (Invitrogen) using Phusion PCR (NEB) and primers BAC16\_downstream\_of\_GFP\_STOP\_overhang\_plus\_Zeo\_3' and BAC16\_upstream\_of\_GFP\_ATG\_antisense\_strand\_overhang\_plus\_EM7\_P\_start and inserting it into BAC16 via recombination. A shuttle construct, Ax185\_pCNSmNeonGreen\_Kana, was created by inserting the i-SceI/Kanamycin cassette of pEPKan-5 (84) into pCNSmNeonGreen using primers mNeonGreen\_463-482\_for plus mNeonGreen\_504-523\_rev for the vector and EPKans5\_reverse\_mNeon\_463-482\_ov plus EPKans\_forward\_mNeon\_504-523\_ov for the insert, followed by Gibson assembly. KSHV\_mNeon-orf65 was generated by inserting the mNeonGreen cassette 5' of the first amino acid of orf65 with the addition of a glycine-serine linker according to the protocol described by Tischer et al. (84). The recombination cassette was generated using primers mNeon-GS-KSHVorf65\_for plus mNeon-GS-KSHVorf65\_rev and Ax185\_pCNSmNeonGreen\_Kana as a template.

T3 Infectious KSHV and RRV reporter viruses were produced as described previously (36). See Table 3 for oligonucleotide sequences.

T4 **Western blotting.** Western blotting was performed as described previously (36) using the respective antibodies (Table 4).

**CRISPR/Cas9-mediated knockout of immune-related IFITMs.** IFITM1, IFITM2, and IFITM3 knockout cell pools were generated by CRISPR/Cas9-mediated knockout by following the protocol described by Sanjana et al. (57), except that PEI transfection was used. In short, the cells intended for knockout were transduced with lentiviruses harboring the CRISPR/Cas9 gene and sgRNAs targeting IFITM1-3 (sgIFITM1/2/3-a, sgIFITM1/2/3-b) or nontargeting sgRNAs (sgNT-a, sgNT-b). For detection of CRISPR/Cas9-mediated knockout, the cells were treated with IFN- $\alpha$  (5,000 U/ml) for 16 h. Thereafter, the cells were harvested and subjected to Western blot analysis.

**Infection experiments.** IFITM-overexpressing cells were seeded in 48-well or 96-well plates at 90% confluence 16 h prior to infection. IFITM1/2/3 knockout cells were seeded in 48-well plates at 70% to 80% confluence. After attachment, cells were treated with IFN- $\alpha$  (5,000 U/ml) or H<sub>2</sub>O (control) for 16 h prior to infection with either KSHV, RRV, IAV-LP, or MLV-LP. For endocytosis inhibitor treatment, the cells were seeded into 96-well plates at 90% confluence and were incubated for 30 min at twice the indicated concentration before virus was added. For EIPA treatment, the medium was changed after 12 h due to toxicity. At 48 h postinfection, cells were trypsinized, trypsin activity was inhibited by adding 5% FCS in PBS, and the cells were washed and fixed with a final concentration of 4% methanol-free formaldehyde (Roth) in PBS. Infection was determined by detection of GFP<sup>+</sup>/YFP<sup>+</sup> cells using an LSRII flow cytometer or ID7000 (Sony); at least 5,000 cells were analyzed.

**Cell-cell fusion assay.** 293T effector cells were seeded in 6-well plates or 10-cm dishes at 70% to 80% confluence and transfected with either empty vector, gH/gL<sub>KSHV</sub> gB<sub>RRV</sub>, or gH/gL<sub>RRV</sub> gB<sub>RRV</sub> and Vp16-Gal4. 293T cells transfected with Gal4-TurboGFP-Luc and pQCXIP-IFITM1-3 were seeded in 48-well plates at 50,000 cells/well. A549 cells double transduced with lentiviruses encoding a Gal4-driven TurboGFP-luciferase reporter and lentiviruses encoding the CRISPR/Cas9 gene and the respective sgRNAs were seeded in 96-well plates at 20,000 cells/well; 6 h after seeding, the cells were treated with IFN- $\alpha$  (5,000 U/ml) for 16 h. Cell-cell fusion was started by adding the glycoprotein-expressing effector cells to the target cells in a 1:1 ratio. After 48 h, the cells were lysed in luciferase cell culture lysis reagent (Promega) and luciferase activity was determined using the Beetle-Juice luciferase assay (PJK Biotech) according to the manufacturer's instructions and a BioTek Synergy 2 plate reader.

AQ: G **Flow cytometry.** For detection of cell surface proteins, A549 IFITM1/2/3 knockout cells were H<sub>2</sub>O or IFN- $\alpha$  treated for 16 h, washed with PBS, detached using EDTA/EGTA (5 mM/5 mM) at 37°C, and washed with cold PBS (4°C). The cells were fixed with 4% methanol-free formaldehyde for 5 min and washed twice with PBS. Following blocking with 10% FCS (blocking buffer) in PBS, the cells were incubated with primary antibody (Table 4) in blocking buffer for 90 min at 4°C. After washing with PBS, the cells were incubated with secondary antibody (Table 4) in blocking buffer for 45 min at room temperature (RT) in the dark. The cells were washed and postfixed with 2% methanol-free formaldehyde in PBS. Analysis

November/December 2021 Volume 12 Issue 6 e02113-21

mbio.asm.org 14

ID: Vinayak.bhelekarTime: 22:12I Path: //mumnasprod/home\$/Vinay.Bhelekar\$/SM-MBIO210767

IFITM-Mediated Restriction of KSHV and RRV



25/11/21 22:12 ArtID: DOI:10.1128/mBio.02113-21 CE: KGL-mar

TABLE 4 Antibodies

Assay type and/or target	Antibody			Secondary antibody			
	Manufacturer	Clone/catalog no. <sup>a</sup>	Species	Type	Manufacturer	Species	Dilution
Western blotting							
IFITM1	R&D Systems	AF4827	Goat	Anti-goat HRP-coupled	Proteintech	Rabbit	1:5,000
IFITM2	Proteintech	66137-1-Ig	Mouse	Anti-mouse HRP-coupled	Dianova	Donkey	1:1,000
IFITM3	Cell Signaling Technology	D8E8G	Rabbit	Anti-rabbit HRP-coupled	Life Technologies	Goat	1:1,000
c-Myc epitope	Santa Cruz Biotechnology	9E10	Mouse	Anti-mouse HRP-coupled	Dianova	Donkey	1:1,000
MxA	R&D Systems	AF7946	Goat	Anti-goat HRP-coupled	Proteintech	Rabbit	1:5,000
GAPDH	GenScript	NA	Mouse	Anti-mouse HRP-coupled	Dianova	Donkey	1:1,000
V5 tag	Bio-Rad	NA	Mouse	Anti-mouse HRP-coupled	Dianova	Donkey	1:1,000
DYKDDDDK (Flag) tag	Cell Signaling Technology	D6W5B	Rabbit	Anti-rabbit HRP-coupled	Life Technologies	Goat	1:1,000
RRV gB	Scott W. Wong (Oregon Health & Science University)	3H8.1	Mouse	Anti-mouse HRP-coupled	Dianova	Donkey	1:1,000
Flow cytometry							
IgG1 isotype	Thermo Fisher Scientific	NA	Mouse	Anti-mouse Alexa Fluor 647	Life Technologies	Donkey	1:500
EphA2	Merck	Clone F2-27	Mouse	Anti-mouse Alexa Fluor 647	Life Technologies	Donkey	1:500
Integrin alpha V/CD51	R&D Systems	P2W7	Mouse	Anti-mouse Alexa Fluor 647	Life Technologies	Donkey	1:500
CD71 (TfR)	Thermo Fisher Scientific	OIK79	Mouse	Anti-mouse Alexa Fluor 647	Life Technologies	Donkey	1:500
Immunofluorescence							
IFITM1	R&D Systems	AF4827	Goat	Anti-goat Alexa Fluor 594 or anti-goat Alexa Fluor 647	Life Technologies	Donkey	1:500
IFITM2	Proteintech	12769-1-AP	Rabbit	Anti-rabbit Alexa Fluor 594 or anti-goat Alexa Fluor 647	Life Technologies	Donkey	1:500
IFITM3	Cell Signaling Technology	D8E8G	Rabbit	Anti-rabbit Alexa Fluor 594 or anti-goat Alexa Fluor 647	Life Technologies	Donkey	1:500
EEA1	BD Laboratories	610456	Mouse	Anti-mouse Alexa Fluor 647	Life Technologies	Donkey	1:500
LAMP-1	Santa Cruz Biotechnology	H5G11	Mouse	Anti-mouse Alexa Fluor 647	Life Technologies	Donkey	1:500
Directly labeled probes				Phalloidin-Fluor 647 conjugate	AAT Bioquest		1:1,000

<sup>a</sup>NA, not applicable.



25/11/21 22:12 ArtID: DOI:10.1128/mBio.02113-21 CE: KGL-mar

Hörnrich et al.



was performed using an LSRII flow cytometer (BD Biosciences) and Flowing software (University of Turku, version 2.5).

**Immunofluorescence.** A549 cells or HUVEC were seeded on 12-mm coverslips (YX03.1; Carl Roth) in 24-well plates at 150,000 cells/well. After attachment, the cells were treated with either H<sub>2</sub>O (control) or IFN- $\alpha$  (5,000 U/ml) for 16 h and cold KSHV\_mNEON-ORF65 was added. Cells were centrifuged (4,200 rpm, 4°C, 30 min), followed by a 10-min incubation at 4°C. After 3 washes with cold PBS, cells were either fixed in 4% methanol-free formaldehyde in PBS for 10 min (0-min time point) or shifted to 37°C after addition of D10 (A549 cells) or endothelial cell growth medium 2 (HUVEC). At the indicated time points, cells were washed once in PBS and fixed in 4% methanol-free formaldehyde in PBS for 10 min. After fixation, cells were washed three times in PBS. Cell permeabilization and blocking were performed in IF buffer (5% FCS, 0.05% saponin [Sigma] in PBS) for 1 h. Primary antibody (Table 4) incubation was performed in IF buffer overnight at 4°C or 2 h at RT. Secondary antibody (Table 4) incubation or incubation with a directly labeled phalloidin probe was performed after three washes with IF buffer for 1 h at RT. Cells were washed once in IF buffer and stained with Hoechst 33342 at 1:10,000 in PBS (catalog no. 62249; Thermo Scientific) for 5 min, followed by a final wash with PBS. The coverslips were dried and mounted in anti-fade fluorescence mounting medium (ab104135; abcam). Images were acquired on a confocal laser scanning microscope (Zeiss LSM800). Laser intensity and signal amplification were maintained for each experiment between different conditions for each antibody staining. All images were processed using Fiji/ImageJ software. For the quantification of colocalization of mNEON and IFITM signals, the Fiji "colocalization" plugin was used. The automatic threshold for IFITM signals was determined using the "IsoData" method, averaged for all analyzed images per experiment, and used in the colocalization analysis of all respective IFITM stainings in this experiment. The threshold for mNEON signals was kept constant in all analyses. Quantification of colocalized particles was performed on the "colocalized points 8-bit" output image using the Fiji built-in "find maxima" function. Quantification of total mNEON-positive particles was performed using the Fiji built-in "find maxima" function on the mNEON channel after thresholding identical to the colocalization analysis. For each experiment and time point, at least three images were analyzed and averaged. For representative images, automatic contrast enhancement on all channels was performed. All images were smoothed prior to processing.

AQ: H

AQ: I

#### SUPPLEMENTAL MATERIAL

Supplemental material is available online only.

**FIG S1**, TIF file, 2 MB.

**FIG S2**, JPG file, 2.3 MB.

**FIG S3**, TIF file, 1.5 MB.

**FIG S4**, JPG file, 2.8 MB.

**FIG S5**, TIF file, 0.5 MB.

#### ACKNOWLEDGMENTS

This work was supported by grants from the Deutsche Forschungsgemeinschaft (<https://www.dfg.de>; grant no. HA 6013/4-1) and the Wilhelm-Sander Foundation (<https://www.wilhelm-sander-stiftung.de>; project no. 2019.027.1).

We thank Stefan Pöhlmann, Michael Winkler, and Michael Farzan for sharing plasmids, Klaus Korn for sharing human foreskin fibroblasts, Rüdiger Behr for sharing rhesus monkey fibroblasts, and Scott Wong for sharing RRV gB antibodies.

#### REFERENCES

- Brass AL, Huang I-C, Benita Y, John SP, Krishnan MN, Feeley EM, Ryan BJ, Weyer JL, van der Weyden L, Fikrig E, Adams DJ, Xavier RJ, Farzan M, Elledge SJ. 2009. The IFITM proteins mediate cellular resistance to influenza A H1N1 virus, West Nile virus, and dengue virus. *cell* 139:1243–1254. <https://doi.org/10.1016/j.cell.2009.12.017>.
- Huang I-C, Bailey CC, Weyer JL, Radoshitzky SR, Becker MM, Chiang JJ, Brass AL, Ahmed AA, Chi X, Dong L, Longobardi LE, Boltz D, Kuhn JH, Elledge SJ, Bavari S, Denison MR, Choe H, Farzan M. 2011. Distinct patterns of IFITM-mediated restriction of filoviruses, SARS coronavirus, and influenza A virus. *PLoS Pathog* 7:e1001258. <https://doi.org/10.1371/journal.ppat.1001258>.
- Wrensch F, Karsten CB, Gnirß K, Hoffmann M, Lu K, Takada A, Winkler M, Simmons G, Pöhlmann S. 2015. Interferon-induced transmembrane protein-mediated inhibition of host cell entry of ebolaviruses. *J Infect Dis* 212 (Suppl 2):S210–S218. <https://doi.org/10.1093/infdis/jiv255>.
- Shi G, Kenney AD, Kudryashova E, Zani A, Zhang L, Lai KK, Hall-Stoodley L, Robinson RT, Kudryashov DS, Compton AA, Yount JS. 2021. Opposing activities of IFITM proteins in SARS-CoV-2 infection. *EMBO J* 40:e106501. <https://doi.org/10.15252/embj.2020106501>.
- Mudhasani R, Tran JP, Retterer C, Radoshitzky SR, Kota KP, Altamura LA, Smith JM, Packard BZ, Kuhn JH, Costantino J, Garrison AR, Schmaljohn CS, Huang I-C, Farzan M, Bavari S. 2013. IFITM-2 and IFITM-3 but not IFITM-1 restrict Rift Valley fever virus. *J Virol* 87:8451–8464. <https://doi.org/10.1128/JVI.03382-12>.
- Bailey CC, Zhong G, Huang I-C, Farzan M. 2014. IFITM-family proteins: the cell's first line of antiviral defense. *Annu Rev Virol* 1:261–283. <https://doi.org/10.1146/annurev-virology-031413-085537>.
- Siegrist F, Ebeling M, Certa U. 2011. The small interferon-induced transmembrane genes and proteins. *J Interferon Cytokine Res* 31:183–197. <https://doi.org/10.1089/jir.2010.0112>.
- Weston S, Czieso S, White IJ, Smith SE, Kellam P, Marsh M. 2014. A membrane topology model for human interferon inducible transmembrane protein 1. *PLoS One* 9:e104341. <https://doi.org/10.1371/journal.pone.0104341>.
- Feeley EM, Sims JS, John SP, Chin CR, Pertel T, Chen L-M, Gaiha GD, Ryan BJ, Donis RO, Elledge SJ, Brass AL. 2011. IFITM3 inhibits influenza A virus infection by preventing cytosolic entry. *PLoS Pathog* 7:e1002337. <https://doi.org/10.1371/journal.ppat.1002337>.

November/December 2021 Volume 12 Issue 6 e02113-21

mbio.asm.org 16

ID: vinayak.bhelekarTime: 22:12 Path: //mumnasprod/home\$/Vinay.Bhelekar/\$M-MBIO210767



25/11/21 22:12 ArtID: DOI:10.1128/mBio.02113-21 CE: KGL-mar

IFITM-Mediated Restriction of KSHV and RRV

mBio

10. Narayana SK, Helbig KJ, McCartney EM, Eyre NS, Bull RA, Eltahl A, Lloyd AR, Beard MR. 2015. The interferon-induced transmembrane proteins, IFITM1, IFITM2, and IFITM3 inhibit hepatitis C virus entry. *J Biol Chem* 290: 25946–25959. <https://doi.org/10.1074/jbc.M115.657346>.
11. Li K, Markosyan RM, Zheng Y-M, Golfetto O, Bungart B, Li M, Ding S, He Y, Liang C, Lee JC, Gratton E, Cohen FS, Liu S-L. 2013. IFITM proteins restrict viral membrane hemifusion. *PLoS Pathog* 9:e1003124. <https://doi.org/10.1371/journal.ppat.1003124>.
12. Desai TM, Marin M, Chin CR, Savidis G, Brass AL, Melikyan GB. 2014. IFITM3 restricts influenza A virus entry by blocking the formation of fusion pores following virus-endosome hemifusion. *PLoS Pathog* 10:e1004048. <https://doi.org/10.1371/journal.ppat.1004048>.
13. Guo X, Steinkühler J, Marin M, Li X, Lu W, Dimova R, Melikyan GB. 2021. Interferon-induced transmembrane protein 3 blocks fusion of diverse enveloped viruses by altering mechanical properties of cell membranes. *ACS Nano* 15:8155–8170. <https://doi.org/10.1021/acsnano.0c10567>.
14. Amini-Bavil-Olyaei S, Choi YJ, Lee JH, Shi M, Huang J-C, Farzan M, Jung JU. 2013. The antiviral effector IFITM3 disrupts intracellular cholesterol homeostasis to block viral entry. *Cell Host Microbe* 13:452–464. <https://doi.org/10.1016/j.chom.2013.03.006>.
15. Suddala KC, Lee CC, Meraner P, Marin M, Markosyan RM, Desai TM, Cohen FS, Brass AL, Melikyan GB. 2019. Interferon-induced transmembrane protein 3 blocks fusion of sensitive but not resistant viruses by partitioning into virus-carrying endosomes. *PLoS Pathog* 15:e1007532. <https://doi.org/10.1371/journal.ppat.1007532>.
16. Shi G, Schwartz O, Compton AA. 2017. More than meets the I: the diverse antiviral and cellular functions of interferon-induced transmembrane proteins. *Retrovirology* 14:53. <https://doi.org/10.1186/s12977-017-0377-y>.
17. Li C, Du S, Tian M, Wang Y, Bai J, Tan P, Liu W, Yin R, Wang M, Jiang Y, Li Y, Zhu N, Zhu Y, Li T, Wu S, Jin N, He F. 2018. The host restriction factor interferon-inducible transmembrane protein 3 inhibits vaccinia virus infection. *Front Immunol* 9:228. <https://doi.org/10.3389/fimmu.2018.00228>.
18. Smith SE, Busse DC, Binter S, Weston S, Diaz Soria C, Laksono BM, Clare S, Van Nieuwkoop S, Van den Hoogen BG, Clement M, Marsden M, Humphreys IR, Marsh M, de Swart RL, Wash RS, Tregoning JS, Kellam P. 2019. Interferon-induced transmembrane protein 1 restricts replication of viruses that enter cells via the plasma membrane. *J Virol* 93:e02003-18. <https://doi.org/10.1128/JVI.02003-18>.
19. Warren CJ, Griffin LM, Little AS, Huang J-C, Farzan M, Peyer D. 2014. The antiviral restriction factors IFITM1, 2 and 3 do not inhibit infection of human papillomavirus, cytomegalovirus and adenovirus. *PLoS One* 9: e96579. <https://doi.org/10.1371/journal.pone.0096579>.
20. Xie M, Xuan B, Shan J, Pan D, Sun Y, Shan Z, Zhang J, Yu D, Li B, Qian Z. 2015. Human cytomegalovirus exploits interferon-induced transmembrane proteins to facilitate morphogenesis of the virion assembly compartment. *J Virol* 89:3049–3061. <https://doi.org/10.1128/JVI.03416-14>.
21. Hussein HAM, Akula SM. 2017. miRNA-36 inhibits KSHV, EBV, HSV-2 infection of cells via stiffling expression of interferon induced transmembrane protein 1 (IFITM1). *Sci Rep* 7:17972. <https://doi.org/10.1038/s41598-017-18225-w>.
22. Hussein HAM, Briestenska K, Mistrikova J, Akula SM. 2018. IFITM1 expression is crucial to gammaherpesvirus infection, in vivo. *Sci Rep* 8:14105. <https://doi.org/10.1038/s41598-018-32350-0>.
23. Tartour K, Nguyen X-N, Apourchoux R, Assil S, Barateau V, Bloyet L-M, Burlaud Gaillard J, Confort M-P, Escudero-Perez B, Gruffat H, Hong SS, Moroso M, Reynard O, Reynard S, Decembre E, Ftaich N, Rossi A, Wu N, Arnaud F, Baize S, Dreux M, Gerlier D, Paranhos-Baccala G, Volchkov V, Roingeard P, Cimagelli A. 2017. Interference with the production of infectious viral particles and bimodal inhibition of replication are broadly conserved antiviral properties of IFITMs. *PLoS Pathog* 13:e1006610. <https://doi.org/10.1371/journal.ppat.1006610>.
24. Damania B, Desrosiers RC. 2001. Simian homologues of human herpesvirus 8. *Philos Trans R Soc Lond B Biol Sci* 356:535–543. <https://doi.org/10.1098/rstb.2000.0782>.
25. Wen KW, Damania B. 2010. Kaposi sarcoma-associated herpesvirus (KSHV): molecular biology and oncogenesis. *Cancer Lett* 289:140–150. <https://doi.org/10.1016/j.canlet.2009.07.004>.
26. Chen Q, Chen J, Li Y, Liu D, Zeng Y, Tian Z, Yunus A, Yang Y, Lu J, Song X, Yuan Y. 2021. Kaposi's sarcoma herpesvirus is associated with osteosarcoma in Xinjiang populations. *Proc Natl Acad Sci U S A* 118:e2016653118. <https://doi.org/10.1073/pnas.2016653118>.
27. Polizzotto MN, Uldrick TS, Hu D, Yarchoan R. 2012. Clinical manifestations of Kaposi sarcoma herpesvirus lytic activation: multicentric Castleman disease (KSHV-MCD) and the KSHV inflammatory cytokine syndrome. *Front Microbiol* 3:73. <https://doi.org/10.3389/fmicb.2012.00073>.
28. Stiller CA. 2007. International patterns of cancer incidence in adolescents. *Cancer Treat Rev* 33:631–645. <https://doi.org/10.1016/j.ctrv.2007.01.001>.
29. Chatlynne LG, Ablashi DV. 1999. Seroepidemiology of Kaposi's sarcoma-associated herpesvirus (KSHV). *Semin Cancer Biol* 9:175–185. <https://doi.org/10.1006/scbi.1998.0089>.
30. Parkin DM, Sitas F, Chirenje M, Stein L, Abratt R, Wabinga H. 2008. Part I: Cancer in Indigenous Africans—burden, distribution, and trends. *Lancet Oncol* 9:683–692. [https://doi.org/10.1016/S1470-2045\(08\)70175-X](https://doi.org/10.1016/S1470-2045(08)70175-X).
31. Amir H, Kaaya EE, Manji KP, Kwasigabo G, Biberfeld P. 2001. Kaposi's sarcoma before and during a human immunodeficiency virus epidemic in Tanzanian children. *Pediatr Infect Dis J* 20:518–521. <https://doi.org/10.1097/00006454-200105000-00009>.
32. Bechtel JT, Liang Y, Hvidding J, Ganem D. 2003. Host range of Kaposi's sarcoma-associated herpesvirus in cultured cells. *J Virol* 77:6474–6481. <https://doi.org/10.1128/jvi.77.11.6474-6481.2003>.
33. Hahn AS, Desrosiers RC. 2013. Rhesus monkey rhadinovirus uses Eph family receptors for entry into B cells and endothelial cells but not fibroblasts. *PLoS Pathog* 9:e1003360. <https://doi.org/10.1371/journal.ppat.1003360>.
34. Dollery SJ. 2019. Towards understanding KSHV fusion and entry. *Viruses* 11:1073. <https://doi.org/10.3390/v11111073>.
35. Hahn AS, Kaufmann JK, Wies E, Naschberger E, Panteleev-Ivlev J, Schmidt K, Holzer A, Schmidt M, Chen J, König S, Ensser A, Myoung J, Brockmeyer NH, Stürzl M, Fleckenstein B, Neipel F. 2012. The ephrin receptor tyrosine kinase A2 is a cellular receptor for Kaposi's sarcoma-associated herpesvirus. *Nat Med* 18:961–966. <https://doi.org/10.1038/nm.2805>.
36. Großkopf AK, Ensser A, Neipel F, Jungnickl D, Schlagowski S, Desrosiers RC, Hahn AS. 2018. A conserved Eph family receptor-binding motif of the gH/gL complex of Kaposi's sarcoma-associated herpesvirus and rhesus monkey rhadinovirus. *PLoS Pathog* 14:e1006912. <https://doi.org/10.1371/journal.ppat.1006912>.
37. Großkopf AK, Schlagowski S, Hörnich BF, Fricke T, Desrosiers RC, Hahn AS. 2019. EphA7 functions as receptor on BJAB cells for cell-to-cell transmission of the Kaposi's sarcoma-associated herpesvirus and for cell-free infection by the related rhesus monkey rhadinovirus. *J Virol* 93:e00064-19. <https://doi.org/10.1128/JVI.00064-19>.
38. Großkopf AK, Schlagowski S, Fricke T, Ensser A, Desrosiers RC, Hahn AS. 2021. Plxhc family members are novel receptors for the rhesus monkey rhadinovirus (RRV). *PLoS Pathog* 17:e1008979. <https://doi.org/10.1371/journal.ppat.1008979>.
39. Hahn A, Birkmann A, Wies E, Dorer D, Mahr K, Stürzl M, Titgemeyer F, Neipel F. 2009. Kaposi's sarcoma-associated herpesvirus gH/gL: glycoprotein export and interaction with cellular receptors. *J Virol* 83:396–407. <https://doi.org/10.1128/JVI.01170-08>.
40. Akula SM, Pramod NP, Wang F-Z, Chandran B. 2002. Integrin  $\alpha 3 \beta 1$  (CD 49c/29) is a cellular receptor for Kaposi's sarcoma-associated herpesvirus (KSHV/HHV-8) entry into the target cells. *Cell* 108:407–419. [https://doi.org/10.1016/S0092-8674\(02\)00628-1](https://doi.org/10.1016/S0092-8674(02)00628-1).
41. Garrigues HJ, DeMaster LK, Rubinchikova YE, Rose TM. 2014. KSHV attachment and entry are dependent on  $\alpha V \beta 3$  integrin localized to specific cell surface microdomains and do not correlate with the presence of heparan sulfate. *Virology* 464-465:118–133. <https://doi.org/10.1016/j.virol.2014.06.035>.
42. Raghu H, Sharma-Walia N, Veetil MV, Sadagopan S, Chandran B. 2009. Kaposi's sarcoma-associated herpesvirus utilizes an actin polymerization-dependent macropinocytotic pathway to enter human dermal microvascular endothelial and human umbilical vein endothelial cells. *J Virol* 83: 4895–4911. <https://doi.org/10.1128/JVI.02498-08>.
43. Akula SM, Naranatt PP, Wallia N-S, Wang F-Z, Fegley B, Chandran B. 2003. Kaposi's sarcoma-associated herpesvirus (human herpesvirus 8) infection of human fibroblast cells occurs through endocytosis. *J Virol* 77: 7978–7990. <https://doi.org/10.1128/jvi.77.14.7978-7990.2003>.
44. Zhang W, Zhou F, Greene W, Gao S-J. 2010. Rhesus rhadinovirus infection of rhesus fibroblasts occurs through clathrin-mediated endocytosis. *J Virol* 84:11709–11717. <https://doi.org/10.1128/JVI.01429-10>.
45. Pertel PE. 2002. Human herpesvirus 8 glycoprotein B (gB), gH, and gL can mediate cell fusion. *J Virol* 76:4390–4400. <https://doi.org/10.1128/jvi.76.9.4390-4400.2002>.
46. Chen J, Schaller S, Jardtzyk TS, Longnecker R. 2020. Epstein-Barr virus gH/gL and Kaposi's sarcoma-associated herpesvirus gH/gL bind to different sites on EphA2 to trigger fusion. *J Virol* 94:e01454-20. <https://doi.org/10.1128/JVI.01454-20>.

November/December 2021 Volume 12 Issue 6 e02113-21

mbio.asm.org 17

ID: vinayak.bhelekarTime: 22:12 Path: //mumnasprod/home\$/VinayBhelekar\$/SM-MBIO210767



47. Myoung J, Ganem D. 2011. Infection of lymphoblastoid cell lines by Kaposi's sarcoma-associated herpesvirus: critical role of cell-associated virus. *J Virol* 85:9767–9777. <https://doi.org/10.1128/JVI.05136-11>.
48. Jarousse N, Chandran B, Coscoy L. 2008. Lack of heparan sulfate expression in B-cell lines: implications for Kaposi's sarcoma-associated herpesvirus and murine gammaherpesvirus 68 infections. *J Virol* 82:12591–12597. <https://doi.org/10.1128/JVI.01167-08>.
49. Dolley SJ, Santiago-Crespo RJ, Kardava L, Moir S, Berger EA. 2013. Efficient infection of a human B cell line with cell-free Kaposi's sarcoma-associated herpesvirus. *J Virol* 88:1748–1757. <https://doi.org/10.1128/JVI.03063-13>.
50. Stoltz M, Klingström J. 2010. Alpha/beta interferon (IFN- $\alpha/\beta$ )-independent induction of IFN- $\lambda$ 1 (interleukin-29) in response to Hantaan virus infection. *J Virol* 84:9140–9148. <https://doi.org/10.1128/JVI.00717-10>.
51. Tissari J, Sirén J, Meri S, Julkunen I, Matikainen S. 2005. IFN- $\alpha$  enhances TLR3-mediated antiviral cytokine expression in human endothelial and epithelial cells by up-regulating TLR3 expression. *J Immunol* 174:4289–4294. <https://doi.org/10.4049/jimmunol.174.7.4289>.
52. Thube MM, Shil P, Kasbe R, Patil AA, Pawar SD, Mullick J. 2018. Differences in type I interferon response in human lung epithelial cells infected by highly pathogenic H5N1 and low pathogenic H1N1 avian influenza viruses. *Virus Genes* 54:414–423. <https://doi.org/10.1007/s11262-018-1556-1>.
53. Spence JS, He R, Hoffmann H-H, Das T, Thion E, Rice CM, Peng T, Chandran K, Hang HC. 2019. IFITM3 directly engages and shuttles incoming virus particles to lysosomes. *Nat Chem Biol* 15:259–268. <https://doi.org/10.1038/s41589-018-0213-2>.
54. Zhao X, Guo F, Liu F, Cuconati A, Chang J, Block TM, Guo J-T. 2014. Interferon induction of IFITM proteins promotes infection by human coronavirus OC43. *Proc Natl Acad Sci U S A* 111:6756–6761. <https://doi.org/10.1073/pnas.1320856111>.
55. Winkler M, Wrensch F, Bosch P, Knoth M, Schindler M, Gärtner S, Pöhlmann S. 2019. Analysis of IFITM-IFITM interactions by a flow cytometry-based FRET assay. *Int J Mol Sci* 20:3859. <https://doi.org/10.3390/ijms20163859>.
56. Rahman K, Coomer CA, Majdoul S, Ding SY, Padilla-Parra S, Compton AA. 2020. Homology-guided identification of a conserved motif linking the antiviral functions of IFITM3 to its oligomeric state. *Elife* 9:e58537. <https://doi.org/10.7554/eLife.58537>.
57. Sanjana NE, Shalem O, Zhang F. 2014. Improved vectors and genome-wide libraries for CRISPR screening. *Nat Methods* 11:783–784. <https://doi.org/10.1038/nmeth.3047>.
58. Tang Y-W, Johnson JE, Browning PJ, Cruz-Gervis RA, Davis A, Graham BS, Brigham KL, Oates JA, Loyd JE, Stecenko AA. 2003. Herpesvirus DNA is consistently detected in lungs of patients with idiopathic pulmonary fibrosis. *J Clin Microbiol* 41:2633–2640. <https://doi.org/10.1128/JCM.41.6.2633-2640.2003>.
59. Lin Y-C, Boone M, Meuris L, Lemmens I, Van Roy N, Soete A, Reumers J, Moisse M, Plaisance S, Drmanac R, Chen J, Speleman F, Lambrechts D, Van de Peer Y, Tavernier J, Callewaert N. 2014. Genome dynamics of the human embryonic kidney 293 lineage in response to cell biology manipulations. *Nat Commun* 5:4767. <https://doi.org/10.1038/ncomms5767>.
60. Stürzl M, Gaus D, Dirks WG, Ganem D, Jochmann R. 2013. Kaposi's sarcoma-derived cell line SLK is not of endothelial origin, but is a contaminant from a known renal carcinoma cell line. *Int J Cancer* 132:1954–1958. <https://doi.org/10.1002/ijc.27849>.
61. Myoung J, Ganem D. 2011. Generation of a doxycycline-inducible KSHV producer cell line of endothelial origin: maintenance of tight latency with efficient reactivation upon induction. *J Virol Methods* 174:12–21. <https://doi.org/10.1016/j.jviromet.2011.03.012>.
62. Williams DEJ, Wu W-L, Grotefend CR, Radic V, Chung C, Chung Y-H, Farzan M, Huang I-C. 2014. IFITM3 polymorphism rs12252-C restricts influenza A viruses. *PLoS One* 9:e110096. <https://doi.org/10.1371/journal.pone.0110096>.
63. John SP, Chin CR, Perreira JM, Feeley EM, Aker AM, Savidis G, Smith SE, Elia AEH, Everitt AR, Vora M, Pertel T, Elledge SJ, Kellam P, Brass AL. 2013. The CD225 domain of IFITM3 is required for both IFITM protein association and inhibition of influenza A virus and dengue virus replication. *J Virol* 87:7837–7852. <https://doi.org/10.1128/JVI.00481-13>.
64. Jia R, Xu F, Qian J, Yao Y, Miao C, Zheng Y-M, Liu S-L, Guo F, Geng Y, Qiao W, Liang C. 2014. Identification of an endocytic signal essential for the antiviral action of IFITM3: endocytosis of IFITM3 and its antiviral activity. *Cell Microbiol* 16:1080–1093. <https://doi.org/10.1111/cmi.12262>.
65. Chesarino NM, McMichael TM, Hach JC, Yount JS. 2014. Phosphorylation of the antiviral protein interferon-inducible transmembrane protein 3 (IFITM3) dually regulates its endocytosis and ubiquitination. *J Biol Chem* 289:11986–11992. <https://doi.org/10.1074/jbc.M114.557694>.
66. Ilangumaran S, Hoessli DC. 1998. Effects of cholesterol depletion by cyclodextrin on the sphingolipid microdomains of the plasma membrane. *Biochem J* 335:433–440. <https://doi.org/10.1042/bj3350433>.
67. Chakraborty S, Valiyaveetil M, Sadagopan S, Paudel N, Chandran B. 2011. c-Cbl-mediated selective virus-receptor translocations into lipid rafts regulate productive Kaposi's sarcoma-associated herpesvirus infection in endothelial cells. *J Virol* 85:12410–12430. <https://doi.org/10.1128/JVI.05953-11>.
68. Koivusalo M, Welch C, Hayashi H, Scott CC, Kim M, Alexander T, Touret N, Hahn KM, Grinstein S. 2010. Amiloride inhibits macropinocytosis by lowering submembranous pH and preventing Rac1 and Cdc42 signaling. *J Cell Biol* 188:547–563. <https://doi.org/10.1083/jcb.200908086>.
69. Zani A, Zhang L, McMichael TM, Kenney AD, Chemudupati M, Kwiek JJ, Liu S-L, Yount JS. 2019. Interferon-induced transmembrane proteins inhibit cell fusion mediated by trophoblast syncytins. *J Biol Chem* 294:19844–19851. <https://doi.org/10.1074/jbc.AC119.010611>.
70. Dutta D, Chakraborty S, Bandyopadhyay C, Valiya Veetil M, Ansari MA, Singh VV, Chandran B. 2013. EphrinA2 regulates clathrin mediated KSHV endocytosis in fibroblast cells by coordinating integrin-associated signaling and c-Cbl directed polyubiquitination. *PLoS Pathog* 9:e1003510. <https://doi.org/10.1371/journal.ppat.1003510>.
71. Perreira JM, Chin CR, Feeley EM, Brass AL. 2013. IFITMs restrict the replication of multiple pathogenic viruses. *J Mol Biol* 425:4937–4955. <https://doi.org/10.1016/j.jmb.2013.09.024>.
72. Hunt CL, Lennemann NJ, Maury W. 2012. Filovirus entry: a novelty in the viral fusion world. *Viruses* 4:258–275. <https://doi.org/10.3390/v4020258>.
73. Vidak E, Javoršek U, Vizovišek M, Turk B. 2019. Cysteine cathepsins and their extracellular roles: shaping the microenvironment. *Cells* 8:264. <https://doi.org/10.3390/cells8030264>.
74. Winkler M, Gärtner S, Wrensch F, Krawczak M, Saueremann U, Pöhlmann S. 2017. Rhesus macaque IFITM3 gene polymorphisms and SIV infection. *PLoS One* 12:e0172847. <https://doi.org/10.1371/journal.pone.0172847>.
75. Wilkins J, Zheng Y-M, Yu J, Liang C, Liu S-L. 2016. Nonhuman primate IFITM proteins are potent inhibitors of HIV and SIV. *PLoS One* 11:e0156739. <https://doi.org/10.1371/journal.pone.0156739>.
76. Hickford D, Frankenberg S, Shaw G, Renfree MB. 2012. Evolution of vertebrate interferon inducible transmembrane proteins. *BMC Genomics* 13:155. <https://doi.org/10.1186/1471-2164-13-155>.
77. Zhang Z, Liu J, Li M, Yang H, Zhang C. 2012. Evolutionary dynamics of the interferon-induced transmembrane gene family in vertebrates. *PLoS One* 7:e49265. <https://doi.org/10.1371/journal.pone.0049265>.
78. Kummer S, Avinoam O, Kräusslich H-G. 2019. IFITM3 clusters on virus containing endosomes and lysosomes early in the influenza A infection of human airway epithelial cells. *Viruses* 11:548. <https://doi.org/10.3390/v11060548>.
79. Ren L, Du S, Xu W, Li T, Wu S, Jin N, Li C. 2020. Current progress on host antiviral factor IFITMs. *Front Immunol* 11:543444. <https://doi.org/10.3389/fimmu.2020.543444>.
80. Buchrieser J, Dufloo J, Hubert M, Monel B, Planas D, Rajah MM, Planchais C, Porrot F, Guivel-Benhassine F, Van der Werf S, Casarelli N, Mouquet H, Bruel T, Schwartz O. 2020. Syncytia formation by SARS-CoV-2-infected cells. *EMBO J* 39. <https://doi.org/10.15252/embj.2020106267>.
81. Hörnich BF, Großkopf AK, Schlagowski S, Tenbusch M, Kleine-Weber H, Neipel F, Stahl-Hennig C, Hahn AS. 2021. SARS-CoV-2 and SARS-CoV spike-mediated cell-cell fusion differ in their requirements for receptor expression and proteolytic activation. *J Virol* 95:e00002-21. <https://doi.org/10.1128/JVI.00002-21>.
82. Prelli Bozzo C, Nchioua R, Volcic M, Koepke L, Krüger J, Schütz D, Heller S, Stürzel CM, Kmiec D, Conzelmann C, Müller J, Zech F, Braun E, Groß R, Wettstein L, Weil T, Weiß J, Diofano F, Rodríguez Alfonso AA, Wiese S, Sauter D, Münch J, Goffinet C, Catanese A, Schön M, Boeckers TM, Stenger S, Sato K, Just S, Klegler A, Sparrer KMJ, Kirchhoff F. 2021. IFITM proteins promote SARS-CoV-2 infection and are targets for virus inhibition in vitro. *Nat Commun* 12:4584. <https://doi.org/10.1038/s41467-021-24817-y>.
83. Ensser A, Yasuda K, Lauer W, Desrosiers RC, Hahn AS. 2020. Rhesus monkey rhadinovirus isolated from hemangioma tissue. *Microbiol Resour Announc* 9:e01347-19. <https://doi.org/10.1128/MRA.01347-19>.
84. Tischer BK, von Einem J, Käufer B, Osterrieder N. 2006. Two-step red-mediated recombination for versatile high-efficiency markerless DNA manipulation in *Escherichia coli*. *Biotechniques* 40:191–197. <https://doi.org/10.2144/000112096>.



25/11/21 22:12 ArtID: DOI:10.1128/mBio.02113-21 CE: KGL-mar



## SUPPLEMENTAL MATERIAL LEGENDS

[Author: Because the full supplemental material legends will appear in the HTML version of the article online, and because the copy editor may have made changes, we have reproduced the legends below. Feel free to enter your changes on this page and we will see that they are conveyed to the online article.]

**FIG S1** Overexpression of IFITM localization mutants and IFITM1 to -3 in HUVEC. (A and B) A549 cells were transduced with pQCXIP constructs to express pQCXIP (empty vector), IFITM1, IFITM3, and IFITM3 43AS, Y20A, and  $\Delta$ 1–21 mutants (A), and HUVEC were transduced with pQCXIP constructs to express IFITM1 to -3 or pQCXIP (empty vector) (B). IFITMs overexpressing cells were infected with KSHV-GFP, RRV-YFP, IAV lentiviral pseudotype (IAV-LP), or MLV lentiviral pseudotype (MLV-LP). Infection was measured using flow cytometry to detect expression of the fluorescent reporter genes. The data show values normalized to pQCXIP empty vector, which was set to 100%, and the error bars represent the standard error of the mean of results of four independent experiments for A549 cells and standard deviation of results of three independent experiments for HUVEC, each performed in triplicate. Statistical significance was determined by ordinary two-way ANOVA; *P* values were corrected for multiple comparisons by Dunnett's method (ns, *P* > 0.05; \*, *P* ≤ 0.05; \*\*, *P* ≤ 0.01; \*\*\*, *P* ≤ 0.001; \*\*\*\*, *P* ≤ 0.0001). (A and B, right panels) Representative Western blots of IFITM-overexpressing cells. Expression of myc-tagged IFITMs was determined using anti-myc antibody, and anti-IFITM3 antibody was used to detect untagged IFITM3 mutants; the  $\Delta$ 1–21 mutant is less well detected due to IFITM3 antibody epitope. GAPDH served as a loading control. (C) Bright-field microscopy images of HUVEC transduced with pQCXIP constructs to express IFITM1 to -3 or pQCXIP (empty vector) at different magnifications.

**FIG S2** Localization of IFITM1/2/3 in A549 cells and HUVEC. (A and B) Confocal microscopy images of A549 cells (A) and HUVEC (B) treated with IFN- $\alpha$  (5,000 U/ml) for 16 h and stained with IFITM1, IFITM2, or IFITM3 antibody (all green). Costaining was performed with antibodies to EEA1, LAMP1, or phalloidin conjugate (all magenta) and Hoechst stain (blue). Scale bars, 10  $\mu$ m.

**FIG S3** KSHV enters A549 cells via an endosomal pH-dependent, macropinocytosis-independent pathway. (A to C) A549 cells (left panel) and HUVEC (right panel) were pretreated for 30 min with twice the indicated concentration of either bafilomycin A1 (A), MBCD (B), or EIPA (C) and incubated with KSHV-GFP, RRV-YFP, IAV lentiviral pseudotype (IAV-LP), or MLV lentiviral pseudotype (MLV-LP) to the final concentration. In the case of EIPA treatment, the medium was changed after 12 h due to cytotoxicity of prolonged incubation. Infection was measured after 48 h using flow cytometry to detect expression of the fluorescent reporter genes. The data show values normalized to the respective solvent control, which was set to 100%, and the error bars represent the standard deviation of the results of one

25/11/21 22:12 ArtID: DOI:10.1128/mBio.02113-21 CE: KGL-mar

mBio

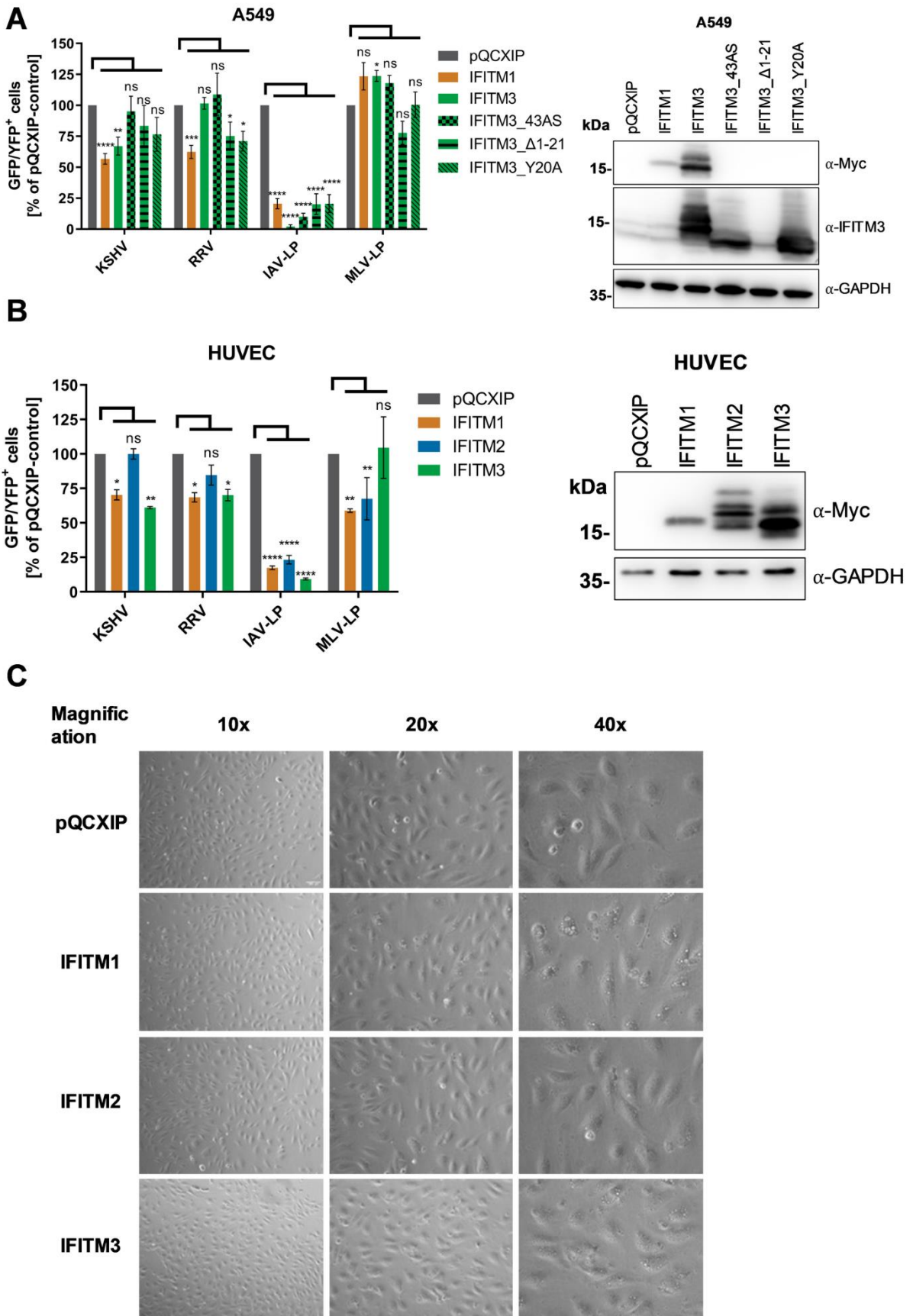
representative experiment performed in triplicate (in duplicate for KSHV with EIPA). Statistical significance was determined by ordinary two-way ANOVA;  $P$  values were corrected for multiple comparisons by Dunnett's method (ns,  $P > 0.05$ ; \*,  $P \leq 0.05$ ; \*\*,  $P \leq 0.01$ ; \*\*\*,  $P \leq 0.001$ ; \*\*\*\*,  $P \leq 0.0001$ ). (D) Cytotoxicity of substances was determined via a CellTiter-Glo assay. A549 cells (left panel) and HUVEC (right panel) were incubated with the substances at the indicated concentrations. In the case of EIPA treatment, the medium was changed after 12 h due to cytotoxicity of prolonged incubation. After 48 h, cell viability was determined using the luciferase-based CellTiter-Glo assay. The data show values normalized to the respective solvent control, which was set to 100%, and the error bars represent the standard deviation of the results of one representative experiment performed in triplicate. Statistical significance was determined by ordinary one-way ANOVA;  $P$  values were corrected for multiple comparisons by Dunnett's method (ns,  $P > 0.05$ ; \*,  $P \leq 0.05$ ; \*\*,  $P \leq 0.01$ ; \*\*\*,  $P \leq 0.001$ ; \*\*\*\*,  $P \leq 0.0001$ ).

**FIG S4** KSHV virus particles in A549 cells and HUVEC. Representative confocal microscopy images of A549 cells (A) and HUVEC (B) treated with 5,000 U/ml IFN- $\alpha$ , infected with KSHV\_mNeon-orf65 (green), and used for the quantification shown in Fig. 5B. Staining was performed using IFITM1, IFITM2, or IFITM3 antibody (magenta) and Hoechst stain (blue). Scale bars, 10  $\mu$ m.

**FIG S5** Cell-cell fusion assay. Effector cells (293T cells transfected with either empty vector [eV] or expression plasmids for the indicated viral glycoproteins together with Vp16-Gal4 expression plasmid) were added to target cells (A549 cells transduced with a Gal4-driven TurboGFP-luciferase construct). After the indicated time points, luciferase activity was measured. The data show fold values relative to empty vector control effector cells. Error bars represent the standard deviation of the results of one representative experiment performed in triplicate. Statistical significance was determined by two-way ANOVA;  $P$  values were corrected for multiple comparisons by Dunnett's method (ns,  $P > 0.05$ ; \*\*,  $P \leq 0.05$ ; \*\*\*,  $P \leq 0.01$ ; \*\*\*\*,  $P \leq 0.001$ ; \*\*\*\*,  $P \leq 0.0001$ ).

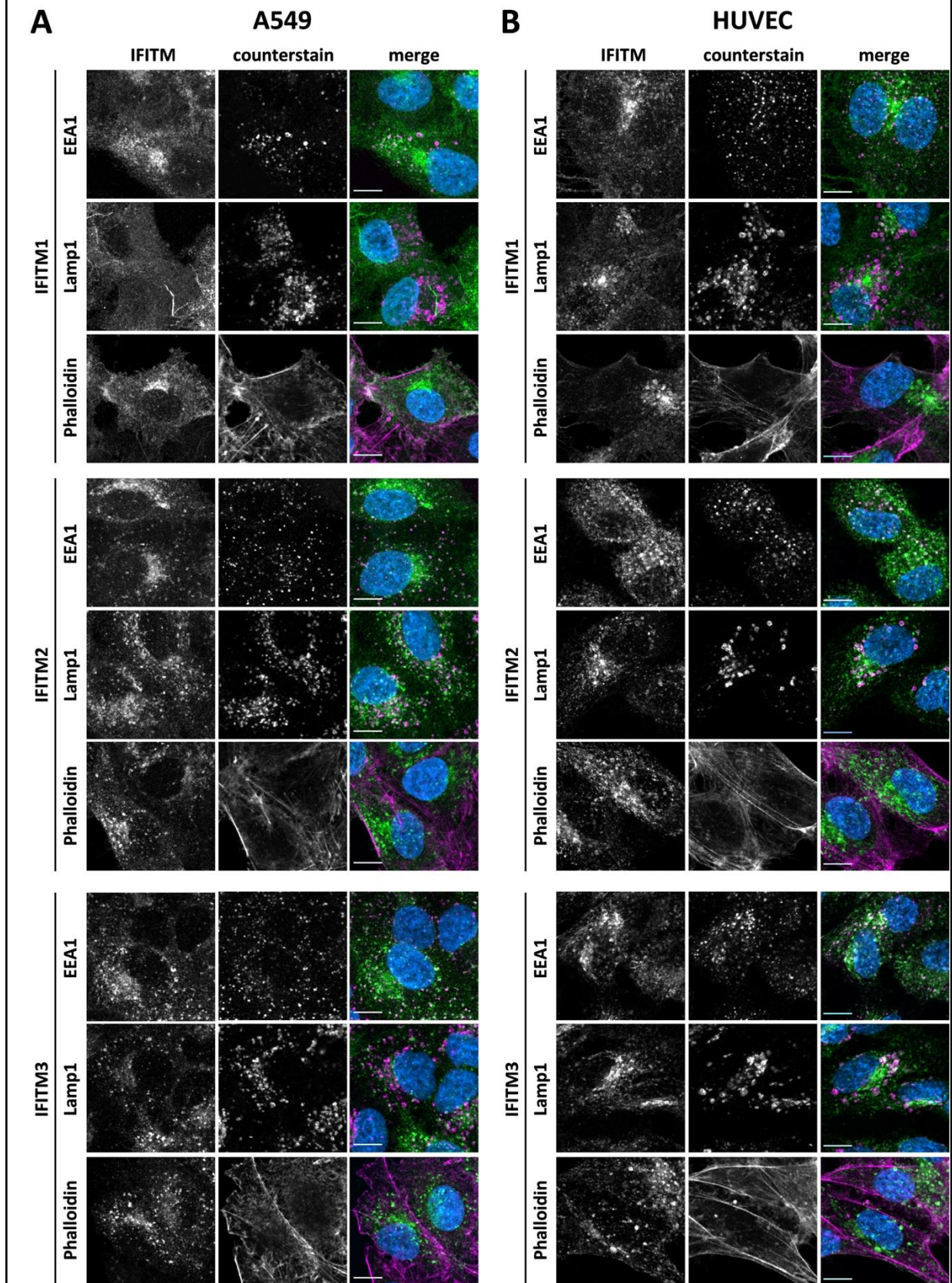


**Supplemental Figure 1**

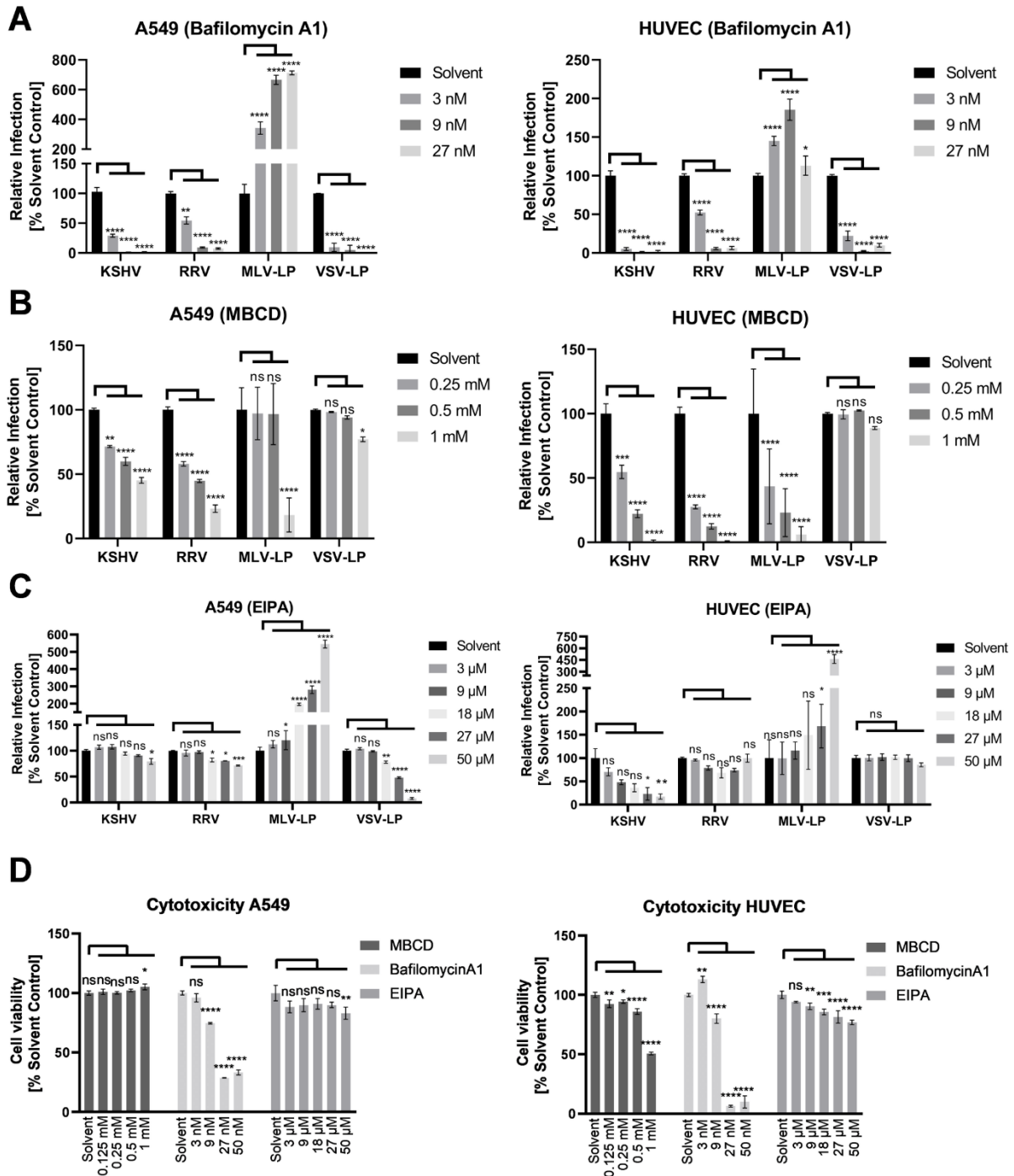




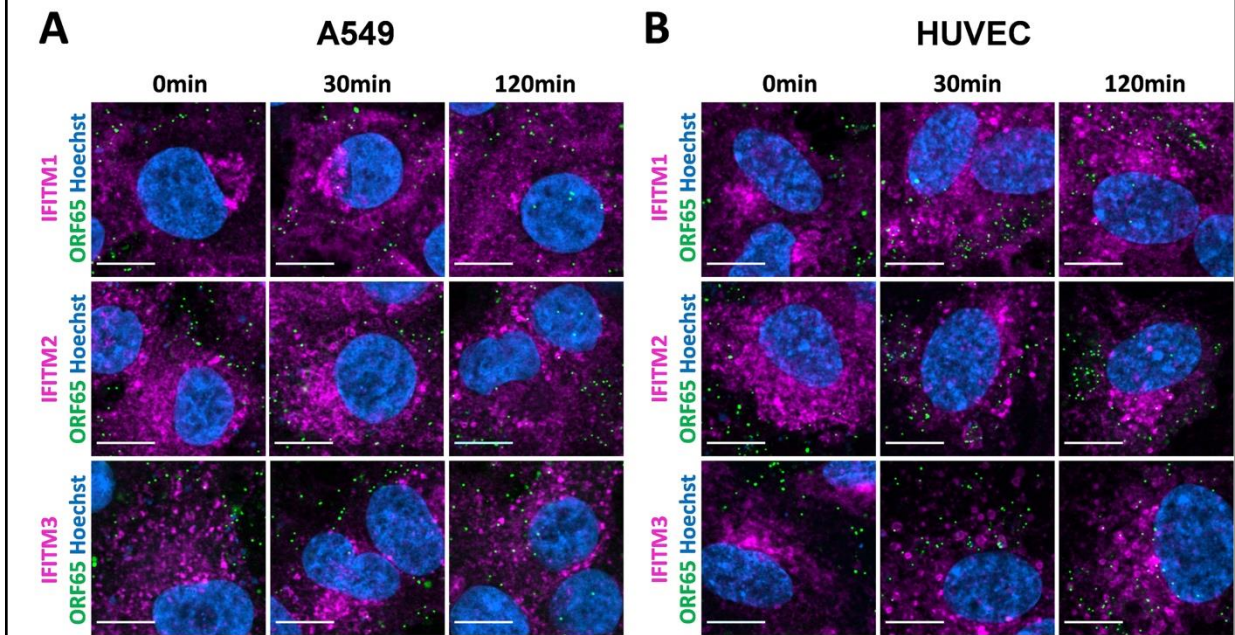
**Supplemental Figure 2**



### Supplemental Figure 3

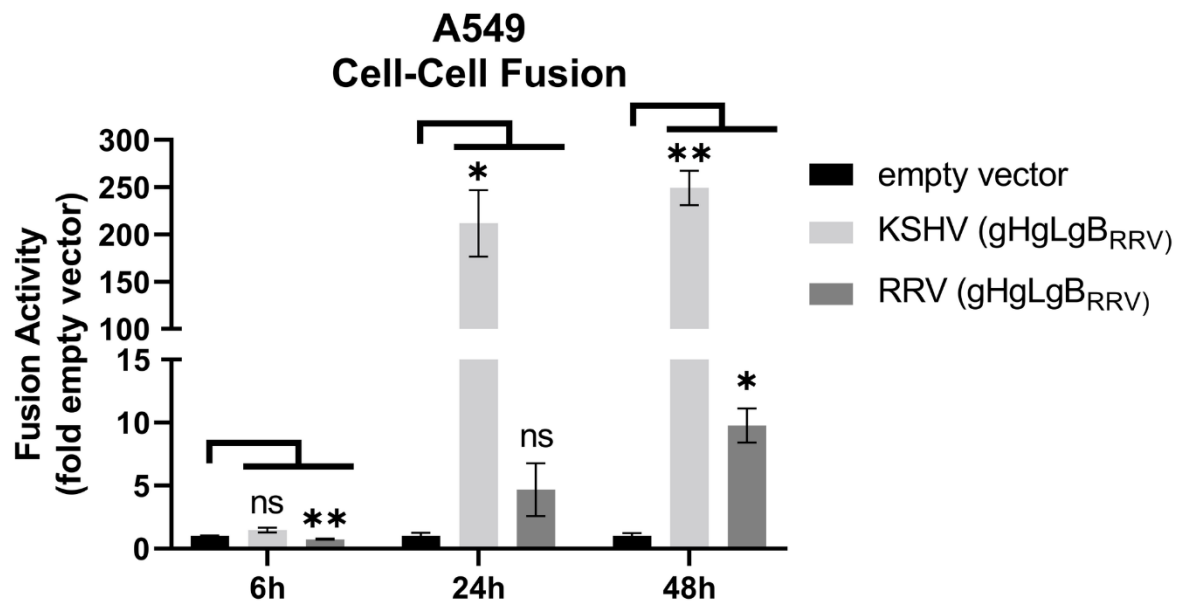


## Supplemental Figure 4





## Supplemental Figure 5



## 4 Discussion

### 4.1 Proteolytic activation of the SARS-CoV-2 Spike– Implications for pathogenesis and clinical intervention strategies.

Zoonotic viruses pose a major threat for humanity by causing severe epidemics and pandemics. The zoonotic virus of unknown origin, named SARS-CoV-2 caused an ongoing pandemic. In order to develop effective intervention strategies and antivirals, a profound knowledge of viral characteristics has to be gained. In the first publication (Publication 1), we analyzed the key features of the SARS-CoV-2 Spike and compared them with the related zoonotic virus SARS-CoV Spike. We used cell-cell fusion and pseudoparticle experiments. We were able to show that there are differences in the receptor requirements and proteolytic activation for cell-cell fusion between the SARS-CoV-2 and SARS-CoV Spike. These are, to a certain degree, owed to the multibasic cleavage motif acquired by the SARS-CoV-2-Spike at the S1/S2-site. Furthermore, we identified the matrix-metalloprotease (MMPs) inhibitor Batimastat to reduce the SARS-CoV-2 Spike mediated cell-cell fusion. We were also able to establish the exact TMPRSS2 priming site within the SARS-CoV-2 Spike for cell-cell and particle fusion. Finally, we could demonstrate activity of the drug Ambroxol against SARS-CoV-2 replication. Thereby this publication contributes to a better understanding how the key features of the SARS-CoV-2 Spike influence proteolytic activation and thus pathogenesis as well as clinical intervention strategies.

#### 4.1.1 The SARS-CoV-2 Spike – Contribution of syncytia formation and matrix-metalloprotease activation to SARS-CoV-2 pathogenesis

When the new coronavirus SARS-CoV-2 emerged, similarities to SARS-CoV regarding the Spike conservation, ACE2 receptor usage and proteolytic activation by TMPRSS2 were identified on an impressive timescale (18). Although both viruses share similarities, there are also important differences. We and others observed that in comparison to the SARS-CoV Spike, the SARS-CoV-2 Spike displays enhanced syncytia formation (Publication 1; (77, 79)). Syncytia allow viral spread without formation of free virus (chapter 2.2) and SARS-CoV-2 Spike mediated syncytia formation was shown to induce a cytopathic effect (77). Concerningly, syncytia were

not only found in lung biopsies (205) of COVID-19 patients, but might also play a role in the risk for cardiac arrhythmia during COVID-19, as SARS-CoV-2 Spike induced syncytia were also observed in a cardiomyocyte model (206). One of the differences between the SARS-CoV and the SARS-CoV-2 Spike is the pre-processing of the SARS-CoV-2 Spike by furin and related enzymes, that recognize a multibasic cleavage motif at the S1/S2-site (chapter 2.3.1).

We and others could show that mutation of this multibasic cleavage motif, which is not present in the SARS-CoV Spike, reduces the SARS-CoV-2 Spike-mediated formation of large multinucleated syncytia (Publication 1, (77, 79)), but not the general cell-cell fusion capability of the Spike when ACE2 and TMPRSS2 are present (Publication 1, (77)). We observed that the quantitative cell-cell fusion of the SARS-CoV, SARS-CoV-2-S1/S2-mutant and SARS-CoV-2 wt Spike is similar, when ACE2 and TMPRSS2 are present. However, the SARS-CoV and SARS-CoV-2-S1/S2-mutant Spikes displayed fusion of only a few cells, whereas the SARS-CoV-2 wt Spike generated large syncytia (Publication 1). This is surprising as the overall capability of the Spike to induce cell-cell fusion and to generate syncytia should be identical. A possible explanation for this observation might be given by experiments of Braga et al. (207), which identified several inhibitors of components of the host cellular  $Ca^{2+}$ -signaling to reduce the SARS-CoV-2 Spike-mediated syncytia formation. These experiments showed that SARS-CoV-2 Spike expression in human cells induces intracellular  $Ca^{2+}$  oscillation and that inhibition or downregulation of the  $Ca^{2+}$ -activated chloride channel TMEM16F reduced the syncytia formation (207). In addition to the chloride channel activity, TMEM16F is also a scramblase that translocates phosphatidylserine (PI) from the inner to the outer leaflet of the membrane (208). Increased PI-levels in the outer leaflet of the membrane is associated to cell-cell fusion events (209). It is therefore possible that the fusion capability of the SARS-CoV-2 Spike is enough to mediate initial cell-cell fusion of only a few cells, while the Spike-mediated  $Ca^{2+}$  oscillation and the resulting signaling is necessary to induce the formation of large syncytia. In line with the observation of reduced syncytia formation, the SARS-CoV Spike does also not induce  $Ca^{2+}$  oscillation similar to the SARS-CoV-2 Spike (207). Due to the absence of the multibasic cleavage motif in the SARS-CoV Spike and the fact that the S1/S2-site mutated SARS-CoV-2 Spike shows reduced syncytia formation, it is plausible to assume that the multibasic cleavage motif might be required for, or at least involved in, the SARS-CoV-2 Spike-mediated  $Ca^{2+}$  oscillation.



Besides the difference in the ability to generate syncytia, we observed differences in the receptor dependency and proteolytic activation of cell-cell fusion between the SARS-CoV-2 and SARS-CoV Spike. We observed that effective SARS-CoV-2 Spike mediated cell-cell fusion was only dependent on ACE2, while TMPRSS2 was dispensable. In contrast, SARS-CoV Spike mediated cell-cell fusion, mainly depended on TMPRSS2 and less on ACE2 (Publication 1). As proteolytic priming of the coronavirus Spike is a prerequisite for fusion activation (chapter 2.3.1 and 2.4.1) and the TMPRSS2 inhibitor Camostat was unable to reduce the cell-cell fusion activity (Publication 1), this suggests that cell-cell fusion activation of the SARS-CoV-2 Spike can occur by additional proteases. We therefore tested several protease inhibitors and identified the MMP-inhibitor Batimastat to effectively inhibit the SARS-CoV-2 Spike-mediated cell-cell fusion when only ACE2 is expressed. Similarly, Nguyen et al. identified the MMP-inhibitors Ilomastat and Marimastat as inhibitors of SARS-CoV-2 Spike-mediated cell-cell fusion (77). It thus seems that Batimastat-sensitive MMPs are capable to activate the SARS-CoV-2 Spike for cell-cell fusion, when ACE2 is present and TMPRSS2 is absent. A similar MMP activation of the SARS-CoV Spike mediated cell-cell fusion was not seen, indicating that there is a difference in the activation potential of the SARS-CoV and the SARS-CoV-2 Spike. Interestingly, mutation of the multibasic cleavage motif at the S1/S2-site reduced the TMPRSS2-independent activation, suggesting that the multibasic cleavage motif might be also relevant for ACE2-dependent MMP-activation of the SARS-CoV-2 Spike.

This raises the question why pre-processing of the S1/S2-site might be necessary for MMP activation. It was demonstrated that pre-cleavage at the S1/S2-site increases the binding of the Spike to ACE2 (14, 142). Structural comparison of SARS-CoV-2 wt and S1/S2-mutant Spikes revealed that in pre-cleaved Spikes, the RBD favors the open conformation and thereby accessibility for ACE2 binding (142). It thus seems plausible to assume that the easier accessibility to ACE2 by pre-cleavage at the S1/S2-site might allow a broader range of proteases to activate the SARS-CoV-2 Spike for cell-cell fusion. Although MMPs activate the SARS-CoV-2 Spike for cell-cell fusion, we were unable to observe an inhibitory effect of Batimastat on the entry of particles pseudotyped with the wt and S1/S2-mutated SARS-CoV-2 Spike into 293T-ACE2/TMPRSS2 cells as well as live virus replication in Calu-3 cells. However, it was shown that the MMP-inhibitors Prinomastat and Marimastat effectively inhibited the spread of SARS-CoV-2 in A549-ACE2 cells (210), which suggests that spread of live

virus in cells devoid of TMPRSS2 expression might be still partially mediated by MMPs. This observation is especially concerning, as MMP-1 and MMP-9 plasma levels were elevated in hospitalized COVID-19 patients and this elevation correlated with hospitalization and in case of MMP-9 with reduced 30-day survival rate after intensive care unit admission (211, 212). MMP expression is also upregulated in response to pro-inflammatory cytokines, which are also released upon SARS-CoV-2 infection, and MMP activity is associated to tissue damage in respiratory diseases (213, 214). Together with the potential MMP activation of cell-cell fusion and the S1/S2-site pre-cleavage mediated syncytia formation, this has the potential to result in a malicious feedback loop that might contribute to the SARS-CoV-2 pathogenesis and clinical outcome of COVID-19.

#### 4.1.2 Proteolytic fusion activation of the SARS-CoV-2 Spike has critical implications for clinical intervention

Although the multibasic cleavage motif at the S1/S2 subunit boarder and the activation by MMPs is a clear difference between SARS-CoV-2 and SARS-CoV, the most critical step of proteolytic priming in the S2-subunit for fusion of viral and host membrane remains the same. Due to the high conservation of the S2-subunit among coronaviruses and the fact that the SARS-CoV as well as the MERS-CoV Spike are activated by the protease TMPRSS2 (215, 78), the SARS-CoV-2 Spike was soon also identified to be activated in a TMPRSS2-dependent manner (18).

The SARS-CoV and MERS-CoV Spikes were demonstrated to be activated at the S2'-site present in the S2-subunit immediately upstream of the fusion peptide (93, 94, 99). This KR-motif is also present in SARS-CoV-2. As proteolytic activation is the key step in the entry and fusion of SARS-CoV-2, we mutated this motif and were able to show that this site is critical for TMPRSS2-mediated activation for cell-cell fusion and particle entry (Publication 1). Similar mutations were already introduced into the Spike of SARS-CoV. However, these mutated Spikes displayed reduced cell surface expression and incorporation into pseudoparticles (94, 216), which hampered the efforts to effectively study the influence of this mutations on the TMPRSS2-mediated activation of the SARS-CoV Spike. The observed reduction in cell-surface expression and pseudoparticle incorporation was likely based on reduced stability of the S2' mutated Spike, as it was possible to increase the incorporation by growing the producer cells at 32°C (94). Nguyen et al. reported that mutation of the SARS-CoV-2 S2'-site,

which displayed, in addition to reduction of TMPRSS2-mediated activation, reduced cleavage at the S1/S2-site (77). The reduction of cleavage into S1- and S2-subunits by mutation of the S2'-site would hint towards a more complicated activation process in which the activation of the S2'-site would be prerequisite for cleavage at the S1/S2-site. However, also the cell surface expression and incorporation into pseudoparticles of this S2'-site mutant was reduced (77), therefore the observed decrease in cleavage at the S1/S2-site is likely result of reduced stability of this mutant, too. After initially identifying the SARS-CoV-2 S2'-AA mutant showing lower surface expression, as well, we screened several mutants and identified the SARS-CoV-2 S2'-GH mutant displaying normal surface expression and particle incorporation. This mutant was still pre-processed at the S1/S2-site similar as the wt Spike. Interestingly, although any TMPRSS2-mediated activation for cell-cell fusion and particle entry was completely abolished, the cell-cell fusion was still inhibited by Batimastat and the particle entry by the cathepsin inhibitor E64-d. A similar observation was already made for the SARS-CoV Spike by Belourzard et al. (94). In their experiments, the SARS-CoV Spike KR-motif mutant R797N was still affected by NH<sub>4</sub>Cl treatment, which raises the endosomal pH required for cathepsin activation, suggesting that this mutant was also still activatable by cathepsins. In agreement with that, computational analysis of the SARS-CoV-2 Spike revealed several potential cathepsin cleavage sites near but not at the S2'-site (217). While this, on one hand demonstrates that the KR-motif in the S2-subunit is the recognition motif for TMPRSS2-mediated fusion activation, it clearly shows on the other hand, that the SARS-CoV-2 Spike can be likely activated redundantly by cathepsins and MMPs at sites distinct to that targeted by TMPRSS2.

Both, the TMPRSS2-mediated entry at the cell-surface and the cathepsin-mediated endocytic entry are utilized by the virus in cell-culture. Cells with high ACE2 and low TMPRSS2 expression are entered primarily in a cathepsin dependent manner, whereas cells with TMPRSS2 expression are entered via direct fusion at the plasma membrane (18, 95, 218). However, while the TMPRSS2-mediated entry also plays a clear role in coronavirus systemic infection (219–221), the in vivo importance of the cathepsin pathway is still under debate. For SARS-CoV it was demonstrated that Camostat inhibited infection in a mouse model, whereas the cysteine protease inhibitor K11777 was without effect on viral replication (219), indicating that the cathepsins are likely not utilized in effective infection of mice. Direct evidence whether the cathepsin



pathway is utilized in SARS-CoV-2 infection remain scarce, but there is some indirect evidence that would imply involvement of this cathepsin-dependent entry in human infection. It was shown that elevated cathepsin B and L plasma-levels of COVID-19 are related to disease severeness and in the same study it was demonstrated that the cathepsin inhibitor E64-d reduced the SARS-CoV-2 pseudoparticle entry in a humanized mouse model (222). Whether these results can be translated to humans is unclear. However, these results at least raise the possibility that both, the TMPRSS2 and cathepsin pathways might be both utilized in vivo. Together with cell-cell fusion, this might give the virus at least three options to propagate, which would have important influence on identification and design of antivirals that try to block the SARS-CoV-2 Spike-mediated entry.

#### 4.1.3 A potential role of Ambroxol in COVID-19 treatment

Being very effective in cell-culture settings, clinical trials using Camostat and related drugs were highly promising (18, 103, 223). However, the recent results of the Camostat clinical trial showed no significant improvement of neither disease progression nor clinical outcome (224). Similarly, studies using chloroquine and hydroxychloroquine, which likely increase the endosomal pH and thus inhibit pH-dependent virus entry (225, 226), were tested in cell-culture with promising results (227, 228), but remained ineffective in clinical trials (229). These observations possibly have several reasons: On one hand, the damages inflicted by SARS-CoV-2 infection are often already severe when clinical symptoms arise and are most likely not completely counteracted by inhibiting viral replication (20, 21). On the other hand, it was demonstrated that Camostat is most effective in Calu-3 cells with high TMPRSS2 expression levels and where the endosomal pathway is not available (18, 95, 103), while it is ineffective in cells which are mainly entered via the endosomal pathway in a cathepsin-dependent manner (95, 230). Vice versa chloroquine/ hydroxychloroquine does not inhibit the entry into cells which can be entered at the cell surface via TMPRSS2-mediated activation (226, 230). Although it is still possible that the bioavailability and the achievable intracellular concentrations of Camostat and chloroquine/hydroxychloroquine are too low, there is also still the possibility that the potential redundancy of the two pathways may result in ineffective inhibition by one of these drugs alone. The redundancy of viral propagation is increased by an additional layer, as MMP-mediated cell-cell fusion might be still possible in the presence of both

Camostat and chloroquine/hydroxychloroquine. Therefore, effective COVID-19 treatment, focusing on entry and fusion, likely must function on multiple layers.

Initially thought as a well-tolerated and widely distributed alternative to Camostat in SARS-CoV-2 inhibition, we tested the over-the-counter medications Ambroxol and Bromhexine. Bromhexine, which was identified to inhibit TMPRSS2 in previous studies (231), is a chemically-related metabolic precursor of Ambroxol. Ambroxol was tested because it has no severe side effects, it can be administered in high doses, and it accumulates in the lung (232–234).

We could show that Ambroxol and Bromhexine inhibit the SARS-CoV-2 replication in Calu-3 cells and in case of Ambroxol, also Spike-mediated cell-cell fusion, in some settings (Publication 1). However, when tested in pseudoparticle infection of 293T-ACE2/TMPRSS2 cells, Bromhexine and Ambroxol remained ineffective. Furthermore, neither the effect of Ambroxol or Bromhexine on SARS-CoV-2 infection of Calu-3 cells nor the effect of Ambroxol on SARS-CoV-2 mediated cell-cell fusion was robust. The missing effect of Ambroxol and Bromhexine on TMPRSS2 activation of the SARS-CoV-2 Spike for cell-cell fusion we observed, might be explained by redundant activation by MMPs. This is also the case for Camostat, which only inhibited the SARS-CoV-2 Spike mediated cell-cell fusion when used together with Batimastat. However, we observed that SARS-CoV-2 Spike-mediated cell-cell fusion was inhibited by Ambroxol and Bromhexine when either the S2'-site or the S1/S2-site was mutated and only ACE2 and not TMPRSS2 was expressed. As basal levels of TMPRSS2 expression are low or not present in 293T cells and the S2'-mutant is not activated by TMPRSS2, it is unlikely that the observed inhibition of Ambroxol and Bromhexine of the S2'-site or the S1/S2-site mutant is related to TMPRSS2. Together with results of Shrimp et al., which are questioning the overall inhibitory effect of Ambroxol and Bromhexine on TMPRSS2 activity (235), this raises the question about the reason for the inhibitory effect we observed. However, results of Olaleye et al. demonstrated that Ambroxol inhibits the interaction of the SARS-CoV-2 Spike with ACE2 (236). This inhibitory effect of Ambroxol would also be a suitable explanation for our observation that the sensitivity of the S2'-site and the S1/S2-site mutants to Ambroxol and Bromhexine is dependent on ACE2 and not TMPRSS2 expression. The inhibition of the SARS-CoV-2 Spike and ACE2 interaction would also explain the inhibitory effect of Ambroxol on SARS-CoV-2 replication observed by Bradfute et al. in Vero cells, which are entered in ACE2-dependent manner (237). In addition, the antiviral effect of

Ambroxol might be also explained by the observed inhibition of the acid sphingomyelinase by Ambroxol in the same cell type (238). In a previous report, the same group demonstrated that SARS-CoV-2 infection depends on ceramides, which are produced as result of acid sphingomyelinase enzyme activity (239). Although the reduction of ACE-binding or acid sphingomyelinase activity might both contribute to the reduced SARS-CoV-2 replication we observed in Calu-3 cells, we also observed an inhibitory effect of Ambroxol on pseudoparticle entry of VSV-G. Ambroxol was already shown to impact endocytosis of rhinovirus by increasing the endosomal pH (240) and thus likely also reduce the endosomal-dependent entry of VSV-G and potentially SARS-CoV-2. While Ambroxol might thereby influence already a variety of points in the viral entry, it was shown to have anti-inflammatory properties and to improve the survival of mice infected with IAV (241). Interestingly, Ambroxol was shown to reduce the cytokine release in human bronchoalveolar mononuclear cells (242) and the mRNA expression levels of MMP-2 in rat lung tissue (243). Furthermore, Ambroxol was successfully applied in the treatment of adult respiratory disease (244, 245), infant respiratory distress syndrome (246) and neonatal respiratory distress syndrome (244), which would add an additional layer in COVID-19 treatment. Together with the impact on viral replication and the good pharmacological properties (244), this would make Ambroxol and attractive candidate for clinical trials together with additional protease inhibitors such as Camostat.

#### **4.2 Differential antiviral activity of IFITMs towards gamma-2-herpesviruses– Hints to the IFITM function and viral evasion strategies**

IFITMs are broadly acting antiviral factors, that restrict the entry of a variety of viruses (see chapter 2.5.2). However, neither the exact mode of action nor the mechanism how some viruses avoid IFITM restriction have been completely clarified. In this work we could show that the entry gamma-2-herpesviruses of KSHV and RRV is, in principle, restricted by IFITM proteins. Furthermore, we could show that this restriction depends on the cell type. While IFITMs only partially colocalize with viral particles, they are able to reduce the fusion protein-mediated cell-cell fusion (Publication 2). Together this suggests that IFITMs can restrict the KSHV/RRV glycoprotein-mediated fusion and that this restriction is potentially avoided by fusion of the viral particles in IFITM-



negative compartments. These results give a better understanding of the IFITM function and how viruses may evade or counteract the IFITM-mediated restriction.

#### 4.2.1 Differential effects of IFITMs on gamma-2-herpesviruses- Implications for the IFITM function

We were able to show that IFITM1 restricts KSHV and RRV infection in a cell-dependent manner, while IFITM2 and IFITM3 were less effective in restricting the entry of KSHV and RRV (Publication 2). Given the fact that the function of IFITMs is still not completely clarified, this observation might give interesting hints regarding the function and interplay of IFITMs. It is a frequent observation that only a single IFITM and in several cases only IFITM1, restricts viral entry. Similar to KSHV and RRV, HSV-1, mumps virus, RSV, Jaagsiekte sheep retrovirus (JSRV) and Murine leukemia virus (MLV)-10A1 are also less affected by IFITM2/3, but highly by IFITM1 (183, 187). Of those, HSV-1, mumps virus and RSV have in common that entry into some cell types is proposed to occur near or at the plasma membrane (70, 247, 248), where also IFITM1 is mainly localized (177, 181, 183).

This raises the question about the function of IFITM1. While there are many proposed functions for IFITM3, IFITM1 is less well studied. IFITM3 was shown to induce negative curvature and increase the lipid order as well as the stiffness of the membrane in which it resides (187, 191). These modifications are proposed to still allow hemifusion but prevent fusion pore opening and thus inhibit fusion of viral and host membranes (187, 190, 191, 200). IFITM3-activity on the biophysical properties of membranes was mapped to its AH (189, 191). Due to the high similarity and the fact that this AH is also present in IFITM1 (Figure 6A), it is reasonable to assume that IFITM1 modifies membranes in a similar manner as IFITM3. In line with that, we observed inhibition of KSHV and RRV glycoprotein-mediated cell-cell fusion activity by IFITM1 and enhancement upon IFITM1/2/3 knockout. Similar to our experiments, cell-cell fusion activity mediated by the glycoproteins of HIV-1 (249), IAV (187, 189), VSV-G (189), JSRV (187) and SARS-CoV-2 (188) was also reduced by IFITMs, in case of SARS-CoV-2 Spike cell-cell fusion most by IFITM1. The activity of IFITM1 towards cell-cell fusion seems plausible, as cell-cell fusion involves fusion of two IFITM1-containing plasma membranes, supporting the idea that IFITM1 modifies membranes in a similar manner as IFITM3. In line with this notion we observed interchangeability of the IFITM

---

effect in our experiments using IFITM3 localization mutants. Mutation of the IFITM3 YxxΦ-motif (chapter 2.5.2, Figure 6), which is also the major difference to IFITM1, resulted in acquisition of an antiviral effect towards RRV that was similar to IFITM1 (Publication 2). It is therefore likely that IFITM1, IFITM2 and IFITM3 exert a similar effect on membrane fusion, but at different subcellular localizations.

While these results together would explain how IFITM1 might prevent viral fusion at the plasma membrane, it would not explain the restriction of KSHV and RRV, because they do not efficiently enter the cells via direct fusion at the plasma membrane. In contrast to RRV gB, which allows cell-cell fusion at neutral or medium pH (Publication 2, (130)) and thus potentially also plasma membrane fusion, KSHV gB apparently does not (own observation, (132)). Furthermore, we and others observed that the entry of KSHV and RRV is sensitive to an increase of endosomal pH by BafilomycinA1 (Publication 2, (113)), suggesting that they enter the cells primarily in an endosomal pH-dependent manner. It is therefore unlikely that the IFITM1 mediated effect towards KSHV and RRV fusion is exerted directly at the plasma membrane. Similarly, JSRV and MLV-10A1 also do not enter most of the tested cells at the plasma membrane (250, 251), but are still primarily restricted by IFITM1 (187). In addition to the plasma membranes, IFITM1 is also found in endosomal vesicles that are distinct from vesicles that colocalize with IFITM2 and IFITM3 (181–183). Interestingly, IFITM1 colocalizes and interacts with caveolin-1 (252). It is therefore possible that IFITM1 restricts viruses, that enter via caveolin-mediated entry. This would correlate with the observation that the IFITM1-restricted viruses MLV-10A1 and RSV enter some cell types via caveolin-mediated entry (250, 253).

However, RRV and JSRV are not associated to caveolin-mediated entry (113, 254) and KSHV as well as RSV enter only a subset of cells in a caveolin-dependent manner (124, 127, 253, 255). While this does not rule out that IFITM1 impacts caveolin-mediated entry, it would not explain restriction of the above-mentioned viruses, that do not exclusively utilize this entry pathway. A common observation made for IFITM1-restricted viruses by us for RRV, KSHV, (Publication 2) and by others for HSV-1, MLV-10A1, JSRV and RSV, is that they are highly sensitive to cholesterol depletion by methyl-beta-cyclodextrin (MBCD) (250, 256–258). Although MBCD influence all cholesterol-dependent fusion events, it also disturbs cholesterol-containing lipid rafts, which are utilized as signaling and entry platforms by a variety of viruses (259). IFITM1 was shown also to be associated to lipid rafts as it interacts with caveolin-1 (252),

---

which in turn colocalizes with lipid rafts and cholesterol (252, 260). Indeed, IFITM1 restricts a variety of viruses that are associated to lipid raft mediated entry (259, 261, 262), including the above mentioned KSHV, HSV-1, MLV-10A1, JSRV, RSV as well as IAV, SARS-CoV, SARS-CoV-2, DENV, EBOV, Marburg virus, WNV and HIV-1 (259, 261, 262). If IFITM1 affects membranes in which it resides in a similar manner as IFITM3, it is possible that IFITM1 influences the fusion of viruses that enter cells from lipid rafts or in a cholesterol-dependent manner. IFITM1 thereby might add an additional layer of restriction against viruses that enter not via the classical clathrin-mediated entry pathway, increasing the range of IFITM-mediated restriction.

#### 4.2.2 IFITM evasion of KSHV and RRV

While our experiments in part may explain the effect of IFITM1 towards KSHV and RRV, the question is still open why IFITM2 and IFITM3 fail to restrict RRV and IFITM2 KSHV, although both viruses enter the cells in an endosomal pH-dependent manner (Publication 2, (113)). A potential explanation how RRV escapes IFITM2 and IFITM3 is given by the fact that RRV gB fusion can be triggered at medium acidic to neutral pH (Publication 2, (130)). This might allow RRV to fuse early in the endosomal pathway and thus avoid IFITM2/IFITM3 containing late endosomes. For KSHV in contrast, we observed partial restriction by IFITM3, and this restriction disappears with IFITM3 delocalization mutants Y20A,  $\Delta$ 1-21 and 43AS, suggesting that the slight antiviral effect of IFITM3 towards KSHV might be exerted in endosomes. Together with the results showing that KSHV is sensitive to Bafilomycin A1, this implies that a proportion of KSHV particles must be localized to IFITM3 containing endosomes. Indeed, we observed partial colocalization of KSHV particles with IFITM2/3 in A549 cells and HUVEC, implying that KSHV enters IFITM2/3 containing endosomes. Still, KSHV is not restricted by IFITM2 and only minor by IFITM3 and knockout of IFITMs remains completely without effect in HUVEC. Together this suggests that there is a mechanism KSHV employs to avoid IFITM restriction.

We observed that entry into HUVEC, in contrast to A549 cells, was sensitive to the macropinocytosis inhibitor 5-(N-Ethyl-N-isopropyl)amiloride (EIPA). It can be speculated that KSHV's avoidance of IFITMs in HUVEC might be the result of macropinocytotic entry. EBOV, IAV and vaccinia virus are known to enter cells via macropinocytosis (263–265) and are restricted by IFITMs (262). However, the fact that they require pH-dependent activation in late endosomes (263–265), which also contain



IFITM2/IFITM3, makes it difficult to make a statement about the IFITM influence on macropinocytotic entry. It is therefore not possible to state whether the missing effect of IFITMs is caused by macropinocytosis or the fact that KSHV has an additional entry pathway available in HUVEC, that is not utilized in A549 cells. In addition to the observed difference in the entry pathway of KSHV, we could also show that KSHV particles colocalize with IFITM1 at a later timepoint in HUVEC than in A549 cells. The importance of colocalization of IFITMs and viral particles was demonstrated in live cell imaging experiments by Spence et al., which tracked IAV particles. It was shown that IAV particles colocalize with IFITM3-positive endosomes (200, 201) and that these particles are trapped in endosomes until they are subjected to degradation in the endolysosomal pathway (200, 202). A comparable effect might be exerted by IFITM1 on KSHV in A549 cells, as we observed similar colocalization of KSHV particles with IFITM1 over the course of the experiment. Interestingly, the percentage of colocalization of KSHV particles mirrored the percentage of IFITM1 restriction in A549 cells. In contrast to A549 cells, colocalization of IFITM1 with KSHV particles was observed in HUVEC at a later timepoint. Again, the lower percentage of colocalization with IFITM1 at this timepoint mirrored the effect of IFITM1 overexpression in these cells (Publication 2). Whether the observed later colocalization of KSHV particles in HUVEC can be assigned to macropinocytotic entry remains unclear, but it seems possible that the sensitivity to EIPA might be related to the difference in the timepoints of colocalization of KSHV particles with IFITM1 between A549 cells and HUVEC.

While we detected increasing colocalization over time for all IFITMs, at least 50% of KSHV particles still did not colocalize with IFITM signals. We frequently observed that KSHV particles are found in areas of low IFITM signal. Although we cannot provide evidence it is still plausible to assume that these particles mediate the actual infection of the cell, when considering the proposed IFITM-mediated inhibition on viral and host fusion. Beside the tracking of IAV particles Spence et al. (200) and Suddala et al. (201) also performed experiments with particles pseudotyped with the LASV glycoprotein. LASV is not restricted by IFITMs (174). By tracking the LASV glycoprotein pseudoparticles it became obvious that they do not colocalize with IFITM3 to the same extent as restricted IAV particles. It is unclear how this is possible as LASV fusion still requires low endosomal pH for fusion activation (266, 267). However, LASV utilizes a clathrin/caveolin independent pathway for entry (268), but is still sensitive to MBCD and BafilomycinA1 (267, 268). Given the fact that the cell-cell fusion activity mediated

by the glycoprotein of LASV is restricted by IFITMs (187), when the fusion requirements are fulfilled, it can be speculated that this clathrin/caveolin-independent entry might allow the IFITM avoidance. Interestingly, LASV entry is also sensitive to EIPA (269, 270), but due to insensitivity to inhibitors of actin remodeling, it was suggested that LASV utilizes an unconventional mode of macropinocytosis (269). Considering the similarities in inhibitor sensitivity and the fact that glycoprotein mediated cell-cell fusion of LASV and KSHV are impacted by IFITMs in a similar manner (Publication 2, (267–270)), it cannot be excluded that KSHV employs a similar strategy as LASV to evade IFITMs. This may also explain why KSHV infection is not impacted by IFITMs to the same degree as IAV (Publication 2). KSHV particles that enter classical IFITM-restricted endocytosis pathways might be restricted by IFITMs, while particles that utilize alternative pathways may escape the restriction, resulting in successful infection. This avoidance mechanism might be only fully available in some cell types like HUVEC and not in others like A549 cells, which are not entered via an EIPA-sensitive pathway. The effect of IFITMs on KSHV infection might be therefore dependent on the type or the availability of redundant entry routes, which may in turn also explain cell-dependent differences.

#### 4.2.3 Viral adaptation to IFITMs and influence on in vivo importance

The observation that KSHV and RRV might employ an avoidance mechanism that is functional in HUVEC but not in A549 cells is interesting, as HUVEC express comparably high endogenous IFITM levels, which are only marginally increased after IFN-treatment. KSHV is an endotheliotropic virus and endothelial cells might play a role in KS development (271, 272). Considering the strong effect of IFITMs on IAV infection (174) and the fact that IFITMs seem to be able to inhibit the in vitro cell-cell fusion of all fusion proteins tested so far (Publication 2, (187–189, 201, 249)), IFITMs likely represent a major membrane fusion barrier for all viruses. Indeed, IAV pseudoparticle infection of HUVEC, was not efficiently possible until IFITM1/2/3-knockout (Publication 2), underlining the potential importance of IFITMs in defense. However, not all viruses are restricted by IFITMs and while IFITMs may reduce infection they don't completely prevent infection. Given the fact that IFITMs are highly conserved and are found in nearly all vertebrate species (172), it is likely that evolutionary adaptation to IFITMs might represent an important process in virus evolution. Viruses utilize a variety of mechanism to adapt to IFITMs. Minor mutations

in the HIV-1 env already allow avoidance and renders transmitted founder viruses resistant against IFITM-mediated restriction (273). It is suggested that plasma membrane fusion of SARS-CoV-2 allows avoidance of the IFITM-mediated effect and might be one reason for the importance of the SARS-CoV-2 Spike multibasic cleavage site (95, 274). Interestingly, SARS-CoV-2 entry into Calu-3 cells was shown to be enhanced by IFITM2 (275). Similarly, also infection of the human coronavirus HCoV-OC43 is enhanced by both, IFITM2 and IFITM3 (276), suggesting that coronaviruses not just evolved a mechanism for IFITM avoidance, but a possibility to utilize IFITMs for infection. In the group of herpesviruses, HCMV is also not restricted by IFITMs and hijacks them for viral particle assembly (277).

Also, earlier reports of the IFITM effect on KSHV infection demonstrated that KSHV infection of BJABs was enhanced upon IFITM1 overexpression (278, 279). Although we observed an enhancement of KSHV infection just for IFITM2 in SLKs, the cell dependency of the IFITM-mediated effect on KSHV infection makes an enhancement of infection in some cell types possible. Whether the enhancing effect of IFITMs on KSHV infection is limited to the reported cell types remains unclear. However, while KSHV effectively suppresses IFN induction by expressing viral Interferon regulatory factors (vIRF) that are homologues to human IRFs (280, 281), we observed that IFITM expression is still enhanced upon KSHV infection of A549 cells. It was shown that, although KSHV is effectively suppressing the IFN-response, the levels of IFITMs are still increased upon KSHV infection (282, 283). It is not further investigated how this is achieved, but it is possible that KSHV induces IFITM expression via its viral interleukin-6 (vIL6). The human and mice IFITM3 are in addition to IFN, also upregulated by IL-6 in a cell type dependent manner (284, 285). Therefore IFITM upregulation might be, at least partially, a result of KSHV vIL-6 expression. It is therefore possible that the observed avoidance of IFITMs by KSHV is an evolutionary adaptation because downregulation of IFITMs is not achieved or evolutionary disfavored, as IFITMs seem to be utilized for entry into some cell types (278, 279).

From our results we cannot conclude whether KSHV evolved the observed IFITM mediated enhancement (278, 279) or avoidance (Publication 2) during course of evolution, but it is at least plausible as a similar adaptation is also observed for CoVs (179, 276) and other herpesviruses (277, 278). Still, the antiviral effect of IFITMs against e.g. IAV is of high importance in vivo. Knockout of the IFITM-Cluster in mice resulted in an drastic increase of disease progression, mortality and higher systemic

viral burden after IAV infection (284). This effect was mainly accounted to IFITM3, as *ifitm3* deletion did not surpass the effect of the *ifitm*-cluster knockout. A similar observation was made in *ifitm3* knockout mice where lethality was greatly enhanced upon WNV infection (286). Interestingly, the IFITM3-mediated restriction was mainly observed in primary cells and cells of fibroblast origin and less in neuronal tissues (286).

We also observed stronger effects of IFITM-knockout in primary cells upon IAV pseudoparticle infection (Publication 2). As these cells displayed as well high levels of basal IFITM expression, it is tempting to speculate that IFITMs play a role in constitutive defense against viruses and thus function as a major barrier for primary infection. Given the importance of IFITMs in cell culture and *in vivo* models it is not surprising that IFITMs might also play a role on a populational level. Single nucleotide polymorphisms (SNP) in IFITM3 are frequently found in the human population and were shown to result in changes of IFITM expression levels (287, 288), or alternative RNA splicing (289). Especially the IFITM3 variant rs12252 is associated with increased disease progression or severeness of HIV (290), IAV (289, 291) and SARS-CoV-2 (292–294) infections. Given the modest effect of IFITMs we observed on KSHV infection of many types of cells, it is unlikely that genetic variants may play a major role for KSHV. However, the dramatic increase in KSHV infection of A549 cells upon IFITM knockout, suggests that IFITMs might play a role in prevention of KSHV infection of specific cell types and may therefore contribute to inhibition of the systemic spread of KSHV.



## 5 Outlook

Although we were able to gain insights into the differences in proteolytic activation and receptor usage of SARS-CoV-2 and SARS-CoV, there are still open questions. While the multibasic cleavage site is clearly involved in the syncytia formation of the SARS-CoV-2 Spike, it is unclear how it facilitates the cell-cell fusion or whether it contributes to the Spike mediated  $Ca^{2+}$  signaling. It might be therefore interesting to test whether S1/S2-mutants still trigger  $Ca^{2+}$ -oscillation. Although syncytia were observed in the lungs of COVID-19 patients and they induce cytopathic effects in vitro, the degree of contribution to the SARS-CoV-2 pathogenesis is not clear and might be addressed in future studies.

While metalloproteases can activate SARS-CoV-2 for cell-cell fusion and metalloprotease inhibitors were shown to reduce the replication of SARS-CoV-2 in A549-ACE2 cells, it remains unknown whether MMPs also play a role in vivo. Identification of the MMP cleavage site in the SARS-COV-2 Spike might give information about the importance of the MMP activation. As several tools for manipulation of the SARS-CoV-2 genome are now available, the mutation of the TMPRSS2-priming site, which we identified, as well as additional proteolytic priming site mutants might be introduced into live virus and tested in mice or ferret models. This would allow the investigation of the in vivo importance of activation via different protease types for SARS-CoV-2 infection and pathogenesis.

The observation that fusion of the SARS-CoV Spike can be triggered with no or reduced ACE2-levels, at least for cell-cell fusion, might hint towards interesting differences in the activation potential and requires further investigation. Especially in the light of an unknown number of coronaviruses still present in bats, with high potential of zoonotic transmission, it is important to fully understand the Spike fusion mechanisms in detail.

Meanwhile there are several vaccines against SARS-CoV-2 available. However, as new mutations with increasing immune escape arise, there is still a demand for effective drugs against COVID-19. We observed that SARS-CoV-2 activation and entry and cell-cell fusion shows a high degree of redundancy regarding proteolytic activation. Although the proteolytic activation is an attractive intervention step, it might not be sufficient to inhibit only a single protease-family. Future investigations and clinical studies therefore have to focus on either combining several protease inhibitors or on

targeting multiple steps in the SARS-CoV-2 replication cycle. We hope that this work might convince towards the use of Ambroxol in combination with protease inhibitors in upcoming clinical trials. While the inhibitory effect of Ambroxol might be mild, the potential to target different steps of the SARS-CoV-2 entry, the pharmacological properties and the fact that it is already used in treatment against respiratory diseases, makes it a good candidate for clinical trials.

In this work we were also able to increase the list of viruses inhibited by the broad-spectrum fusion restrictors IFITMs. Although the effect of IFITMs against KSHV and RRV was rather mild, the differences in the restriction potential of individual IFITMs and the cell-dependency of the IFITM restriction gave interesting insights into the overall IFITM function. Our approach of complete IFITMs knockout gave us the chance to study IFITM function at basal expression levels, which reduces chance of overexpression artifacts and might thereby give future directions in how to study IFITM function. This is especially true as we saw a discrepancy between overexpression and knockout experiments.

Furthermore, in future studies IFITMs might be utilized together with endocytic inhibitors to block potential redundant entry pathways. It might be also interesting to perform live particle tracking experiments with KSHV and RRV particles that identify the actual site of viral fusion to see whether these sites correlate with IFITM positive or negative compartments. Mutations in the AH of IFITM1 might also show whether the effect of IFITM1 on KSHV, RRV and other IFITM1 restricted viruses is similar as observed for IFITM3. While it is unlikely that IFITMs can be used as intervention against KSHV, our results together with the observation of others that all IFITMs are in principle able to restrict viral fusion protein mediated cell-cell fusion and that the activity likely depends on IFITM localization might lead to the development of a new generation of broad-spectrum fusion inhibitors. As recent results showed that the amphipathic helix is sufficient to exhibit the observed IFITM restriction, it might be possible to generate small peptide drugs that base on the structure of the IFITM amphipathic helix, similar to amphiphilic thiazolidine derivatives (165, 166) and rigid amphipathic fusion inhibitors (167, 168). For that, future studies must focus on the question how viruses evade the IFITM function, in order to design potential mimics in a way that avoidance is counteracted.

## 6 References

1. Worobey M, Han G-Z, Rambaut A. 2014. Genesis and pathogenesis of the 1918 pandemic H1N1 influenza A virus. *PNAS* 111:8107–8112.
2. Sharp PM, Hahn BH. 2011. Origins of HIV and the AIDS Pandemic. *Cold Spring Harb perspect med* 1:a006841–a006841.
3. Holmes EC, Dudas G, Rambaut A, Andersen KG. 2016. The evolution of Ebola virus: Insights from the 2013–2016 epidemic. *Nature* 538:193–200.
4. Zhao X, Ding Y, Du J, Fan Y. 2020. 2020 update on human coronaviruses: One health, one world. *Medicine in Novel Technology and Devices* 8:100043.
5. Finkel Y, Mizrahi O, Nachshon A, Weingarten-Gabbay S, Morgenstern D, Yahalom-Ronen Y, Tamir H, Achdout H, Stein D, Israeli O, Beth-Din A, Melamed S, Weiss S, Israely T, Paran N, Schwartz M, Stern-Ginossar N. 2021. The coding capacity of SARS-CoV-2. *Nature* 589:125–130.
6. Zhou P, Yang X-L, Wang X-G, Hu B, Zhang L, Zhang W, Si H-R, Zhu Y, Li B, Huang C-L, Chen H-D, Chen J, Luo Y, Guo H, Jiang R-D, Liu M-Q, Chen Y, Shen X-R, Wang X, Zheng X-S, Zhao K, Chen Q-J, Deng F, Liu L-L, Yan B, Zhan F-X, Wang Y-Y, Xiao G-F, Shi Z-L. 2020. A pneumonia outbreak associated with a new coronavirus of probable bat origin. *Nature* 579:270–273.
7. Lu R, Zhao X, Li J, Niu P, Yang B, Wu H, Wang W, Song H, Huang B, Zhu N, Bi Y, Ma X, Zhan F, Wang L, Hu T, Zhou H, Hu Z, Zhou W, Zhao L, Chen J, Meng Y, Wang J, Lin Y, Yuan J, Xie Z, Ma J, Liu WJ, Wang D, Xu W, Holmes EC, Gao GF, Wu G, Chen W, Shi W, Tan W. 2020. Genomic characterisation and epidemiology of 2019 novel coronavirus: implications for virus origins and receptor binding. *The Lancet* 395:565–574.
8. Lytras S, Hughes J, Martin D, de Klerk A, Lourens R, Kosakovsky Pond SL, Xia W, Jiang X, Robertson DL. 2021. Exploring the natural origins of SARS-CoV-2 in the light of recombination. preprint, *Evolutionary Biology*.
9. Zhang T, Wu Q, Zhang Z. 2020. Probable Pangolin Origin of SARS-CoV-2 Associated with the COVID-19 Outbreak. *Curr Biol* 30:1578.
10. Lam TT-Y, Jia N, Zhang Y-W, Shum MH-H, Jiang J-F, Zhu H-C, Tong Y-G, Shi Y-X, Ni X-B, Liao Y-S, Li W-J, Jiang B-G, Wei W, Yuan T-T, Zheng K, Cui X-M, Li J, Pei G-Q, Qiang X, Cheung WY-M, Li L-F, Sun F-F, Qin S, Huang J-C, Leung GM, Holmes EC, Hu Y-L, Guan Y, Cao W-C. 2020. Identifying SARS-CoV-2-related coronaviruses in Malayan pangolins. *Nature* 583:282–285.
11. Lytras S, Xia W, Hughes J, Jiang X, Robertson DL. 2021. The animal origin of SARS-CoV-2. *Science* 373:968–970.
12. Temmam S, Vongphayloth K, Salazar EB, Munier S, Bonomi M, Régnauld B, Douangboubpha B, Karami Y, Chretien D, Sanamxay D, Xayaphet V, Paphaphanh P, Lacoste V, Somlor S, Lakeomany K, Phommavanh N, Pérot P, Donati F, Bigot T, Nilges M, Rey F, Werf S van der, Brey P, Eloit M. 2021. Coronaviruses with a SARS-CoV-2-like receptor-binding domain allowing ACE2-mediated entry into human cells isolated from bats of Indochinese peninsula. preprint, In Review.
13. Holmes EC, Goldstein SA, Rasmussen AL, Robertson DL, Crits-Christoph A, Wertheim JO, Anthony SJ, Barclay WS, Boni MF, Doherty PC, Farrar J, Geoghegan JL, Jiang X, Leibowitz JL, Neil SJD, Skern T, Weiss SR, Worobey M, Andersen KG, Garry RF, Rambaut A. 2021. The origins of SARS-CoV-2: A critical review. *Cell* 184:4848–4856.
14. Wrobel AG, Benton DJ, Xu P, Roustan C, Martin SR, Rosenthal PB, Skehel JJ, Gamblin SJ. 2020. SARS-CoV-2 and bat RaTG13 spike glycoprotein structures

- inform on virus evolution and furin-cleavage effects. *Nat Struct Mol Biol* 27:763–767.
15. Morawska L, Cao J. 2020. Airborne transmission of SARS-CoV-2: The world should face the reality. *Environ Int* 139:105730.
  16. Meyerowitz EA, Richterman A, Gandhi RT, Sax PE. 2021. Transmission of SARS-CoV-2: A Review of Viral, Host, and Environmental Factors. *Ann Intern Med* 174:69–79.
  17. Malaiyan J, Arumugam S, Mohan K, Gomathi Radhakrishnan G. 2021. An update on the origin of SARS-CoV-2: Despite closest identity, bat (RaTG13) and pangolin derived coronaviruses varied in the critical binding site and O-linked glycan residues. *J Med Virol* 93:499–505.
  18. Hoffmann M, Kleine-Weber H, Schroeder S, Krüger N, Herrler T, Erichsen S, Schiergens TS, Herrler G, Wu N-H, Nitsche A, Müller MA, Drosten C, Pöhlmann S. 2020. SARS-CoV-2 Cell Entry Depends on ACE2 and TMPRSS2 and Is Blocked by a Clinically Proven Protease Inhibitor. *Cell* 181:271-280.e8.
  19. Wang CC, Prather KA, Sznitman J, Jimenez JL, Lakdawala SS, Tufekci Z, Marr LC. 2021. Airborne transmission of respiratory viruses. *Science* 373:eabd9149.
  20. Guan W, Ni Z, Hu Y, Liang W, Ou C, He J, Liu L, Shan H, Lei C, Hui DSC, Du B, Li L, Zeng G, Yuen K-Y, Chen R, Tang C, Wang T, Chen P, Xiang J, Li S, Wang J, Liang Z, Peng Y, Wei L, Liu Y, Hu Y, Peng P, Wang J, Liu J, Chen Z, Li G, Zheng Z, Qiu S, Luo J, Ye C, Zhu S, Zhong N. 2020. Clinical Characteristics of Coronavirus Disease 2019 in China. *N Engl J Med* 382:1708–1720.
  21. Zeng H, Ma Y, Zhou Z, Liu W, Huang P, Jiang M, Liu Q, Chen P, Luo H, Chen Y. 2021. Spectrum and Clinical Characteristics of Symptomatic and Asymptomatic Coronavirus Disease 2019 (COVID-19) With and Without Pneumonia. *Front Med* 8:645651.
  22. Wu C, Chen X, Cai Y, Xia J, Zhou X, Xu S, Huang H, Zhang L, Zhou X, Du C, Zhang Y, Song J, Wang S, Chao Y, Yang Z, Xu J, Zhou X, Chen D, Xiong W, Xu L, Zhou F, Jiang J, Bai C, Zheng J, Song Y. 2020. Risk Factors Associated With Acute Respiratory Distress Syndrome and Death in Patients With Coronavirus Disease 2019 Pneumonia in Wuhan, China. *JAMA Intern Med* 180:934.
  23. Tian J, Yuan X, Xiao J, Zhong Q, Yang C, Liu B, Cai Y, Lu Z, Wang J, Wang Y, Liu S, Cheng B, Wang J, Zhang M, Wang L, Niu S, Yao Z, Deng X, Zhou F, Wei W, Li Q, Chen X, Chen W, Yang Q, Wu S, Fan J, Shu B, Hu Z, Wang S, Yang X-P, Liu W, Miao X, Wang Z. 2020. Clinical characteristics and risk factors associated with COVID-19 disease severity in patients with cancer in Wuhan, China: a multicentre, retrospective, cohort study. *The Lancet Oncology* 21:893–903.
  24. Sudre CH, Murray B, Varsavsky T, Graham MS, Penfold RS, Bowyer RC, Pujol JC, Klaser K, Antonelli M, Canas LS, Molteni E, Modat M, Jorge Cardoso M, May A, Ganesh S, Davies R, Nguyen LH, Drew DA, Astley CM, Joshi AD, Merino J, Tsereteli N, Fall T, Gomez MF, Duncan EL, Menni C, Williams FMK, Franks PW, Chan AT, Wolf J, Ourselin S, Spector T, Steves CJ. 2021. Attributes and predictors of long COVID. *Nat Med* 27:626–631.
  25. Islam MF, Cotler J, Jason LA. 2020. Post-viral fatigue and COVID-19: lessons from past epidemics. *Fatigue: Biomedicine, Health & Behavior* 8:61–69.
  26. Hampshire A, Trender W, Chamberlain SR, Jolly AE, Grant JE, Patrick F, Mazibuko N, Williams SC, Barnby JM, Hellyer P, Mehta MA. 2021. Cognitive deficits in people who have recovered from COVID-19. *EClinicalMedicine* 39:101044.
  27. Ramcharan T, Nolan O, Lai CY, Prabhu N, Krishnamurthy R, Richter AG, Jyothish D, Kanthimathinathan HK, Welch SB, Hackett S, Al-Abadi E, Scholefield BR,



- Chikermane A. 2020. Paediatric Inflammatory Multisystem Syndrome: Temporally Associated with SARS-CoV-2 (PIMS-TS): Cardiac Features, Management and Short-Term Outcomes at a UK Tertiary Paediatric Hospital. *Pediatr Cardiol* 41:1391–1401.
28. Davies P, Evans C, Kanthimathinathan HK, Lillie J, Brierley J, Waters G, Johnson M, Griffiths B, du Pré P, Mohammad Z, Deep A, Playfor S, Singh D, Inwald D, Jardine M, Ross O, Shetty N, Worrall M, Sinha R, Koul A, Whittaker E, Vyas H, Scholefield BR, Ramnarayan P. 2020. Intensive care admissions of children with paediatric inflammatory multisystem syndrome temporally associated with SARS-CoV-2 (PIMS-TS) in the UK: a multicentre observational study. *The Lancet Child & Adolescent Health* 4:669–677.
  29. Krammer F. 2020. SARS-CoV-2 vaccines in development. *Nature* 586:516–527.
  30. Creech CB, Walker SC, Samuels RJ. 2021. SARS-CoV-2 Vaccines. *JAMA* 325:1318.
  31. Korr G, Thamm M, Czogiel I, Poethko-Mueller C, Bremer V, Jansen K. 2017. Decreasing seroprevalence of herpes simplex virus type 1 and type 2 in Germany leaves many people susceptible to genital infection: time to raise awareness and enhance control. *BMC Infect Dis* 17:471.
  32. Wen L, Qiu Y, Cheng S, Jiang X, Ma Y-P, Fang W, Wang W, Cui J, Ruan Q, Zhao F, Hu F, Luo M-H. 2018. Serologic and viral genome prevalence of HSV, EBV, and HCMV among healthy adults in Wuhan, China. *J Med Virol* 90:571–581.
  33. McGeoch DJ, Cook S, Dolan A, Jamieson FE, Telford EAR. 1995. Molecular Phylogeny and Evolutionary Timescale for the Family of Mammalian Herpesviruses. *J Mol Biol* 247:443–458.
  34. Stempel M, Chan B, Brinkmann MM. 2019. Coevolution pays off: Herpesviruses have the license to escape the DNA sensing pathway. *Med Microbiol Immunol* 208:495–512.
  35. Kaufer BB, Flamand L, Cohrs RJ, Dewals BG, Muylkens B. 2020. Herpesvirus Latency. *Front Microbiol* 169.
  36. Grinde B. 2013. Herpesviruses: latency and reactivation – viral strategies and host response. *J Oral Microbiol* 5:22766.
  37. Roizman B, Carmichael LE, Deinhardt F, de-The G, Nahmias AJ, Plowright W, Rapp F, Sheldrick P, Takahashi M, Wolf K. 1981. Herpesviridae. *Intervirology* 16:201–217.
  38. Sinclair J, Sissons P. 2006. Latency and reactivation of human cytomegalovirus. *J Gen Virol* 87:1763–1779.
  39. Broussard G, Damania B. 2020. Regulation of KSHV Latency and Lytic Reactivation. *Viruses* 12:1034.
  40. Deshmane SL, Fraser NW. 1989. During latency, herpes simplex virus type 1 DNA is associated with nucleosomes in a chromatin structure. *J Virol* 63:943–947.
  41. Stoeger T, Adler H. 2019. “Novel” Triggers of Herpesvirus Reactivation and Their Potential Health Relevance. *Front Microbiol* 9:3207.
  42. Kobayashi M, Wilson AC, Chao MV, Mohr I. 2012. Control of viral latency in neurons by axonal mTOR signaling and the 4E-BP translation repressor. *Genes Dev* 26:1527–1532.
  43. Freeman ML, Sheridan BS, Bonneau RH, Hendricks RL. 2007. Psychological Stress Compromises CD8<sup>+</sup> T Cell Control of Latent Herpes Simplex Virus Type 1 Infections. *J Immunol* 179:322–328.
  44. Stowe R, Kozlova E, Yetman D, Walling D, Goodwin J, Glaser R. 2007. Chronic herpesvirus reactivation occurs in aging. *Exp Gerontol* 42:563–570.
  45. Chang Y, Moore PS, Weiss RA. 2017. Human oncogenic viruses: nature and

- discovery. *Phil Trans R Soc B* 372:20160264.
46. Wen KW, Damania B. 2010. Kaposi sarcoma-associated herpesvirus (KSHV): Molecular biology and oncogenesis. *Cancer Letters* 289:140–150.
  47. Sathish N, Wang X, Yuan Y. 2012. Tegument Proteins of Kaposi's Sarcoma-Associated Herpesvirus and Related Gamma-Herpesviruses. *Front Microbio* 3.
  48. Kaposi. 1872. Idiopathisches multiples Pigmentsarkom der Haut. *Arch f Dermat* 4:265–273.
  49. Dutz W, Stout AP. 1960. Kaposi's sarcoma in infants and children. *Cancer* 13:684–694.
  50. Beral V, Newton R. 1998. Overview of the Epidemiology of Immunodeficiency-Associated Cancers. *JNCI Monographs* 1998:1–6.
  51. Barozzi P, Luppi M, Facchetti F, Mecucci C, Alù M, Sarid R, Rasini V, Ravazzini L, Rossi E, Festa S, Crescenzi B, Wolf DG, Schulz TF, Torelli G. 2003. Post-transplant Kaposi sarcoma originates from the seeding of donor-derived progenitors. *Nat Med* 9:554–561.
  52. Cesarman E, Knowles DM. 1995. Kaposi's Sarcoma–Associated Herpesvirus-Like DNA Sequences in AIDS-Related Body-Cavity–Based Lymphomas. *N Engl J Med* 332:6.
  53. Soulier J, Grollet L, Oksenhendler E, Cacoub P, Cazals-Hatem D, Babinet P, d'Agay M, Clauvel J, Raphael M, Degos L, Sigaux F. 1995. Kaposi's sarcoma-associated herpesvirus-like DNA sequences in multicentric Castleman's disease. *Blood* 86:1276–1280.
  54. Polizzotto MN, Uldrick TS, Wyvill KM, Aleman K, Marshall V, Wang V, Whitby D, Pittaluga S, Jaffe ES, Millo C, Tosato G, Little RF, Steinberg SM, Sereti I, Yarchoan R. 2016. Clinical Features and Outcomes of Patients With Symptomatic Kaposi Sarcoma Herpesvirus (KSHV)-associated Inflammation: Prospective Characterization of KSHV Inflammatory Cytokine Syndrome (KICS). *Clin Infect Dis* 62:730–738.
  55. Chen Q, Chen J, Li Y, Liu D, Zeng Y, Tian Z, Yunus A, Yang Y, Lu J, Song X, Yuan Y. 2021. Kaposi's sarcoma herpesvirus is associated with osteosarcoma in Xinjiang populations. *PNAS* 118:e2016653118.
  56. Minhas V, Wood C. 2014. Epidemiology and Transmission of Kaposi's Sarcoma-Associated Herpesvirus. *Viruses* 6:4178–4194.
  57. Cesarman E, Damania B, Krown SE, Martin J, Bower M, Whitby D. 2019. Kaposi sarcoma. *Nat Rev Dis Primers* 5:9.
  58. Parkin DM, Sitas F, Chirenje M, Stein L, Abratt R, Wabinga H. 2008. Part I: Cancer in Indigenous Africans—burden, distribution, and trends. *The Lancet Oncology* 9:683–692.
  59. Amir H, Kaaya EE, Manji KP, Kwesigabo G, Biberfeld P. 2001. Kaposi's sarcoma before and during a human immunodeficiency virus epidemic in Tanzanian children: *J Pediatr Infect Dis* 20:518–521.
  60. Ryu W-S. 2017. Virus Life Cycle, p. 31–45. *In* *Molecular Virology of Human Pathogenic Viruses*. Elsevier.
  61. Koehler M, Delguste M, Sieben C, Gillet L, Alsteens D. 2020. Initial Step of Virus Entry: Virion Binding to Cell-Surface Glycans. *Annu Rev Virol* 7:143–165.
  62. Olofsson S, Bergström T. 2005. Glycoconjugate glycans as viral receptors. *Annals of Medicine* 37:154–172.
  63. Di Giovine P, Settembre EC, Bhargava AK, Luftig MA, Lou H, Cohen GH, Eisenberg RJ, Krummenacher C, Carfi A. 2011. Structure of Herpes Simplex Virus Glycoprotein D Bound to the Human Receptor Nectin-1. *PLoS Pathog* 7:e1002277.
  64. Krummenacher C, Supekari VM, Whitbeck JC, Lazear E, Connolly SA, Eisenberg

- RJ, Cohen GH, Wiley DC, Carfi A. 2005. Structure of unliganded HSV gD reveals a mechanism for receptor-mediated activation of virus entry: Structure of unliganded HSV gD. *The EMBO Journal* 24:4144–4153.
65. Helenius A, Kartenbeck J, Simons K, Fries E. 1980. On the entry of semliki forest virus into BHK-21 cells. *J Cell Biol* 84:404–420.
  66. Snyers L, Zwickl H, Blaas D. 2003. Human Rhinovirus Type 2 Is Internalized by Clathrin-Mediated Endocytosis. *J Virol* 77:5360–5369.
  67. Sieben C, Sezgin E, Eggeling C, Manley S. 2020. Influenza A viruses use multivalent sialic acid clusters for cell binding and receptor activation. *PLoS Pathog* 16:e1008656.
  68. Pernet O, Pohl C, Ainouze M, Kweder H, Buckland R. 2009. Nipah virus entry can occur by macropinocytosis. *Virology* 395:298–311.
  69. Herold N, Anders-Ößwein M, Glass B, Eckhardt M, Müller B, Kräusslich H-G. 2014. HIV-1 Entry in SupT1-R5, CEM-ss, and Primary CD4<sup>+</sup> T Cells Occurs at the Plasma Membrane and Does Not Require Endocytosis. *J Virol* 88:13956–13970.
  70. Lycke E, Hamark B, Johansson M, Krotowil A, Lycke J, Svennerholm B. 1988. Herpes simplex virus infection of the human sensory neuron: An electron microscopy study. *Arch Virol* 101:87–104.
  71. Mercer J, Schelhaas M, Helenius A. 2010. Virus Entry by Endocytosis. *Annu Rev Biochem* 79:803–833.
  72. Mercer J, Helenius A. 2009. Virus entry by macropinocytosis. *Nat Cell Biol* 11:510–520.
  73. Rampersad S, Tennant P. 2018. Replication and Expression Strategies of Viruses, p. 55–82. *In* *Viruses*. Elsevier.
  74. Hoggan MD, Roizman B. 1959. THE ISOLATION AND PROPERTIES OF A VARIANT OF HERPES SIMPLEX PRODUCING MULTINUCLEATED GIANT CELLS IN MONOLAYER CULTURES IN THE PRESENCE OF ANTIBODY1. *Am J Epidemiol* 70:208–219.
  75. Sodroski J, Goh WC, Rosen C, Campbell K, Haseltine WA. 1986. Role of the HTLV-III/LAV envelope in syncytium formation and cytopathicity. *Nature* 322:470–474.
  76. Wright PF, Ikizler MR, Gonzales RA, Carroll KN, Johnson JE, Werkhaven JA. 2005. Growth of Respiratory Syncytial Virus in Primary Epithelial Cells from the Human Respiratory Tract. *J Virol* 79:8651–8654.
  77. Nguyen HT, Zhang S, Wang Q, Anang S, Wang J, Ding H, Kappes JC, Sodroski J. 2020. Spike glycoprotein and host cell determinants of SARS-CoV-2 entry and cytopathic effects. *J Virol* 2304–20.
  78. Shirato K, Kawase M, Matsuyama S. 2013. Middle East Respiratory Syndrome Coronavirus Infection Mediated by the Transmembrane Serine Protease TMPRSS2. *J Virol* 87:12552–12561.
  79. Hoffmann M, Kleine-Weber H, Pöhlmann S. 2020. A Multibasic Cleavage Site in the Spike Protein of SARS-CoV-2 Is Essential for Infection of Human Lung Cells. *Mol Cell* 78:779-784.e5.
  80. Leroy H, Han M, Woottum M, Bracq L, Bouchet J, Xie M, Benichou S. 2020. Virus-Mediated Cell-Cell Fusion. *IJMS* 21:9644.
  81. Coutard B, Valle C, de Lamballerie X, Canard B, Seidah NG, Decroly E. 2020. The spike glycoprotein of the new coronavirus 2019-nCoV contains a furin-like cleavage site absent in CoV of the same clade. *Antivir Res* 176:104742.
  82. Liu K, Pan X, Li L, Yu F, Zheng A, Du P, Han P, Meng Y, Zhang Y, Wu L, Chen Q, Song C, Jia Y, Niu S, Lu D, Qiao C, Chen Z, Ma D, Ma X, Tan S, Zhao X, Qi J, Gao GF, Wang Q. 2021. Binding and molecular basis of the bat coronavirus

- RaTG13 virus to ACE2 in humans and other species. *Cell* 184:3438-3451.e10.
83. Yang J, Petitjean SJL, Koehler M, Zhang Q, Dumitru AC, Chen W, Derclaye S, Vincent SP, Soumilion P, Alsteens D. 2020. Molecular interaction and inhibition of SARS-CoV-2 binding to the ACE2 receptor. *Nat Commun* 11:4541.
  84. Lan J, Ge J, Yu J, Shan S, Zhou H, Fan S, Zhang Q, Shi X, Wang Q, Zhang L, Wang X. 2020. Structure of the SARS-CoV-2 spike receptor-binding domain bound to the ACE2 receptor. *Nature* 581:215–220.
  85. Walls AC, Park Y-J, Tortorici MA, Wall A, McGuire AT, Veerler D. 2020. Structure, Function, and Antigenicity of the SARS-CoV-2 Spike Glycoprotein. *Cell* 181:281-292.e6.
  86. Daly JL, Simonetti B, Klein K, Chen K-E, Williamson MK, Antón-Plágaro C, Shoemark DK, Simón-Gracia L, Bauer M, Hollandi R, Greber UF, Horvath P, Sessions RB, Helenius A, Hiscox JA, Teesalu T, Matthews DA, Davidson AD, Collins BM, Cullen PJ, Yamauchi Y. 2020. Neuropilin-1 is a host factor for SARS-CoV-2 infection. *Science* 370:861–865.
  87. Cantuti-Castelvetri L, Ojha R, Pedro LD, Djannatian M, Franz J, Kuivanen S, van der Meer F, Kallio K, Kaya T, Anastasina M, Smura T, Levanov L, Szivovics L, Tobi A, Kallio-Kokko H, Österlund P, Joensuu M, Meunier FA, Butcher SJ, Winkler MS, Mollenhauer B, Helenius A, Gokce O, Teesalu T, Hepojoki J, Vapalahti O, Stadelmann C, Balistreri G, Simons M. 2020. Neuropilin-1 facilitates SARS-CoV-2 cell entry and infectivity. *Science* 370:856–860.
  88. Liu L, Chopra P, Li X, Bouwman KM, Tompkins SM, Wolfert MA, de Vries RP, Boons G-J. 2021. Heparan Sulfate Proteoglycans as Attachment Factor for SARS-CoV-2. *ACS Cent Sci* 7:1009–1018.
  89. Zhang Q, Chen CZ, Swaroop M, Xu M, Wang L, Lee J, Wang AQ, Pradhan M, Hagen N, Chen L, Shen M, Luo Z, Xu X, Xu Y, Huang W, Zheng W, Ye Y. 2020. Heparan sulfate assists SARS-CoV-2 in cell entry and can be targeted by approved drugs in vitro. *Cell Discov* 6:80.
  90. Fantini J, Di Scala C, Chahinian H, Yahi N. 2020. Structural and molecular modelling studies reveal a new mechanism of action of chloroquine and hydroxychloroquine against SARS-CoV-2 infection. *Int J Antimicrob Agents* 55:105960.
  91. Baker AN, Richards S-J, Guy CS, Congdon TR, Hasan M, Zwetsloot AJ, Gallo A, Lewandowski JR, Stansfeld PJ, Straube A, Walker M, Chessa S, Pergolizzi G, Dedola S, Field RA, Gibson MI. 2020. The SARS-COV-2 Spike Protein Binds Sialic Acids and Enables Rapid Detection in a Lateral Flow Point of Care Diagnostic Device. *ACS Cent Sci* 6:2046–2052.
  92. Jaimes JA, Millet JK, Whittaker GR. 2020. Proteolytic Cleavage of the SARS-CoV-2 Spike Protein and the Role of the Novel S1/S2 Site. *iScience* 23:101212.
  93. Millet JK, Whittaker GR. 2014. Host cell entry of Middle East respiratory syndrome coronavirus after two-step, furin-mediated activation of the spike protein. *PNAS* 111:15214–15219.
  94. Belouzard S, Chu VC, Whittaker GR. 2009. Activation of the SARS coronavirus spike protein via sequential proteolytic cleavage at two distinct sites. *PNAS* 106:5871–5876.
  95. Peacock TP, Goldhill DH, Zhou J, Baillon L, Frise R, Swann OC, Kugathasan R, Penn R, Brown JC, Sanchez-David RY, Braga L, Williamson MK, Hassard JA, Staller E, Hanley B, Osborn M, Giacca M, Davidson AD, Matthews DA, Barclay WS. 2021. The furin cleavage site in the SARS-CoV-2 spike protein is required for transmission in ferrets. *Nat Microbiol* 6:899–909.
  96. Sasaki M, Uemura K, Sato A, Toba S, Sanaki T, Maenaka K, Hall WW, Orba Y,



- Sawa H. 2021. SARS-CoV-2 variants with mutations at the S1/S2 cleavage site are generated in vitro during propagation in TMPRSS2-deficient cells. *PLoS Pathog* 17:e1009233.
97. Davidson AD, Williamson MK, Lewis S, Shoemark D, Carroll MW, Heesom KJ, Zambon M, Ellis J, Lewis PA, Hiscox JA, Matthews DA. 2020. Characterisation of the transcriptome and proteome of SARS-CoV-2 reveals a cell passage induced in-frame deletion of the furin-like cleavage site from the spike glycoprotein. *Genome Med* 12:68.
  98. Johnson BA, Xie X, Bailey AL, Kalveram B, Lokugamage KG, Muruato A, Zou J, Zhang X, Juelich T, Smith JK, Zhang L, Bopp N, Schindewolf C, Vu M, Vanderheiden A, Winkler ES, Swetnam D, Plante JA, Aguilar P, Plante KS, Popov V, Lee B, Weaver SC, Suthar MS, Routh AL, Ren P, Ku Z, An Z, Debbink K, Diamond MS, Shi P-Y, Freiberg AN, Menachery VD. 2021. Loss of furin cleavage site attenuates SARS-CoV-2 pathogenesis. *Nature* 591:293–299.
  99. Kleine-Weber H, Elzayat MT, Hoffmann M, Pöhlmann S. 2018. Functional analysis of potential cleavage sites in the MERS-coronavirus spike protein. *Sci Rep* 8:16597.
  100. Shang J, Wan Y, Luo C, Ye G, Geng Q, Auerbach A, Li F. 2020. Cell entry mechanisms of SARS-CoV-2. *PNAS* 202003138.
  101. Zang R, Gomez Castro MF, McCune BT, Zeng Q, Rothlauf PW, Sonnek NM, Liu Z, Brulois KF, Wang X, Greenberg HB, Diamond MS, Ciorba MA, Whelan SPJ, Ding S. 2020. TMPRSS2 and TMPRSS4 promote SARS-CoV-2 infection of human small intestinal enterocytes. *Sci Immunol* 5:eabc3582.
  102. Kishimoto M, Uemura K, Sanaki T, Sato A, Hall WW, Kariwa H, Orba Y, Sawa H, Sasaki M. 2021. TMPRSS11D and TMPRSS13 Activate the SARS-CoV-2 Spike Protein. *Viruses* 13:384.
  103. Hoffmann M, Hofmann-Winkler H, Smith JC, Krüger N, Arora P, Sørensen LK, Søgaard OS, Hasselstrøm JB, Winkler M, Hempel T, Raich L, Olsson S, Danov O, Jonigk D, Yamazoe T, Yamatsuta K, Mizuno H, Ludwig S, Noé F, Kjolby M, Braun A, Sheltzer JM, Pöhlmann S. 2021. Camostat mesylate inhibits SARS-CoV-2 activation by TMPRSS2-related proteases and its metabolite GBPA exerts antiviral activity. *EBioMedicine* 65:103255.
  104. Bayati A, Kumar R, Francis V, McPherson PS. 2021. SARS-CoV-2 infects cells after viral entry via clathrin-mediated endocytosis. *J Biol Chem* 296:100306.
  105. Murgolo N, Therien AG, Howell B, Klein D, Koeplinger K, Lieberman LA, Adam GC, Flynn J, McKenna P, Swaminathan G, Hazuda DJ, Olsen DB. 2021. SARS-CoV-2 tropism, entry, replication, and propagation: Considerations for drug discovery and development. *PLoS Pathog* 17:e1009225.
  106. Connolly SA, Jardetzky TS, Longnecker R. 2021. The structural basis of herpesvirus entry. *Nat Rev Microbiol* 19:110–121.
  107. Chandran B. 2010. Early Events in Kaposi's Sarcoma-Associated Herpesvirus Infection of Target Cells. *J Virol* 84:2188–2199.
  108. Zhu FX, Chong JM, Wu L, Yuan Y. 2005. Virion Proteins of Kaposi's Sarcoma-Associated Herpesvirus. *J Virol* 79:800–811.
  109. Hahn A, Birkmann A, Wies E, Dorer D, Mahr K, Stürzl M, Titgemeyer F, Neipel F. 2009. Kaposi's Sarcoma-Associated Herpesvirus gH/gL: Glycoprotein Export and Interaction with Cellular Receptors. *J Virol* 83:396–407.
  110. Birkmann A, Mahr K, Ensser A, Yağuboğlu S, Titgemeyer F, Fleckenstein B, Neipel F. 2001. Cell Surface Heparan Sulfate Is a Receptor for Human Herpesvirus 8 and Interacts with Envelope Glycoprotein K8.1. *J Virol* 75:11583–11593.
  111. Wang F-Z, Akula SM, Sharma-Walia N, Zeng L, Chandran B. 2003. Human

- Herpesvirus 8 Envelope Glycoprotein B Mediates Cell Adhesion via Its RGD Sequence. *J Virol* 77:3131–3147.
112. Hahn AS, Kaufmann JK, Wies E, Naschberger E, Panteleev-Ivlev J, Schmidt K, Holzer A, Schmidt M, Chen J, König S, Ensser A, Myoung J, Brockmeyer NH, Stürzl M, Fleckenstein B, Neipel F. 2012. The ephrin receptor tyrosine kinase A2 is a cellular receptor for Kaposi's sarcoma-associated herpesvirus. *Nat Med* 18:961–966.
113. Hahn AS, Desrosiers RC. 2013. Rhesus Monkey Rhadinovirus Uses Eph Family Receptors for Entry into B Cells and Endothelial Cells but Not Fibroblasts. *PLoS Pathog* 9:e1003360.
114. Chakraborty S, Veettil MV, Bottero V, Chandran B. 2012. Kaposi's sarcoma-associated herpesvirus interacts with EphrinA2 receptor to amplify signaling essential for productive infection. *PNAS* 109:E1163–E1172.
115. Großkopf AK, Schlagowski S, Hörnich BF, Fricke T, Desrosiers RC, Hahn AS. 2019. EphA7 Functions as Receptor on BJAB Cells for Cell-to-Cell Transmission of the Kaposi's Sarcoma-Associated Herpesvirus and for Cell-Free Infection by the Related Rhesus Monkey Rhadinovirus. *J Virol* 93.
116. Bechtel JT, Liang Y, Hvidding J, Ganem D. 2003. Host Range of Kaposi's Sarcoma-Associated Herpesvirus in Cultured Cells. *J Virol* 77:6474–6481.
117. Dollery SJ, Santiago-Crespo RJ, Kardava L, Moir S, Berger EA. 2014. Efficient Infection of a Human B Cell Line with Cell-Free Kaposi's Sarcoma-Associated Herpesvirus. *J Virol* 88:1748–1757.
118. Großkopf AK, Ensser A, Neipel F, Jungnickl D, Schlagowski S, Desrosiers RC, Hahn AS. 2018. A conserved Eph family receptor-binding motif on the gH/gL complex of Kaposi's sarcoma-associated herpesvirus and rhesus monkey rhadinovirus. 2. *PLoS Pathog* 14:e1006912.
119. TerBush AA, Hafkamp F, Lee HJ, Coscoy L. 2018. A Kaposi's Sarcoma-Associated Herpesvirus Infection Mechanism Is Independent of Integrins  $\alpha 3\beta 1$ ,  $\alpha V\beta 3$ , and  $\alpha V\beta 5$ . *Journal of Virology* 92:22.
120. Dutta D, Chakraborty S, Bandyopadhyay C, Valiya Veettil M, Ansari MA, Singh VV, Chandran B. 2013. EphrinA2 Regulates Clathrin Mediated KSHV Endocytosis in Fibroblast Cells by Coordinating Integrin-Associated Signaling and c-Cbl Directed Polyubiquitination. *PLoS Pathog* 9:e1003510.
121. Veettil MV, Sadagopan S, Sharma-Walia N, Wang F-Z, Raghu H, Varga L, Chandran B. 2008. Kaposi's Sarcoma-Associated Herpesvirus Forms a Multimolecular Complex of Integrins ( $\alpha V\beta 5$ ,  $\alpha V\beta 3$ , and  $\alpha 3\beta 1$ ) and CD98-xCT during Infection of Human Dermal Microvascular Endothelial Cells, and CD98-xCT Is Essential for the Postentry Stage of Infection. *J Virol* 82:12126–12144.
122. Garrigues HJ, Rubinchikova YE, DiPersio CM, Rose TM. 2008. Integrin  $\alpha v \beta 3$  Binds to the RGD Motif of Glycoprotein B of Kaposi's Sarcoma-Associated Herpesvirus and Functions as an RGD-Dependent Entry Receptor. *J Virol* 82:1570–1580.
123. Rappocciolo G, Jenkins FJ, Hensler HR, Piazza P, Jais M, Borowski L, Watkins SC, Rinaldo CR. 2006. DC-SIGN Is a Receptor for Human Herpesvirus 8 on Dendritic Cells and Macrophages. *J Immunol* 176:1741–1749.
124. Kerur N, Veettil MV, Sharma-Walia N, Sadagopan S, Bottero V, Paul AG, Chandran B. 2010. Characterization of entry and infection of monocytic THP-1 cells by Kaposi's sarcoma associated herpesvirus (KSHV): Role of heparan sulfate, DC-SIGN, integrins and signaling. *Virology* 406:103–116.
125. Rappocciolo G, Hensler HR, Jais M, Reinhart TA, Pegu A, Jenkins FJ, Rinaldo CR. 2008. Human Herpesvirus 8 Infects and Replicates in Primary Cultures of

- Activated B Lymphocytes through DC-SIGN. *J Virol* 82:4793–4806.
126. Jarousse N, Chandran B, Coscoy L. 2008. Lack of Heparan Sulfate Expression in B-Cell Lines: Implications for Kaposi's Sarcoma-Associated Herpesvirus and Murine Gammaherpesvirus 68 Infections. *J Virol* 82:12591–12597.
  127. Raghu H, Sharma-Walia N, Veetil MV, Sadagopan S, Chandran B. 2009. Kaposi's Sarcoma-Associated Herpesvirus Utilizes an Actin Polymerization-Dependent Macropinocytic Pathway To Enter Human Dermal Microvascular Endothelial and Human Umbilical Vein Endothelial Cells. *J Virol* 83:4895–4911.
  128. Akula SM, Naranatt PP, Walia N-S, Wang F-Z, Fegley B, Chandran B. 2003. Kaposi's Sarcoma-Associated Herpesvirus (Human Herpesvirus 8) Infection of Human Fibroblast Cells Occurs through Endocytosis. *J Virol* 77:7978–7990.
  129. Inoue N, Winter J, Lal RB, Offermann MK, Koyano S. 2003. Characterization of Entry Mechanisms of Human Herpesvirus 8 by Using an Rta-Dependent Reporter Cell Line. *J Virol* 77:8147–8152.
  130. Großkopf AK, Schlagowski S, Fricke T, Ensser A, Desrosiers RC, Hahn AS. 2021. P1xdc family members are novel receptors for the rhesus monkey rhadinovirus (RRV). *PLoS Pathog* 17:e1008979.
  131. Pertel PE. 2002. Human Herpesvirus 8 Glycoprotein B (gB), gH, and gL Can Mediate Cell Fusion. *J Virol* 76:4390–4400.
  132. Chen J, Schaller S, Jardetzky TS, Longnecker R. 2020. Epstein-Barr Virus gH/gL and Kaposi's Sarcoma-Associated Herpesvirus gH/gL Bind to Different Sites on EphA2 To Trigger Fusion. *J Virol* 94.
  133. Chernomordik LV, Zimmerberg J, Kozlov MM. 2006. Membranes of the world unite! *J Cell Biol* 175:201–207.
  134. Harrison SC. 2008. Viral membrane fusion. *Nat Struct Mol Biol* 15:690–698.
  135. Schibli DJ, Weissenhorn W. 2004. Class I and class II viral fusion protein structures reveal similar principles in membrane fusion (Review). *Mol Membr Biol* 21:361–371.
  136. Doms RW, Moore JP. 2000. HIV-1 Membrane Fusion: Targets of Opportunity. *The Journal of Cell Biology* 151:5.
  137. Galloway SE, Reed ML, Russell CJ, Steinhauer DA. 2013. Influenza HA Subtypes Demonstrate Divergent Phenotypes for Cleavage Activation and pH of Fusion: Implications for Host Range and Adaptation. *PLoS Pathog* 9:e1003151.
  138. White JM, Delos SE, Brecher M, Schornberg K. 2008. Structures and Mechanisms of Viral Membrane Fusion Proteins: Multiple Variations on a Common Theme. *Crit Rev Biochem Mol Biol* 43:189–219.
  139. Backovic M, Jardetzky TS. 2009. Class III viral membrane fusion proteins. *Curr Opin Struct Biol* 19:189–196.
  140. Ou X, Liu Y, Lei X, Li P, Mi D, Ren L, Guo L, Guo R, Chen T, Hu J, Xiang Z, Mu Z, Chen X, Chen J, Hu K, Jin Q, Wang J, Qian Z. 2020. Characterization of spike glycoprotein of SARS-CoV-2 on virus entry and its immune cross-reactivity with SARS-CoV. 1. *Nat Commun* 11:1620.
  141. Fan X, Cao D, Kong L, Zhang X. 2020. Cryo-EM analysis of the post-fusion structure of the SARS-CoV spike glycoprotein. *Nat Commun* 11:3618.
  142. Benton DJ, Wrobel AG, Xu P, Roustan C, Martin SR, Rosenthal PB, Skehel JJ, Gamblin SJ. 2020. Receptor binding and priming of the spike protein of SARS-CoV-2 for membrane fusion. *Nature* 588:327–330.
  143. Ke Z, Oton J, Qu K, Cortese M, Zila V, McKeane L, Nakane T, Zivanov J, Neufeldt CJ, Cerikan B, Lu JM, Peukes J, Xiong X, Kräusslich H-G, Scheres SHW, Bartenschlager R, Briggs JAG. 2020. Structures and distributions of

- 
- SARS-CoV-2 spike proteins on intact virions. *Nature* 588:498–502.
144. Wrapp D, Wang N, Corbett KS, Goldsmith JA, Hsieh C-L, Abiona O, Graham BS, McLellan JS. 2020. Cryo-EM structure of the 2019-nCoV spike in the prefusion conformation. *Science* 367:1260–1263.
  145. Eisenberg RJ, Atanasiu D, Cairns TM, Gallagher JR, Krummenacher C, Cohen GH. 2012. Herpes Virus Fusion and Entry: A Story with Many Characters. *Viruses* 4:800–832.
  146. Heldwein EE, Lou H, Bender FC, Cohen GH, Eisenberg RJ, Harrison SC. 2006. Crystal structure of glycoprotein B from herpes simplex virus 1. *Science* 313:217–220.
  147. Vallbracht M, Brun D, Tassinari M, Vaney M-C, Pehau-Arnaudet G, Guardado-Calvo P, Haouz A, Klupp BG, Mettenleiter TC, Rey FA, Backovic M. 2018. Structure-Function Dissection of Pseudorabies Virus Glycoprotein B Fusion Loops. *J Virol* 92.
  148. Burke HG, Heldwein EE. 2015. Crystal Structure of the Human Cytomegalovirus Glycoprotein B. *PLoS Pathog* 11:e1005227.
  149. Backovic M, Longnecker R, Jardetzky TS. 2009. Structure of a trimeric variant of the Epstein–Barr virus glycoprotein B. *PNAS* 106:2880–2885.
  150. Vollmer B, Pražák V, Vasishtan D, Jefferys EE, Hernandez-Duran A, Vallbracht M, Klupp BG, Mettenleiter TC, Backovic M, Rey FA, Topf M, Grünewald K. 2020. The prefusion structure of herpes simplex virus glycoprotein B. *Sci Adv* 6:eabc1726.
  151. Liu Y, Heim KP, Che Y, Chi X, Qiu X, Han S, Dormitzer PR, Yang X. 2021. Prefusion structure of human cytomegalovirus glycoprotein B and structural basis for membrane fusion. *Sci Adv* 7:eabf3178.
  152. Madavaraju K, Koganti R, Volety I, Yadavalli T, Shukla D. 2021. Herpes Simplex Virus Cell Entry Mechanisms: An Update. *Front Cell Infect Microbiol* 10:617578.
  153. Cooper RS, Georgieva ER, Borbat PP, Freed JH, Heldwein EE. 2018. Structural basis for membrane anchoring and fusion regulation of the herpes simplex virus fusogen gB. *Nat Struct Mol Biol* 25:416–424.
  154. Vollmer B. 2020. Herpesvirus membrane fusion a team effort. *Curr Opin Struct Biol* 62:112–120.
  155. Pattnaik GP, Chakraborty H. 2020. Entry Inhibitors: Efficient Means to Block Viral Infection. *J Membrane Biol* 253:425–444.
  156. Berkhout B, Eggink D, Sanders RW. 2012. Is there a future for antiviral fusion inhibitors? *Curr Opin Virol* 2:50–59.
  157. Yao X, Chong H, Zhang C, Qiu Z, Qin B, Han R, Waltersperger S, Wang M, He Y, Cui S. 2012. Structural Basis of Potent and Broad HIV-1 Fusion Inhibitor CP32M. *J Biol Chem* 287:26618–26629.
  158. Wang R-R, Yang L-M, Wang Y-H, Pang W, Tam S-C, Tien P, Zheng Y-T. 2009. Sifuvirtide, a potent HIV fusion inhibitor peptide. *Biochem Biophys Res Commun* 382:540–544.
  159. Dwyer JJ, Wilson KL, Davison DK, Freel SA, Seedorff JE, Wring SA, Tvermoes NA, Matthews TJ, Greenberg ML, Delmedico MK. 2007. Design of helical, oligomeric HIV-1 fusion inhibitor peptides with potent activity against enfuvirtide-resistant virus. *PNAS* 104:12772–12777.
  160. Lambert DM, Barney S, Lambert AL, Guthrie K, Medinas R, Davis DE, Bucy T, Erickson J, Merutka G, Petteway SR. 1996. Peptides from conserved regions of paramyxovirus fusion (F) proteins are potent inhibitors of viral fusion. *PNAS* 93:2186–2191.
  161. Young JK, Li D, Abramowitz MC, Morrison TG. 1999. Interaction of Peptides



- with Sequences from the Newcastle Disease Virus Fusion Protein Heptad Repeat Regions. *J Virol* 73:5945–5956.
162. Xia S, Yan L, Xu W, Agrawal AS, Algaissi A, Tseng C-TK, Wang Q, Du L, Tan W, Wilson IA, Jiang S, Yang B, Lu L. 2019. A pan-coronavirus fusion inhibitor targeting the HR1 domain of human coronavirus spike. *Sci Adv* 5:eaav4580.
163. Xia S, Liu M, Wang C, Xu W, Lan Q, Feng S, Qi F, Bao L, Du L, Liu S, Qin C, Sun F, Shi Z, Zhu Y, Jiang S, Lu L. 2020. Inhibition of SARS-CoV-2 (previously 2019-nCoV) infection by a highly potent pan-coronavirus fusion inhibitor targeting its spike protein that harbors a high capacity to mediate membrane fusion. *Cell Res* 30:343–355.
164. Zhou G, Wu D, Snyder B, Ptak RG, Kaur H, Gochin M. 2011. Development of Indole Compounds as Small Molecule Fusion Inhibitors Targeting HIV-1 Glycoprotein-41. *J Med Chem* 54:7220–7231.
165. Vigant F, Santos NC, Lee B. 2015. Broad-spectrum antivirals against viral fusion. *Nat Rev Microbiol* 13:426–437.
166. Wolf MC, Freiberg AN, Zhang T, Akyol-Ataman Z, Grock A, Hong PW, Li J, Watson NF, Fang AQ, Aguilar HC, Porotto M, Honko AN, Damoiseaux R, Miller JP, Woodson SE, Chantasirivisal S, Fontanes V, Negrete OA, Krogstad P, Dasgupta A, Moscona A, Hensley LE, Whelan SP, Faull KF, Holbrook MR, Jung ME, Lee B. 2010. A broad-spectrum antiviral targeting entry of enveloped viruses. *PNAS* 107:3157–3162.
167. Hakobyan A, Galindo I, Nañez A, Arabyan E, Karalyan Z, Chistov AA, Streshnev PP, Korshun VA, Alonso C, Zakaryan H. 2018. Rigid amphipathic fusion inhibitors demonstrate antiviral activity against African swine fever virus. *J Gen Virol* 99:148–156.
168. St.Vincent MR, Colpitts CC, Ustinov AV, Muqadas M, Joyce MA, Barsby NL, Epand RF, Epand RM, Khramyshev SA, Valueva OA, Korshun VA, Tyrrell DLJ, Schang LM. 2010. Rigid amphipathic fusion inhibitors, small molecule antiviral compounds against enveloped viruses. *PNAS* 107:17339–17344.
169. Watabe N, Ishida Y, Ochiai A, Tokuoka Y, Kawashima N. 2007. Oxidation Decomposition of Unsaturated Fatty Acids by Singlet Oxygen in Phospholipid Bilayer Membranes. *J Oleo Sci* 56:73–80.
170. Vigant F, Lee J, Hollmann A, Tanner LB, Akyol Ataman Z, Yun T, Shui G, Aguilar HC, Zhang D, Meriwether D, Roman-Sosa G, Robinson LR, Juelich TL, Buczkowski H, Chou S, Castanho MARB, Wolf MC, Smith JK, Banyard A, Kielian M, Reddy S, Wenk MR, Selke M, Santos NC, Freiberg AN, Jung ME, Lee B. 2013. A Mechanistic Paradigm for Broad-Spectrum Antivirals that Target Virus-Cell Fusion. *PLoS Pathog* 9:e1003297.
171. Vigant F, Santos NC, Lee B. 2015. Broad-spectrum antivirals against viral fusion. *Nat Rev Microbiol* 13:426–437.
172. Zhang Z, Liu J, Li M, Yang H, Zhang C. 2012. Evolutionary Dynamics of the Interferon-Induced Transmembrane Gene Family in Vertebrates. *PLoS ONE* 7:e49265.
173. Hickford D, Frankenberg S, Shaw G, Renfree MB. 2012. Evolution of vertebrate interferon inducible transmembrane proteins. *BMC Genomics* 13:155.
174. Brass AL, Huang I-C, Benita Y, John SP, Krishnan MN, Feeley EM, Ryan BJ, Weyer JL, van der Weyden L, Fikrig E, Adams DJ, Xavier RJ, Farzan M, Elledge SJ. 2009. The IFITM Proteins Mediate Cellular Resistance to Influenza A H1N1 Virus, West Nile Virus, and Dengue Virus. *Cell* 139:1243–1254.
175. Huang I-C, Bailey CC, Weyer JL, Radoshitzky SR, Becker MM, Chiang JJ, Brass AL, Ahmed AA, Chi X, Dong L, Longobardi LE, Boltz D, Kuhn JH, Elledge

- SJ, Bavari S, Denison MR, Choe H, Farzan M. 2011. Distinct Patterns of IFITM-Mediated Restriction of Filoviruses, SARS Coronavirus, and Influenza A Virus. 1. *PLoS Pathog* 7:e1001258.
176. Wrensch F, Karsten CB, Gnirß K, Hoffmann M, Lu K, Takada A, Winkler M, Simmons G, Pöhlmann S. 2015. Interferon-Induced Transmembrane Protein-Mediated Inhibition of Host Cell Entry of Ebolaviruses. *suppl 2. J Infect Dis* 212:S210–S218.
177. Mudhasani R, Tran JP, Retterer C, Radoshitzky SR, Kota KP, Altamura LA, Smith JM, Packard BZ, Kuhn JH, Costantino J, Garrison AR, Schmaljohn CS, Huang I-C, Farzan M, Bavari S. 2013. IFITM-2 and IFITM-3 but Not IFITM-1 Restrict Rift Valley Fever Virus. *Journal of Virology* 87:8451–8464.
178. Bailey CC, Zhong G, Huang I-C, Farzan M. 2014. IFITM-Family Proteins: The Cell's First Line of Antiviral Defense. 1. *Annu Rev Virol* 1:261–283.
179. Shi G, Kenney AD, Kudryashova E, Zani A, Zhang L, Lai KK, Hall-Stoodley L, Robinson RT, Kudryashov DS, Compton AA, Yount JS. 2021. Opposing activities of IFITM proteins in SARS-CoV-2 infection. *EMBO J* 40.
180. Siegrist F, Ebeling M, Certa U. 2011. The Small Interferon-Induced Transmembrane Genes and Proteins. *J Interferon Cytokine Res* 31:183–197.
181. Weston S, Czieso S, White IJ, Smith SE, Kellam P, Marsh M. 2014. A Membrane Topology Model for Human Interferon Inducible Transmembrane Protein 1. 8. *PLoS ONE* 9:e104341.
182. Narayana SK, Helbig KJ, McCartney EM, Eyre NS, Bull RA, Eltahla A, Lloyd AR, Beard MR. 2015. The Interferon-induced Transmembrane Proteins, IFITM1, IFITM2, and IFITM3 Inhibit Hepatitis C Virus Entry. 43. *J Biol Chem* 290:25946–25959.
183. Smith SE, Busse DC, Binter S, Weston S, Diaz Soria C, Laksono BM, Clare S, Van Nieuwkoop S, Van den Hoogen BG, Clement M, Marsden M, Humphreys IR, Marsh M, de Swart RL, Wash RS, Tregoning JS, Kellam P. 2018. Interferon-Induced Transmembrane Protein 1 Restricts Replication of Viruses That Enter Cells via the Plasma Membrane. *J Virol* 93:2003–18.
184. Jia R, Xu F, Qian J, Yao Y, Miao C, Zheng Y-M, Liu S-L, Guo F, Geng Y, Qiao W, Liang C. 2014. Identification of an endocytic signal essential for the antiviral action of IFITM3: Endocytosis of IFITM3 and its antiviral activity. *Cell Microbiol* 16:1080–1093.
185. John SP, Chin CR, Perreira JM, Feeley EM, Aker AM, Savidis G, Smith SE, Elia AEH, Everitt AR, Vora M, Pertel T, Elledge SJ, Kellam P, Brass AL. 2013. The CD225 Domain of IFITM3 Is Required for both IFITM Protein Association and Inhibition of Influenza A Virus and Dengue Virus Replication. *J Virol* 87:7837–7852.
186. Shi G, Schwartz O, Compton AA. 2017. More than meets the I: the diverse antiviral and cellular functions of interferon-induced transmembrane proteins. 1. *Retrovirology* 14:53.
187. Li K, Markosyan RM, Zheng Y-M, Golfetto O, Bungart B, Li M, Ding S, He Y, Liang C, Lee JC, Gratton E, Cohen FS, Liu S-L. 2013. IFITM Proteins Restrict Viral Membrane Hemifusion. *PLOS Pathog* 9:18.
188. Buchrieser J, Dufloo J, Hubert M, Monel B, Planas D, Rajah MM, Planchais C, Porrot F, Guivel-Benhassine F, Van der Werf S, Casartelli N, Mouquet H, Bruel T, Schwartz O. 2020. Syncytia formation by SARS-CoV-2-infected cells. *EMBO J* 39.
189. Chesarino NM, Compton AA, McMichael TM, Kenney AD, Zhang L, Soewarna V, Davis M, Schwartz O, Yount JS. 2017. IFITM 3 requires an amphipathic helix

- for antiviral activity. 10. *EMBO Rep* 18:1740–1751.
190. Desai TM, Marin M, Chin CR, Savidis G, Brass AL, Melikyan GB. 2014. IFITM3 Restricts Influenza A Virus Entry by Blocking the Formation of Fusion Pores following Virus-Endosome Hemifusion. 4. *PLoS Pathog* 10:e1004048.
  191. Guo X, Steinkühler J, Marin M, Li X, Lu W, Dimova R, Melikyan GB. 2021. Interferon-Induced Transmembrane Protein 3 Blocks Fusion of Diverse Enveloped Viruses by Altering Mechanical Properties of Cell Membranes. *ACS Nano* 15:8155–8170.
  192. Fu B, Wang L, Li S, Dorf ME. 2017. ZMPSTE24 defends against influenza and other pathogenic viruses. *Exp Med* 214:919–929.
  193. Li C, Du S, Tian M, Wang Y, Bai J, Tan P, Liu W, Yin R, Wang M, Jiang Y, Li Y, Zhu N, Zhu Y, Li T, Wu S, Jin N, He F. 2018. The Host Restriction Factor Interferon-Inducible Transmembrane Protein 3 Inhibits Vaccinia Virus Infection. *Front Immunol* 9:228.
  194. Muñoz-Moreno R, Cuesta-Geijo MÁ, Martínez-Romero C, Barrado-Gil L, Galindo I, García-Sastre A, Alonso C. 2016. Antiviral Role of IFITM Proteins in African Swine Fever Virus Infection. *PLoS ONE* 11:e0154366.
  195. Weston S, Czieso S, White IJ, Smith SE, Wash RS, Diaz-Soria C, Kellam P, Marsh M. 2016. Alphavirus Restriction by IFITM Proteins: IFITMs Inhibit Cellular Infection by Alphaviruses. *Traffic* 17:997–1013.
  196. Wee YS, Roundy KM, Weis JJ, Weis JH. 2012. Interferon-inducible transmembrane proteins of the innate immune response act as membrane organizers by influencing clathrin and v-ATPase localization and function. *Innate Immun* 18:834–845.
  197. Amini-Bavil-Olyaei S, Choi YJ, Lee JH, Shi M, Huang I-C, Farzan M, Jung JU. 2013. The Antiviral Effector IFITM3 Disrupts Intracellular Cholesterol Homeostasis to Block Viral Entry. *Cell Host & Microbe* 13:452–464.
  198. Peng T, Hang HC. 2015. Bifunctional Fatty Acid Chemical Reporter for Analyzing S-Palmitoylated Membrane Protein–Protein Interactions in Mammalian Cells. *J Am Chem Soc* 137:556–559.
  199. Wrensch F, Winkler M, Pöhlmann S. 2014. IFITM Proteins Inhibit Entry Driven by the MERS-Coronavirus Spike Protein: Evidence for Cholesterol-Independent Mechanisms. *Viruses* 6:3683–3698.
  200. Spence JS, He R, Hoffmann H-H, Das T, Thinon E, Rice CM, Peng T, Chandran K, Hang HC. 2019. IFITM3 directly engages and shuttles incoming virus particles to lysosomes. 3. *Nat Chem Biol* 15:259–268.
  201. Suddala KC, Lee CC, Meraner P, Marin M, Markosyan RM, Desai TM, Cohen FS, Brass AL, Melikyan GB. 2019. Interferon-induced transmembrane protein 3 blocks fusion of sensitive but not resistant viruses by partitioning into virus-carrying endosomes. 1. *PLoS Pathog* 15:e1007532.
  202. Kummer S, Avinoam O, Kräusslich H-G. 2019. IFITM3 Clusters on Virus Containing Endosomes and Lysosomes Early in the Influenza A Infection of Human Airway Epithelial Cells. 6. *Viruses* 11:548.
  203. Cloud-Based Informatics Platform for Life Sciences R&D | Benchling.
  204. Sun F, Xia Z, Han Y, Gao M, Wang L, Wu Y, Sabatier J-M, Miao L, Cao Z. 2020. Topology, Antiviral Functional Residues and Mechanism of IFITM1. *Viruses* 12:295.
  205. Bussani R, Schneider E, Zentilin L, Collesi C, Ali H, Braga L, Volpe MC, Colliva A, Zanconati F, Berlot G, Silvestri F, Zacchigna S, Giacca M. 2020. Persistence of viral RNA, pneumocyte syncytia and thrombosis are hallmarks of advanced COVID-19 pathology. *EBioMedicine* 61:103104.

- 
206. Clemens DJ, Ye D, John Kim C, Pease DR, Navaratnarajah CK, Barkhymer A, J. Nelson T, Cattaneo R, Schneider JW, Ackerman MJ. 2021. B-AB18-03 SARS-COV-2 DIRECT CARDIAC DAMAGE THROUGH SPIKE-MEDIATED CARDIOMYOCYTE FUSION MAY CONTRIBUTE TO INCREASED ARRHYTHMIC RISK IN COVID-19. *Heart Rhythm* 18:S35.
  207. Braga L, Ali H, Secco I, Chiavacci E, Neves G, Goldhill D, Penn R, Jimenez-Guardeño JM, Ortega-Prieto AM, Bussani R, Cannatà A, Rizzari G, Collesi C, Schneider E, Arosio D, Shah AM, Barclay WS, Malim MH, Burrone J, Giacca M. 2021. Drugs that inhibit TMEM16 proteins block SARS-CoV-2 spike-induced syncytia. *Nature* 594:88–93.
  208. Malvezzi M, Andra KK, Pandey K, Lee B-C, Falzone ME, Brown A, Iqbal R, Menon AK, Accardi A. 2018. Out-of-the-groove transport of lipids by TMEM16 and GPCR scramblases. *PNAS* 115:E7033–E7042.
  209. Whitlock JM, Chernomordik LV. 2021. Flagging fusion: Phosphatidylserine signaling in cell–cell fusion. *J Biol Chem* 296:100411.
  210. Stukalov A, Girault V, Grass V, Karayel O, Bergant V, Urban C, Haas DA, Huang Y, Oubraham L, Wang A, Hamad MS, Piras A, Hansen FM, Tanzer MC, Paron I, Zinzula L, Engleitner T, Reinecke M, Lavacca TM, Ehmann R, Wölfel R, Jores J, Kuster B, Protzer U, Rad R, Ziebuhr J, Thiel V, Scaturro P, Mann M, Pichlmair A. 2021. Multilevel proteomics reveals host perturbations by SARS-CoV-2 and SARS-CoV. *Nature* 594:246–252.
  211. Syed F, Li W, Relich RF, Russell PM, Zhang S, Zimmerman MK, Yu Q. 2021. Excessive Matrix Metalloproteinase-1 and Hyperactivation of Endothelial Cells Occurred in COVID-19 Patients and Were Associated With the Severity of COVID-19. *J Infect Dis* 224:60–69.
  212. Jordakieva G, Budge-Wolfram RM, Budinsky AC, Nikfardjam M, Delle-Karth G, Girard A, Godnic-Cvar J, Crevenna R, Heinz G. 2021. Plasma MMP-9 and TIMP-1 levels on ICU admission are associated with 30-day survival. *Wien Klin Wochenschr* 133:86–95.
  213. Elkington PTG. 2006. Matrix metalloproteinases in destructive pulmonary pathology. *Thorax* 61:259–266.
  214. Oikonomidi S, Kostikas K, Tsilioni I, Tanou K, Gourgoulianis K, Kiropoulos T. 2009. Matrix Metalloproteinases in Respiratory Diseases: From Pathogenesis to Potential Clinical Implications. *Curr Med Chem* 16:1214–1228.
  215. Matsuyama S, Nagata N, Shirato K, Kawase M, Takeda M, Taguchi F. 2010. Efficient Activation of the Severe Acute Respiratory Syndrome Coronavirus Spike Protein by the Transmembrane Protease TMPRSS2. *J Virol* 84:12658–12664.
  216. Kam Y-W, Okumura Y, Kido H, Ng LFP, Bruzzone R, Altmeyer R. 2009. Cleavage of the SARS Coronavirus Spike Glycoprotein by Airway Proteases Enhances Virus Entry into Human Bronchial Epithelial Cells In Vitro. *PLoS ONE* 4:e7870.
  217. Bollavaram K, Leeman TH, Lee MW, Kulkarni A, Upshaw SG, Yang J, Song H, Platt MO. 2021. Multiple sites on SARS-CoV -2 spike protein are susceptible to proteolysis by cathepsins B, K, L, S, and V. *Protein Sci* 30:1131–1143.
  218. Koch J, Uckelej ZM, Doldan P, Stanifer M, Boulant S, Lozach P. 2021. TMPRSS2 expression dictates the entry route used by SARS-CoV-2 to infect host cells. *EMBO J* 40.
  219. Zhou Y, Vedantham P, Lu K, Agudelo J, Carrion R, Nunneley JW, Barnard D, Pöhlmann S, McKerrow JH, Renslo AR, Simmons G. 2015. Protease inhibitors targeting coronavirus and filovirus entry. *Antivir Res* 116:76–84.



- 
220. Iwata-Yoshikawa N, Okamura T, Shimizu Y, Hasegawa H, Takeda M, Nagata N. 2019. TMPRSS2 Contributes to Virus Spread and Immunopathology in the Airways of Murine Models after Coronavirus Infection. *J Virol* 93.
221. Li K, Meyerholz DK, Bartlett JA, McCray PB. 2021. The TMPRSS2 Inhibitor Nafamostat Reduces SARS-CoV-2 Pulmonary Infection in Mouse Models of COVID-19. *mBio* 12.
222. Zhao M-M, Yang W-L, Yang F-Y, Zhang L, Huang W-J, Hou W, Fan C-F, Jin R-H, Feng Y-M, Wang Y-C, Yang J-K. 2021. Cathepsin L plays a key role in SARS-CoV-2 infection in humans and humanized mice and is a promising target for new drug development. *Sig Transduct Target Ther* 6:134.
223. Hoffmann M, Schroeder S, Kleine-Weber H, Müller MA, Drosten C, Pöhlmann S. 2020. Nafamostat mesylate blocks activation of SARS-CoV-2: New treatment option for COVID-19. *Antimicrob Agents Chemother* AAC.00754-20, aac;AAC.00754-20v1.
224. Gunst JD, Staerke NB, Pahus MH, Kristensen LH, Bodilsen J, Lohse N, Dalgaard LS, Brønnum D, Frøbert O, Hønge B, Johansen IS, Monrad I, Erikstrup C, Rosendal R, Vilstrup E, Mariager T, Bove DG, Offersen R, Shakar S, Cajander S, Jørgensen NP, Sritharan SS, Breining P, Jespersen S, Mortensen KL, Jensen ML, Kolte L, Frattari GS, Larsen CS, Storgaard M, Nielsen LP, Tolstrup M, Sædder EA, Østergaard LJ, Ngo HTT, Jensen MH, Højen JF, Kjolby M, Søgaard OS. 2021. Efficacy of the TMPRSS2 inhibitor camostat mesilate in patients hospitalized with Covid-19—a double-blind randomized controlled trial. *EClinicalMedicine* 35:100849.
225. Rolain J-M, Colson P, Raoult D. 2007. Recycling of chloroquine and its hydroxyl analogue to face bacterial, fungal and viral infections in the 21st century. *Int J Antimicrob Agents* 30:297–308.
226. Ou T, Mou H, Zhang L, Ojha A, Choe H, Farzan M. 2021. Hydroxychloroquine-mediated inhibition of SARS-CoV-2 entry is attenuated by TMPRSS2. *PLoS Pathog* 17:e1009212.
227. Wang M, Cao R, Zhang L, Yang X, Liu J, Xu M, Shi Z, Hu Z, Zhong W, Xiao G. 2020. Remdesivir and chloroquine effectively inhibit the recently emerged novel coronavirus (2019-nCoV) in vitro. *Cell Res* 30:269–271.
228. Yao X, Ye F, Zhang M, Cui C, Huang B, Niu P, Liu X, Zhao L, Dong E, Song C, Zhan S, Lu R, Li H, Tan W, Liu D. 2020. In Vitro Antiviral Activity and Projection of Optimized Dosing Design of Hydroxychloroquine for the Treatment of Severe Acute Respiratory Syndrome Coronavirus 2 (SARS-CoV-2). *Clin Infect Dis* 71:732–739.
229. Axfors C, Schmitt AM, Janiaud P, van't Hooft J, Abd-El Salam S, Abdo EF, Abella BS, Akram J, Amaravadi RK, Angus DC, Arabi YM, Azhar S, Baden LR, Baker AW, Belkhir L, Benfield T, Berrevoets MAH, Chen C-P, Chen T-C, Cheng S-H, Cheng C-Y, Chung W-S, Cohen YZ, Cowan LN, Dalgard O, de Almeida e Val FF, de Lacerda MVG, de Melo GC, Derde L, Dubee V, Elfakir A, Gordon AC, Hernandez-Cardenas CM, Hills T, Hoepelman AIM, Huang Y-W, Igau B, Jin R, Jurado-Camacho F, Khan KS, Kremsner PG, Kreuels B, Kuo C-Y, Le T, Lin Y-C, Lin W-P, Lin T-H, Lyngbakken MN, McArthur C, McVerry BJ, Meza-Meneses P, Monteiro WM, Morpeth SC, Mourad A, Mulligan MJ, Murthy S, Naggie S, Narayanasamy S, Nichol A, Novack LA, O'Brien SM, Okeke NL, Perez L, Perez-Padilla R, Perrin L, Remigio-Luna A, Rivera-Martinez NE, Rockhold FW, Rodriguez-Llamazares S, Rolfe R, Rosa R, Røsjø H, Sampaio VS, Seto TB, Shahzad M, Soliman S, Stout JE, Thirion-Romero I, Troxel AB, Tseng T-Y, Turner NA, Ulrich RJ, Walsh SR, Webb SA, Weehuizen JM, Velinova M, Wong

- H-L, Wrenn R, Zampieri FG, Zhong W, Moher D, Goodman SN, Ioannidis JPA, Hemkens LG. 2021. Mortality outcomes with hydroxychloroquine and chloroquine in COVID-19 from an international collaborative meta-analysis of randomized trials. *Nat Commun* 12:2349.
230. Hoffmann M, Mösbauer K, Hofmann-Winkler H, Kaul A, Kleine-Weber H, Krüger N, Gassen NC, Müller MA, Drosten C, Pöhlmann S. 2020. Chloroquine does not inhibit infection of human lung cells with SARS-CoV-2. *Nature* 585:588–590.
231. Lucas JM, Heinlein C, Kim T, Hernandez SA, Malik MS, True LD, Morrissey C, Corey E, Montgomery B, Mostaghel E, Clegg N, Coleman I, Brown CM, Schneider EL, Craik C, Simon JA, Bedalov A, Nelson PS. 2014. The Androgen-Regulated Protease TMPRSS2 Activates a Proteolytic Cascade Involving Components of the Tumor Microenvironment and Promotes Prostate Cancer Metastasis. *Cancer Discovery* 4:1310–1325.
232. Malerba M, Ragnoli B. 2008. Ambroxol in the 21st century: pharmacological and clinical update. *Exp Opin Drug Metabol Toxicol* 4:1119–1129.
233. Kim Y-M, Yum M-S, Heo SH, Kim T, Jin HK, Bae J, Seo GH, Oh A, Yoon HM, Lim HT, Kim H-W, Ko T-S, Lim H, Osborn MJ, Tolar J, Cozma C, Rolfs A, Zimran A, Lee BH, Yoo H-W. 2020. Pharmacologic properties of high-dose ambroxol in four patients with Gaucher disease and myoclonic epilepsy. *J Med Genet* 57:124–131.
234. Silveira CRA, MacKinley J, Coleman K, Li Z, Finger E, Bartha R, Morrow SA, Wells J, Borrie M, Tirona RG, Rupar CA, Zou G, Hegele RA, Mahuran D, MacDonald P, Jenkins ME, Jog M, Pasternak SH. 2019. Ambroxol as a novel disease-modifying treatment for Parkinson’s disease dementia: protocol for a single-centre, randomized, double-blind, placebo-controlled trial. *BMC Neurol* 19:20.
235. Shrimp JH, Kales SC, Sanderson PE, Simeonov A, Shen M, Hall MD. 2020. An Enzymatic TMPRSS2 Assay for Assessment of Clinical Candidates and Discovery of Inhibitors as Potential Treatment of COVID-19. *ACS Pharmacol Transl Sci* 3:997–1007.
236. Olaleye OA, Kaur M, Onyenaka CC. 2020. Ambroxol Hydrochloride Inhibits the Interaction between Severe Acute Respiratory Syndrome Coronavirus 2 Spike Protein’s Receptor Binding Domain and Recombinant Human ACE2. preprint, *Pharmacology and Toxicology*.
237. Bradfute SB, Ye C, Clarke EC, Kumar S, Timmins GS, Deretic V. 2020. Ambroxol and Ciprofloxacin Show Activity Against SARS-CoV2 in Vero E6 Cells at Clinically-Relevant Concentrations. preprint, *Microbiology*.
238. Carpinteiro A, Gripp B, Hoffmann M, Pöhlmann S, Hoertel N, Edwards MJ, Kamler M, Kornhuber J, Becker KA, Gulbins E. 2021. Inhibition of acid sphingomyelinase by ambroxol prevents SARS-CoV-2 entry into epithelial cells. *J Biol Chem* 296:100701.
239. Carpinteiro A, Edwards MJ, Hoffmann M, Kochs G, Gripp B, Weigang S, Adams C, Carpinteiro E, Gulbins A, Keitsch S, Sehl C, Soddemann M, Wilker B, Kamler M, Bertsch T, Lang KS, Patel S, Wilson GC, Walter S, Hengel H, Pöhlmann S, Lang PA, Kornhuber J, Becker KA, Ahmad SA, Fassbender K, Gulbins E. 2020. Pharmacological Inhibition of Acid Sphingomyelinase Prevents Uptake of SARS-CoV-2 by Epithelial Cells. *Cell Rep Med* 1:100142.
240. Yamaya M, Nishimura H, Nadine LK, Ota C, Kubo H, Nagatomi R. 2014. Ambroxol inhibits rhinovirus infection in primary cultures of human tracheal epithelial cells. *Arch Pharm Res* 37:520–529.
241. Yang B, Yao DF, Ohuchi M, Ide M, Yano M, Okumura Y, Kido H. 2002. Ambroxol

- suppresses influenza-virus proliferation in the mouse airway by increasing antiviral factor levels. *Eur Respir J* 19:952–958.
242. Pfeifer S, Zissel G, Kienast K, Müller-Quernheim J. 1997. Reduction of cytokine release of blood and bronchoalveolar mononuclear cells by ambroxol. *Eur J Med Res* 2:129–132.
243. Zhi Q-M, Yang L, Sun H. 2011. Protective Effect of Ambroxol against Paraquat-induced Pulmonary Fibrosis in Rats. *Intern Med* 50:1879–1887.
244. Kantar A, Klimek L, Cazan D, Sperl A, Sent U, Mesquita M. An overview of efficacy and safety of ambroxol for the treatment of acute and chronic respiratory diseases with a special regard to children. *Multidis Res Med* 15:11.
245. Gupta P. 2010. Ambroxol - Resurgence of an old molecule as an anti-inflammatory agent in chronic obstructive airway diseases. *Lung India* 27:46.
246. Zhang Z-Q, Wu Q-Q, Huang X-M, Lu H. 2012. Prevention of Respiratory Distress Syndrome in Preterm Infants by Antenatal Ambroxol: A Meta-Analysis of Randomized Controlled Trials. *Amer J Perinatol* 30:529–536.
247. Smith EC, Popa A, Chang A, Masante C, Dutch RE. 2009. Viral entry mechanisms: the increasing diversity of paramyxovirus entry: The increasing diversity of paramyxovirus entry. *FEBS Journal* 276:7217–7227.
248. Srinivasakumar N, Ogra PL, Flanagan TD. 1991. Characteristics of fusion of respiratory syncytial virus with HEp-2 cells as measured by R18 fluorescence dequenching assay. *J Virol* 65:4063–4069.
249. Yu J, Li M, Wilkins J, Ding S, Swartz TH, Esposito AM, Zheng Y-M, Freed EO, Liang C, Chen BK, Liu S-L. 2015. IFITM Proteins Restrict HIV-1 Infection by Antagonizing the Envelope Glycoprotein. *Cell Reports* 13:145–156.
250. Beer C, Andersen DS, Rojek A, Pedersen L. 2005. Caveola-Dependent Endocytic Entry of Amphotropic Murine Leukemia Virus. *J Virol* 79:10776–10787.
251. Bertrand P, Côté M, Zheng Y-M, Albritton LM, Liu S-L. 2008. Jaagsiekte Sheep Retrovirus Utilizes a pH-Dependent Endocytosis Pathway for Entry. *J Virol* 82:2555–2559.
252. Xu Y, Yang G, Hu G. 2009. Binding of IFITM1 enhances the inhibiting effect of caveolin-1 on ERK activation. *Acta Biochim Biophys Sin* 41:488–494.
253. Werling D, Hope JC, Chaplin P, Collins RA, Taylor G, Howard CJ. 1999. Involvement of caveolae in the uptake of respiratory syncytial virus antigen by dendritic cells. *J Leukoc Biol* 66:50–58.
254. Zhang W, Zhou F, Greene W, Gao S-J. 2010. Rhesus Rhadinovirus Infection of Rhesus Fibroblasts Occurs through Clathrin-Mediated Endocytosis. *J Virol* 84:11709–11717.
255. Krzyzaniak MA, Zumstein MT, Gerez JA, Picotti P, Helenius A. 2013. Host Cell Entry of Respiratory Syncytial Virus Involves Macropinocytosis Followed by Proteolytic Activation of the F Protein. *PLoS Pathog* 9:e1003309.
256. Chang T-H, Segovia J, Sabbah A, Mgbemena V, Bose S. 2012. Cholesterol-rich lipid rafts are required for release of infectious human respiratory syncytial virus particles. *Virology* 422:205–213.
257. Bender FC, Whitbeck JC, Ponce de Leon M, Lou H, Eisenberg RJ, Cohen GH. 2003. Specific Association of Glycoprotein B with Lipid Rafts during Herpes Simplex Virus Entry. *J Virol* 77:9542–9552.
258. Bertrand P. 2010. Understanding the mechanisms of entry of Jaagsiekte sheep retrovirus. McGill University Libraries, Ottawa.
259. Ripa I, Andreu S, López-Guerrero JA, Bello-Morales R. 2021. Membrane Rafts: Portals for Viral Entry. *Front Microbiol* 12:631274.

260. Murata M, Peranen J, Schreiner R, Wieland F, Kurzchalia TV, Simons K. 1995. VIP21/caveolin is a cholesterol-binding protein. *PNAS* 92:10339–10343.
261. Perreira JM, Chin CR, Feeley EM, Brass AL. 2013. IFITMs Restrict the Replication of Multiple Pathogenic Viruses. *J Mol Biol* 425:4937–4955.
262. Ren L, Du S, Xu W, Li T, Wu S, Jin N, Li C. 2020. Current Progress on Host Antiviral Factor IFITMs. *Front Immunol* 11:543444.
263. Aleksandrowicz P, Marzi A, Biedenkopf N, Beimforde N, Becker S, Hoenen T, Feldmann H, Schnittler H-J. 2011. Ebola Virus Enters Host Cells by Macropinocytosis and Clathrin-Mediated Endocytosis. *J Infect Dis* 204:S957–S967.
264. Mercer J, Helenius A. 2008. Vaccinia Virus Uses Macropinocytosis and Apoptotic Mimicry to Enter Host Cells. *Science* 320:531–535.
265. de Vries E, Tscherne DM, Wienholts MJ, Cobos-Jiménez V, Scholte F, García-Sastre A, Rottier PJM, de Haan CAM. 2011. Dissection of the Influenza A Virus Endocytic Routes Reveals Macropinocytosis as an Alternative Entry Pathway. *PLoS Pathog* 7:e1001329.
266. Rojek JM, Sanchez AB, Nguyen NT, de la Torre J-C, Kunz S. 2008. Different Mechanisms of Cell Entry by Human-Pathogenic Old World and New World Arenaviruses. *J Virol* 82:7677–7687.
267. Jae LT, Raaben M, Herbert AS, Kuehne AI, Wirchnianski AS, Soh TK, Stubbs SH, Janssen H, Damme M, Saftig P, Whelan SP, Dye JM, Brummelkamp TR. 2014. Lassa virus entry requires a trigger-induced receptor switch. *Science* 344:1506–1510.
268. Vela EM, Zhang L, Colpitts TM, Davey RA, Aronson JF. 2007. Arenavirus entry occurs through a cholesterol-dependent, non-caveolar, clathrin-mediated endocytic mechanism. *Virology* 369:1–11.
269. Oppliger J, Torriani G, Herrador A, Kunz S. 2016. Lassa Virus Cell Entry via Dystroglycan Involves an Unusual Pathway of Macropinocytosis. *J Virol* 90:6412–6429.
270. Iwasaki M, Ngo N, de la Torre JC. 2014. Sodium Hydrogen Exchangers Contribute to Arenavirus Cell Entry. *J Virol* 88:643–654.
271. Boshoff C, Schulz TF, Kennedy MM, Graham AK, Fisher C, Thomas A, McGee JO, Weiss RA, O’Leary JJ. 1995. Kaposi’s sarcoma-associated herpesvirus infects endothelial and spindle cells. *Nat Med* 1:1274–1278.
272. DiMaio TA, Gutierrez KD, Lagunoff M. 2011. Latent KSHV Infection of Endothelial Cells Induces Integrin Beta3 to Activate Angiogenic Phenotypes. *PLoS Pathog* 7:e1002424.
273. Foster TL, Wilson H, Iyer SS, Coss K, Doores K, Smith S, Kellam P, Finzi A, Borrow P, Hahn BH, Neil SJD. 2016. Resistance of Transmitted Founder HIV-1 to IFITM-Mediated Restriction. *Cell Host & Microbe* 20:429–442.
274. Hoffmann M, Pöhlmann S. 2021. How SARS-CoV-2 makes the cut. *Nat Microbiol* 6:828–829.
275. Prelli Bozzo C, Nchioua R, Volcic M, Koepke L, Krüger J, Schütz D, Heller S, Stürzel CM, Kmiec D, Conzelmann C, Müller J, Zech F, Braun E, Groß R, Wettstein L, Weil T, Weiß J, DiOfano F, Rodríguez Alfonso AA, Wiese S, Sauter D, Münch J, Goffinet C, Catanese A, Schön M, Boeckers TM, Stenger S, Sato K, Just S, Kleger A, Sparrer KMJ, Kirchhoff F. 2021. IFITM proteins promote SARS-CoV-2 infection and are targets for virus inhibition in vitro. *Nat Commun* 12:4584.
276. Zhao X, Guo F, Liu F, Cuconati A, Chang J, Block TM, Guo J-T. 2014. Interferon induction of IFITM proteins promotes infection by human coronavirus OC43.



- PNAS 111:6756–6761.
277. Xie M, Xuan B, Shan J, Pan D, Sun Y, Shan Z, Zhang J, Yu D, Li B, Qian Z. 2015. Human Cytomegalovirus Exploits Interferon-Induced Transmembrane Proteins To Facilitate Morphogenesis of the Virion Assembly Compartment. 6. *J Virol* 89:3049–3061.
  278. Hussein HAM, Akula SM. 2017. miRNA-36 inhibits KSHV, EBV, HSV-2 infection of cells via stifling expression of interferon induced transmembrane protein 1 (IFITM1). 1. *Sci Rep* 7:17972.
  279. Hussein HAM, Briestenska K, Mistrikova J, Akula SM. 2018. IFITM1 expression is crucial to gammaherpesvirus infection, in vivo. 1. *Sci Rep* 8:14105.
  280. Jacobs SR, Gregory SM, West JA, Wollish AC, Bennett CL, Blackbourn DJ, Heise MT, Damania B. 2013. The Viral Interferon Regulatory Factors of Kaposi's Sarcoma-Associated Herpesvirus Differ in Their Inhibition of Interferon Activation Mediated by Toll-Like Receptor 3. *J Virol* 87:798–806.
  281. Perry ST, Compton T. 2006. Kaposi's Sarcoma-Associated Herpesvirus Virions Inhibit Interferon Responses Induced by Envelope Glycoprotein gpK8.1. *J Virol* 80:11105–11114.
  282. Poole LJ, Yu Y, Kim PS, Zheng Q-Z, Pevsner J, Hayward GS. 2002. Altered Patterns of Cellular Gene Expression in Dermal Microvascular Endothelial Cells Infected with Kaposi's Sarcoma-Associated Herpesvirus. *J Virol* 76:3395–3420.
  283. Naranatt PP, Krishnan HH, Svojanovsky SR, Bloomer C, Mathur S, Chandran B. 2004. Host Gene Induction and Transcriptional Reprogramming in Kaposi's Sarcoma-Associated Herpesvirus (KSHV/HHV-8)-Infected Endothelial, Fibroblast, and B Cells: Insights into Modulation Events Early during Infection. *Cancer Res* 64:72–84.
  284. Bailey CC, Huang I-C, Kam C, Farzan M. 2012. Ifitm3 Limits the Severity of Acute Influenza in Mice. *PLoS Pathog* 8:e1002909.
  285. Ranjbar S, Haridas V, Jasenosky LD, Falvo JV, Goldfeld AE. 2015. A Role for IFITM Proteins in Restriction of Mycobacterium tuberculosis Infection. *Cell Reports* 13:874–883.
  286. Gorman MJ, Poddar S, Farzan M, Diamond MS. 2016. The Interferon-Stimulated Gene *Ifitm3* Restricts West Nile Virus Infection and Pathogenesis. *J Virol* 90:8212–8225.
  287. Allen EK, Randolph AG, Bhangale T, Dogra P, Ohlson M, Oshansky CM, Zamora AE, Shannon JP, Finkelstein D, Dressen A, DeVincenzo J, Caniza M, Youngblood B, Rosenberger CM, Thomas PG. 2017. SNP-mediated disruption of CTCF binding at the IFITM3 promoter is associated with risk of severe influenza in humans. *Nat Med* 23:975–983.
  288. Shen C, Wu X, Jiao W, Sun L, Feng W, Xiao J, Miao Q, Liu F, Yin Q, Zhang C, Guo Y, Shen A. 2013. A Functional Promoter Polymorphism of IFITM3 Is Associated with Susceptibility to Pediatric Tuberculosis in Han Chinese Population. *PLoS ONE* 8:e67816.
  289. The GenISIS Investigators, The MOSAIC Investigators, Everitt AR, Clare S, Pertel T, John SP, Wash RS, Smith SE, Chin CR, Feeley EM, Sims JS, Adams DJ, Wise HM, Kane L, Goulding D, Digard P, Anttila V, Baillie JK, Walsh TS, Hume DA, Palotie A, Xue Y, Colonna V, Tyler-Smith C, Dunning J, Gordon SB, Smyth RL, Openshaw PJ, Dougan G, Brass AL, Kellam P. 2012. IFITM3 restricts the morbidity and mortality associated with influenza. 7395. *Nature* 484:519–523.
  290. Zhang Y, Makvandi-Nejad S, Qin L, Zhao Y, Zhang T, Wang L, Repapi E, Taylor S, McMichael A, Li N, Dong T, Wu H. 2015. Interferon-induced transmembrane

- 
- protein-3 rs12252-C is associated with rapid progression of acute HIV-1 infection in Chinese MSM cohort. *AIDS* 29:889–894.
291. Zhang Y-H, Zhao Y, Li N, Peng Y-C, Giannoulatou E, Jin R-H, Yan H-P, Wu H, Liu J-H, Liu N, Wang D-Y, Shu Y-L, Ho L-P, Kellam P, McMichael A, Dong T. 2013. Interferon-induced transmembrane protein-3 genetic variant rs12252-C is associated with severe influenza in Chinese individuals. *Nat Commun* 4:1418.
292. Zhang Y, Qin L, Zhao Y, Zhang P, Xu B, Li K, Liang L, Zhang C, Dai Y, Feng Y, Sun J, Hu Z, Xiang H, Knight JC, Dong T, Jin R. 2020. Interferon-Induced Transmembrane Protein 3 Genetic Variant rs12252-C Associated With Disease Severity in Coronavirus Disease 2019. *J Infect Dis* 222:34–37.
293. Gómez J, Albaiceta GM, Cuesta-Llavona E, García-Clemente M, López-Larrea C, Amado-Rodríguez L, López-Alonso I, Melón S, Alvarez-Argüelles ME, Gil-Peña H, Vidal-Castiñeira JR, Corte-Iglesias V, Saiz ML, Alvarez V, Coto E. 2021. The Interferon-induced transmembrane protein 3 gene (IFITM3) rs12252 C variant is associated with COVID-19. *Cytokine* 137:155354.
294. Alghamdi J, Alaamery M, Barhoumi T, Rashid M, Alajmi H, Aljasser N, Alhendi Y, Alkhalaf H, Alqahtani H, Algablan O, Alshaya AI, Tashkandi N, Massadeh S, Almuzzaini B, Ehaideb SN, Bosaeed M, Ayoub K, Yezli S, Khan A, Alaskar A, Bouchama A. 2021. Interferon-induced transmembrane protein-3 genetic variant rs12252 is associated with COVID-19 mortality. *Genomics* 113:1733–1741.

## 7 Appendix

### 7.1 List of Figures

Figure 1: Simplified viral replication cycle

Figure 2: SARS-CoV-2 Spike protein structure and particle entry

Figure 3: Viral Membrane fusion

Figure 4: Schematic representation of the proposed model of SARS-CoV-2 Spike-mediated membrane fusion

Figure 5: Schematic representation of the proposed model of herpesviral gB-mediated fusion

Figure 6: IFITM domain structure and proposed models for IFITM function

### 7.2 List of Abbreviations

Abbreviation		Abbreviation	
6HB	six alpha-helices	L	leucine
A	alanine	Lassa virus	LASV
ACE2	angiotensin-converting enzyme 2	M	methionine
AH	amphipathic helix	MBCD	methyl-beta-cyclodextrin
approx.	approxiamtely	MCD	multicentric Castleman disease
ATP	Adenosine triphosphate	MERS-CoV	Middle East Respiratory Syndrome coronavirus
C	cysteine	MLV	Murine leukemia virus
C-terminal	carboxy terminal	MMPs	matrix-metalloproteases
Ca	Calcium	MPR	membrane proximal region
CH	central helix	N	asparagine
CIL	conserved intracellular loop	N-terminal	amino terminus
COVID-19	coronavirus disease 2019	NH <sub>4</sub> Cl	Ammonium Chloride
CoVs	coronaviruses	nm	nanometer
CTD	cytoplasmic tail domain	NTD	N-terminal domain
D	Domain	ORF	Open reading frame
D	aspartic acid	P	proline

DC-SIGN	Dendritic Cell-Specific Intercellular adhesion molecule-3-Grabbing Nonintegrin	PEL	primary effusion lymphoma
DENV	Dengue virus	PI	phosphatidylserine
Deoxyribonucleic acid	DNA	Q	glutamine
E	glutamic acid	R	arginine
EBOV	Ebola virus	RBD	receptor binding domain
EBV	Epstein-Barr virus	Ribonucleic acid	RNA
EIPA	5-(N-Ethyl-N-isopropyl)amiloride	RRV	rhesus monkey rhadinovirus
EphA2	Ephrin type-A receptor 2	RSV	respiratory syncytial virus
et al.	et alii	S	Spike
F	phenylalanine	S	serine
FP	fusion peptide	S1	Subunit 1
g	glycoproteins	S2	Subunit 2
G	glycine	SARS-CoV	severe acute respiratory syndrome coronavirus
H	histidine	SARS-CoV-2	severe acute respiratory syndrome coronavirus 2
HA	hemagglutinin	SD3	subdomain 3
hACE2	human angiotensin-converting enzyme 2	small interfering RNA	siRNA
HCMV	Human Cytomegalovirus	T	threonine
HD	hydrophobic domain	TM	transmembrane domain
HFF	Human Foreskin Fibroblast	TMEM16F	Transmembrane protein 16F
HIV	human immunodeficiency virus	TMPRSS2	transmembrane protease serine subtype 2
HMVEC-d	Human dermal microvascular endothelial cell	UH	upstream helices
HR1	heptad repeat regions 1	USA	United States of America
HR2	heptad repeat regions 2	V	valine
HSPG	heparan sulfate proteoglycan	VAPA	Vesicle-membrane-protein-associated protein
HSV-1	Herpes simplex virus 1	vIL6	viral interleukin-6
HUVEC	Human Umbilical Vein Endothelial Cells	vIRF	viral Interferon regulatory factors
I	isoleucine	W	tryptophan
IAV	influenza A virus	WNV	West Nile Virus
IFITM1	Interferon-inducible transmembrane protein 1	wt	wild type



IFITM10	Interferon-inducible transmembrane protein 10	Y	tyrosine
IFITM2	Interferon-inducible transmembrane protein 2	ZMPSTE24	Zinc Metallopeptidase STE24
IFITM3	Interferon-inducible transmembrane protein 3		
IFITM5	Interferon-inducible transmembrane protein 5		
IFITMs	Interferon-inducible transmembrane proteins		
IFN	Interferon		
IL-6	interleukin-6		
IRFs	Interferon regulatory factors		
JSRV	Jaagsiekte sheep retrovirus		
K	lysine		
kb	Kilobases		
KS	Kaposi's sarcoma		
KSHV	Kaposi's sarcoma herpesvirus		
L	linker domain		

### 7.3 List of publications

- 2021 **Hörnich B.F.**, Großkopf A.K., Dcosta C.J., Schlagowski S., Hahn A.S. Interferon-Induced Transmembrane Proteins Inhibit Infection by the Kaposi's Sarcoma-Associated Herpesvirus and the Related Rhesus Monkey Rhadinovirus in a Cell-Specific Manner. *mBio* **2021**, DOI:10.1128/mBio.02113-21
- 2021 Hoffmann M., Arora P., Groß R., Seidel A., **Hörnich B.F.** et al. SARS-CoV-2 Variants B.1.351 and P.1 Escape from Neutralizing Antibodies. *Cell* **2021**, 184 (9), 2384-2393
- 2021 **Hörnich B.F.**, Großkopf A.K., Schlagowski S., Tenbusch M., et al. SARS-CoV-2 and SARS-CoV Spike-Mediated Cell-Cell Fusion Differ in Their Requirements for Receptor Expression and Proteolytic Activation. *J Virol* **2021**, 95 (9)
- 2021 Lüdke D., Roth C., Kamrad S.A., Messerschmidt J., Hartken D., Appel J., **Hörnich B. F.** et al. Functional Requirement of the *Arabidopsis* Importin- $\alpha$  Nuclear Transport Receptor Family in Autoimmunity Mediated by the NLR Protein SNC1. *Plant J* **2021**, 105 (4), 994–1009
- 2019 Großkopf A.K., Schlagowski S., **Hörnich B.F.**, Fricke T., Desrosiers R.C., Hahn A.S. EphA7 Functions as Receptor on BJAB Cells for Cell-to-Cell Transmission of the Kaposi's Sarcoma-Associated Herpesvirus and for Cell-Free Infection by the Related Rhesus Monkey Rhadinovirus. *J Virol* **2019**, 93 (15)

### 7.4 Conference participations

- 2019 Düsseldorf, DE 28<sup>th</sup> Annual meeting of the society for virology: Interaction between interferon-induced trans-membrane proteins and gamma-2-Herpesviruses, Poster Presentation
- 2019 Braunschweig, DE 14<sup>th</sup> Mini-Herpesvirus Workshop: Interaction between interferon induced trans-membrane proteins and gamma-2-Herpes viruses, Poster Presentation
- 2021 Hannover, DE 30<sup>th</sup> Annual meeting of the society for virology: SARS-CoV-2 and SARS-CoV Spike-Mediated Cell-Cell Fusion Differ in Their Requirements for Receptor Expression and Proteolytic Activation, Poster Presentation

## 7.5 Acknowledgement

First, I like to state that I prefer personal thanks instead of written ones and that some written words cannot sufficiently express my gratitude.

So here just in short:

At first, I would like to thank Dr. Alexander Hahn for the opportunity to work at this project and the possibility to follow my own ideas. The constant scientific exchange is the base of the successful outcome of this work and the publications it is based on.

I would also like to thank Stefan Pöhlmann for being the second reviewer of this thesis.

Special thanks go to the members of my Thesis Advisory Committee Lutz Walter and Christiane Stahl-Hennig for the helpful advice and feedback.

Additional thanks also go to the members of the Infection Biology Unit, in particular Markus Hoffman and Michael Winkler, for the great collaboration and helpful ideas.

The most important thanks must go to the members of the NWG Herpesviren for the great atmosphere, constant support, and scientific input.

At last, I have to thank my parents.

---

## 7.6 Curriculum vitae

**Bojan Fabio Hörnich**

<hr/>	
	<b>Personal Information</b>
Date of birth	14.08.1991
Place of birth	Berlin
Nationality	German
<hr/>	
	<b>Academic Carrier</b>
Since 05/2018	Dissertation, within the doctoral program Emerging Infectious Diseases (EIDIS) of the Georg-August University School of Science (GAUSS)
<hr/>	
	<b>Education</b>
10/2015-06/2018	M. Sc. in Molecular Life Sciences: Microbiology, Biotechnology and Biochemistry, Georg-August-Universität Göttingen Master thesis: Functional analysis of a resistance-like protein pair in Arabidopsis using CRISPR/Cas9 and subcellular localization studies
10/2011- 10/2015	B. Sc. in Biochemistry, Georg-August-Universität Göttingen Bachelor thesis: Synthese einer photoabspaltbaren Schutzgruppe für Cystein zur Untersuchung der SNARE- vermittelten Membranfusion
08/2008-06/2011	Abitur at the Gymnasium Einbeck
<hr/>	
	<b>Engagement</b>
Since 2020	Student representative, Graduate School for Emerging Infectious Diseases (EIDIS)
<hr/>	
	<b>Languages</b>
German	Native speaker
English	C1
Spanish	Basic